AD-A053 395 NAVAL RESEARCH LAB WASHINGTON D C F/G 20/1
SPATIAL IMPULSE RESPONSE OF AN ACOUSTIC LINE RADIATOR - A STUDY--ETC(U)
FEB 78 A J RUDGERS

UNCLASSIFIED NRL-8191 SBIE-AD-E000 134 NL

1 OF 3
ADA
053395

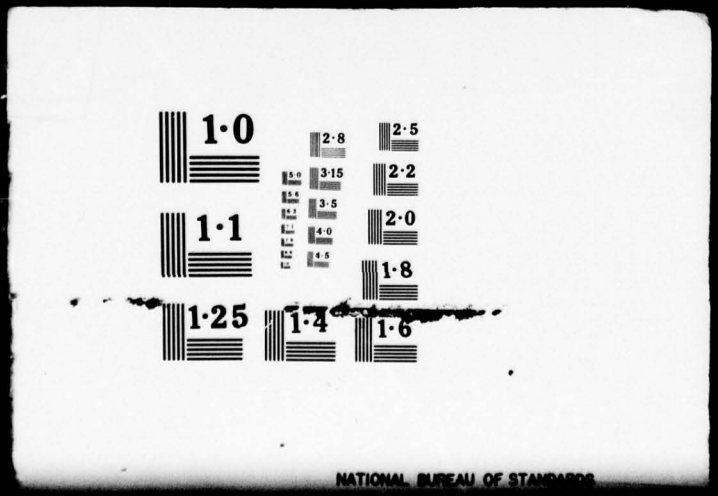

NRL Report 8191

Spatial Impulse Response of an Acoustic Line Radiator— A Study of Boundary-Diffraction-Wave Phenomena and Their Experimental Detection

ANTHONY J. RUDGERS

Standards Branch
Underwater Sound Reference Division

February 22, 1978

NAVAL RESEARCH LABORATORY
Underwater Sound Reference Division
P.O. Box 8337, Orlando, Florida 32856

This report is a facsimile of a dissertation submitted in 1977 to the faculty of the School of Engineering and Architecture of The Catholic University of America, Washington, D.C., in partial fulfillment of the requirements for the degree of Doctor of Philosophy. The director of the dissertation work was Dr. Ronald L. Spooner; the readers were Dr. Edward B. Magrab and Dr. Frank A. Andrews. The research described was simultaneously a part of the program of the Naval Research Laboratory.

Manuscript submitted January 18, 1978.

SECURITY CLASSIFICATION OF THIS PAGE *(When Data Entered)*

REPORT DOCUMENTATION PAGE

READ INSTRUCTIONS BEFORE COMPLETING FORM

1. REPORT NUMBER NRL Report 8191	2. GOVT ACCESSION NO.
3. RECIPIENT'S CATALOG NUMBER	
4. TITLE *(and Subtitle)* SPATIAL IMPULSE RESPONSE OF AN ACOUSTIC LINE RADIATOR - A STUDY OF BOUNDARY-DIFFRACTION-WAVE PHENOMENA AND THEIR EXPERIMENTAL DETECTION.	5. TYPE OF REPORT & PERIOD COVERED Interim report on a continuing NRL problem.
	6. PERFORMING ORG. REPORT NUMBER
7. AUTHOR(s) Anthony J. Rudgers	8. CONTRACT OR GRANT NUMBER(s) RR011080 RR011080842
9. PERFORMING ORGANIZATION NAME AND ADDRESS Underwater Sound Reference Division Naval Research Laboratory P.O. Box 8337, Orlando, FL 32856	10. PROGRAM ELEMENT, PROJECT, TASK AREA & WORK UNIT NUMBERS NRL Problem S02-46 PE: 61153N-11 Project: RR011-08-42
11. CONTROLLING OFFICE NAME AND ADDRESS Naval Research Laboratory Washington, D.C. 20375	12. REPORT DATE February 1978
	13. NUMBER OF PAGES 238 (240 p.)
14. MONITORING AGENCY NAME & ADDRESS *(if different from Controlling Office)* SBIE AD-E000 134	15. SECURITY CLASS. *(of this report)* UNCLASSIFIED
	15a. DECLASSIFICATION/DOWNGRADING SCHEDULE

16. DISTRIBUTION STATEMENT *(of this Report)*

Approved for public release; distribution unlimited.

17. DISTRIBUTION STATEMENT *(of the abstract entered in Block 20, if different from Report)*

18. SUPPLEMENTARY NOTES

19. KEY WORDS *(Continue on reverse side if necessary and identify by block number)*

Acoustic radiation theory	Boundary diffraction waves
Acoustic diffraction theory	Geometrical waves
Acoustic field structure	Young's boundary wave
Rubinowicz-Maggi diffraction theory	Radiated field components
Schoch radiation theory	Diffracted field components (Cont'd)

20. ABSTRACT *(Continue on reverse side if necessary and identify by block number)*

The field radiated by a finite-length line source was investigated theoretically and experimentally. A new closed-form, time-domain theoretical expression of this field was derived. This result, which supports the ideas advanced in the Rubinowicz-Maggi diffraction theory, shows the field of a line source to be comprised of three components: a spatially discontinuous cylindrical wave ("geometrical wave") and two directional boundary diffraction

(Continues)

251 950

19. Key Words (Continued)

Line acoustic sources
Planar acoustic sources
Finite acoustic sources
Transient acoustic fields
Active points
Active regions
Spatial impulse response functions
Measurement of acoustic radiation
Crosscorrelation techniques
Digital acoustical instrumentation
Measurement of radiated noise
Acoustic test tanks
Acoustic transducers
USRD Type F36 transducer
Pseudorandom Gaussian noise
Solutions of the wave equation
Integral transform techniques
Generalized functions
Pseudofunctions
Correlation functions

20. Abstract (Continued)

waves radiated by the ends of the line. The theory is tested by measuring the spatial impulse response of a line transducer. The experiments were conducted in a water tank, using bursts of pseudorandom noise to excite the transducer electrically. By crosscorrelating these electric signals with the acoustic signals that the transducer radiates, the waveform of the source's spatial impulse response is obtained at a number of observation points. Experimental waveforms are compared to the waveforms theoretically expected. Agreement between theory and experiment is excellent. The experiments constitute the first definitive test of the Rubinowicz-Maggi theory in acoustics. Existence of the geometrical and boundary diffraction waves was confirmed. Moreover, since a standard underwater transducer was used as a source in the experiments, this research demonstrates that the Rubinowicz-Maggi theory is applicable in practical situations.

CONTENTS

ACKNOWLEDGEMENTS

I deeply appreciate the employee-training policy of the Naval Research Laboratory that enabled me to carry out my graduate work and dissertation research in conjunction with my official duties. I am particularly grateful for the opportunity to participate in the Edison Memorial Graduate Training Program. I sincerely thank my former supervisor, Mr. W. James Trott of the Acoustics Division, for his encouragement and for providing me, in times of ever-shrinking budgets, with resources that were sufficient to allow me to complete the research work reported here.

I am greatly indebted to many individuals throughout the Naval Research Laboratory, who aided me during the course of my dissertation work. I wish to specially thank Ms. Renee A. Walker, A Federal Junior Fellow, for her able assistance, both in the laboratory and with the massive amount of computer work that this research effort entailed. Special thanks go also to Mr. Charles E. Balfourd, who took the particular set of experimental data that resulted in most of the spatial-impulse-response-function waveforms reported here. Mr. Eddie L. Shepler deserves special appreciation for his competence and his helpfulness in planning and expediting the fabrication of much of the experimental apparatus, and for constructing several pieces of specialized laboratory equipment. Mr. George C. Wiedemann was also very helpful in constructing equipment during the early stages of this research effort. My sincere appreciation goes to Mr. Dorsey J. G. Gregan, not only for helping me to align the transducer-mounting assembly, but also for his untiring assistance in solving the myriad of technical problems that accompany experimental acoustic work in a water tank. Thanks also go to Mr. Delfus J. Dorsey for helping me on countless occasions both in setting up and in maintaining the laboratory equipment, and to Mr. Josephus Neeley, who measured the response characteristics of some of the electronic equipment that I used.

I appreciate the help that I received from many persons in the support groups at the Naval Research Laboratory, particularly those in

Research Computation Center, in the Technical Information Division, and in the Engineering Services Division. Persons in the Research Computation Center who deserve particular thanks are Mr. Edward L. Aiken and Mr. R. D. "Mac" McCulloch, without whose help it would not have been possible to construct the necessary data-handling computer programs. Thanks also go to Mr. Irwin J. Levy and to Mr. John W. Carpenter for making it possible to efficiently handle paper-tape data with the CDC 3800 computer. Two persons in the Engineering Services Division deserve my particular thanks: Mr. John O'Toole, the former supervisor of the satellite shop where much of the laboratory equipment was built and Mr. John Reese of Instrument Repair, whose prompt attention to instrumentation problems kept the experimental electronic system in operation.

The efforts of Mrs. Pamela J. Nuckols, of Ms. Marian E. Bruemmer, and especially of Mrs. Yolanda S. Pelosi in typing the many manuscripts of this dissertation are greatly appreciated. My deepest thanks, however, go to Mrs. Louise E. Maiden, who patiently and expertly typed the final draft.

A special acknowledgement is due my family. Without the help, understanding, and encouragement of my wife Karen and our children Nathan, Ben, and Erika during the many years of my graduate studies, it would have been difficult for me to carry these studies to completion.

Finally, I wish to express my warmest thanks to Dr. Sam Hanish for the encouragement, empathy, and advice that he has given me.

PRECIS

Introduction

Acoustical radiation, diffraction, and scattering problems have been treated using a variety of analytical techniques. However, none of the present techniques are capable of providing solutions to all of the problems that are of theoretical and practical significance. For this reason, it is important to examine new approaches to the solution of such problems. It is particularly important to examine those new approaches that may prove of value in solving whole classes of problems that one cannot now treat by means of conventional methods.

One such alternative approach, which can be used to attack general problems arising in the study of acoustical radiation phenomena, is based upon the Rubinowicz-Maggi formulation of diffraction theory. In the Rubinowicz-Maggi formulation, the radiated field of an acoustic source is envisioned as being comprised of components of two types. First, there is a geometrical field component. This is a wavefield with spatially discontinuous wavefronts whose shape conforms to the shape of the radiating surface of the source. Second, there are one or more boundary-diffraction-wave field components that are radiated by the edges of the source's surface. Radiation associated with such boundary-diffraction-wave components may often be localized to particular points on the edges of the source's radiating surface. Boundary-diffraction-wave components, like the geometrical component, are spatially discontinuous, but their discontinuities are such that they exactly compensate for the discontinuity in the geometrical component. Thus, the source's total radiated field, consisting of the superposition of the geometrical and boundary-diffraction-wave components, is continuous everywhere.

This picture of the structure of radiation fields that results from the Rubinowicz-Maggi formulation has, potentially, important

consequences from both a theoretical and a practical standpoint. On the theoretical side, the radiation of particular field components can be associated with definite geometrical features of the radiating source. Thus, the shape and nature of an acoustic source's edge, as much as the shape and curvature of its radiating surface, determines the structure of its radiated field. This being the case, it is conceivable, on the basis of tne Rubinowicz-Maggi theory, that one can eventually theoretically predict the acoustic field radiated by a source of arbitrary shape, once a geometrical description of the source is given. An enhanced ability to design acoustic sources, receivers, and scatterers would be the practical result of this new theoretical understanding.

While the theoretical basis for the Rubinowicz-Maggi formulation is reasonably well-established, there is at present very little experimental work either supporting or refuting it. This holds true, not only in the field of acoustics, but in optics as well. The aim of the work reported in this dissertation is to provide definitive experimental confirmation for the Rubinowicz-Maggi theory by performing laboratory experiments in which the field structure of a sound-radiating source is investigated. It is shown here that the features of the source's radiated field that are experimentally observed are precisely those that are theoretically predicted on the basis of the concepts of the Rubinowicz-Maggi formulation of diffraction and radiation theory. The acoustic radiator whose field is investigated is a line source of finite length. The radiated field of this source is described by the spatial impulse response function, which expresses the field of the finite line source in the time domain rather than in the frequency domain. In addition to designing and implementing a laboratory experiment to measure the spatial impulse response function of a finite-line acoustic source, it is also necessary to develop a suitable theoretical expression for the field of such a source, before experimental and theoretical results can be compared.

Background

The Rubinowicz-Maggi theory resulted from the study of optical diffraction phenomena. Many of the concepts embodied in the Rubinowicz-Maggi theory can be traced to the formulation of diffraction theory advanced by Thomas Young early in the nineteenth century. Young's formulation, however, seemed at the time to have certain shortcomings that led to its rejection and to its replacement by a formulation of diffraction theory that is based upon the ideas of Fresnel and of Kirchhoff. At the present time, the conventional theory of acoustic radiation rests upon this latter formulation of diffraction theory. However, throughout the long history of diffraction theory, investigators of optical diffraction phenomena have continually returned to Young's concepts. In particular, Sommerfeld's exact treatment of the problem of diffraction of a plane electromagnetic wave by a perfectly reflecting half-plane suggested that a diffracting edge acts as a directional source of waves. These diffraction waves appear to interfere with the incident light in the half-plane's directly illuminated region and to radiate into the region of its geometrical shadow.

Sommerfeld's work led Rubinowicz to reformulate Kirchhoff's theory of scalar-wave diffraction. Rubinowicz was able to express the diffracted field of an edge or an aperture as the superposition of a geometrical wave field and a boundary-diffraction-wave field. In the Rubinowicz formulation, the boundary-diffraction-wave field can be expressed in terms of a line integral taken along the edge of the diffracting object. This is in contrast to the results of the usual formulation of diffraction theory in which the diffracted field, which is not separated from the geometrical field, is expressed as a surface integral taken over that portion of an incident wavefront that is not obstructed by the diffracting object. By pointing out how the line-integral expressions for the boundary-diffraction-wave fields could be evaluated by an asymptotic technique, Rubinowicz showed that the radiation of boundary diffraction waves by the edge of a diffracting body

can be localized to small regions in the vicinity of active points. Active points are those points on the diffracting edge that are defined by extremum values of the optical path, passing through the diffracting edge, that connects the source point to the observation point in question.

The Rubinowicz-Maggi theory was applied to the study of acoustic radiation phenomena by Schoch. Schoch obtained general expressions for the radiated field of a finite planar piston source, which was located in an infinite rigid baffle and which radiated into a fluid-filled half-space. Schoch separated the fluid-filled region into two subregions by means of a hypothetical cylindrical surface, normal to the plane of the baffle, whose generating lines pass through the periphery of the radiating piston. Within the semi-infinite cylinder defined by this hypothetical surface, Schoch showed that the piston's radiated field is comprised of two components. The first such component is a geometrical wave. This is a finite plane wave with wavefronts parallel to the piston face. Since these wavefronts terminate abruptly at the surface of the cylinder, the geometrical wavefield propagates in a beam-like fashion away from the piston face. There is also a boundary-diffraction-wave field component within the cylindrical subregion that is directly in front of the piston. This boundary-diffraction-wave component, which is radiated by the edge of the piston, is expressed by a line integral taken along the piston's edge. The boundary-diffraction-wave component interferes with the geometrical wave within the cylindrical subregion and also changes discontinuously at the subregion's surface. Outside of the cylindrical subregion, Schoch's analysis showed that there is no geometrical wave component. Only a boundary-diffraction-wave component exists there, which, like the boundary-diffraction-wave component within the cylindrical surface, is expressed by a line integral taken along the edge of the piston. Both the boundary-diffraction-wave component and the geometrical component of the piston's radiated field change discontinuously as the cylindrical boundary surface between the two subregions is crossed. However, the piston's total radiated field, which is the superposition

of these two components, remains continuous everywhere, owing to the fact that the discontinuous change in the boundary-diffraction-wave component exactly compensates for the discontinuous change in the geometrical wave component.

Schoch's expressions for the boundary-diffraction-wave components in the two subregions remain in the form of line integrals. Schoch does, however, point out how it would be possible to evaluate these integrals by an asymptotic procedure and to thereby obtain results analogous to those obtained by Rubinowicz in the case of a light-diffracting aperture. Because of the apparent difficulty, no one previously has carried out this asymptotic evaluation of the boundary-diffraction-wave line integrals, except in a few very restricted cases. Nevertheless, it proved possible to perform this analysis in a straightforward fashion for the case of a piston whose boundary is defined by a general, smooth, convex curve. The results and their range of validity are reported in this dissertation. The analysis presented, however, is both complex and lengthy. It requires one to pay considerable attention to the details of the geometry of the curve defining the piston's periphery. The expressions obtained for the piston's radiated field, as a result of the analysis, are likewise lengthy. They show, however, that there are localized active points on the piston's periphery, the neighborhoods of which, radiate boundary diffraction waves to an observation point. These active points are defined by extremum values of the distance that separates an observation point from points on the piston's boundary.

Using a Green's-function technique, one can also obtain a time-domain expression for the radiated field of a planar piston. This result of conventional radiation theory expresses the piston's field as a surface integral taken over the radiating piston face. The surface-integral expression gives no hint that the radiated field of the piston is a composite comprised of geometrical and boundary-diffraction-wave components.

Theory of the Finite Line Source

The line radiator of finite length is a far more suitable source to use in laboratory acoustical experiments than is a planar piston in an infinite rigid baffle. Presently, however, there is no closed-form analytic expression for the radiated field of a finite line source in the time domain. For this reason, it is necessary to derive such a result.

An expression for the spatial impulse response function of an idealized line radiator with finite length is obtained by solving the inhomogeneous wave equation. Owing to the symmetry of the line source, this is essentially a two-dimensional problem, in which the wave equation can be expressed in cylindrical coordinates. The solution to the wave equation is obtained by using integral-transform techniques, but in order to do so it is necessary to work with the wave equation for the acoustic velocity-potential field rather than that for the acoustic pressure field. The velocity potential must be transformed with respect to three variables. A Hankel transform of order zero is taken with respect to the radial cylindrical coordinate, an exponential Fourier transform is taken with respect to the axial cylindrical coordinate, and a Laplace transform is taken with respect to the time. Once an expression for the transformed velocity potential is found, the three transforms can be inverted, through use of results found in the Bateman tables, in order to obtain an expression for the line source's velocity-potential field in the time domain.

The expression for the velocity-potential field of the source is differentiated with respect to time in order to obtain a corresponding expression for the source's acoustic pressure field. However, since the velocity potential is expressed in terms of generalized functions of time and functions with temporal singularities, in order to correctly perform the required differentiation, it is necessary to apply techniques from the theory of distributions. The result of the analysis is the following expression for the spatial impulse response of a finite line source:

$$p(r,z,t) = -\frac{\rho Q}{4\pi}[2\psi(r,\ 0,\ t) - \psi(r,\ \tfrac{1}{2}L-z,\ t) - \psi(r,\ \tfrac{1}{2}L+z,\ t)], \quad \text{(P1a)}$$

for $-\frac{1}{2}L \le z \le \frac{1}{2}L$ and

$$p(r,z,t) = -\frac{\rho Q}{4\pi}\mathrm{sgn}(z)[\psi(r,\ \tfrac{1}{2}L-z,\ t) - \psi(r,\ \tfrac{1}{2}L+z,\ t)], \quad \text{(P1b)}$$

for $|z| > \frac{1}{2}L$, where L is the length of the line source, r and z are, respectively, the radial and axial cylindrical coordinates of the observation point, and t is the time. The generalized function ψ appearing in Eqs. (P1) is the pseudofunction

$$\psi(r,u,t) = \mathrm{Psf}\left[\frac{u[t - (r^2 + u^2)^{\frac{1}{2}}/c]t}{[t^2 - (r^2 + u^2)/c^2]^{3/2}}\right] \quad \text{(P2)}$$

In Eq. (P2), u designates the unit step function and the sign function sgn in Eq. (P1b) assumes the value -1 for $z < 0$ and 1 for $z > 0$. The quantity Q in Eqs. (P1) is the source strength of the line radiator per unit length. The line source is considered to be surrounded by a fluid having density ρ and soundspeed c. The line source is situated on the z axis of the cylindrical coordinate system and is symmetrically disposed about the coordinate origin.

It is to be noted from Eqs. (P1) that the theoretical expression for the spatial impulse response function of the finite line is of a different form in each of two subregions of the fluid-filled medium surrounding the source. These two subregions are defined by a pair of hypothetical infinite planes, which are each normal to the line source and which pass through its respective ends. In the subregion between these two planes, the radiated pressure field, which is expressed by Eq. (P1a), is a composite of three distinct components--a geometrical wave component and two boundary-diffraction-wave components. The impulsive geometrical wave, which is expressed by the term $2\psi(r,\ 0,\ t)$ in Eq. (P1a), is a finite cylindrical wave concentric with the source, whose wavefronts terminate abruptly at the two hypothetical planes. In this subregion

also, impulsive boundary diffraction waves radiate from each end of the line. These are given by the two terms of the form $\Psi(r, \frac{1}{2}L \pm z, t)$ in Eq. (P1a). Both of the boundary diffraction waves have the same polarity, or sense, which is opposite to the polarity of the geometrical wave in the subregion between the hypothetical planes, so that in this subregion they tend to interfere constructively with one another and destructively with the geometrical wave.

In either of the two subregions outside one of the hypothetical planes, only the two boundary diffraction waves, which are radiated by the ends of the line, exist. This situation is described by Eq. (P1b). However, as an observation point passes across one such plane, the boundary diffraction wave radiated from the end of the line through which that plane passes changes discontinuously. The most conspicuous feature of this discontinuous change is an abrupt change in the polarity of the impulsive boundary diffraction wave. This change in polarity can be noted from the opposite signs of $\psi(r, \frac{1}{2}L-z, t)$ and $\psi(r, \frac{1}{2}L+z, t)$ in Eq. (P1b). Thus outside either of the two hypothetical planes, the two boundary diffraction waves, which are radiated from opposite ends of the line, tend to interfere destructively with one another. The discontinuous change in the boundary diffraction wave at the hypothetical plane again just compensates for the discontinuous change in the cylindrical geometrical wave, so that the line source's total pressure field again remains continuous everywhere.

It is apparent that the structural features of the pressure field radiated by a finite line source, as they are predicted on the basis of the analysis that is developed, are analogous to those predicted for a planar piston, according to Schoch's theory. Thus, for example, the finite cylindrical wave in the case of the line radiator is the analog of the finite plane wave that is the geometrical component of the radiated field of a planar piston. Similarly, the components radiated from the ends of the finite line source are analogous to the field component radiated by active points on a planar piston's periphery. The line source's pressure field, as given by the spatial impulse response

function is, however, expressed in closed form. The expression for this field is exact, in contrast to the corresponding approximate expression that one obtains for the spatial impulse response function of a piston, owing to the introduction of the asymptotic method for evaluating line integrals in this latter case. Moreover, also in contrast to the expression obtained in the case of the piston, the expression for the line source's spatial impulse response function is valid both far from the source as well as near to it.

Since the theoretical spatial impulse response function of the finite line source is expressed in terms of generalized functions that contain singularities, it is necessary to obtain, in addition to the theoretical result given by Eqs. (P1), an analytical expression that is everywhere finite so that theoretical predictions can be compared to experimental results. Moreover, in this finite form of the source's spatial impulse response function, it is also necessary to account for a number of characteristics of the experimental system. It is found that the important features of the theoretical spatial impulse response function are those that significantly influence the result obtained when the spatial impulse response function is convolved with another function. Consequently, the singularities of the spatial impulse response function, their relative weights, and their sequence of occurrence in time appear to be the function's essential characteristics. The singularities of the function can easily be represented by finite impulse functions with their relative weights obtained directly from the theoretical analysis. However, theoretical results are to be compared with the experimental results obtained from a sampled-data measurement system. Therefore, the theoretical spatial impulse response function must also be expressed as a sampled temporal function. This fact introduces a difficulty in representing the theoretical spatial impulse response function by means of finite impulse functions of the usual type, since the experimental sampling points do not coincide in time with the instant at which such impulse functions occur. A method is devised, however, which allows one

to correctly represent the impulse functions at an arbitrary instant of time that does not correspond to an experimental sampling time. Use of this method, which is based upon the five point Lagrange interpolation formula, is an important factor in developing a theoretical representation of the line source's spatial impulse response function that can be compared to the results that are obtained experimentally.

Experimental Design

The spatial impulse response of an acoustic source is the acoustic pressure signal resulting from a uniform particle-velocity distribution on the radiating surface of the source, which has a time-variation that is described by a δ-function. The spatial impulse response function of a source is analogous to the usual temporal impulse response of a linear system. However, the spatial impulse response function characterizes the geometry of the source as it relates to the field that the source radiates, rather than characterizing the internal nature of a linear system, as does the usual temporal impulse response function. It is a well-known result of the statistical theory of communication that the temporal impulse response function of an arbitrary linear system can be obtained by exciting the input of the system with a continuous white-noise signal and crosscorrelating this input signal with the resulting output signal from the linear system. This same input-output crosscorrelation technique is applied to obtain the spatial impulse response of the finite line source. One may do this since the line source and its radiated field constitute a linear system.

Measurements are made of the spatial impulse response of a Type F36 line transducer. The Type F36, which is designed to operate as a source in the frequency range from 1 to 20 kHz, is a transducer currently in widespread use in the field of underwater acoustics. The experiments to measure the radiated field of this transducer were conducted in a large water tank, using bursts of bandlimited pseudorandom white Gaussian noise to excite the Type F36 electrically.

Designing and building the unique experimental system that was used to conduct the experiments confirming the Rubinowicz-Maggi radiation theory was a major part of the work reported here. In this experimental system, a large computer is coupled to both the input and the output of the laboratory equipment. The computer is used at the input of the laboratory system to generate, in digital form, the pseudorandom noise-bursts that excite the Type F36 source transducer. A record of each such digital noiseburst is first written on magnetic tape and then read into a semiconductor memory that is part of the laboratory electronic equipment. Under control of a digital timing system, the digital data residing in the memory is transmitted sequentially at high speed to a digital-to-analog converter unit. The resulting signal at the output of the digital-to-analog converter unit is, after low-pass filtering, a time-varying voltage that duplicates the waveform of the noiseburst originally generated by the computer.

The output signal of the digital-to-analog converter unit is supplied to the Type F36 source and the pressure signal that is radiated by the source as a result of this excitation is measured with a small hydrophone. The noiseburst signal at the output of the measuring hydrophone is then converted to digital form by a transient recorder and written on punched paper tape. The output of the laboratory system is digital paper-tape data records of this kind. These records are supplied to the computer and used to calculate the input-output crosscorrelation functions that define the spatial impulse response function of the Type F36 transducer.

Once the acoustic-measurement system was in operation, it was found that two important experimental problems had to be dealt with. The first of these problems concerns accounting for the fact that the Type F36 transducer is not the ideal line source for which the theoretical analysis is developed. The theoretical line source considered has a vanishingly small extension in all directions normal to its length. It is also considered to be excited so as to produce a uniform particle

velocity everywhere on its surface, which has a time-variation that is given by a δ-function. In contrast to this situation, the Type F36 source consists of an array of seven endcapped ferroelectric shells of finite diameter and is excited by applying an electrical signal, in the form of a noiseburst, to it. Consequently, it is necessary to devise a means to separate the purely geometrical effects, i.e., those characterized by the source's spatial impulse response function, from those effects introduced by the electromechanical behavior of the Type F36 when it is excited by a broadband noiseburst.

Theoretical analysis of an equivalent-circuit representation of a ferroelectric vibrating shell and preliminary experimental results showed that two procedures are necessary in order to remove the effects of the Type F36 transducer's electromechanical behavior from the measured input-output crosscorrelation functions. First, before pseudorandom noiseburst voltages are applied to the input of the Type F36, they must be passed through a low-pass filter network that has a transfer characteristic with a very large slope above the high-frequency cutoff. This type of input-signal filtering is necessary in order to prevent excitation of a multitude of high-frequency electromechanical resonances within the Type F36. Second, for constant-voltage excitation of the input of the Type F36 source, at frequencies well below the first electromechanical resonance of one of the ferroelectric shells comprising the array in Type F36, it is necessary to filter the measured input-output crosscorrelation functions in order to account for the mechanical compliance of the ferroelectric shells. It is shown that this can be done by convolving the measured input-output crosscorrelation functions with a unit step function, which is chosen so as to have a step-height such that the mean-squared value of each correlation function is the same after convolution as it is before.

The second important experimental problem that must be dealt with concerns the fact that the input-output correlation experiments are performed using bursts of pseudorandom noise, which are bandlimited signals

of finite duration and are not the ideal continuous white-noise signals considered in the theory upon which the experimental design is based. Moreover, all experimental signals must be represented in the computer in sampled form. Also, the maximum duration of the experimental noisebursts is dictated by the size of the water tank in which experiments are performed. Under no circumstances can this duration be made much greater than 4 ms for the tank used, and for most experimental geometries it is less than 3 ms. A straightforward analysis shows that, from the input-output correlation function of sampled, pseudorandom noisebursts, one can obtain an estimate of the input-output crosscorrelation function that would have been obtained, if the Type F36 had been excited by a continuous white-noise signal. However, both experiment and theory point out that the correlation function of a single pair of 3 ms or 4 ms noisebursts does not provide an adequate estimate of this input-output correlation function, owing to the short duration of the signal records. But this experimental difficulty can be circumvented. It is shown theoretically and confirmed experimentally that by averaging a number of the input-output cross-correlation functions, which are obtained using the short experimental noisebursts, one can obtain an input-output correlation function that is equivalent to the function that would have been obtained if arbitrarily long samples of continuous input and output signals had been cross-correlated. This is a consequence of the fact that the pseudorandom noisebursts, which are used as input signals in the experiments, simulate samples of an ergodic stochastic process. That many short noisebursts may be used to obtain the equivalent of an arbitrarily long noise record is a significant result, since it demonstrates that one can conduct acoustical experiments in a water tank, even though those experiments require noise-signal record lengths much longer than the maximum duration of the pulses that are compatible with the size of the tank.

Experimental Results

A small hydrophone measures the radiated field of the Type F36 source at 29 angular positions, all of which are at a distance of 1.3 m

from the source's center. Orientations of the measuring hydrophone with respect to the Type F36 line transducer are specified by the angle ϕ. When ϕ is equal to 180° or to 0°, the hydrophone is located on the longitudinal axis of the Type F36, while when ϕ is equal to 270° or to 90°, the hydrophone is broadside to the source. At each angular position ϕ, the Type F36 is excited with a set of eight pseudorandom noisebursts. Each exciting noiseburst has a 2.8 ms duration. A spatial-impulse-response-function waveform is computed from the eight input-output correlation functions obtained for each angular position. Representative experimental spatial-impulse-response-function waveforms are reported and discussed.

Before the experimental spatial-impulse-response-function waveforms can be compared to those theoretically predicted, it is necessary to obtain a value for the equivalent length of the Type F36 source. This value cannot be obtained from a knowledge of the internal structure of the Type F36, but rather must be obtained by experiment. The equivalent length of the Type F36 source is determined by measuring the angular positions of nulls in the directional response patterns that are obtained when the Type F36 is excited by tonebursts at each of six different frequencies. A modification of the experimental apparatus is necessary in order to be able to generate the various tonebursts required in these measurements.

Once the equivalent length of the Type F36 is determined, its value is used in the analytical expressions that are obtained from the theoretical development. A computer is then used to construct theoretical spatial-impulse-response-function waveforms. These are compared to the corresponding experimental waveforms that are observed at a number of different angular orientations of the source and receiver. A comparison of the theoretical and experimental waveforms for $\phi = 230°$ and for $\phi = 120°$ is shown in Fig. P1. The agreement between the theoretical predictions and the experimental results is seen to be excellent in these two examples in spite of the quite different shape spatial-impulse-

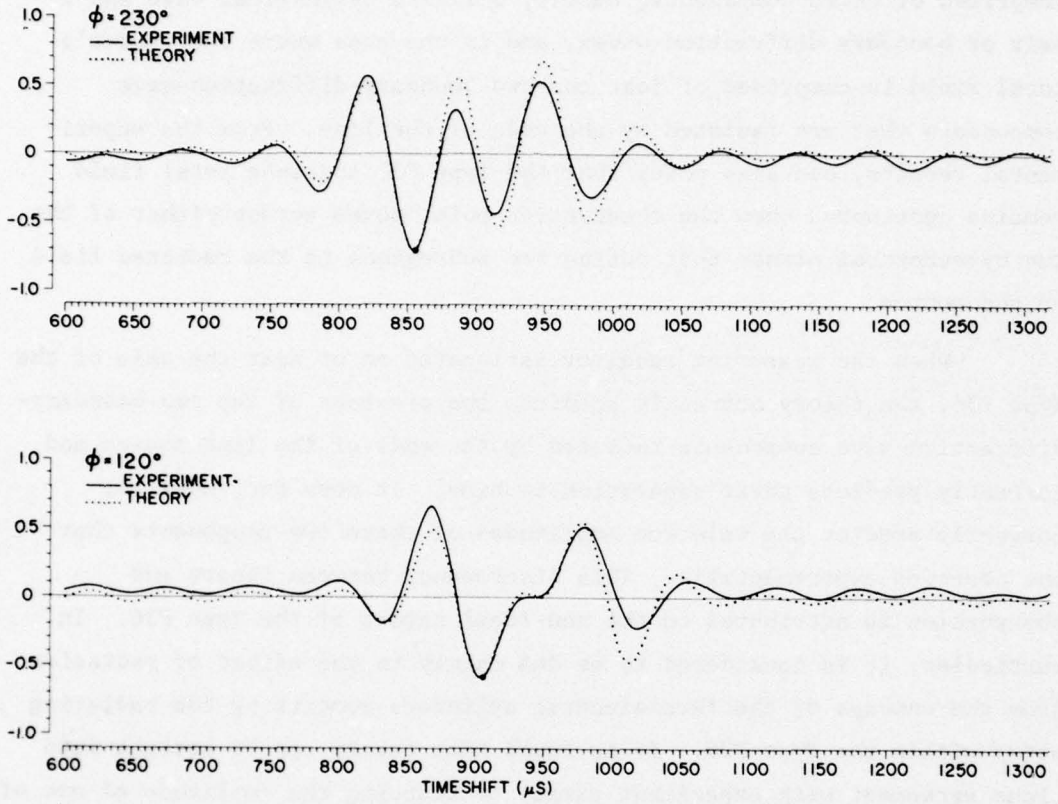

Fig. P1--A comparison of theoretical and experimental spatial-impulse-response-function waveforms

response-function waveform in each of the two cases. Likewise, at angular orientations for which the measuring receiver is not on or near the longitudinal axis of the Type F36, the agreement between the theoretical and the experimental spatial-impulse-response-function waveforms is excellent in all of the other cases examined. In particular, it is found that the theoretical and experimental waveforms are in close agreement both inside the subregion defined by the two hypothetical planes passing through the ends of the line and in the two symmetric subregions outside these two planes. That is, the theoretical and experimental waveforms agree both in the case where the total field of the Type F36 source is

comprised of three components, namely, a finite cylindrical wave and a pair of boundary diffraction waves, and in the case where the source's total field is comprised of just the two boundary-diffraction-wave components that are radiated by the ends of the line. From the experimental results, one also notes that the Type F36 source's total field remains continuous when the observation point moves across either of the two hypothetical planes that define the subregions in the radiated field of the source.

When the measuring receiver is located on or near the axis of the Type F36, the theory correctly predicts the presence of the two boundary-diffraction-wave components radiated by the ends of the line source and correctly predicts their separation in time. It does not, however, correctly predict the relative amplitudes of these two components that one observes experimentally. This discrepancy between theory and observation is attributed to the non-ideal nature of the Type F36. In particular, it is considered to be due mainly to the effect of radiation from the endcaps of the ferroelectric cylinders comprising the radiating array within the Type F36. It is found that theory can be brought into close agreement with experiment simply by reducing the amplitude of one of the boundary-diffraction-wave components used to construct the theoretical spatial-impulse-response-function waveforms in cases of axial or near-axial source and receiver orientations. The fact that the discrepancy between the theoretical and the experimental waveforms can be removed by such a simple expedient lends support to the ideas embodied in the Rubinowicz-Maggi theory, rather than casts doubt upon them, for one notes that it is possible to modify the Rubinowicz-Maggi theory to account for the non-ideal nature of the line source that is used in the experiments. This modification can be effected only because it is possible to decompose the radiated field of the source into the components predicted on the basis of the Rubinowicz-Maggi theory. If, on the other hand, one had a theoretical spatial-impulse-response-function waveform of the line source that was constructed on the basis of the conventional radiation theory,

which contains no hint of the composite nature of the source's total field, it would have been impossible to perceive how to make the correct modification of the theoretical waveform in order to bring it into agreement with observation.

Minor departures of experimental results from the results expected theoretically also occur. Their causes are discussed and some errors inherent in the measurement system are evaluated. It is found that in some particular instances it is fortuitous that small experimental errors are present, since these perturb the symmetry inherent in the experiments. This perturbation makes it possible to describe the behavior of the Type F36 source's spatial-impulse-response-function waveform in regions of angular orientation where large changes in the shape of the waveform result from small changes in the angle ϕ.

Summary of the Contributions of this Research

The research reported here makes three major and six secondary contributions to present knowledge. The three major contributions are as follows. First, the Rubinowicz-Maggi formulation of diffraction theory is verified by the experiments reported here. Not only does this dissertation report the first quantitative comparison of the Rubinowicz-Maggi theory with the results of acoustic-radiation experiments, but if one includes experiments in optical diffraction as well, the research here provides one of the few existing experimental investigations of the phenomena predicted by the Rubinowicz-Maggi theory. The reported experiments confirm the existence of geometrical and boundary diffraction waves in the radiated field of a line source. These field components are found experimentally to have the characteristics that are expected on the basis of the theory.

The second major contribution of this research is the development of a new theoretical expression for the field of an acoustic line source of finite length. This result is an exact expression describing the time-domain behavior of the finite line source's pressure field everywhere--

both in the source's nearfield and farfield regions. The new result reported here is potentially useful in analyzing a variety of general problems in acoustic-radiation theory.

Design and development of the unique experimental system described in this dissertation is the third major contribution of this research. The waveform-generating equipment in the electronic system, which is used in the experiments to produce pseudorandom noisebursts and tonebursts of variable frequency, can, in fact, be used to produce, in real time, any waveform that can be generated in digital form by the computer. A second unique feature of this measurement system is its ability to digitize electrical signals, under digital control, and to record these signals directly in a form that is suitable for computer processing. A third unique feature of the experimental system is the digital timebase that permits all subunits of the system to operate in complete synchronism under the control of a single master clock. Coupled with the accurate positioning apparatus that was used in the experimental arrangement, the electronic system described in this dissertation made it possible to conduct laboratory acoustic-radiation experiments with a degree of precision greater than that which is generally attained elsewhere.

The six secondary contributions of the research reported here are as follows. First, since the Type F36 source is a transducer presently in widespread use in underwater acoustics, the research shows that the concepts of the Rubinowicz-Maggi theory are of practical, rather than of purely theoretical, significance. Just as these concepts are used here to analyze the radiated field of the Type F36, they may likewise be used in understanding the phenomena occurring in other practical problems involving acoustic radiation, reception, or scattering. Second, it is shown both theoretically and experimentally that the equivalent of very long noise-signal records can be obtained by combining the results produced by a number of much shorter signal records. This means that experiments that require long records of noise signals can be performed in a confined volume of water--a tank or lake--where the boundaries of

the water volume limit the length of the signal record with which one can work. Third, Schoch's analysis has been carried out, for the first time, for the general case of a planar piston defined by a convex boundary curve. The result is a new asymptotic expression for the field of such a piston that is far more general than the results that have been reported previously. Fourth, a new experimental method for generating tonebursts has been devised. Since tonebursts are widely used as acoustic test signals, this method should be of interest to other experimenters. Fifth, a new technique for representing sampled records of impulse functions has been devised that is based upon Lagrangian interpolation formulas. This method should have more general applicability, for example, in certain problems associated with the representation of complex signals and their spectra by means of the fast-Fourier transform. Sixth and finally, a codification and analysis of the historical development of the Rubinowicz-Maggi theory is presented. This is useful, not just from a cultural standpoint, but also for the insight it gives one into the physical bases of radiation, diffraction, and scattering phenomena. This insight is vital if knowledge is to be extended beyond those areas that can be dealt with using only the conventional theories of the present time.

Preview

The development of the physical concepts embodied in the Rubinowicz-Maggi formulation of diffraction theory is traced in Chapter I of this dissertation. In Chapter II, the notion of the spatial impulse response of an acoustic radiator is introduced by deriving a time-domain expression for the field of a planar source using the conventional approach to radiation theory. Schoch's analysis of the radiated field of a piston source, which he developed on the basis of the Rubinowicz-Maggi diffraction theory, is discussed in the first part of Chapter III. In the second part of that chapter, the general integral expressions that result from Schoch's analysis are evaluated by the method of stationary phase and the new asymptotic formula for the spatial impulse response of a planar source is found. The theoretical development in Chapter IV results in the new

time-domain expression for the radiated field of a line source of finite length. The methodology behind the experimental determination of the spatial impulse response of an actual line transducer, by means of input-output cross-correlation measurements, is discussed in Chapter V, while the experimental equipment and techniques used to carry out such measurements are described in Chapter VI. The experimentally obtained spatial-impulse-response-function waveforms are reported in Chapter VII, and compared in this chapter to theoretical waveforms constructed on the basis of the analysis developed in Chapter IV.

INDEX OF TABLES

INDEX OF FIGURES

CHAPTER I

INTRODUCTION

The research reported here is a study of the acoustic field radiated by a line source of finite length. Although it might appear at first glance that the finite line source, as a radiator of sound, is so simple and so well-understood that any further effort to analyze its characteristics would be banal, this dissertation will demonstrate that, contrary to this appearance, the radiated field of the line source is a composite of several components, whose existence has, heretofore, been only vaguely suspected and whose characteristics have not been previously understood. In particular, an examination of the composite field radiated by a line source, enables one to experimentally detect the so-called "boundary diffraction waves" and to measure their characteristics, as well as to experimentally explore other physical phenomena associated with them. Indeed, as will be shown subsequently, the use the finite line source naturally suggests itself, when one is designing a definitive experiment to detect boundary diffraction waves. Prior to the work reported here, such a definitive experiment has not been done in acoustics.

It is the purpose of the research reported here to experimentally examine the consequences of the analysis that predicts the occurrence of boundary diffraction waves, in addition to other such component waves, in a radiated, a diffracted, or a scattered field. The corpus of analytic and experimental results describing radiated, diffracted, or scattered fields in terms of such component waves may be referred to as the Rubinowicz-Maggi theory. This theory originated from the study of optical diffraction phenomena, but it has, as will be shown by the work presented here, important ramifications in the theory of acoustic radiation. In order to introduce the requisite theory and to enable one

to place the present research in its proper context with respect to this theory, it is useful to begin the discussion with a historical account of the development of the Rubinowicz-Maggi theory and of the origin of certain other related results. Much of the historical information presented below can be found scattered throughout the technical references to be cited. In addition, one should refer to the historical paper by Rubinowicz [1] and to the books by Baker and Copson [2] and by Born and Wolf [3] for accounts of the background of the Rubinowicz-Maggi theory. Also the book by Mach [4] is useful for an account of the historical background of what can be called conventional diffraction theory. In the historical summary to follow, the emphasis will be placed upon the physical ideas involved in the Rubinowicz-Maggi theory and upon the phenomenological description of its significant features, rather than upon the analytic expression of the theory, except where it becomes necessary to introduce mathematical results in order to clarify the presentation.

The conceptual genesis of the boundary diffraction wave actually antedates the conventional formulation of diffraction theory. Grimaldi [5], in 1665, reported the first systematic experiments concerning the diffraction of light. Shortly thereafter, Newton repeated Grimaldi's experiments and, in addition, made a number of original observations of diffraction phenomena. In one of Newton's experiments, he observed the diffraction pattern that was caused by the edge of a knife when a narrow beam of sunlight fell upon it through a small aperture. When Newton viewed the light-diffracting knife-edge, with his eye in the region of the geometrical shadow of the knife, he observed [6] that the portion of the knife-edge illuminated by the sunlight appeared as a thin luminous line. In addition to this observation, Newton noted [7] that, when he moved his eye parallel to the knife-edge, the knife-edge still appeared bright, even when his eye was not directly behind the aperture through which the sunlight passed before falling upon the knife. Moreover, Newton also noted that the luminous line became finer as he moved his

eye farther into the shadow region [8].

In Newton's diffraction experiment, the knife-edge appeared as a source of light. This line source radiated into the region of the knife's geometrical shadow and, moreover, appeared to have directional properties. According to the Rubinowicz-Maggi theory, the diffraction pattern of a semi-infinite screen (Newton's knife-edge), in the region of the screen's geometrical shadow, results from a boundary diffraction wave radiated by the screen's edge, while outside of the geometrical shadow, the screen's diffraction pattern is caused by the interference between this boundary diffraction wave and the incident light that by-passes the screen. Moreover, the boundary diffraction wave in the Rubinowicz-Maggi theory possesses directional properties, since it gives rise to the observed diffraction pattern both within and outside of the region of the screen's geometrical shadow. Newton's observations of the luminous knife-edge thus constitute the first evidence of boundary-diffraction-wave phenomena.

Young commenced his study of optics in 1799. Since Young had command of a considerable knowledge of acoustics, he was able to apply the then conjectural hypothesis, that light is a wave phenomenon, to explain in a straightforward fashion many of the earlier observations that resulted from interference and diffraction experiments. Young's wave-theoretical model of the half-plane diffraction problem evolved between 1799 and 1804. Young maintained that the diffraction pattern, produced by a semi-infinite screen, resulted from interference between those light waves in the incident beam that passed far from the edge of the screen, and which, consequently, were little influenced by it, and those light waves that passed so near the edge of screen that their course was altered. Diffraction, i.e., interference, fringes would thereby be produced, owing to the different paths traversed by the deviated and undeviated waves. The deviation, or as Young called it "inflection", of waves by the screen's edge was first thought by Young to be due a refraction-like effect [9]. The screen, being composed of

ponderable matter, was conceived by Young to influence the medium of propagation of the light waves (i.e., the "aether"). This influence of the screen was thought to depend on some power of the distance. Thus, Young believed that the properties of the aether in the vicinity of the edge of screen were altered to a greater degree than they were far from the screen. Consequently, the waves passing near the screen would suffer a greater deviation and, hence, would travel over a greater distance than would the practically undeviated waves far from the screen. Owing to the resulting phase difference at the observation point, the deviated and undeviated waves would produce, by interference, the bright and dark fringes in the diffraction pattern.

In formulating his model of diffraction by a semi-infinite screen, Young also included waves, which after deviation by the aetherial medium were, supposedly, then reflected from the edge of the diffracting screen [10,11]. However, until 1803, Young apparently retained the notion that a change in the properties of the aether, induced by the presence of the screen, was the primary cause that produced deviation of the waves that pass near the screen's edge. He viewed the role of reflection at the edge of the screen as secondary. But after Young conducted a series of diffraction experiments, which were reported late in 1803, he abandoned his view that diffraction phenomena resulted from a variation in the properties of the aether [12]. Young did not, however, abandon his conceptual picture in which he viewed the diffraction pattern of a semi-infinite screen as the result of an interference between undeviated waves in the incident light beam and waves that suffer a modification at the edge of the screen.

Young refers to this modification as a "reflection" of the waves by the edge of the screen, much like the reflection he had earlier viewed as a possible secondary contribution to the interference that produced a diffraction pattern. Now, however, this formerly secondary contribution became an essential element in Young's model of diffraction; the diffraction pattern resulted from interference between waves in the

incident light beam and waves reflected at the screen's edge [12,13]. It is clear that Young did not regard this reflection process, taking place at the edge of the screen, as being reflection of an ordinary sort. First, he was certainly familiar with the results of a diffraction experiment that had been performed by Hooke, even prior to Newton's investigations. Hooke had used the blade of a straight-razor [14] and had separately observed both the diffraction pattern produced by the sharp edge of the blade and that produced by its blunt side. There was found to be no difference in the diffraction patterns produced in the two cases. Since the sharp and blunt sides of the blade would reflect light much differently, one would certainly expect quite different diffraction patterns in the two instances, if one component in the blade's diffracted field were generated through an ordinary reflection process. Moreover, even if one could account for the diffraction pattern of a screen, in the region directly illuminated by the incident light, as the result of an interference taking place between this incident light and light undergoing an ordinary reflection process at the screen's edge, such an interference can hardly account for the diffraction fringes observed within the region of the screen's geometrical shadow where there is no incident light. Not only is there this difficulty, when attempting to explain the nature of the process taking place at the edge of the screen in terms of reflection, but one must account for Newton's observation that the illuminated part of screen's edge appears as a luminous line, even if the eye is placed deep in the region of the screen's geometrical shadow. Since, in an ordinary reflection of the incident light, it is required that the angles of reflection and incidence be equal, there is no way that light can be reflected deep into the region of the screen's geometrical shadow.

Although Young referred to the process taking place at the screen's edge as "reflection" he used the term somewhat vaguely, as if for want of a better word. He knew that light of low intensity could be found deep in the screen's geometrical shadow region [15], but he admitted

that he did not yet understand how it reached there from the diffracting edge. What Young did realize was that, in the directly illuminated region (i.e., the region outside of the screen's geometrical shadow), he could describe the results of his diffraction experiments very well in terms of an interference between light in the incident beam and light arriving at the observation point from the edge of the screen [16], even though the observed diffraction pattern did differ in certain instances from that expected on the basis of this model [17]. Subsequently, Young refined his model [18,19] and considered that the edge of the diffracting screen was a source of waves, which interfered with the incident wave in the directly illuminated region and which diverged from the screen's edge into the geometrical shadow region.

It is worth examining the development of Young's conceptions in detail, since his studies had led him to a rudimentary, but in many respects a fundamentally correct, model of diffraction phenomena. According to the Rubinowicz-Maggi theory, the diffraction by a semi-infinite plane would be described in just such a fashion. However, while this modern model of the diffraction process is much like that conceived by Young, there is one important difference. The wave from the screen boundary envisioned by Young was simple. In the illuminated region, where it interfered with the incident light, Young regarded it as a uniform cylindrical wave. However, according to the Rubinowicz-Maggi theory, the boundary diffraction wave, as it will be seen subsequently, not only has directional properties, but, in the region of the geometrical shadow, it has a phase opposite to that which it possesses in the illuminated region. Had Young been able to attribute proper directional and phase characteristics to his boundary wave, he could have correctly described the several observations that called his theory into question. Fresnel pointed out that there were serious problems with Young's diffraction model. Since the knowledge of diffraction then available to Young was not sufficient to allow him to refute Fresnel's arguments, Young's theory of diffraction came to be

regarded as incorrect.

Fresnel's early view of diffraction phenomena was quite similar to that of Young, but he was led to reject this view as a result of a series of careful experiments. Fresnel studied the diffraction patterns produced by a slit. In his initial investigations, Fresnel found that he could describe the diffraction pattern of a slit, at least to a good approximation, by using the model of Young. Since a slit possesses two edges, the interference effects of three component waves, one wave from each edge and the wave owing to the incident light, must actually be accounted for in this situation, when one adopts Young's viewpoint. However, if Fresnel attributed the diffraction pattern observed in different regions to the interference of different pairs of these component waves, then the appearance of the fringe system in the diffraction pattern of the slit could be explained reasonably well, save for two of its features. First, as Young had earlier noted [17], some of the observed diffraction fringes were displaced from the positions predicted for them on the basis of the interference model. Second, in explaining the fringe system using the model of Young, it was necessary for Fresnel to assume that a component wave from the boundary of the slit started out with a phase opposite to that of the wave characterizing the incident light. If this was not done, and the interference between waves was calculated only on the basis of path differences, Young's model predicted intensity maxima where minima should lie in the diffraction pattern and vice versa. Young apparently knew [16] of the necessity for introducing a phase change of π into his boundary wave, but never attempted explain its introduction on a physical basis.

Fresnel tested by experiment the hypothesis that it is the interference between pairs of waves which gives rise to the observed diffraction pattern of a slit. He reasoned that, if the diffraction pattern in a certain region is produced by the interference of a particular pair of waves, then it should be possible to modify one part of the

diffraction pattern, and at the same time leave another part unaltered, by changing the conditions of diffraction at a single edge of the slit. However, when Fresnel displaced one edge of the slit and left the other edge fixed, he noted that the entire diffraction pattern changed. From this experiment, Fresnel concluded that it is the mutual interference of all the light passing through the slit that gives rise to the diffraction pattern observed at each point, and not the interference produced by the type of waves described by Young.

Fresnel went on to put his own new conception of diffraction on a mathematical basis. In his analytical formulation, he adopted the view of Huygens and regarded the incident light wave as arising from the mutual interference of an ensemble of elementary waves (Huygens' wavelets), to each of which Fresnel attributed directionality by means of an obliquity factor. By considering that a slit, or any diffracting aperture, deletes certain of these wavelets from the incident light, Fresnel was able to explain how the resulting diffraction pattern, produced by that aperture, can be regarded as the mutual interference pattern owing to the remaining wavelets. Most damaging to Young's diffraction model was the fact that the predictions of Fresnel's theory were much more closely in agreement with experiment than were those predications made on the basis of Young's ideas. Thus, Fresnel could calculate the positions of all the bright and dark fringes observed in the diffraction pattern of a slit, while Young's theory gave incorrect results for some fringe positions. Moreover, in Fresnel's model, there was no need to introduce an unexplainable phase shift of π into the interference process in order to obtain diffraction maxima and minima in their correct positions.

On the basis of Fresnel's theory, in which conventional optical diffraction theory has its origin, Fresnel and others who followed him were able to simply and accurately predict the diffraction effects observed in a wide variety of experiments. To be sure, certain questions concerning Fresnel's theory arose during its early years, such as that of the physical basis of the obliquity factor and that of the origin of

certain phase shifts that one was required to introduce into the Huygens' wavelets in order to formulate an incident field correctly. However, all these questions concerning the otherwise completely successful theory appeared to be satisfactorily answered when Kirchhoff, in 1882, formulated Fresnel's ideas in terms of a scalar field described by a wave equation.

Even Young, who corresponded with Fresnel, came to regard the latter's theory as superior to his own. However, it would be well at this juncture to take a second look at the experiment that led Fresnel to reject Young's conceptual picture of diffraction phenomena. Fresnel considered that the diffracted field of the slit at any observation point must arise from the interference of a pair of component waves, if one adopts the view of Young. Thus, according to Fresnel's interpretation of Young's model [20], in the slit's directly illuminated region, there will be two regions in which one boundary wave or the other interferes with the incident wave. These regions will be symmetrically disposed about the center of the slit. There will also be a region near the center of the diffraction pattern where, presumably, the boundary waves interfere with each other, but not with the incident wave. It was perhaps quite reasonable for Fresnel to believe that the critical test of Young's diffraction model involved the idea that the diffracted field of the slit arose from the interference of particular pairs of waves, since the observed features of the slit's diffraction pattern could be explained fairly accurately in terms of such interferences. However, if there are two boundary waves originating at the slit's edges, in addition to the incident wave, it is hard to see why one should not consider that the diffracted field at any observation point results from the mutual interference all three of the component waves, rather than from one particular pair of these waves. If the diffracted field at every observation point arises from the interference of all three component waves, then varying the diffraction conditions at one slit edge by moving that edge alone, as Fresnel did in his experiment, will cause the diffraction pattern of the slit to be altered everywhere, which is

exactly the effect Fresnel observed. Thus, it must be emphasized that the result of Fresnel's experiment does not contradict the basic concept of Young's diffraction model, if one conceives that the diffraction pattern arises from the mutual interference of three component waves, rather than from the interference of two such waves, which was the hypothesis of Fresnel and, apparently, also of Young.

With Kirchhoff's analytical formulation of the ideas of Fresnel, the conventional diffraction theory of scalar waves took on the basic form it retains to this day. After the establishment of Fresnel's concept of diffraction, Young's earlier ideas passed into eclipse for many years, but were neither totally forgotten nor entirely discarded. In 1886, Gouy [21,22] reported the results of experiments in which he studied the diffraction of light by a semi-infinite metal screen, but took into consideration the polarization of the incident light, the material from which the screen was fabricated, and the shape of the screen's diffracting edge. Gouy discovered, or one should say re-discovered, since Newton's prior observations seem to have been forgotten [22], that the edge of the diffracting screen appeared as a luminous line. Gouy, like Young, considered the edge to act as a source that radiates diffracted light into both the directly illuminated region and the region of the screen's geometrical shadow. When Gouy examined the diffracted light, he noted that its color and its state of polarization depended, not only upon the state of polarization of the incident light, but also very strongly upon the material from which the screen was made and the extent to which the screen's diffracting edge was rounded when it was fabricated. Kirchhoff's scalar-wave theory of diffraction could certainly not be expected to account for the observed polarization and color effects in the diffracted light [23]. To understand such effects, the electromagnetic theory of light is required. However, Gouy's work, and subsequent work along the same lines by Wien [24], led Maey to examine the question of whether the phenomenon of the semi-infinite screen's luminous edge could be understood on the basis of Kirchhoff's

scalar-wave diffraction theory, or whether electromagnetic theory was needed to explain it.

Maey [25] reported in 1893 that, indeed, one could use the scalar-wave diffraction theory and derive as a consequence that the edge of a semi-infinite screen should act as a light source. Maey also recognized that a number of the results of his rather recondite mathematical analysis could readily be interpreted in terms of the diffraction model of Young. Maey was able to express the total scalar field, in the region directly illuminated by the incident light, in terms of an interference between the incident wave and a secondary wave. In the directly illuminated region, this secondary wave was found to have an amplitude equal to that of the incident wave, but a phase angle differing from the incident wave by π . It will be recalled that Young had to introduce just such a phase difference in order to account for the observed positions of maxima and minima in the diffraction patterns he observed. Also, Maey concluded that the secondary wave exhibited opposite phases, when observed on either side of the boundary plane defining the screen's geometrical shadow region. Moreover, this secondary wave appeared to possess other complex phase characteristics, both within and outside the screen's geometrical shadow region. It thus had far more complex properties than those of the simple cylindrical boundary wave that Young invoked when using his model to explain the diffraction pattern of a semi-infinite screen.

Maey tried to understand the consequences of the Kirchhoff theory in the problem of light diffraction by a semi-infinite screen in order to be able to separate the purely geometrical effects of diffraction from those effects dependent on the electromagnetic properties of light and of the diffracting screen. Shortly afterward, Sommerfeld [26] published his profound and fundamental theoretical paper on diffraction of light by an infinitely thin, perfectly conducting half-plane. As is well known, Sommerfeld was able to solve exactly the boundary-value problem for the electromagnetic field described by Maxwell's equations. What is pertinent

to the discussion here, is the fact that Sommerfeld's exact theoretical solution is readily interpreted in terms of a diffraction model like that of Young.

Consider the case in which an E-polarized monochromatic plane wave

$$E_z^{(i)} = Ae^{jkr\cos(\theta - \alpha)} \tag{1}$$

is the incident upon the perfectly conducting half-plane that is depicted in Fig. 1. As shown in Fig. 1, the wave normal of the plane wave, which

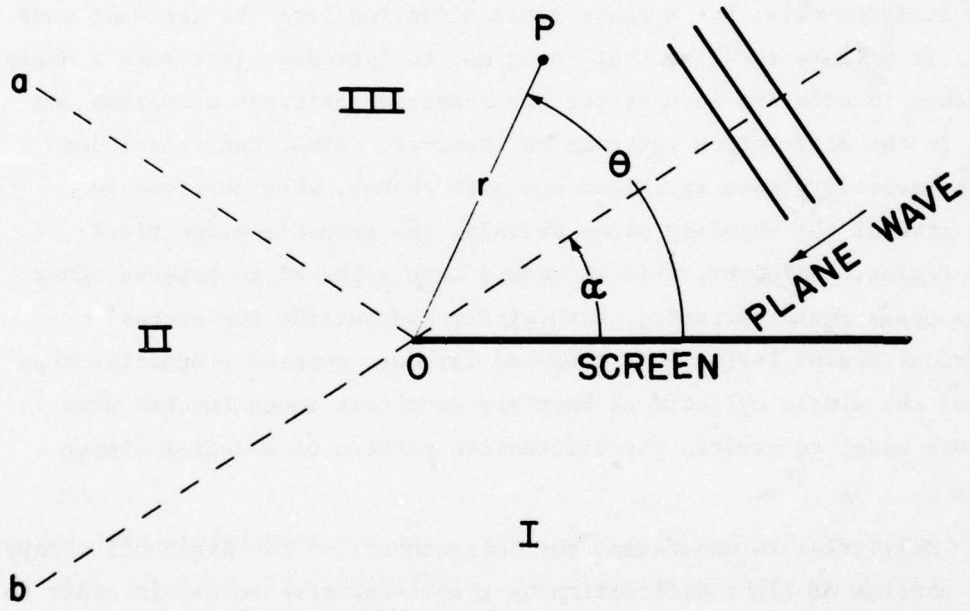

Fig. 1--Diffraction by a semi-infinite plane screen

specifies its direction of incidence, is at the angle α with respect to the half-plane. The edge of the half-plane is coincident with the z-axis of a cylindrical coordinate system. In this coordinate system, an

observation point P may be located by the polar coordinates r and θ. The quantity k is the wavenumber of the incident wave and A is its amplitude. The electric vector of the wave points in the direction of the z-axis. That is, this vector is parallel to the edge of the screen. The total field may be expressed [27] as

$$E_z = E_z^{(g)} + E_z^{(d)}, \tag{2}$$

in which $E_z^{(g)}$ is a geometrical field given by the expression

$$E_z^{(g)} = \begin{cases} Ae^{jkr\cos(\theta - \alpha)} - Ae^{jkr\cos(\theta + \alpha)}, & 0 \le \theta < \pi - \alpha \\ Ae^{jkr\cos(\theta - \alpha)}, & \pi - \alpha < \theta < \pi + \alpha \\ 0, & \pi + \alpha < \theta \le 2\pi \end{cases} \tag{3}$$

and $E_z^{(d)}$ is a diffraction field. From Eq. (3) and Fig. 1, it is seen that the geometrical field is the sum of the incident field and a specularly reflected field in region III, where $0 \le \theta < \pi - \alpha$. Region III is defined by the screen and by plane Oa in Fig. 1. On the other hand, in the directly illuminated region II, between the planes Oa and Ob, the geometrical field is due to the incident wave alone. Region I, the geometrical shadow region, lies between plane Ob and the screen. In the shadow region, $\pi + \alpha < \theta \le 2\pi$. Here the geometrical wave vanishes. Note that the geometrical wavefield, given by Eq. (3), changes discontinuously when the observation point passes from one region to another.

If kr is large, that is, if P is many wavelengths from the edge of the screen, the diffraction field may be expressed

$$E_z^{(d)} \sim A(\tfrac{1}{2}\pi kr)^{-\frac{1}{2}} e^{-j(kr + \frac{\pi}{4})} \left\{ \frac{\sin(\frac{1}{2}\theta)\sin(\frac{1}{2}\alpha)}{\cos\theta + \cos\alpha} \right\} \tag{4}$$

This asymptotic expression for the diffraction field is valid everywhere, except in the vicinity of the boundary planes Oa and Ob. Equation (4) shows that the diffraction field has the form of a directional cylindrical wave that emanates from the edge of the screen. Since the diffracting screen in the Sommerfeld problem is a perfect conductor, it is also perfectly reflecting. This is in contrast to the nature of the diffracting screens usually considered in the scalar-wave theory. In scalar-wave diffraction theory, the screens considered are perfectly absorbing, i.e., "black", in which case, there is no contribution to the diffraction pattern owing to the light falling on the side of the screen facing the incoming light wave. The cylindrical wave from the edge of the screen, which is expressed by Eq. (4), contains such a bright-side component in addition to the pure-diffraction component that would appear if the diffracting screen were perfectly black. The bright-side and pure-diffraction components can be separated by expressing Eq. (4) in the form

$$E_z^{(d)} \sim A(8\pi kr)^{-\frac{1}{2}} e^{-j(kr + \frac{\pi}{4})} \left\{ \frac{1}{\cos[\frac{1}{2}(\theta + \alpha)]} - \frac{1}{\cos[\frac{1}{2}(\theta - \alpha)]} \right\}. \quad (5)$$

The first term within the braces of Eq. (5) is associated with the bright side of the screen [28], that is, with the "reflected" contribution to the cylindrical wave from the edge of the screen. The second term within the braces, the term containing the factor $\cos[\frac{1}{2}(\theta - \alpha)]$ in its denominator, is the pure-diffraction component, like that which would be present in the case of diffraction by a black screen. Note that in region II this pure-diffraction component has a sign opposite to that of the incident wave. Consequently, the diffracted component interferes destructively with the incident wave there, just as the boundary wave does in the model of Young. Moreover, in region I, the region the screen's geometrical shadow, this pure-diffraction component has a sign opposite to that which it has in the directly illuminated region, that is, which it has in region II. Thus, this pure-diffraction component changes signs when one crosses the plane Ob that delineates the screen's geometrical

shadow. Whether or not the field owing to this diffraction component changes discontinuously at the shadow-boundary plane Ob cannot be deduced from Eq. (5), since the asymptotic formula is not valid in the vicinity of this plane. It might be mentioned, incidentally, that, if the magnetic vector **H**, rather than the electric vector **E**, of the incident plane wave were parallel to the edge of the diffracting screen, results very similar to those expressed by Eqs. (2) through (5) would be obtained. Sommerfeld's exact theory of the diffracting half-plane thus predicts a diffracted wave emanating from the edge of the screen, which interferes with the incident wave in the illuminated region and which radiates into the screen's geometrical shadow region. If the same objections to this model are raised that were raised to the model of Young, they are readily refuted [29] by taking into account the directional and phase properties of the wave emanating from the screen's boundary. Nevertheless, in spite of the fact that the solution of Sommerfeld analytically yields up an expression for a wave originating at the boundary of a diffracting screen, many investigators [30], including Sommerfeld himself [31], do not regard this wave as being physically real. This view persists to the present day.

Rubinowicz [32] made a fundamental contribution to the theory of the boundary diffraction wave when, in 1917, he reformulated the scalar-wave diffraction theory of Kirchhoff. In Kirchhoff's formulation of diffraction theory, which follows from the original conceptions of Fresnel, one is concerned with calculating two-dimensional integrals. Such integrals sum up the contributions at the observation point of all the Huygens' wavelets that are not blocked by the diffracting screen. Thus, such integrations are taken over the surface of the diffracting aperture. Rubinowicz showed that the total field in a diffraction problem could be decomposed into the sum of a primary field and a diffracted field. The primary field in Rubinowicz's theory is geometric in nature. On the side of the diffracting screen opposite the light source, this primary field is the same as the field of the incident wave,

if one observes it in the directly illuminated region. On the other hand, the primary field is zero, if one observes it in the geometrical shadow region of the screen. This primary field, like the geometrical field expressed by Eq. (3), is thus discontinuous across the surface delineating the shadow boundary.

Rubinowicz's formulation of the diffracted field is extremely significant. Rubinowicz showed that the diffracted field could be expressed as a line integral taken along the boundary of the diffracting aperture, rather than as a surface integral over the aperture itself. Thus, in the formulation of Rubinowicz, the diffracted field truly arises at the edge of the diffracting aperture. In this formulation of diffraction theory, as in the early diffraction model of Young, a wave emanates from the edge of the diffracting aperture. In the directly illuminated region, this boundary diffraction wave interferes with the primary wave to produce the diffraction pattern there. In the screen's geometrical shadow region, where the primary wave is not present, the boundary diffraction wave alone gives rise the observed diffraction pattern of the aperture. The field of the boundary diffraction wave changes discontinuously across the surface delineating the geometrical shadow region, but in such a way that the total field, which is the sum of the primary wave field of the boundary diffraction wave, remains continuous everywhere. Such a continuity of the total field requires that the field of the boundary diffraction wave have a phase opposite to that of the primary wave in the directly illuminated region and suffer a phase change of π when the shadow boundary is crossed. Moreover, the boundary diffraction wave has, in addition to such unique phase characteristics, definite directional properties. Thus, in contrast to the simple boundary wave envisioned by Young, the Rubinowicz boundary diffraction wave is capable of accounting for the observed features of a diffraction pattern as faithfully as they can be accounted for in the Fresnel-Kirchhoff model. Indeed, this must be the case, since the Rubinowicz and the Fresnel-Kirchhoff models of diffraction are two

different analytical formulations describing the same physical phenomena.

It is important to note that the basic properties of the boundary diffraction wave deduced by Rubinowicz, as well as some of those properties deduced even earlier by Maey on the basis of scalar-wave diffraction theory, are quite like the properties of the pure-diffraction wave that appears to originate at the edge of the diffracting half-plane in the problem that Sommerfeld solved exactly. Rubinowicz's decomposition of the total field in a diffraction problem into a geometrical field and a diffracted field and his expression of the diffracted field as a line integral along the edge of the diffracting aperture thus appears to provide a description, in terms of scalar-wave theory, of those diffraction phenomena that are not strongly dependent upon the electromagnetic properties of the screen. One must note that even before Sommerfeld solved the half-plane problem, Maggi [33], using the scalar-wave theory of Kirchhoff, showed that the total field in a diffraction problem could be decomposed into the sum of a geometrical and a diffracted field, thus anticipating this aspect of the later work of Rubinowicz. However, Maggi apparently did not express his diffracted field as a line integral taken along the edge of the diffracting aperture as did Rubinowicz, and, therefore, did not necessarily associate the diffracted component with the edge of the aperture. Maggi's work lay in obscurity until Kottler [34] rediscovered it in 1923 and showed that one could transform Maggi's diffraction component into the line-integral form of Rubinowicz. It is for this reason that the name of Maggi is usually associated with the theory of the boundary diffraction wave.

In 1924 Rubinowicz [38] examined some further consequences of his reformulation of scalar-wave diffraction theory. If the Rubinowicz-Maggi theory is applied to the problem of light diffraction by apertures in plane screens, additional boundary-diffraction-wave phenomena become manifest. The field of the boundary diffraction wave in the case of a diffracting aperture is given by an integral along the edge of the aperture, but all points on the aperture boundary are not equally

effective contributors to the diffracted field at an observation point. Suppose one considers all possible optical paths, which connect the source point of the incident light wave with the observation point and which pass through points on the boundary of the aperture. One then finds that it is those boundary points for which the length of such paths assumes an extremum value that determine the diffracted-wave field at the observation point. Each such "active point" [36] on the boundary of the aperture, which defines an extremum of the path length, has surrounding it an "active region" that radiates light to the observation point. The contributions to the field at the observation point from the remainder of the aperture boundary may be considered to be negligible. For example, suppose light from a point source is diffracted by a circular aperture in a plane screen, with the source point situated on an axis perpendicular to the screen that passes through the center of the aperture. If one observes the aperture from a point not situated on the aforementioned axis, two bright spots will be seen on the edge of the aperture. The centers of these bright spots will be at opposite ends of a diameter of the aperture. Passing through the two aperture-boundary points defined by this diameter, will be two optical paths connecting the source and observation points; one of these paths will be maximum in length and the other will be minimum.

One can analytically demonstrate the existence of active points and active regions on the aperture boundary by evaluating the line integral, which expresses the field of the boundary diffraction wave, by an asymptotic technique, such as the method of stationary phase. If this is done, the only significant contributions to the value of the line integral come from neighborhoods of those points on the aperture boundary for which the length of the optical path connecting boundary points to the source and to the observation point takes on an extremum value. The physical interpretation of this result can be formulated in terms reminiscent of Fresnel's concept of the interference of Huygens' wavelets. One has, at the observation point, diffracted-field contributions

arriving from all parts of the aperture boundary. However, the phase of the contributions arriving at the observation point from the various differential length elements of the aperture boundary is a rapidly varying quantity, except in the vicinity of active points. Consequently, all the contributions from the aperture boundary cancel one another by destructive interference, save for those arriving at the observation point from the active regions.

Additional theoretical details of the Rubinowicz-Maggi model of diffraction phenomena were elucidated in the 1930's. Rubinowicz [37] examined the nature of the discontinuous phase change that occurs in the diffraction wave at the boundary of the geometrical shadow of a diffracting aperture. He also addressed the related question of the discontinuous phase change suffered by a spherical wave when it is brought to a focus. In this problem, if one examines the wavefield near the focus, he finds that the phase of the diverging spherical wave on one side of the focal point is opposite that of the converging spherical wave on the other side. Bouwkamp [38] also considered this problem in 1940, but, while he adopted Rubinowicz's boundary-diffraction-wave concept, he criticized the introduction of discontinuous phase changes by Rubinowicz.

From the foregoing chronology, it is seen that the theoretical concept of the boundary diffraction wave grew out of the accumulated experience with optical diffraction phenomena in the period stretching from Newton's investigations, which were made in about 1665, to the year 1940. After Young's initial efforts, the most significant theoretical advances came as a result of Sommerfeld's 1896 paper and Rubinowicz's paper of 1917. Despite this long history, only a limited number of optical diffraction experiments appear to have been conducted, which have a direct bearing upon the diffraction model resulting from the Rubinowicz-Maggi theory.

Kalaschnikow [39] is reported to have experimentally proven, in 1912, that the diffraction wave, which is predicted on the basis

Sommerfeld's analysis, actually originates on the edge of the diffracting screen. To accomplish this, Kalaschnikow cast shadows of wires, which were placed in the field of the diffracted wave, upon a photographic plate. From the position of these shadows, he then deduced the place of origin of the diffracted wave.

In 1919, Banerji [40] experimentally investigated the formation of boundary diffraction waves at the edges of circular and polygonial apertures and slits. Banerji formed the image of the diffracting aperture using a dark-field optical system that excluded all direct light from the image by means of a properly placed stop. With this arrangement, Banerji could observe only the diffracted light coming from the edge of an aperture, even if he made the observation in the directly illuminated region of that aperture. When he observed the light coming from one edge of a slit, Banerji found that there was a very fine dark line at the center of the bright line that coincided with the slit edge. Although, Banerji was apparently unaware of the earlier work of Rubinowicz, he explained the cause of this phenomenon just as it would be explained on the basis of the Rubinowicz-Maggi diffraction model. That is, Banerji regarded each portion of the edge of an aperture as radiating beams of light in two different directions, with one beam on each side of the wave normal of the incident wave. Moreover, Banerji concluded that the light waves in the respective beams had opposite phases.

Banerji supported these conclusions with arguments based upon the results of Sommerfeld's analysis, much like those discussed above. Banerji also theoretically calculated the intensity distributions that he would expect to observe with his dark-field optical system, when using circular or rectangular apertures. These calculations, which were made using the conventional Kirchhoff diffraction theory, predicted the occurrence of the fine dark fringe at center of the luminous edge of a diffracting aperture just like those that Banerji actually observed.

Unfortunately, the diffraction images Banerji observed experimentally depended very much upon the size and shape of the stops used in

his optical system. For this reason, Banerji did not observe such phenomena as the radiation of light by active points on the edges of his diffracting apertures. Neither could his calculations lead him to suspect the existence of such phenomena, since these calculations included effects of the transmission characteristics of his optical system and these effects tended to obscure those effects due solely to the boundary diffraction wave. Nevertheless, Banerji's observations appear to provide the best direct experimental confirmation of the Rubinowicz-Maggi optical diffraction model, although there is one other noteworthy experimental result.

In 1922, Noack [41] also observed the dark line at the center of the luminous edge of a diffracting screen. Noack, too, used a dark-field optical system to exclude the effect of the incident light wave when observing the diffracted field, although his system differed from that of Banerji. However, Noack brought the images of the bright fringes on either side of the dark line together optically and observed the interference pattern that resulted. Noack then inserted a half-wave plate into the optical path of the light beam corresponding to one of the two bright fringes, and, thereby, retarded the light wave constituting this beam by a half-period. Noack was able to show from the change produced in the interference pattern that the waves from the two bright fringes must differ in phase by π in the absence of the half-wave plate. Thus, Noack confirmed experimentally that the phase of the boundary diffraction wave, in the geometrical shadow of a diffracting aperture, differs by π from the phase of this wave in the directly illuminated region.

The Rubinowicz-Maggi theory and the boundary-diffraction-wave concept did not enter the science of acoustics until 1941. In that year, Schoch [42] introduced a new expression describing the acoustic field radiated by a planar piston. Schoch's formulation, which was based on the ideas set forth by Rubinowicz, will be dealt with in detail in Chapter III of this dissertation. At this juncture, it is sufficient

to note that Schoch's analysis of the problem of radiation by a piston introduces into radiation theory, either explicitly or implicitly, all of the concepts that were previously discussed in connection with optical diffraction phenomena--boundary diffraction waves radiated by the edge of the piston, geometrical waves directly in front of the piston, active points and active regions on the piston's periphery, regions in the piston's radiated field that are analogous to the geometrical shadow region and to the directly illuminated region in the case of optical diffraction, discontinuous changes in the phases of radiation-field components, etc.

Knowledge of Schoch's analysis has become widespread. For example, Stenzel [43] used Schoch's integral, which expresses the radiated boundary diffraction wave, in constructing an exact solution to the problem of the radiating circular piston. Similarly, Carter and Williams [44] incorporated Schoch's formulation in their analysis of the radiated field of such piston. Also Kozina and Makarov [45,46] have analyzed the transient fields radiated by plane pistons of arbitrary shape, using Schoch's analytical results as a starting point. In addition, numerous references to Schoch's 1941 paper may be found scattered throughout the acoustical literature in many of the papers that treat the radiation fields of pistons or problems associated with transient radiation by acoustic sources. It also should be mentioned that, in studying light diffraction by a circular aperture, Ramachandran [47] developed expressions that are quite similar to those obtained by Schoch for the piston radiator. Also, in a 1951 paper by Chetayev [48], one may find an analytic representation of the radiated field of a piston that is the same as Schoch's.

There are few experimental investigations in acoustics that deal with boundary-diffraction-wave phenomena in any direct fashion. In 1941, Osterhammel [49] studied both the sound fields radiated by thin brass plates that were driven by vibrating quartz bars and the sound fields radiated by such bars themselves. All the vibrating quartz bars

Osterhammel used were long and thin and were cut from the mother crystal so that they vibrated in a thickness mode. Thus, Osterhammel investigated the acoustic radiation from vibrators that approximated rectangular pistons with faces that were very long in comparison with their widths. Osterhammel immersed these vibrators either in xylol or benzol and observed their radiated pressure fields optically by using a dark-field schlieren system. The long edge of the rectangular piston face was aligned, in each case, parallel to the direction of the collimated light beam, so that the short edge of the piston appeared in the optical image when the schlieren system viewed the sound field directly in front of the piston. The optical images of radiated sound fields thus obtained were photographed by Osterhammel and the positions of the bright and dark spots on the pictures were measured.

Osterhammel had earlier noted when observing sound fields optically, that a long, thin rectangular piston produces an essentially two-dimensional sound field in the region directly in front of the piston. That is, directly in front of the vibrating surface, the sound field of a long, thin rectangular piston produces an optical image that approximates closely the image that would be produced by the sound field of an infinitely long vibrating strip that had the same width as the long, thin piston. To explain the observed distribution of bright and dark spots in his photographs, which correspond to pressure maxima and minima in the sound fields of his piston radiators, Osterhammel invoked the diffraction model of Young. Osterhammel analyzed the radiation fields in front of the pistons exactly as Fresnel analyzed the diffraction pattern of a slit on the basis of Young's model. That is, Osterhammel supposed simple cylindrical waves to diverge from each of the two long edges of a piston face and supposed a progressive plane wave, with wavefronts parallel to the piston face, to exist in the region directly in front of that piston. Osterhammel argued that it is the interference between particular pairs of the three existing waves that causes the loci of the pressure maxima and minima in front of the piston to be hyperbolae.

He constructed such hyperbolae on the basis of this theoretical model and compared the positions of the bright and dark spots in his photograph to them. Osterhammel concluded that his experimental results agreed with theory to within 1 to 2 percent.

Young knew [50] that the bright and dark spots in the diffraction pattern of a straight-edge generally lay on equilateral hyperbolae. As was pointed out earlier however, Young also knew that the position of all fringes could not be predicted exactly using his diffraction model. Moreover, as was also pointed out earlier, it is necessary to assign a phase shift of π to the cylindrical wave diverging from the diffracting edge in order to predict the locations of the observed maxima and minima. It will be recalled that it was just such problems with Young's model that led Fresnel to reject it as incorrect and to develop, in its place, his own, more accurate method of treating diffraction problems. However, Osterhammel describes no significant deviations of his observed results from the predictions made according to the theoretical model of Young, nor does he indicate that he introduced a phase shift of π into his edge waves when computing the theoretical positions of the bright and dark spots on his photographs. As far as the detection of those bright and dark spots that do not lie at the positions predicted for them on the basis of Young's theory, one may speculate somewhat and argue that Osterhammel's photographic method was not sensitive enough to resolve the differences between the predictions of Young's approximate model and those of the more precise Fresnel-Kirchhoff theory. That is, the light intensity maxima and minima on Osterhammel's photographs are not precise points, but are, rather, a pattern of somewhat diffuse patches, having various shades of grey. For this reason, one might suspect that it was not possible for Osterhammel to obtain the precise positions of the intensity maxima and minima, and, consequently, of the corresponding pressure maxima and minima in the sound field, with quite the accuracy that he claimed.

Osterhammel gives no discussion of the phase shift of π that must be introduced into Young's model in order to have the interference,

between the boundary wave from the piston edge and the plane wave in front of the piston, yield maxima and minima in the correct positions. However, Gessert and Hiedemann [51] later examined this question experimentally. These investigators used an "ultrasonic stroboscope" to examine, among other things, the field radiated by a quartz-crystal radiator with a rectangular face 25.4 mm (1 in) long and 2.49 mm (0.0980 in) wide, immersed in carbon tetrachloride (for which, the sound speed is 940 m/s). The crystal was driven at a frequency of 4.42 MHz. Gessert and Hiedemann's ultrasonic stroboscope, like Osterhammel's schlieren apparatus, utilized an optical system to form an image of the piston's radiated sound field that could be photographed. Gessert and Hiedemann concluded from such a photograph, that the experimental image obtained was more consistent with the result expected, if there is a phase difference of π between the boundary wave and the plane wave in front of the piston, than it is with the result that would be obtained if no such phase difference existed. Moreover, when the photographs published by Osterhammel were also examined by Gessert and Hiedemann, they could reach this same conclusion from Osterhammel's results.

The remaining experimental paper dealing with boundary-diffraction-wave acoustical phenomena, and probably the best such investigation, heretofore, is that published by Dehn [52] in 1960. Dehn was aware of the work of Schoch and experimentally tested some of the conclusions of Schoch's theory both qualitatively and quantitatively. Radiation in the nearfield region of a circular piston was examined. The radiating piston was immersed in photographic developing fluid. Sheets of photographic paper, placed in front of the radiating piston, were used to detect the pressure field. The plane of such a sheet was placed parallel to the face of the piston and the sheet kept in the developing solution for several minutes, during which time, the action of the sound field caused a series of concentric bright and dark circular bands to appear on the paper. Sheets were placed at different distances from the piston. On any such sheet, a bright spot existed at the center of the circular

band system when a pressure minimum occurred at the point on the axis of the piston where it intersected the paper. Similarly, a dark spot occurred at the center of the band system if the paper was placed so that a pressure maximum existed at the point where the piston axis intersected the paper. The alternating dark and bright circular bands surrounding these bright or dark spots, in effect, allowed Dehn to map out the pressure maxima and minima in the nearfield of the piston.

The positions of the nearfield axial pressure maxima and minima, observed by Dehn, corresponded very closely to those expected on the basis of radiation theory. (It should be pointed out that the nearfield pressure on the axis of a circular piston is very easy to calculate theoretically.) Arguments based on Schoch's theory were then set forth by Dehn in an attempt to predict the positions of the concentric bright and dark bands on his photographs of the circular piston's sound field. Dehn drew a diagram such as is shown in Fig. 2 and invoked some of Schoch's results in the course of producing the expression

$$\phi = (jv/k)(\tfrac{1}{2}\exp\{-jk[z^2 + (a + x)^2]^{\frac{1}{2}}\} + \tfrac{1}{2}\exp\{-jk[z^2 + (a - x)^2]^{\frac{1}{2}}\} + \exp\{-jk[z + (n - \tfrac{1}{2})\lambda]\}) \qquad (6)$$

to describe the radiated sound field of the circular piston. In Eq. (6), the quantity z represents the axial distance of the observation point from the piston face, x represents the radial distance of the observation point from the piston axis, a represents the piston radius, and λ is the wavelength of the radiated sound. The factor $(n - \frac{1}{2})\lambda$, in the last term of Eq. (6), which contains the arbitrary integer n, changes the phase of the plane wave in front of the piston by an odd multiple of π. Dehn introduced this factor to make his formula conform to the theoretical solution on the piston axis.

Dehn called his model, describing the radiated field in front of a circular piston, the "three-ray method", because there are three

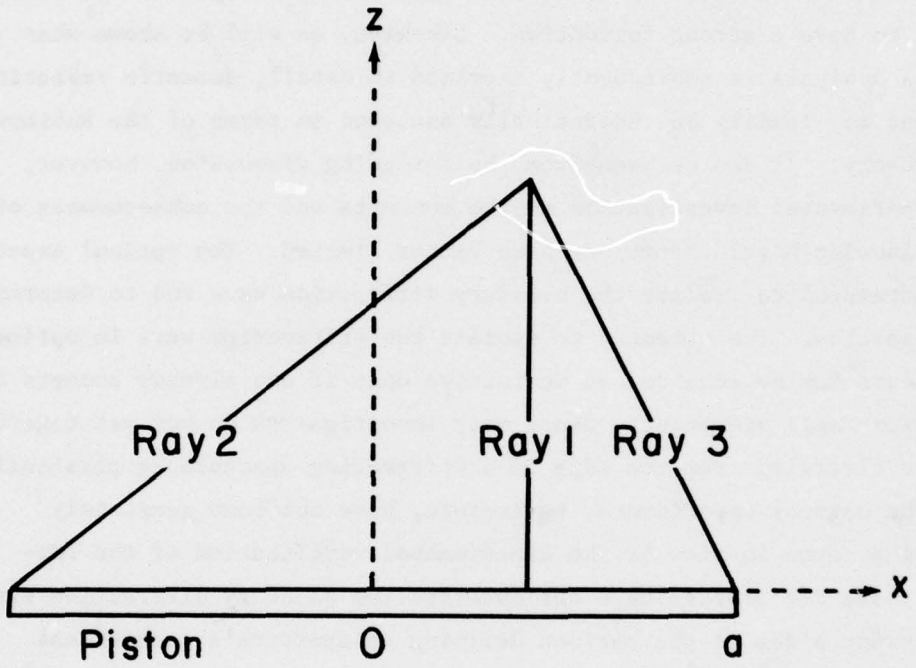

Fig. 2--Dehn's model of the radiated field of a circular piston

interfering components in Eq. (6). To describe the radiated field in Dehn's terms, one would say that each of the first two terms in Eq. (6) describes a plane wave or "ray" from an edge of the piston while the last term describes a plane wave or "ray" coming directly from the piston face. Dehn discussed the positions and intensities of the circular bands in his photographs in terms of this three-ray model. In many cases, Dehn could obtain approximate agreement between the predicted band positions and intensities and those positions and intensities that he observed. In other cases, he could obtain a qualitative description of his observed band patterns using his three-ray model, although to do

so he had to assign relative amplitudes and phases to the waves that characterized his three rays somewhat arbitrarily.

Theoretically, the Rubinowicz-Maggi theory of optical diffraction appears to have a strong foundation. Likewise, as will be shown when Schoch's analysis is subsequently examined in detail, acoustic radiation phenomena may readily be theoretically analyzed in terms of the Rubinowicz-Maggi theory. It can be seen from the foregoing discussion, however, that experimental investigation of the concepts and the consequences of the Rubinowicz-Maggi theory has been rather limited. The optical experiments attempted to isolate the boundary diffraction wave and to determine its properties. The attempts to isolate the diffraction wave in optical experiments may be regarded as definitive only if one already accepts the Rubinowicz-Maggi viewpoint. Since many investigators do not yet regard the wave diverging from the edge of a diffracting aperture as physically real, the optical experiments, heretofore, have not been completely convincing, even in view of the experimental verification of the predicted phase differences when one observes the boundary diffraction wave on different sides of the surface defining an aperture's geometrical shadow region. Previously performed acoustical experiments provide even less convincing evidence of the existence of boundary diffraction waves. In order to describe his results, Osterhammel did little more than invoke the diffraction model of Young, which, for the reasons discussed previously, is known to be defective. Gessert and Hiedemann, on the other hand, actually experimentally investigated a question relevant to the Rubinowicz-Maggi theory when they examined the field of the rectangular piston in order to determine the phase of the wave originating at the piston's edge.

Dehn's acoustical experiments deal with the important problem of the radiating circular piston, but do not actually verify any of the theoretical predictions of Schoch's theory. For instance, mathematically, Schoch's analysis does not lead to Eq. (6) and to Dehn's three-ray model.

Equation (6) is, by Dehn's own admission, an ad hoc result, and one which should be considered to give only an approximate description of the acoustic pressure in the circular piston's nearfield region. One rather obvious shortcoming of Eq. (6) is that all three wave components in it lack both directionality and range-dependent amplitudes, so that one could hardly expect to predict the radiated pressure throughout the nearfield region using such an expression.

The lack of definitive experimental evidence of boundary-diffraction-wave phenomena, particularly in the acoustical radiation and scattering literature, motivated the work that is reported here. As was stated previously, the primary thrust of this work is experimental. However, some useful new theoretical results also have been derived, which describe the acoustic field of a line radiator of finite length in the time domain. These new theoretical results, which are derived in Chapter IV, clearly show that the radiated field of the line source is comprised of three components. First, there is a geometrical component. This component is a finite cylindrical wave diverging from the line. The geometrical component exists only in the region that lies between two hypothetical parallel planes, which pass through the ends of the line source and to which the line is perpendicular. There is also a boundary-diffraction-wave component radiated by each of the two ends of the line source. The boundary-diffraction-wave components both have a "phase" opposite to that of the geometrical component within the region between the two hypothetical planes. If the boundary-diffraction-wave component radiated by one end of the line is observed on opposite sides of the hypothetical plane passing through that end of the line, it is found that this component suffers a discontinuous change in phase of π at the plane in question. This discontinuous phase change, however, ensures that the total field radiated by the line source is everywhere continuous. Boundary-diffraction-wave components are, moreover, directional, so that the entire radiated field of the line source, in both the nearfield and farfield regions, can be described as the superposition, i.e., the inter-

ference, of the geometrical wave component and the two boundary-diffraction-wave components.

The theoretical picture of the radiated field of a line source of finite length, which is outlined in the preceeding paragraph was verified experimentally. The experiments to be described subsequently use a technique that is quite different from those used in most experimental diffraction and radiation studies heretofore. The methodology behind the experimental technique, the experimental system used to implement it, and the experiments will be discussed in detail in Chapters V, VI, and VII, respectively. The basic idea involved in the experimental method, however, is to deal with the radiated field of a finite source in the time domain, rather than in the frequency domain. In this way, the effects of the various components in the radiated field of the source may be spearated and observed directly. This is in contrast to the situation usually encountered in a diffraction or a radiation experiment. Usually, one uses a monochromatic incident light signal in a diffraction experiment or else a harmonic excitation of the source in a radiation experiment. The result in either case is a complex interference pattern in which the effects of all individual component waves in the field become merged together. Consequently, in the usual experiments, the effects and properties of each individual component wave cannot be observed separately, but can only be indirectly inferred from measurement of the amplitude and phase of the harmonic field that results when two or more of these component waves mutually interfere.

To describe the field of a radiator in the time domain, one requires the concept of the spatial impulse response function of that radiator. This concept is a natural extension of the notion of the temporal impulse response of a linear system. Such a function was apparently first used, in 1958, by Kennaugh and Cosgriff [53] for describing scattered electromagnetic fields. In an acoustical radiation problem, the spatial impulse response function relates the acoustic

pressure (or, conceivably, any other field variable) to the geometry of the radiating source. A spatial impulse response function may be envisioned as the pressure field that results from a spatially uniform velocity distribution on the radiator, which has a time history that is described by a δ-function. Therefore, if the radiation process is indeed localized, so that different radiated-field components actually originate at different points on the source, it should be possible to deduce the origin of such components from measurements of the source's spatial impulse response function in the radiated field, since the components from the various points on the source will, in general, arrive at an observation point at different times. Moreover, if the various radiated-field components present in the source's spatial impulse response function can be separated in time, then it should be possible, in principle at least, to study the effects and properties of each such component separately.

In the investigation of acoustical boundary-diffraction-wave phenomena, one finds that the line radiator of finite length is an excellent sound source to study from both a theoretical and an experimental standpoint. From the theoretical point of view, this source is unique because one can find an exact solution that expresses its radiated field in the time domain by solving the two-dimensional inhomogeneous wave equation using integral-transform techniques. In this solution, which expresses the source's spatial impulse response function in terms of generalized functions, the three radiated-field components, discussed previously, are clearly evident. In contrast to this situation, one finds that, in case of the radiating piston treated by Schoch, the equations describing the field contain line-integral expressions. These line-integral expressions must be evaluated by means of an asymptotic technique before the boundary-diffraction-wave components in the radiated field can be localized and considered to originate at specific active points on the piston's edge. Moreover, in obtaining a theoretical solution to the radiating-piston problem, one is required to assume that

the piston is located in an infinite rigid baffle, whereas in the case of the finite line source, it is not necessary to assume that any baffle at all is present.

The differences, which exist between the kind of theoretical expressions that one obtains for the radiated field in the case of a baffled piston source and in the case of an unbaffled finite line source, have important implications from an experimental point of view. First, suppose that one of the experimental objectives is to attempt to isolate boundary-diffraction-wave components and to see if one can actually localize the origin of such components to specific points on the radiating source's periphery. If, in order to accomplish this objective, one elected to experimentally investigate the field of a piston source, then it would be necessary to experimentally satisfy those assumptions made in Schoch's theory when evaluating the pertinent line integrals by means of an asymptotic method. It will be shown in Chapter III, that there are a number of different circumstances for which such asymptotic evaluations should yield adequate theoretical expressions for components of the piston's radiated field. However, by far the most common of these circumstances is that in which the size of the piston is very large in comparison to the wavelengths of all spectral components in the radiated sound field. Thus, in order to be able to compare experimental results to theoretical predictions in the case of a radiating piston, one must either use a very large piston source at frequencies in the audio range or else use a piston of moderate dimensions and work at very high frequencies. Neither of these choices is appealing when designing a practical laboratory experiment. Using a very large piston requires that one have a very large fluid volume available in which to conduct the radiation experiment. On the other hand, operating in a very high frequency range introduces difficulties in constructing reliable experimental transducers and in positioning these acoustic devices precisely without unduly perturbing the radiation field of the source by the introduction of the positioning fixtures and the field-measuring

transducer. Moreover, constructing a piston source that vibrates in such a way that a uniform velocity distribution is obtained on its radiating face is quite difficult if the size of the piston is very large in comparison to the acoustic wavelength of the radiated sound. Unless they are specially constructed, planar radiators in practice do not usually act as vibrating membranes, but rather act as vibrating plates, when the acoustic wavelength is but small fraction of the piston diameter. Such plate-like vibration causes a non-uniform velocity distribution to be created on the face of the piston. Yet the theory of Schoch requires that experiments be performed with a membrane-like piston radiator having a spatially uniform surface velocity. In addition to these difficulties, the piston radiator must, theoretically, be surrounded by a rigid baffle that is of infinite extent. While it is possible, experimentally, to achieve the effect of an infinite baffle with a baffle of finite size, use of any baffle means that the size of the experimental fluid volume must be increased to accommodate it. Moreover, if the fluid in the acoustic medium is to be a liquid such as water, then one is confronted with an additional experimental difficulty, namely, the difficulty of constructing a baffle that approximates a rigid surface, since, in water, all common solid materials exhibit an elastic response to an acoustic field.

Other experimental problems in designing a definitive boundary-diffraction-wave experiment could be cited, but the list above is sufficient to point out the desirability of studying the radiated field of a finite line source, rather than that of a planar baffled piston. One may outline the work to be presented subsequently in this dissertation as follows. As was mentioned before, Schoch's analysis for a planar piston source is examined in detail in Chapter III, in order to illustrate the application of the Rubinowicz-Maggi theory to an acoustic radiation problem. In particular, the spatial impulse response function of the piston source is derived in Chapter III. Before proceeding with this examination of Schoch's analysis, however, it is useful to introduce the

notion of the spatial impulse response function of an acoustic source. It is also worthwhile to obtain an expression for the spatial impulse response function of a piston radiator using the conventional formulation of radiation theory, so that one can compare this result with the corresponding result obtained on the basis of Schoch's analysis. For these reasons, the spatial impulse response of a piston source is derived in Chapter II by means of a Green's-function formulation.

In Chapter II, the Green's-function approach is used to derive the spatial impulse response function of a radiating piston with an arbitrary shape that is surrounded by an infinite baffle. The spatial impulse response function that results from this derivation is expressed as a surface integral taken over the surface of the piston. On the other hand, when Schoch's theory is developed in Chapter III, the resulting expression for the spatial impulse response of a piston involves a line integral taken along the periphery of the radiating piston face, rather than a surface integral. As shown in Chapter III, an asymptotic evaluation of this line-integral expression shows that there are active points on the piston's periphery, which radiate sound to the observation point. For a convex planar piston, which is the case analyzed in Chapter III, these active points are found to be those points on the piston's periphery for which the distance to the observation point from the periphery assumes an extremum value. Thus, the structure of the acoustic radiation field of a convex planar piston can be described in terms of the concepts that were put forth by Rubinowicz when analyzing the problem of optical diffraction by an aperture in a plane screen. It should be mentioned that Kozina and Makarov [45] analyzed the problem of transient acoustic radiation by a convex planar piston using Schoch's formulation of the radiation problem. However, the treatment given in Chapter III is more general than that of these authors, since Kozina and Makarov consider in their analysis only piston radiators that possess an axis of symmetry in the plane of the baffle and they only consider observation points that lie on a plane, normal to the baffle, which passes through this

axis of symmetry. The results derived in Chapter III for the field of a convex planar piston are, therefore, new.

As was mentioned earlier, a new theoretical solution to the problem of radiation by a finite line source is developed in Chapter IV, which shows clearly the composite nature of the field that this source radiates. The structure of this composite field is completely in accord with that expected on the basis of the Rubinowicz-Maggi theory. Since the spatial impulse response function of a line source with finite length can be expressed in a closed form, no integrals need be evaluated in order to determine the behavior of the radiated field at an observation point.

In order to experimentally examine boundary-diffraction-wave phenomena, the spatial impulse response function of an actual line source was measured and compared to that predicted on the basis of the analysis developed in Chapter IV. The experiments were conducted in a large water tank. In the experiments, bursts of pseudorandom noise excited the line transducer and this source's spatial impulse response function was determined by crosscorrelating these exciting noisebursts with the acoustic signals that these bursts caused the line source to radiate. The rationale behind the use of pseudorandom noise signals for determining the source's spatial impulse response function, which results from the application of concepts originating in the statistical theory of communication, is discussed in Chapter V.

In order to conduct the pertinent radiation experiments using pseudorandom noise signals, it was necessary to develop a unique acoustic measurement system, which combines both digital and analog electronic instrumentation and which utilizes the capabilities of a large digital computer. This measurement system, the only one of its kind now in existence, is described in Chapter VI. The experimental measurements of the spatial impulse response function of a finite line source that were made using the measurement system are discussed in Chapter VII. Also in that chapter, the measured spatial impulse response function for the line

transducer used in the experiments is compared to the theoretically predicted spatial impulse response function of an ideal line source. The agreement between theory and experiment is found to be excellent.

The acoustic experiments reported here thus provide a definitive verification of the conceptual model of radiation fields arising from the Rubinowicz-Maggi theory. Moreover, they also establish the fact that this theory is applicable in practical problems. This view, that the Rubinowicz-Maggi theory is of practical importance, comes with the realization that it is used, in the work reported here, to analyze the field radiated by a real transducer. That is, the Rubinowicz-Maggi radiation theory has been applied in order to understand the behavior of an acoustic device that is in widespread use at the present time. It is obvious from this that the theory is not restricted to the analysis of idealized radiation problems, but is of potential value in analyzing the fields encountered in a wide variety of real acoustic radiation, scattering, and diffraction problems.

Two important subjects should also be considered before ending this introductory chapter. The first of these subjects is that of the development of the Rubinowicz-Maggi diffraction theory that has taken place since the publication of Schoch's paper. The second of these subjects concerns the relationship of the concepts derived from the Rubinowicz-Maggi theory to the concepts that arise from other models for radiated or scattered fields. These two subjects will be taken up in order and discussed briefly in what follows.

Further advances have been made in the theory of the boundary diffraction wave in recent years. It was known for a long time that Rubinowicz's formulation of diffraction problems had a peculiar limitation. Using the analytical technique of Rubinowicz, one can only transform the expression for the total field in a diffraction problem into the superposition of a geometrical field and a boundary-wave field, with the boundary-wave field expressed as a line integral along the diffracting edge, in two particular cases. Either the incident field

must be a spherical wave or else it must be a plane wave. Since one could not formulate the theory of boundary diffraction waves analytically for incident fields of a general nature, the validity of the Rubinowicz-Maggi model of diffracted fields was questioned [54] by van Kampen.

In 1955, Ingarden [55] attempted to generalize the Rubinowicz-Maggi theory by employing an eikonal expression for the incident field and then making certain approximations in the resulting equations. Ingarden's success with this approach was limited. The decomposition of the total field in a diffraction problem, with an arbitrary incident wavefield, could only be accomplished to a certain degree of approximation using Ingarden's technique. Moreover, even this approximate decomposition could only be achieved for certain special classes of incident waves.

However, in 1962, Miyamoto and Wolf [56-58] developed a new general theory of optical boundary-diffraction-wave phenomena. Using the theory, one can express monochromatic scalar wavefields of a general nature in terms a new vector potential function that Miyamoto and Wolf devised. With this vector potential function, Miyamoto and Wolf could attack the problem of diffraction by an aperture that is illuminated by an arbitrary incident field. Miyamoto and Wolf found that when an arbitrary wave field suffers diffraction at an aperture, the total field on the side of the aperture opposite the light source may be decomposed into the sum of a primary field and a diffracted field, just as it could be decomposed in the Rubinowicz-Maggi theory. Moreover, the diffracted field can be expressed as a line integral of the vector potential function, taken along the boundary of the diffracting aperture. In view of the line-integral expression of the diffracted field, Miyamoto and Wolf consider that the edge of the aperture gives rise to a boundary diffraction wave like that envisioned in the Rubinowicz-Maggi diffraction model.

In the formulation of Miyamoto and Wolf, the primary-wave component of the total field does not appear to be an extension of the incident field into the directly illuminated region beyond the plane of

the diffracting aperture. Rather, this primary component consists of the superposition of waves arriving from particular points, called "critical points", that lie within the aperture. Thus, in the general Miyamoto-Wolf formulation, the primary wave is somewhat different from the geometrical wave arising out of the Rubinowicz-Maggi theory.

If the incident field in a diffraction problem is either that of a spherical or of a plane wave, then the equations expressing the primary and boundary-diffraction-wave fields in the formulation of Miyamoto and Wolf reduce to the equations that Rubinowicz derived for the geometrical and boundary-wave field components. The Miyamoto-Wolf formulation is thus a generalization of the Rubinowicz-Maggi theory. However, in addition to the difference between the primary-wave field, in the Miyamoto-Wolf formulation, and the geometrical wave field, in the Rubinowicz-Maggi theory, there is also an apparent difference in the nature of the boundary-diffraction-wave fields in the two cases. One finds Rubinowicz [59] discussing this point in a tutorial paper. Rubinowicz regards diffraction as a local effect in his formulation of diffraction theory. That is, he conceives that the boundary diffraction wave diverging from each infinitesimal line element on the edge of the aperture must depend only upon the local behavior of the incident field at that line element. Thus, Rubinowicz conceives that the boundary diffraction wave should truly originate on the boundary of the diffracting aperture and not depend upon the properties of the wavefield elsewhere. On the other hand, the boundary diffraction wave in the formulation of Miyamoto and Wolf is expressed as the line integral of a vector potential function taken along the edge of the aperture. But in order to know the value of this vector potential function at each point on the aperture edge, one is required to know the value of this function at each point on that surface that delineates the geometrical shadow region of the diffracting aperture. Therefore, the properties of boundary diffraction wave in the Miyamoto-Wolf formulation depend upon the behavior of the wavefield at points other than those that lie on the

boundary of the diffracting aperture. For this reason, Rubinowicz distinguishes the boundary diffraction wave arising out of the Miyamoto-Wolf formulation from the type of boundary wave that he considers to be a realization of the conception of Young. One can find some of the important ramifications of Miyamoto and Wolf's new formulation of wave-fields discussed by Rubinowicz [59-63] and by Wolf [64].

The Rubinowicz-Maggi theory and the conventional scalar-wave diffraction theory, which is based upon the ideas of Fresnel and Kirchhoff, provide alternative descriptions of optical diffraction phenomena. In acoustic radiation theory, there are, likewise, alternative descriptions for radiation-field phenomena. In discussions of such radiation-field phenomena, the theoretical results of Freedman [65-70] and of Stephanishen [71-74] are of particular interest and are certainly relevant to the understanding of the physical basis of the Rubinowicz-Maggi theory. Relevant, too, is the geometrical diffraction theory of Keller [75]. Unfortunately, however, a comprehensive evaluation of Freedman's, Stephanishen's, and Keller's results, and of a number of other highly relevant subjects, such as the theory of transient radiation, is far beyond the scope of this dissertation and will not be presented here.

CHAPTER II

GREEN'S-FUNCTION FORMULATION OF THE SPATIAL IMPULSE RESPONSE OF A PLANAR ACOUSTIC SOURCE

Consider the planar radiator S_0 depicted in Fig. 3. This radiator is located in the $z = 0$ plane of a cartesian coordinate system. At time $t = 0$, let the radiator be excited with an impulsive velocity that is of uniform amplitude on its surface. The portion of the $z = 0$ plane surrounding S_0 is considered to act as a rigid baffle. If $\mathbf{U}(\mathbf{r},t)$ is the acoustic particle velocity at an observation point P, which is located with respect to the coordinate origin 0_0 by the vector $\mathbf{r}$, then in the space $z > 0$, the velocity potential $\varphi(\mathbf{r},t)$ satisfies the wave equation

$$\left[\nabla^2 - \frac{1}{c^2}\frac{\partial^2}{\partial t^2}\right]\varphi(\mathbf{r},t) = 0 \ . \tag{7}$$

subject to the boundary conditions that

$$U^z(\mathbf{r},t) = U_0\delta(t) \ , \tag{8a}$$

for P on S_0, with U_0 a constant, and

$$U^z(\mathbf{r},t) = 0 \tag{8b}$$

elsewhere on the $z = 0$ plane. The superscript z in Eqs. (8) denotes the z component of the particle-velocity vector $\mathbf{U} = \text{grad}\ \varphi$. If written in terms of the velocity potential, the boundary conditions expressed by Eqs. (8) become

$$\frac{\partial\varphi(\mathbf{r},t)}{\partial z} = U_0\delta(t) \ , \tag{9a}$$

for P on S_0 and

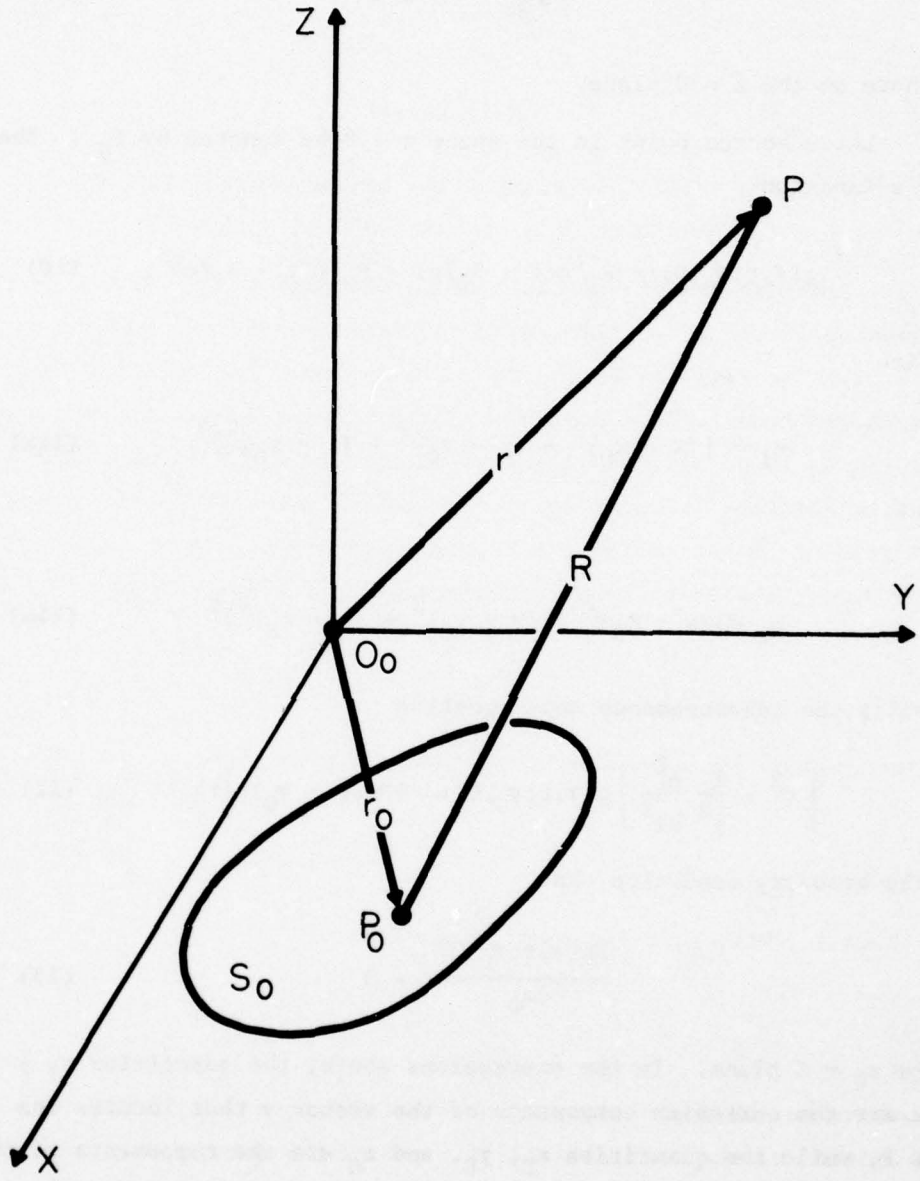

Fig. 3--Planar acoustic source

$$\frac{\partial \varphi(\mathbf{r},t)}{\partial z} = 0 \qquad (9b)$$

elsewhere on the $z = 0$ plane.

Let a source point in the space $z \geq 0$ be denoted by P_0. The Green's function

$$g(\mathbf{r},t;\mathbf{r}_0,0) = R_1^{-1}\delta(t - R_1/c) + R_2^{-1}\delta(t - R_2/c) , \qquad (10)$$

in which

$$R_1 = [(x - x_0)^2 + (y - y_0)^2 + (z - z_0)^2]^{\frac{1}{2}} \qquad (11a)$$

and

$$R_2 = [(x - x_0)^2 + (y - y_0)^2 + (z + z_0)^2]^{\frac{1}{2}} \qquad (11b)$$

satisfies the inhomogeneous wave equation

$$\left[\nabla^2 - \frac{1}{c^2}\frac{\partial^2}{\partial t^2}\right] g(\mathbf{r},t;\mathbf{r}_0,0) = -4\pi\delta(\mathbf{r} - \mathbf{r}_0)\delta(t) \qquad (12)$$

and the boundary condition that

$$\frac{\partial g(\mathbf{r},t;\mathbf{r}_0,0)}{\partial z_0} = 0 \qquad (13)$$

on the $z_0 = 0$ plane. In the expressions above, the quantities x, y and z are the cartesian components of the vector $\mathbf{r}$ that locates the point P, while the quantities x_0, y_0, and z_0 are the components of the vector $\mathbf{r}_0$ that locates P_0. It is also seen from Eqs. (10) and (11), that if either the point P_0 or the point P is located at a finite distance from the origin, then both $g(\mathbf{r},t;\mathbf{r}_0,0)$ and its gradient tend to zero as the other point moves toward infinity.

The Laplace transform on the time variable t is applied respectively to Eq. (7) and to Eq. (12), producing the expressions

$$[\nabla^2 - (s/c)^2]\varphi_L(\mathbf{r},s) = 0 \tag{14}$$

and

$$[\nabla^2 - (s/c)^2]g_L(\mathbf{r},s;\mathbf{r}_0,0) = -4\pi\delta(\mathbf{r} - \mathbf{r}_0) \ . \tag{15}$$

The following definitions are used for the Laplace-transform pair:

$$f_L(s) = \int_0^\infty \exp(-st)f(t)\ dt \tag{16a}$$

and

$$f(t) = \frac{1}{2\pi j}\int_{\sigma-j\infty}^{\sigma+j\infty} \exp(st)f_L(s)\ ds, \tag{16b}$$

in which σ is so chosen that the path of integration lies to the right of all singularities in the complex s-plane. If the Laplace transform Green's function given by Eq. (10) is taken, it is seen that the reciprocity relation

$$g_L(\mathbf{r},s;\mathbf{r}_0,0) = g_L(\mathbf{r}_0,s;\mathbf{r},0) \tag{17}$$

is satisfied when the source point and observation point exchange roles. Suppose $\mathbf{r}$ and $\mathbf{r}_0$ are interchanged in Eqs. (14) and (15) and that Eq. (14) is then multiplied by $g_L(\mathbf{r}_0,s;\mathbf{r},0)$ and that Eq. (15) is multiplied by $\varphi_L(\mathbf{r}_0,s)$. If the resulting equations are subtracted and their difference integrated over the volume of a region Σ that contains both P and P_0, the expression

$$\varphi_L(\mathbf{r},s) = \frac{1}{4\pi}\int_\Sigma [g_L(\mathbf{r}_0,s;\mathbf{r},0)\nabla_0^2\varphi_L(\mathbf{r}_0,s) - \varphi_L(\mathbf{r}_0,s)\nabla_0^2 g_L(\mathbf{r}_0,s;\mathbf{r},0)]\ d(\mathbf{r}_0) \tag{18}$$

is obtained, in which the zero subscript on the Laplacian operator indicates that it is to be taken using the components of $\mathbf{r}_0$. The infinitesimal $d(\mathbf{r}_0)$ in Eq. (18) is a volume element in the region Σ. The particular region Σ throughout which the volume integral is taken is that between the $z_0 = 0$ plane and a large hemisphere of radius R_∞ with its center at the origin. The hemisphere is taken in the region where $z_0 \geq 0$. The surface bounding Σ is comprised of a hemispherical surface S_∞ and a circular region S' of the $z_0 = 0$ plane. It is assumed that R_∞ can be taken so large that the planar radiator S_0 lies entirely within S'. This is always possible if the planar radiator is of finite size.

Except at the point of discontinuity $\mathbf{r} = \mathbf{r}_0$, the transformed Green's function g_L possesses continuous first derivatives within Σ and on its boundary and continuous second derivatives within Σ. The transformed velocity potential φ_L is, likewise, assumed to be sufficiently well-behaved that it possesses similar continuity properties. Green's theorem can therefore be used to convert the volume integral over Σ in Eq. (18) into a surface integral over the surface $S' + S_\infty$. Owing to the properties of the Green's function, the contribution to the integral from the surface S_∞ becomes negligible for R_∞ sufficiently large. One then has

$$\varphi_L(\mathbf{r},s) = \frac{1}{4\pi}\int_{S'} [g_L(\mathbf{r}_0,s;\mathbf{r},0)\nabla_0\varphi_L(\mathbf{r}_0,s) - \varphi_L(\mathbf{r}_0,s)\nabla_0 g_L(\mathbf{r}_0,s;\mathbf{r},0)] \cdot d\mathbf{S}', \quad (19)$$

where the vector $d\mathbf{S}'$ is a directed element of the surface S'. This infinitesimal vector is normal to the $z_0 = 0$ plane and points outward, away from the region Σ. Owing to the direction of $d\mathbf{S}'$, only the z_0 component of each gradient contributes to the scalar product in Eq. (19) and one can thus write Eq. (19) in the form

$$\varphi_L(\mathbf{r},s) = -\frac{1}{4\pi}\int_{S'}\left[g_L(\mathbf{r}_0,s;\mathbf{r},0)\,\frac{\partial\varphi_L(\mathbf{r}_0,s)}{\partial z_0} - \varphi_L(\mathbf{r}_0,s)\,\frac{\partial g_L(\mathbf{r}_0,s;\mathbf{r},0)}{\partial z_0}\right]dS' \,, \qquad (20)$$

in which dS' is an elemental area on the $z_0 = 0$ plane. In view of the boundary condition imposed on the Green's function--this condition being expressed by the Laplace-transformed version of Eq. (13)--the second term in the integrand of Eq. (20) must vanish everywhere on S'. Moreover, if the boundary conditions imposed on the velocity potential, which are expressed by Eqs. (9), are likewise transformed and the results inserted into Eq. (14), then this latter equation becomes

$$\varphi_L(\mathbf{r},s) = -\frac{U_0}{4\pi}\int_{S_0} g_L(\mathbf{r}_0,s;\mathbf{r},0)\,dS' \,, \qquad (21)$$

with only the surface S_0 of the planar radiator now contributing to the surface integral. Finally, by taking the Laplace transform of Eq. (10), one obtains the result that

$$g_L(\mathbf{r},s;\mathbf{r}_0,0) = R_1^{-1}\exp(-sR_1/c) + R_2^{-1}\exp(-sR_2/c) \,. \qquad (22)$$

For $z_0 = 0$, the expression in Eq. (22) becomes

$$g_L(\mathbf{r},s;\mathbf{r}_0,0) = 2R^{-1}\exp(-sR/c) \,, \qquad (23)$$

where

$$R = [(x - x_0)^2 + (y - y_0)^2 + z^2]^{\frac{1}{2}} \,. \qquad (24)$$

If Eq. (23) is inserted into Eq. (21), the result is

$$\varphi_L(\mathbf{r},s) = -\frac{U_0}{2\pi}\int_{S_0}\frac{\exp(-sR/c)}{R}\,dS \,, \qquad (25)$$

in which the prime superscript on the elemental area dS has been dropped.

Upon taking the inverse Laplace transform of Eq. (25), one converts Eq. (25) to

$$\varphi(\mathbf{r},t) = -\frac{U_0}{2\pi}\int_{S_0}\frac{\delta(t - R/c)}{R}\,dS\ . \qquad (26)$$

The pressure in the radiated field is related to the velocity potential by the expression

$$p(\mathbf{r},t) = -\rho\frac{\partial\varphi(\mathbf{r},t)}{\partial t}\ , \qquad (27)$$

in which ρ is the density of the unperturbed fluid. The radiated pressure field produced when the planar source is given an impulsive excitation uniformly over its surface is obtained by applying the definition embodied in Eq. (27) to Eq. (26). This result is expressed

$$p(\mathbf{r},t) = \frac{\rho U_0}{2\pi}\int_{S_0}\frac{\delta'(t - R/c)}{R}dS\ . \qquad (28)$$

Equation (28) gives the spatial impulse response of the planar acoustic radiator. In the integrand of Eq. (28), the prime denotes the first derivative of the δ-function with respect to the variable t. The quantity R is expressed by Eq. (24).

CHAPTER III

RADIATION OF SOUND BY PLANAR PISTONS DESCRIBED USING THE RUBINOWICZ-MAGGI THEORY

Schoch's Transformation of the Radiated Field of A Planar Acoustic Source

As was shown in the preceding chapter, the radiated field produced at an observation point P by a uniformly excited planar source can be expressed as a surface integral over the area of the radiator. It was possible for Schoch [42] to transform this surface-integral field representation in a simple way and to thereby obtain a new means of expressing the radiated field of a planar source. Schoch's technique transforms the surface integral into an expression that incorporates both line integrals taken along the radiator's periphery and a separate term describing a propagating beam of plane waves. Schoch's analytic results show that the acoustic field of the source may be decomposed into interfering components. One type of component, the boundary diffraction wave, [3] originates at the periphery of the source and is expressed in terms of line integrals. The second type of component, the geometrical wave, [3] exists only within the semi-infinite cylindrical region C that is directly in front of the planar source. Subsequently it will be shown that the boundary diffraction wave itself can be considered a composite of several components. These boundary-wave components appear to radiate to an observation point P from virtual sources or "active points" [1] located on the planar radiator's periphery. A virtual source arises whenever an extremum occurs in the distance between the observation point P and a peripheral point on the planar source.

In the following discussion, the analysis of Schoch is applied to determine the spatial impulse response of a planar acoustic source. An arbitrarily shaped planar source could be treated, but it is sufficient to consider only the case in which the shape of the planar source is defined by a smooth closed curve that is everywhere convex, since analysis of this

case exhibits all the essential features of Schoch's method without unnecessary mathematical complication. The basic geometry of Fig. 3 is again considered. However, the halfspace $z \geq 0$ is separated into two regions and the radiated field of the source is analyzed separately in each. The two regions of the halfspace are separated by the semi-infinite cylindrical surface that has the source's periphery as its directrix and its generating lines perpendicular to the $z = 0$ plane. Denote the cylindrical region extending outward from the source as C and the remainder of the $z \geq 0$ halfspace, which is outside this cylinder, as C^c

Consider first the case in which the observation point P is located in the region C. This situation is depicted in Fig. 4. A perpendicular can be erected from some point 0_1 on the surface of the planar source to the point P. The point 0_1 is taken as the origin of a local cartesian coordinate system whose axes X_1 and Y_1 are respectively parallel to the axes X and Y in the original cartesian system. If the location of any source point P_0 on the planar radiator is described by the coordinates x_1 and y_1 with respect to the origin 0_1, then Eq. (24) becomes

$$R = (x_1^2 + y_1^2 + z^2)^{\frac{1}{2}} , \tag{29a}$$

or

$$R = (r_1^2 + z^2)^{\frac{1}{2}} , \tag{29b}$$

if plane polar coordinates (r_1, θ) with an origin at 0_1 are introduced. In terms of these polar coordinates, Eq. (25) can be expressed

$$\varphi_L(\mathbf{r}, s) = -\frac{U_0}{2\pi} \int_0^{2\pi} d\theta \int_0^{r_B(\theta)} \frac{\exp(-sR/c)}{R} r_1 \, dr_1, \tag{30}$$

in which $r_B(\theta)$ is the radial coordinate of the point B that lies on the source's periphery at the angular position θ. In view of Eq. (29b), a

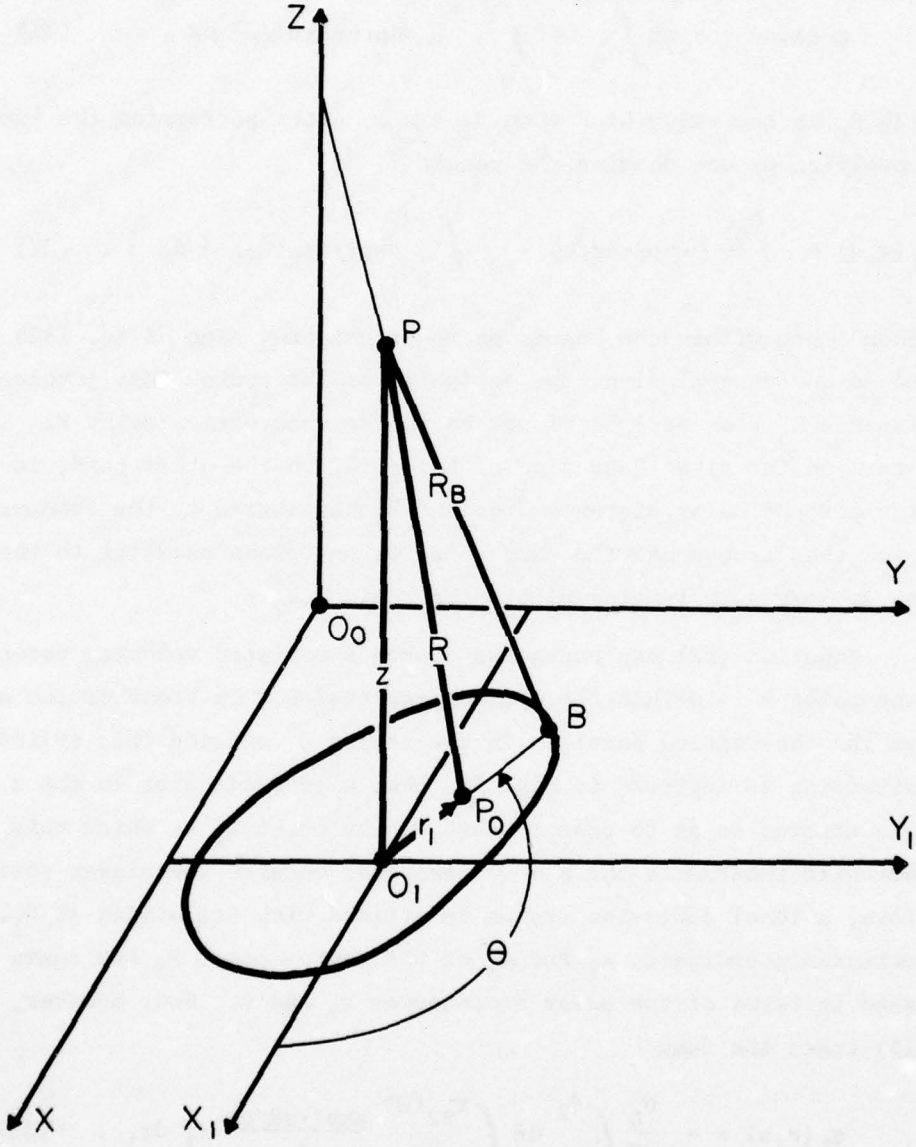

Fig. 4--Planar acoustic source with the observation point in region C

change of variable from r_1 to R transforms Eq. (30) into the expression

$$\varphi_L(\mathbf{r},s) = -\frac{U_0}{2\pi}\int_0^{2\pi} d\theta \int_z^{R_B(\theta)} \exp[-sR(\theta)/c]\, dR\ , \qquad (31)$$

in which R_B is the value of R when $r_1 = r_B$. After performing the integration involving R, one obtains the result

$$\varphi_L(\mathbf{r},s) = -\frac{U_0 c}{s}\left\{\exp(-sz/c) - \frac{1}{2\pi}\int_0^{2\pi} \exp[-sR_B(\theta)/c]\, d\theta\right\}. \qquad (32)$$

The second term within the braces on the right-hand side of Eq. (32) is seen to be an integral along the periphery of the source that involves the distance R_B from peripheral points to the observation point P. The first term on the right-hand side of Eq. (32), on the other hand, involves only the perpendicular distance from the planar source to the observation point and thus always has the same value on any plane parallel to the source, so long as P remains within the region C.

Equation (32) expresses the source's radiated velocity potential when the point P is within the cylindrical region C in front of the source. Suppose the observation point is in the region C^c outside this cylinder. This situation is depicted in Fig. 5. When a perpendicular to the z = 0 plane is erected so as to pass through P, the point 0_1 at which this perpendicular intersects the z = 0 plane lies outside the planar source. As before, a local cartesian system is defined with its origin at 0_1. The cartesian coordinates x_1 and y_1 of the source point P_0 are again expressed in terms of the polar coordinates r_1 and θ. Now, however, Eq. (25) takes the form

$$\varphi_L(\mathbf{r},s) = -\frac{U_0}{2\pi}\int_{\theta_1}^{\theta_2} d\theta \int_{r_{B1}(\theta)}^{r_{B2}(\theta)} \frac{\exp(-sR/c)}{R}\, r_1\, dr_1\ . \qquad (33)$$

The quantities r_{B1} and r_{B2} in the limits of the innermost integral on the right-hand side of Eq. (33) are, respectively, the radial coordinates

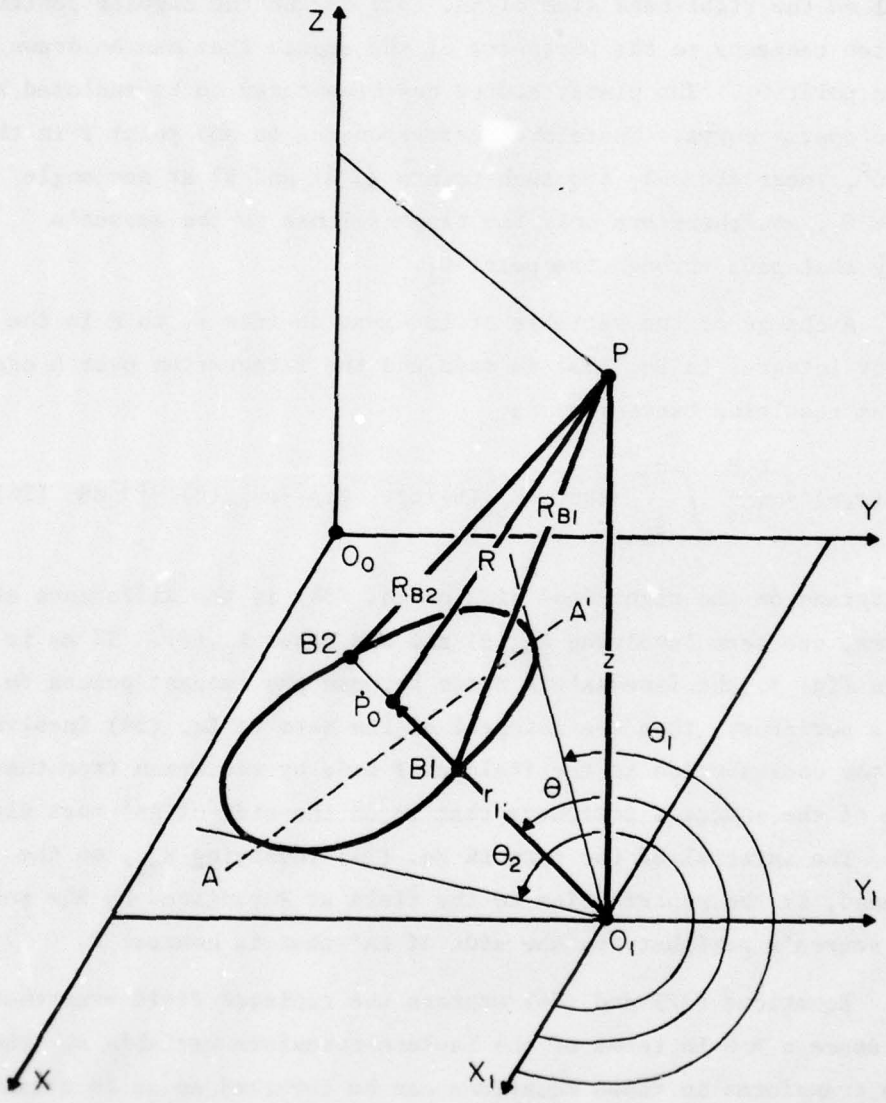

Fig. 5--Planar acoustic source with the observation point in region C^c

of the two points B1 and B2 that lie on the source's periphery at the angular position θ. The angles θ_1 and θ_2 in the limits of the outer integral on the right-hand side of Eq. (33) define the angular positions of the two tangents to the periphery of the source that can be drawn from the point O_1. The planar source has been taken to be enclosed by a smooth convex curve. Therefore, corresponding to any point P in the region C^c, there are only two such points as B1 and B2 at any angle $\theta_1 < \theta < \theta_2$, and there are only two tangent lines to the source's boundary that pass through the point O_1.

A change of the variable of integration from r_1 to R in the innermost integral in Eq. (33) is made and the integration over R carried out. The resulting expression is

$$\varphi_L(\mathbf{r},s) = \frac{U_0 c}{2\pi s} \int_{\theta_1}^{\theta_2} \{\exp[-sR_{B2}(\theta)/c] - \exp[-sR_{B1}(\theta)/c]\}\, d\theta \quad (34)$$

The integrand on the right-hand side of Eq. (34) is the difference of two terms, one term involving $R_{B2}(\theta)$ and the other $R_{B1}(\theta)$. If as is shown in Fig. 5, the line AA' is drawn between the tangent points to the source's periphery, then the integral of the term in Eq. (34) involving R_{B2} is the contribution to the field at P made by radiation from that portion of the source's periphery that is on the side of AA' most distant from P. The integral of the term in Eq. (34) involving R_{B1}, on the other hand, is the contribution to the field at P radiated by the portion of the source's periphery on the side of AA' that is nearest P.

Equations (32) and (34) express the radiated field everywhere in the space $z > 0$ in terms of the Laplace-transform variable s. The Laplace transforms in these equations can be inverted so as to obtain the temporal behavior of the planar source's radiated velocity potential. One has the expression

$$\varphi(\mathbf{r},t) = -U_0 c \left\{ u(t - z/c) - \frac{1}{2\pi} \int_0^{2\pi} u[t - R_B(\theta)/c]\, d\theta \right\} \quad (35a)$$

for P in the region C and the expression

$$\varphi(\mathbf{r},t) = \frac{U_0 c}{2\pi} \int_{\theta_1}^{\theta_2} \{u[t - R_{B2}(\theta)/c] - u[t - R_{B1}(\theta)/c]\, d\theta \,, \qquad (35b)$$

for P in the region C^c. In Eqs. (35), the quantity u designates the unit step function

$$u(x) = \begin{cases} 0 \,, & x < 0 \\ \frac{1}{2} \,, & x = 0 \\ 1 \,, & x > 0 \,. \end{cases} \qquad (36)$$

The radiated pressure field produced by the planar source can be obtained from the results expressed in Eqs. (35) and the definition embodied in Eq. (27). The radiated pressure field is given by the equation

$$p(\mathbf{r},t) = U_0 \rho c \left\{ \delta(t - z/c) - \frac{1}{2\pi} \int_0^{2\pi} \delta[t - R_B(\theta)/c]\, d\theta \right\} , \qquad (37a)$$

when the observation point is in the cylindrical region directly in front of the planar source, and by the equation

$$p(\mathbf{r},t) = - \frac{U_0 \rho c}{2\pi} \int_{\theta_1}^{\theta_2} \{\delta[t - R_{B2}(\theta)/c] - \delta[t - R_{B1}(\theta)/c]\}\, d\theta \,, \qquad (37b)$$

when P is outside this region. Equations (37) express the spatial impulse response of a planar acoustic radiator--the same result expressed by Eq. (26), transformed, however, by the technique of Schoch. In Eqs. (37), terms that involve integrals of functions of θ express contributions to the radiated field made by boundary diffraction waves. The component of the radiated field that is expressed by $U_0 \rho c \delta(t - z/c)$ in Eq. (37a) is the geometrical wave, which is seen to be an impulsive plane wave propagating in a beamlike fashion away from the source.

Decomposition of the Boundary-Diffraction-Wave Field of a Planar Acoustic Source by an Asymptotic Evaluation of the Line Integrals Expressing This Field

It was shown in the previous part of this chapter that when Schoch's technique is used, the surface integral that expresses the radiated field of a planar acoustic source can be transformed in such a way that the resulting equations, describing the field, involve boundary-diffraction-wave components. These boundary-diffraction-wave components appear as line-integral terms in the equations that express the source's radiated field, both in the cylindrical region C directly in front of the source and in the region C^c outside this cylinder. In each of the two regions, the composition of the field produced by boundary-diffraction-wave components is different. In the region C, contributions to the field at P from the entire periphery interfere constructively. On the other hand, in the region C^c, the boundary-diffraction-wave component radiated from the portion of the source's periphery on the side of AA' most distant from P will interfere destructively with the boundary-diffraction-wave component radiated by that portion of the source's periphery on the side of AA' that is nearest P. Moreover, as was stated previously, the boundary diffraction waves themselves can be decomposed into several components. Each such component appears to radiate to the observation point P from a virtual source (i.e., active point) located on the planar radiator's periphery at a point where the distance between P and the source's periphery takes on an extremum value.

To show the composite nature of the boundary diffraction waves, one evaluates the line integrals expressing the boundary-diffraction-wave contributions to the source's radiated field using the method of stationary phase. The form of the dominant terms in the resulting asymptotic expressions indicates that boundary-diffraction-wave generation is associated with critical points [76] on the source's periphery. In order for an asymptotic technique to yield a useful approximation of the field in a radiation problem, it is, of course,

necessary to restrict the range of observation in both space and time. This restriction implies that localization of boundary-diffraction-wave radiation to particular source points may not be completely realized in regions of observation for which the method of stationary phase fails to provide a good approximation for the boundary-diffraction-wave line integrals.

The principle of stationary phase [77] permits an asymptotic evaluation of integrals of the form

$$I(\mu;a,b) = \int_a^b \psi(x)\exp[j\mu f(x)]\, dx \ , \tag{38}$$

in which $f(x)$ and $\psi(x)$ are real functions and $\mu \to +\infty$. The principle asserts that the dominant terms in the asymptotic expansion of $I(\mu;a,b)$ arise from the immediate neighborhood of the end points of the interval $a \le x \le b$ and from the immediate neighborhoods of the points at which $\mu f(x)$ is stationary, that is, the points at which f' vanishes. It is clear also that if $\mu \to -\infty$, the dominant terms in $I(\mu;a,b)$ in this case are just the complex conjugates of those terms obtained for the case when $\mu \to +\infty$. Copson states the following theorem, which holds if $f(z)$ and $\psi(z)$ are analytic functions of the complex variable z that are regular in a simply connected open region containing the interval $a \le x \le b$ and if $f(z)$ is real on the real axis: (I) if $f(x)$ has no stationary points in the interval $\alpha \le x \le \beta$, then as $\mu \to +\infty$

$$I(\mu;\alpha,\beta) = \left[\frac{\psi(\beta)}{j\mu f'(\beta)}\right] \exp[j\mu f(\beta)]$$

$$-\left[\frac{\psi(\alpha)}{j\mu f'(\alpha)}\right] \exp[j\mu f(\alpha)] + O(\mu^{-2}); \tag{39a}$$

(II) if $f(x)$ has one stationary point in the interval $\alpha \le x \le \beta$, namely at $x = \alpha$, and if $f''(\alpha) \neq 0$, then as $\mu \to +\infty$

$$I(\mu;\alpha,\beta) = \left[\frac{\pi}{2\mu \mid f''(\alpha)\mid}\right]^{\frac{1}{2}} \psi(\alpha)\exp[j\mu f(\alpha) \pm \tfrac{1}{4}j\pi] + 0(\mu^{-1}) , \quad (39b)$$

with the plus sign in the exponential pertaining to the case in which $f''(\alpha) > 0$ and the minus sign pertaining to the case in which $f''(\alpha) < 0$; and (III) if $f(x)$ has one stationary point in the interval $\alpha \le x \le \beta$, namely at $x = \beta$, and if $f''(\beta) \neq 0$, then as $\mu \to +\infty$

$$I(\mu;\alpha,\beta) = \left[\frac{\pi}{2\mu \mid f''(\beta)\mid}\right]^{\frac{1}{2}} \psi(\beta)\exp[j\mu f(\beta) \pm \tfrac{1}{4}j\pi] + 0(\mu^{-1}), \quad (39c)$$

with the plus and minus signs in the exponential again pertaining, respectively, to the cases in which $f''(\beta) > 0$ and $f''(\beta) < 0$. In Eqs. (39), the order symbol is denoted by 0 and the values of α and β are finite. Since $f(z)$ is regular in a domain containing the interval $a \le x \le b$, so is $f'(z)$. Therefore, $f'(x)$ can have only a finite number of zeros on the interval $a \le x \le b$ and these zeros will be isolated from one another. Consequently, it will always be possible to divide the interval $a \le x \le b$ into a set of closed subintervals $\alpha \le x \le \beta$ such that each interval either contains no stationary point of $f(x)$ or else contains just one stationary point located at the left-hand or the right-hand end-point. These are the three cases to which Eqs. (39a), (39b), and (39c), respectively, apply. The case in which f'' and f' vanish simultaneously cannot occur for a curve with no points of inflection and will therefore not be considered. It will be noted from Eqs. (39) that the dominant term in $I(\mu;\alpha,\beta)$, owing to an interval containing a stationary point in f, is $0(\mu^{-\frac{1}{2}})$, while the dominant term in $I(\mu;\alpha,\beta)$, owing to an interval with no stationary point is $0(\mu^{-1})$. Thus the contribution of a stationary point to an integral is of greater importance as $\mu \to \infty$ than the contribution of an end point.

Asymptotic expressions for the line integrals in Eqs. (32) and (34) can be found by applying Copson's stationary-phase theorem outlined above. In both Eqs. (32) and (34), one has integrals of the form

$$I = \int_{\theta_a}^{\theta_b} \exp[-sR_B(\theta)/c]\, d\theta \qquad (40)$$

to evaluate. When the observation point P is in the region C, there is one such integral to evaluate. For this integral, $\theta_a = 0$ and $\theta_b = 2\pi$. On the other hand, when P is in the region C^c, there are two integrals of the form of Eq.(40). The first of these integrals expresses the boundary-diffraction-wave contribution at P owing to the portion of the source's periphery on the side of AA' most distant from P. (See Fig. 5.) For this integral, $\theta_a = \theta_1$ and $\theta_b = \theta_2$. The second integral in the case where P is in C^c expresses the boundary-diffraction-wave contribution owing to the portion source's periphery on the side of AA' nearest P. For this integral also, $\theta_a = \theta_1$ and $\theta_b = \theta_2$.

The two cases, the first with P in C and the second with P in C^c, will be treated separately. Certain transformations of the form of the integral in Eq. (40) are necessary, however, in both cases. In both cases, one has an equation of the form

$$R_B(\theta) = [z^2 + r_B^2(\theta)]^{\frac{1}{2}} ,$$

in which r_B is the radial polar coordinate from the point O_1 to a point on the periphery of the source. If primes denote derivatives of quantities with respect to θ, then, for any fixed z and non-zero value of r_B, one has $R_B'(\theta) = 0$ only when $r_B'(\theta) = 0$. Moreover, by writing

$$r_B(\theta) = \Omega + \chi(\theta) , \qquad (42a)$$

with Ω a suitably chosen constant, one can express $R_B(\theta)$ in the form

$$R_B(\theta) = (z^2 + \Omega^2)^{\frac{1}{2}} h(\theta) , \qquad (42b)$$

in which

$$h(\theta) = \{1 + [2\Omega X(\theta) + \chi^2(\theta)]/[z^2 + \Omega^2]\}^{\frac{1}{2}} . \qquad (42c)$$

Also, one expresses the complex Laplace-transform parameter s in terms of the wavenumber k, which is a real quantity:

$$s = jkc . \qquad (43)$$

Since the integrand in Eq. (40) contains no singularities in the right half of the s-plane, Eq. (43) specifies that the contour of integration in Eq. (16b) is along the imaginary axis, with an infinitesimal indentation made at s = 0 to account for the s^{-1} factor in Eqs. (32) and (34). Using the results expressed by Eqs. (42b) and (43), one can write Eq. (40) in the form

$$I = \int_{\theta_a}^{\theta_b} \exp[-j\mu h(\theta)]\, d\theta , \qquad (44)$$

where

$$\mu = k(z^2 + \Omega^2)^{\frac{1}{2}} . \qquad (45)$$

Equation (44) has the form of Eq. (38) with $\psi(\theta) = 1$. The parameter μ given by Eq. (45) is that which is taken to be large when evaluating the integral in Eq. (44) in asymptotic form.

The stationary points of $h(\theta)$ in Eq. (44) are the points for which $r_B'(\theta) = 0$. The periphery of the planar source has earlier been restricted to be a smooth closed curve that is everywhere convex. The periphery will be sufficiently smooth for the following analysis if $r_B''(\theta)$ is a continuous function and if there is no arc of finite length between angles Θ_α and Θ_β on the periphery such that $r_B(\theta)$ is constant for all $\Theta_\alpha \le \theta \le \Theta_\beta$. The radial coordinate $r_B(\theta)$ from a point 0_1 in the z = 0 plane to a point on the periphery of a smooth convex closed curve can assume N maximum and N minimum values. This is true whether the point 0_1 lies inside the curve, as shown in Fig. 4, or outside it

as shown in Fig. 5. The form of the curve and the location of the point O_1 determine the value of N. Thus, for example, an ellipse can have either one maximum and one minimum value ($N = 1$) or else two maximum and two minimum values ($N = 2$) of $r_B(\theta)$. Both the $N = 1$ and $N = 2$ cases are possible for O_1 inside as well as for O_1 outside the ellipse. For the ellipse and in the general case as well, the maxima and minima of $r_B(\theta)$ must alternate, since $r_B(\theta)$ is a continuous function and not constant on any finite arc of the source's periphery. At the maximum and minimum values of $r_B(\theta)$, the first derivative $r_B'(\theta)$ is zero and the second derivative $r_B''(\theta)$ is alternately negative and positive.

Consider first the case in which the observation point P is in the region C, so that O_1 lies on the planar source (Fig. 4). Choose some initial point $[r_B(\theta_{a1}), \theta_{a1}]$ on the source's periphery that is neither at a maximum nor a minimum value of $r_B(\theta)$. Maxima in $r_B(\theta)$ will occur at angles $(\theta_{M1}, \theta_{M2}, \ldots \theta_{Mn}, \ldots \theta_{MN})$ and minima at angles $(\theta_{m1}, \theta_{m2}, \ldots \theta_{mn}, \ldots \theta_{mN})$. It is possible to choose 2N points θ_{an} and θ_{bn} between the alternating maxima and minima so that

$$\begin{aligned} \theta_{a1} < \theta_{m1} < \theta_{b1} < \theta_{M1} < \theta_{a2} < \theta_{m2} < \theta_{b2} \\ < \theta_{M2} < \ldots < \theta_{an} < \theta_{mn} < \theta_{bn} < \theta_{Mn} < \ldots \\ < \theta_{aN} < \theta_{mN} < \theta_{bN} < \theta_{MN} < (\theta_{a1} + 2\pi) , \end{aligned} \qquad (46)$$

with the set including the initial point on the periphery at θ_{a1}. The points on the periphery defined by θ_{a1} and by $(\theta_{a1} + 2\pi)$ will of course coincide. The stationary points of the function $h(\theta)$ in Eq. (44) will occur at the 2N angles θ_{mn} and θ_{Mn} at which $h'(\theta) = 0$. A change of variable is made in the integral appearing in Eq. (44) so that the lower limit θ_a of the integral corresponds to the initial point θ_{a1} and so that the upper limit θ_b becomes $(\theta_{a1} + 2\pi)$. The integral is then written as

the sum of 4N integrals over the angular intervals specified by Eq. (46). Thus, the first integral will have lower limit θ_{a1} and upper limit θ_{m1}, the second integral will have lower limit θ_{m1} and upper limit θ_{b1}, and so on. Each of the 4N integrals is performed over an interval that contains a single stationary point of $h(\theta)$ and this stationary point occurs at one end point of the interval. Each stationary point of $h(\theta)$ contributes to two of the 4N integrals. Using the results of Copson's theorem embodied in Eqs. (39b) and (39c), one can write the asymptotic form of Eq. (32) as

$$\Phi_L(\mathbf{r},s) \sim -\frac{U_0 c}{s}\left\{\exp(-sz/c) - \left(\frac{c}{2\pi s}\right)^{\frac{1}{2}} \sum_{n=1}^{N}\left[\frac{\exp[-sR_B(\theta_{mn})/c]}{[\,|R_B''(\theta_{mn})|\,]^{\frac{1}{2}}} + \frac{\exp[-sR_B(\theta_{Mn})/c]}{[\,|R_B''(\theta_{Mn})|\,]^{\frac{1}{2}}}\right]\right\}. \tag{47}$$

In establishing Eq. (47) in terms of the Laplace-transform parameter s, rather than in terms of the wavenumber k, the square root of $j = \sqrt{-1}$ that yields a physical (i.e., real) solution in the time domain must be chosen.

The case for which the observation point P is in the region C^c is slightly more complicated to treat than that for which P is in the region C. Consider Fig. 6 that depicts the z = 0 plane of Fig. 5. The origin O_1 lies outside the source. The line AA' intersects the source's periphery at points a and a' and through these points pass the two tangent lines from O_1, which are defined by the respective angles θ_2 and θ_1. It will now be proven that on the arc a(B1)a', the radial coordinate $r_B(\theta)$, and hence the function $h(\theta)$, has just one extremum value--the minimum at θ_{m1}. It will also be shown that an extremum value of $r_B(\theta)$ occurs neither at the point a nor at the point a'. This

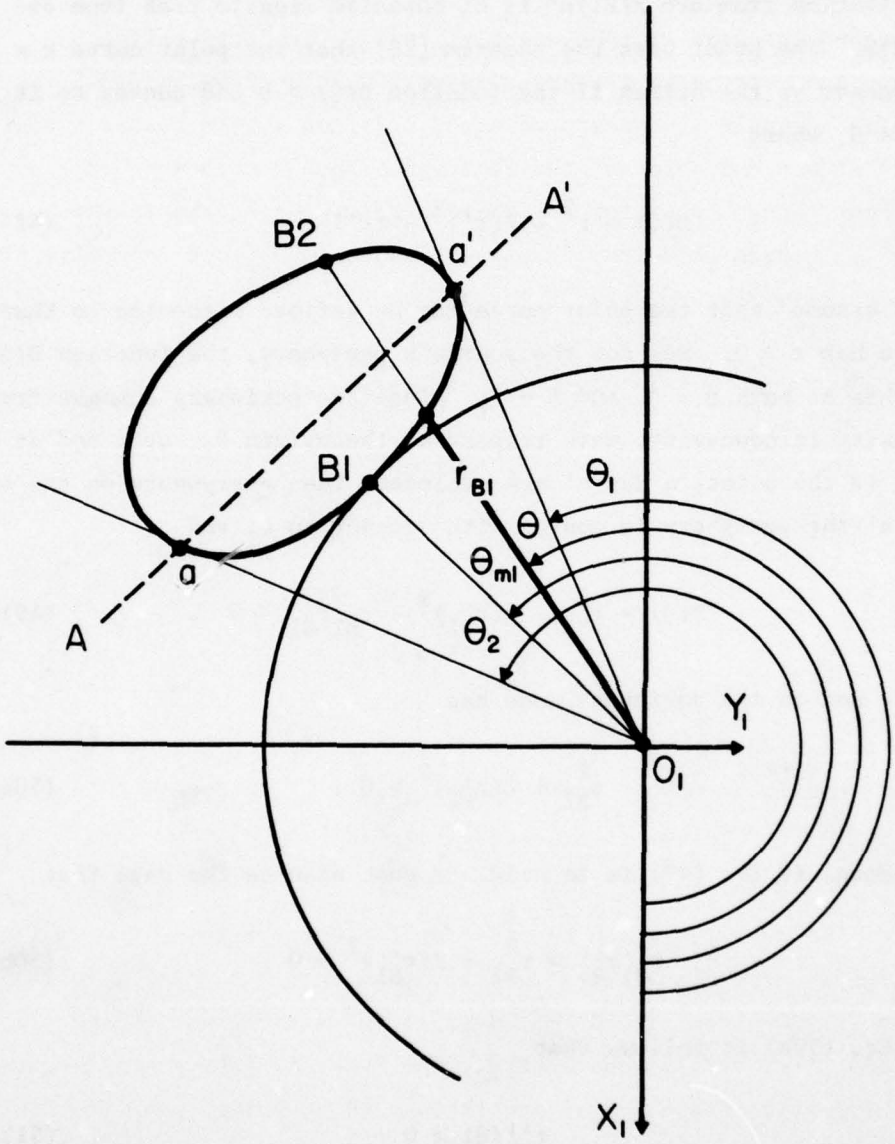

Fig. 6--The z = 0 plane when the observation point is in region C^c

proof is necessary, since in Eq. (34) the boundary-diffraction-wave contribution from arc a(B1)a' is of opposite sign to that from arc a'(B2)a. The proof uses the theorem [78] that the polar curve $r = r(\theta)$ is concave to the origin if the function $D(\theta) > 0$ and convex to it if $D(\theta) < 0$, where

$$D(\theta) = r^2 + 2(r')^2 - rr'' \ . \tag{48}$$

It is assumed that the polar curve may be defined piecewise so that one always has $r \geq 0$. Now for the source's periphery, the function $D(\theta)$, vanishes at both $\theta = \theta_1$ and $\theta = \theta_2$, since the periphery changes from convexity to concavity, with respect to the origin 0_1, at a and at a'. Thus, if the points a and a' are excluded, then everywhere on the arc a(B1)a' the periphery is convex with respect to 0_1 and

$$D(\theta) = r_{B1}^2 + 2(r'_{B1})^2 - r_{B1}r''_{B1} < 0 \ . \tag{49}$$

For 0_1 not on the periphery, one has

$$r_{B1}^2 + 2(r'_{B1})^2 > 0 \ . \tag{50a}$$

Therefore, if Eq. (49) is to hold, it must also be the case that

$$r_{B1}r''_{B1} > r_{B1}^2 + 2(r'_{B1})^2 > 0 \ . \tag{50b}$$

From Eq. (50b) it follows that

$$r''_{B1}(\theta) > 0 \tag{51}$$

everywhere on a(B1)a', exclusive of the end points, so that $r_{B1}(\theta)$ can have no maximum on this arc. Since maxima and minima must occur alternately for a continuous non-constant function, the portion of the

source's periphery defined by arc a(b1)a' has no minimum of $r_{B1}(\theta)$, save that at θ_{m1}.

Moreover, neither a maximum nor a minimum of $r_B(\theta)$ can occur at either the point a or the point a'. For suppose such an extremum value of r_B occurred, for example, at a'. Then one would have $r'_B(\theta_1) = 0$ and, since $D(\theta_1) = 0$, one would also have from Eq. (49) the result that

$$r^2_{B1}(\theta_1) = r_{B1}(\theta_1) r''_{B1}(\theta_1)$$

or that

$$r''_{B1}(\theta_1) > 0 \ , \tag{52}$$

since $r_{B1}(\theta_1) > 0$. Equation (52) implies that if $r'_{B1}(\theta_1) = 0$, then only a minimum of $r_{B1}(\theta)$ is possible at $\theta = \theta_1$ and not a maximum, since a maximum would require that $r''_{B1}(\theta_1) < 0$. However, there is a minimum of $r_{B1}(\theta)$ at $\theta = \theta_{m1}$ and no maximum on the interval $\theta_{m1} \leq \theta < \theta_1$. Therefore, there cannot be a minimum at $\theta = \theta_1$, since there is no intervening maximum. A similar result can be established for the point a. Since there is neither a maximum nor a minimum of $r_{B1}(\theta)$ at a or at a', it follows that $r'_{B1} \neq 0$ at both these points. This in turn implies that $r''_{B1} > 0$ at both a and a', since for $\theta = \theta_1$ or $\theta = \theta_2$

$$r''_{B1} = r_{B1} + r^{-1}_{B1}(r'_{B1})^2 \ . \tag{53}$$

If $r''_{B1} > 0$ at a and at a' and $r''_{B1}(\theta)$ is continuous, then there is some neighborhood of a and some neighborhood of a' throughout which

$$r''_B(r) > 0 \ . \tag{54}$$

In Eq. (54) the subscript on r'' is written as B rather than as B1,

since points on the arc a'(B2)a also lie in any neighborhood of a or of a'. Since the arc a(B1)a' has no maximum of $r_B(\theta)$, any maxima in $r_B(\theta)$, therefore, lie on the arc a'(B2)a at a finite angular separation from both the point a and the point a'.

The analysis in the foregoing two paragraphs establishes the fact that there is only one stationary point of $h(\theta)$ between the points a and a' on the arc a(B1)a', regardless of the number of extremum values of $h(\theta)$ that occur. One can now proceed in a way similar to that used to find an asymptotic expression for Eq. (32) in the case in which P was in the region C. Again suppose there are N maxima and N minima of $h(\theta)$. Let the maxima, which all occur on the arc a'(B2)a, be designated by the angles (θ_{M1}, θ_{M2}, ... θ_{Mn}, ... θ_{MN}). The minimum at $\theta = \theta_{m1}$ occurs on the arc a(B1)a', while the remaining (N - 1) minima occur on the arc a'(B2)a at angles (θ_{m2}, θ_{m3}, ... θ_{mn}, ... θ_{mN}). On the arc a'(B2)a, choose (2N - 2) points that lie between the alternating maxima and minima of $h(\theta)$. Designate the corresponding (2N - 2) angles by θ_{an} and θ_{bn}. One then has the relation

$$\begin{aligned} \theta_1 < \theta_{M1} < \theta_{a2} < \theta_{m2} < \theta_{b2} \\ < \theta_{M2} < \ldots < \theta_{an} < \theta_{mn} < \theta_{bn} < \theta_{Mn} < \ldots \\ < \theta_{aN} < \theta_{mN} < \theta_{bN} < \theta_{MN} < \theta_2 \, , \end{aligned} \tag{55a}$$

on the arc a'(B2)a. Similarly, on the arc a'(B1)a, one has

$$\theta_1 < \theta_{m1} < \theta_2 \, . \tag{55b}$$

The integral in Eq. (34) is separated into the sum of an integral on the arc a'(B2)a and an integral on the arc a'(B1)a. Each of these two integrals is cast in the form of Eq. (44) and evaluated using Copson's theorem. The integral on the arc a'(B2)a is first subdivided

AD-A053 395 NAVAL RESEARCH LAB WASHINGTON D C F/G 20/1
SPATIAL IMPULSE RESPONSE OF AN ACOUSTIC LINE RADIATOR - A STUDY--ETC(U)
FEB 78 A J RUDGERS

UNCLASSIFIED NRL-8191 SBIE-AD-E000 134 NL

2 OF 3
ADA
053395

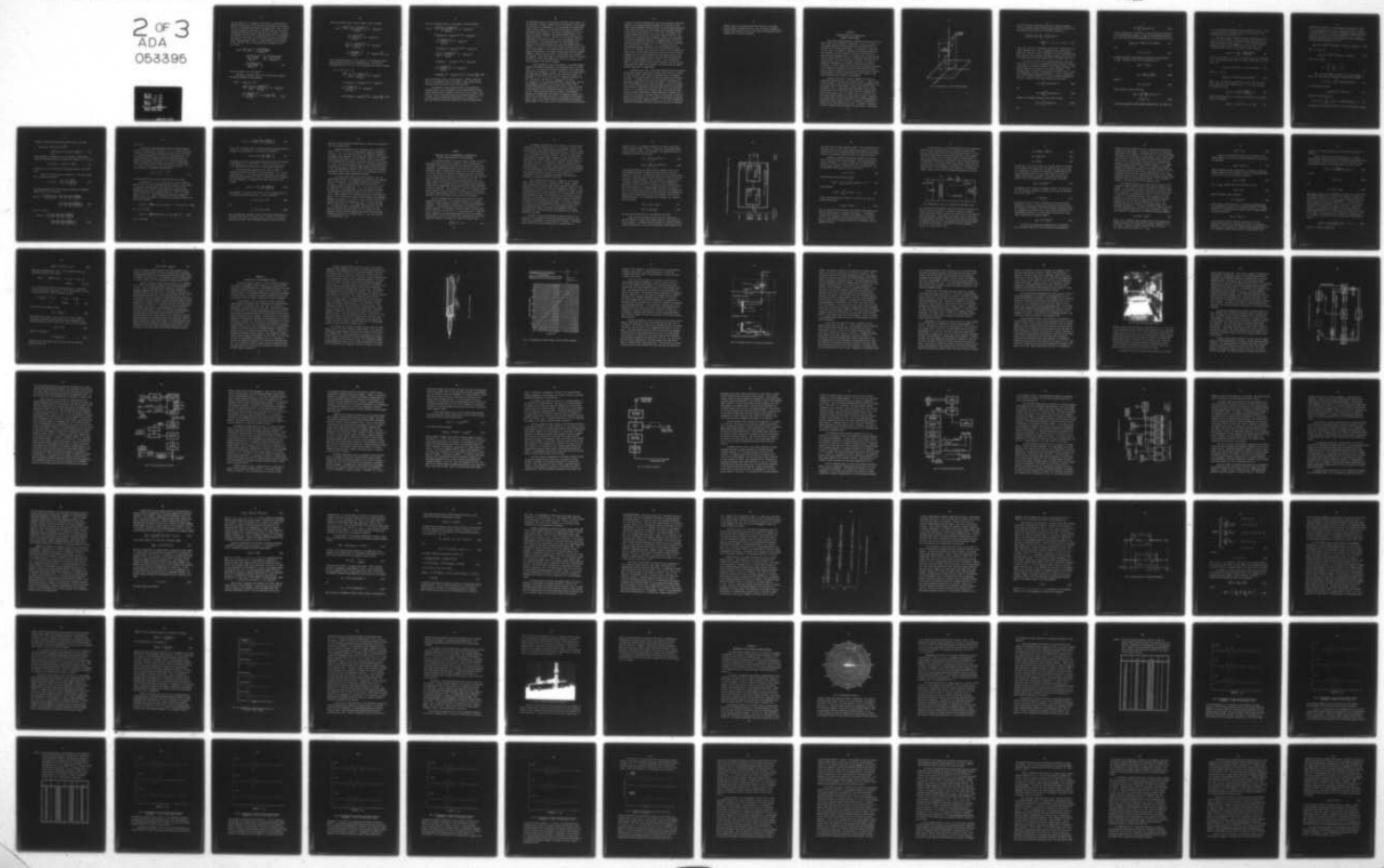

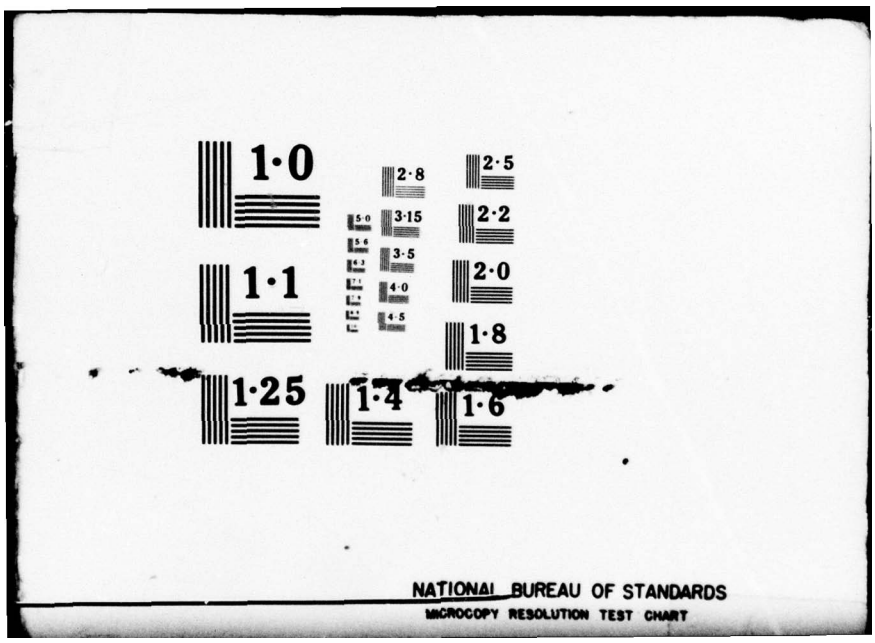
1·0
1·1
1·25
2·8
3·15
3·5
4·0
4·5
2·5
2·2
2·0
1·8
1·4
1·6
NATIONAL BUREAU OF STANDARDS
MICROCOPY RESOLUTION TEST CHART

into the sum of (4N - 2) integrals, each taken on an interval with a single stationary point of $h(\theta)$ located at an end point of the interval. The (4N - 2) intervals are defined by the angles in Eq. (55a). That is, the first integral has lower limit θ_1 and upper limit θ_{M1}, the second integral has lower limit θ_{M1} and upper limit θ_{a2}, and so on. Similarly, the integral on the arc a'(B1)a is written as the sum of two integrals, the first with lower limit θ_1 and upper limit θ_{m1} and the second with lower limit θ_{m1} and upper limit θ_2. Again using the results embodied in Eqs. (39b) and (39c), one can then write the asymptotic form of Eq. (34) as

$$\varphi_L(\mathbf{r},s) \sim \frac{U_0 c}{s}\left(\frac{c}{2\pi s}\right)^{\frac{1}{2}}\left\{\frac{\exp[-sR_{B2}(\theta_{M1})/c]}{[\,|R''_{B2}(\theta_{M1})|\,]^{\frac{1}{2}}}\right.$$

$$-\frac{\exp[-sR_{B1}(\theta_{m1})/c]}{[\,|R''_{B1}(\theta_{m1})|\,]^{\frac{1}{2}}}+\sum_{n=2}^{N}\left[\frac{\exp[-sR_{B2}(\theta_{mn})/c]}{[\,|R''_{B2}(\theta_{mn})|\,]^{\frac{1}{2}}}\right.$$

$$\left.\left.+\frac{\exp[-sR_{B2}(\theta_{Mn})/c]}{[\,|R''_{B2}(\theta_{Mn})|\,]^{\frac{1}{2}}}\right]\right\}, \qquad (56)$$

for the case where P is in the region C^c.

The Laplace transforms in Eqs. (47) and (56) can be inverted. The velocity potential is then expressed

$$\varphi(\mathbf{r},t) \sim -U_0 c\left\{u(t-z/c)\right.$$

$$-\frac{(2c)^{\frac{1}{2}}}{\pi}\sum_{n=1}^{N}\left[\left(\frac{t-R_B(\theta_{mn})/c}{|R''_B(\theta_{mn})|}\right)^{\frac{1}{2}}u[t-R_B(\theta_{mn})/c]\right.$$

$$\left.\left.+\left(\frac{t-R_B(\theta_{Mn})/c}{|R''_B(\theta_{Mn})|}\right)^{\frac{1}{2}}u[t-R_B(\theta_{Mn})/c]\right]\right\}, \qquad (57a)$$

when the observation point is in the region C, and is expressed

$$\varphi(\mathbf{r},t) \sim \frac{U_0 c(2c)^{\frac{1}{2}}}{\pi} \left\{ \left(\frac{t - R_{B2}(\theta_{M1})/c}{|R''_{B2}(\theta_{M1})|} \right)^{\frac{1}{2}} u[t - R_{B2}(\theta_{M1})/c] \right.$$

$$- \left(\frac{t - R_{B1}(\theta_{m1})/c}{|R''_{B1}(\theta_{m1})|} \right)^{\frac{1}{2}} u[t - R_{B1}(\theta_{m1})/c]$$

$$+ \sum_{n=2}^{N} \left[\left(\frac{t - R_{B2}(\theta_{mn})/c}{|R''_{B2}(\theta_{mn})|} \right)^{\frac{1}{2}} u[t - R_{B2}(\theta_{mn})/c] \right.$$

$$\left. \left. + \left(\frac{t - R_{B2}(\theta_{Mn})/c}{|R''_{B2}(\theta_{Mn})|} \right)^{\frac{1}{2}} u[t - R_{B2}(\theta_{Mn})/c] \right] \right\} \quad (57b)$$

when the observation point is in the region C^c. The radiated pressure field produced by the source is obtained from Eqs. (57) using the definition embodied in Eq. (27). For the pressure, one obtains expression

$$p(\mathbf{r},t) \sim U_0 \rho c \left\{ \delta(t - z/c) \right.$$

$$- \frac{(2c)^{\frac{1}{2}}}{\pi} \sum_{n=1}^{N} \left[\left(\frac{t - R_B(\theta_{mn})/c}{|R''_B(\theta_{mn})|} \right)^{\frac{1}{2}} \delta[t - R_B(\theta_{mn})/c] \right.$$

$$- \tfrac{1}{2} \{ |R''_B(\theta_{mn})| [t - R_B(\theta_{mn})/c] \}^{-\frac{1}{2}} u[t - R_B(\theta_{mn})/c]$$

$$+ \left(\frac{t - R_B(\theta_{Mn})/c}{|R''_B(\theta_{Mn})|} \right)^{\frac{1}{2}} \delta[t - R_B(\theta_{Mn})/c]$$

$$\left. \left. + \tfrac{1}{2} \{ |R''_B(\theta_{Mn})| [t - R_B(\theta_{Mn})/c] \}^{-\frac{1}{2}} u[t - R_B(\theta_{Mn})/c] \right] \right\}, \quad (58a)$$

when the observation point is in the region C, and the expression

$$p(\mathbf{r},t) \sim -\frac{U_0 c(2c)^{\frac{1}{2}}}{\pi}\left\{\left(\frac{t - R_{B2}(\theta_{M1})/c}{|R''_{B2}(\theta_{M1})|}\right)^{\frac{1}{2}} \delta[t - R_{B2}(\theta_{M1})/c]\right.$$

$$+ \tfrac{1}{2}\{[R''_{B2}(\theta_{M1})|[t - R_{B2}(\theta_{M1})/c]\}^{-\frac{1}{2}}\, u[t - R_{B2}(\theta_{M1})/c]$$

$$- \left(\frac{t - R_{B1}(\theta_{m1})/c}{|R''_{B1}(\theta_{m1})|}\right)^{\frac{1}{2}} \delta[t - R_{B1}(\theta_{m1})/c]$$

$$- \tfrac{1}{2}\{|R''_{B1}(\theta_{m1})|\,[t - R_{B1}(\theta_{m1})/c]\}^{-\frac{1}{2}}\, u[t - R_{B1}(\theta_{m1})/c]$$

$$+ \sum_{n=2}^{N}\left[\left(\frac{t - R_{B2}(\theta_{mn})/c}{|R''_{B2}(\theta_{mn})|}\right)^{\frac{1}{2}} \delta[t - R_{B2}(\theta_{mn})/c]\right.$$

$$+ \tfrac{1}{2}\{|R''_{B2}(\theta_{mn})|[t - R_{B2}(\theta_{mn})/c]\}^{-\frac{1}{2}}\, u[t - R_{B2}(\theta_{mn})/c]$$

$$+ \left(\frac{t - R_{B2}(\theta_{Mn})/c}{|R''_{B2}(\theta_{Mn})|}\right)^{\frac{1}{2}} \delta[t - R_{B2}(\theta_{Mn})/c]$$

$$\left.\left. + \tfrac{1}{2}\{|R''_{B2}(\theta_{Mn})|\,[t - R_{B2}(\theta_{Mn})/c]\}^{-\frac{1}{2}}\, u[t - R_{B2}(\theta_{Mn})/c]\right]\right\}, \quad (58b)$$

when the observation point is in the region C^c. Equations (58a) and (58b) are the asymptotic forms of the planar source's spatial impulse response expressed previously by Eqs. (37a) and (37b).

The asymptotic results produced using the stationary-phase technique provide a good representation of the planar source's spatial impulse response when the parameter μ given by Eq. (45) is large. This can occur in three situations, which are not mutually exclusive. First, μ becomes large for sufficiently large values of z, provided $k \neq 0$. Thus, the asymptotic expressions describe the source's radiation when

the observation point P is in the source's farfield, that is, when P is far from the z = 0 plane. Second, if $k \neq 0$, the quantity μ can be large for any value of z, including z = 0, if the constant Ω is sufficiently large. From Eq. (42a), it is seen that Ω can be used as a measure of the average distance from 0_1 to the source's periphery when P is in C and can be used as a measure of the average distance from 0_1 to the planar source when P is in C^c. That is, if 0_1 is near the center of a large source, in the case in which P is in C, the constant Ω will be large compared to the variable function $\chi(\theta)$, which measures the deviation of the radial coordinate $r_B(\theta)$ from the "average" radius Ω. Similarly, if P is in C^c and 0_1 is far outside the planar source, Ω will also be large compared to the variable function $\chi(\theta)$, which in this case measures the deviation of the radial coordinate $r_B(\theta)$ from the "average" distance Ω between 0_1 and the source. For any value of z, therefore, the parameter μ can be made large if the observation point P is such that the point 0_1, which is the projection of P on the z = 0 plane, is far from all points on the source's periphery.

In the foregoing two cases, the parameter μ can be made large by suitably restricting the position of the observation point in the half-space $z \geq 0$. The third case in which the parameter μ can be made large occurs when the wavenumber k is large. This restricts the observation of the planar source's radiated field in time rather than in space. In particular, if $(z^2 + \Omega^2)^{\frac{1}{2}}$ is not large, the asymptotic expressions of Eqs. (57) and Eqs. (58) hold as $[t - R_B(\theta_{Mn})/c] \rightarrow 0+$ and as $[t - R_B(\theta_{mn})/c] \rightarrow 0+$ for each particular value of θ_{mn} and θ_{Mn}. That is, these asymptotic expressions hold near the onset of each of the boundary-diffraction-wave components that arrive at P from the virtual sources associated with the stationary points of the function $h(\theta)$ in Eq. (44). This conclusion follows from certain of the Tauberian theorems for transform pairs that connect the asymptotic behavior of a function in the time domain with that of its transform in the frequency domain. Thus, if the relation between the time-domain and frequency-domain behavior of the planar source's radiated field had been formulated

in terms of a Fourier-transform pair, then the correspondence between the behavior of the frequency-domain description of the field for large values of the wavenumber k and the behavior of the time-domain description of the field near the onset of the boundary-diffraction-wave-component arrivals would follow directly [79]. By Eq. (43), the behavior of the frequency-domain description of the source's radiated field for large values of k is associated with the behavior of $\varphi_L(\mathbf{r},s)$ for large values of the Laplace-transform parameter s. Tauberian theorems [80, 81] for the Laplace transform show that when the asymptotic form of a transform, which is valid in the s domain for $s \to \infty$, is inverted, then the corresponding asymptotic expression in the time domain will be valid when $t \to 0+$. Therefore, one can not only use Eqs. (58) to describe the planar source's spatial impulse response at points far from the source's periphery, but can use these equations near the source as well, if one considers only the temporal behavior of each boundary-diffraction-wave component at times immediately after its onset. As the observation point P is placed farther from the source's periphery, the time interval, during which the asymptotic expressions of the source's spatial impulse response remain valid, becomes longer.

According to Eqs. (58), the boundary-diffraction-wave contributions to the spatial impulse response of the planar source consist of a series of discrete arrivals, each of which is associated with an extremum in the value of the distance between the source's periphery and the observation point. A radiating point source can therefore be associated with each such extremum point on the source's periphery. Such point sources may be called "virtual sources" since the number, position, and strength of such sources is different for different positions of the observation point P. Such localized sources appear owing to the destructive interference and mutual cancellation of boundary-diffraction radiation from all points on the source's periphery other than those points at which the phase of the exponential term, in the integrals expressing the boundary-diffraction-wave field, becomes stationary. It is, in fact, through such destructive interference and mutual cancellation that all the radiating

elements, which are distributed over the entire area of the planar source, generate a radiated field with only two types of components--a planewave beam directly in front of the source and boundary-diffraction radiation from the source's periphery.

CHAPTER IV

RADIATED FIELD OF AN ACOUSTIC LINE SOURCE OF FINITE LENGTH

The radiated field produced by a uniformly excited line source of finite length can be expressed in closed form. This is in contrast to the integral expression previously given for the radiated field of a uniformly excited planar piston source. It is found that the field of the line source is a composite consisting of two boundary-diffraction-wave components, which are radiated by the ends of the line, and a geometrical wave component, which is a spatially finite cylindrical wave that is coaxial with the line source. An analytical expression for the radiated field of the finite line source is obtained by solving the appropriate inhomogeneous wave equation, using integral-transform techniques. In order to make use of extant tables of integral transforms, it is convenient to formulate and solve the field problem in terms of acoustic velocity potential and to obtain the radiated pressure field by differentiating the velocity-potential solution with respect to time, using techniques from the theory of distributions.

Consider a line source of length L located on the axis of a cylindrical coordinate system, as is depicted in Fig. 7. Clearly, there is axial symmetry, so that the field of the source is independent of the polar angle θ and can be described in terms of the radial and axial coordinates r and z. Suppose that axial coordinates z_1 and z_2 locate the end points of the line source and that the line is symmetrically disposed with respect to the $z = 0$ plane. Then $z_1 = -\frac{1}{2}L$ and $z_2 = \frac{1}{2}L$. The spatial impulse response of the line source is sought. Therefore, one considers that the line source imparts to the fluid surrounding it an impulsive volume velocity at time $t = 0$, which has a strength of Q volume units per unit length per unit time. The impulse is applied to the fluid uniformly along the length of the line source. If the field

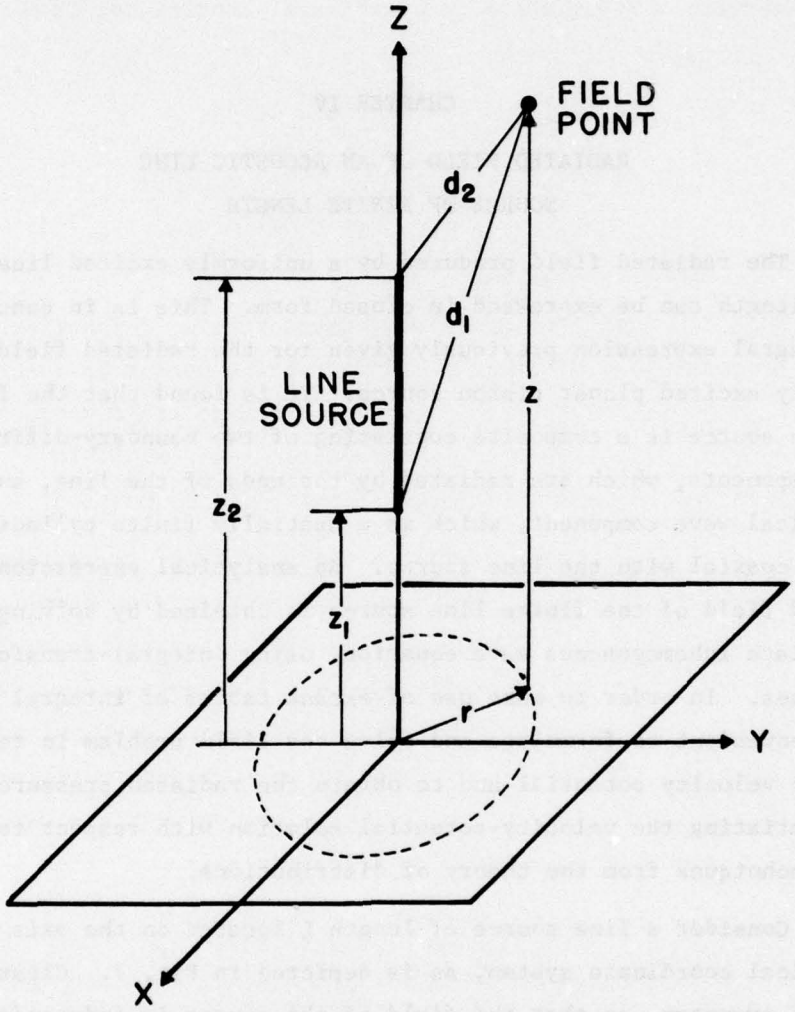

Fig. 7--Line acoustic source of finite length

of the line source is described in terms of the velocity potential $\varphi(r,z,t)$, where $\mathbf{U}$ = grad φ, with $\mathbf{U}$ the acoustic particle velocity, then the appropriate wave equation in cylindrical coordinates is

$$\left[\frac{1}{r}\frac{\partial}{\partial r}\left(r\frac{\partial}{\partial r}\right) + \frac{\partial^2}{\partial z^2} - \frac{1}{c^2}\frac{\partial^2}{\partial t^2}\right]\varphi(r,z,t)$$

$$= -\frac{Q\delta(r)}{\pi|r|}[u(z - z_1) - u(z - z_2)]\delta(t) \ . \qquad (59)$$

In Eq. (59), $\delta(r)$ and $\delta(t)$ designate, respectively, δ-functions of the radial coordinate and of time, u designates the unit step function, given by Eq. (36), and c is the soundspeed in the fluid surrounding the line. Once Eq. (59) is solved, the radiated pressure field $p(r,z,t)$ can be obtained from the velocity potential $\varphi(r,z,t)$ by means of Eq. (27).

In order to solve Eq. (59), a Laplace transform is taken of φ with respect to the time t, an exponential Fourier transform is taken of φ with respect to the axial coordinate z, and a Hankel transform of zero order is taken of φ with respect to the radial coordinate r. The following forms of the three transform pairs are adopted, with s, w, and q the transformed variables corresponding to t, z and r, respectively. First, for the Laplace transform, one uses the definitions embodied in Eqs. (16). Second, for the Fourier-transform pair one takes

$$f_F(w) = \int_{-\infty}^{\infty} \exp(-jwz) f(z)\, dz \ , \qquad (60a)$$

and

$$f(z) = \frac{1}{2\pi}\int_{-\infty}^{\infty} \exp(jwz) f_F(w)\, dw \ . \qquad (60b)$$

Finally, for the Hankel transform of zero order, one uses

$$f_H(q) = \int_0^{\infty} J_0(rq) f(r) r\, dr \qquad (61a)$$

and

$$f(r) = \int_0^\infty J_0(rq) f_H(q) q \, dq \ , \tag{61b}$$

for the transform pair, in which $J_0(x)$ is the zero-order Bessel function of the first kind with argument x. Using the relationships embodied in Eqs. (16), (60), and (61), one transforms Eq. (59) and obtains the result

$$\varphi_{LFH}(q,w,s) = Q[\pi w(w^2 + b^2)]^{-1} \sin(\tfrac{1}{2}wL) \ , \tag{62}$$

with

$$b^2 = q^2 + (s/c)^2 \ . \tag{63}$$

Two Hankel-transform relationships are necessary in the derivation of Eq. (62). The first of these [82] relationships is that

$$g_H(q) = - q^2 f_H(q) \ , \tag{64a}$$

if

$$g(r) = \frac{1}{r} \frac{d}{dr} \left(r \frac{d}{dr} \right) f(r) \ . \tag{64b}$$

Second, if

$$f(r) = \delta(r)/|r| \ , \tag{65a}$$

then, by using Eq. (61a), one obtains

$$f_H(q) = \tfrac{1}{2} \int_{-\infty}^{\infty} \frac{\delta(r)}{|r|} J_0(|r|q) \, |r| \, dr$$

$$= \tfrac{1}{2} J_0(0) = \tfrac{1}{2} \ . \tag{65b}$$

It has been assumed when taking Laplace transforms that, for times prior

to t = 0, both $\varphi(r,z,t)$ and $\partial\varphi(r,z,t)/\partial t$ are zero for all r and z. That is, no acoustic field is assumed to exist in the fluid prior to the excitation of the line source at t = 0.

The inverse Laplace, Fourier, and Hankel transforms must now be taken of Eq. (62), in order to obtain the velocity potential $\varphi(r,z,t)$ from the transformed quantity $\varphi_{LFH}(q,w,s)$. First, the inverse Fourier transform is taken using the definition given in Eq. (60b). The resulting integral can be put in the form of a cosine transform

$$\varphi_{LH}(q,z,s) = \frac{Q}{\pi^2}\int_0^\infty \frac{\sin(\frac{1}{2}w)\cos(wz)}{w(w^2 + b^2)}\, dw . \qquad (66)$$

It will be noted from Eq. (66) that, as expected, φ_{LH} is an even function of z. Using transform tables [83], one obtains, for the case z > 0, the result that

$$\varphi_{LH}(q,z,s) = Q(2\pi b^2)^{-1}[1 - \exp(-\tfrac{1}{2}Lb)\cosh(bz)], \qquad (67a)$$

when $0 < z < \frac{1}{2}L$, and

$$\varphi_{LH}(q,z,s) = Q(2\pi b^2)^{-1}[\exp(-bz)\sinh(\tfrac{1}{2}Lb)] \qquad (67b)$$

when $z > \frac{1}{2}L$. The value of φ_{LH}, given by Eq. (67a), equals that given by Eq. (67b) when $z = \frac{1}{2}L$. Moreover, when z = 0, Eq. (66) becomes the sine-transform integral

$$\varphi_{LH}(q,0,x) = \frac{Q}{\pi^2}\int_0^\infty \frac{\sin(\frac{1}{2}w)}{w(w^2 + b^2)}\, dw . \qquad (68)$$

Using transform tables [84], one evaluates the integral in Eq. (68) and obtains the expression

$$\varphi_{LH}(q,0,s) = Q(2\pi b^2)^{-1}[1 - \exp(-\tfrac{1}{2}Lb)]. \qquad (69)$$

Equation (69) is identical to the expression obtained when the value $z = 0$ is substituted into Eq. (67a). Therefore, Eq. (67a) is valid on the closed interval $0 \le z \le \frac{1}{2}L$ and the expression for $\varphi_{LH}(q,z,s)$, given by Eqs. (67), is valid for the entire interval $0 \le z < \infty$. If the hyperbolic functions in Eqs. (67) are written in terms of exponentials, one may put these equations in the form

$$\varphi_{LH}(q,z,s) = Q(4\pi b^2)^{-1}[2\exp(-b\beta_0) - \exp(-b\beta_1) - \exp(-b\beta_2)] , \quad (70a)$$

when $0 \le z \le \frac{1}{2}L$, and

$$\varphi_{LH}(q,z,s) = Q(4\pi b^2)^{-1}[\exp(-b\beta_1) - \exp(-b\beta_2)] , \quad (70b)$$

when $z > \frac{1}{2}L$, in which

$$\beta_i = \begin{cases} 0, & i = 0 \\ \frac{1}{2}L - z, & i = 1 \\ \frac{1}{2}L + z, & i = 2 \end{cases} . \quad (71)$$

Next, the inverse Hankel transform of Eqs. (70) is taken. In order to do this, one first considers the Hankel-transform integral

$$f_L(r,z,s;\beta_i) = \int_0^\infty b^{-2} J_0(qr)\exp(-b\beta_i) q \, dq \quad (72)$$

of the transformed equation

$$f_{LH}(q,z,s;\beta_i) = b^{-2}\exp(-b\beta_i) . \quad (73)$$

Equation (72) may be written as

$$f_L(r,z,s;\beta_i) = \int_{s/c}^\infty b^{-1} J_0\{[b^2 - (s/c)^2]^{\frac{1}{2}} r\}\exp(-b\beta_i) \, db . \quad (74)$$

The integral on the right-hand side of Eq. (74) has the form of a Laplace

transform. Again [85] from integral-transform tables, the result

$$f_L(r,z,s;\beta_i) = \exp[-(s/c)(r^2 + \beta_i^2)^{\frac{1}{2}}] \times \int_0^\infty \exp(-\xi)[\xi^2 + 2(s/c)(r^2 + \beta_i^2)^{\frac{1}{2}}\xi]\, d\xi \ . \qquad (75)$$

can be obtained. The integral in Eq. (75) has been tabulated [86]. Using this tabulated result, one can express the quantity f_L in Eq. (75) as

$$f_L(r,z,s;\beta_i) = - K_0[(s/c)(r^2 + \beta_i^2)^{\frac{1}{2}}] \ , \qquad (76)$$

in which $K_0(x)$ is the zero-order modified Bessel function of the third kind.

Finally, the inverse Laplace transform of Eq. (76) may be taken [87] to obtain the expression

$$f(r,z,t;\beta_i) = - \frac{u[t - (r^2 + \beta_i^2)^{\frac{1}{2}}/c]}{[t^2 - (r^2 + \beta_i^2)/c^2]^{\frac{1}{2}}} \ . \qquad (77)$$

The results embodied in Eqs. (69) through (77) allow the transformed version of Eqs. (70) to be written

$$\varphi(r,z,t) = - \frac{Q}{4\pi}\left[\frac{2u(t - r/c)}{(t^2 - r^2/c)^{\frac{1}{2}}} - \frac{u\{t - [r^2 + (\frac{1}{2}L - z)^2]^{\frac{1}{2}}/c\}}{\{t^2 - [r^2 + (\frac{1}{2}L - z)^2]/c^2\}^{\frac{1}{2}}} - \frac{u\{t - [r^2 + (\frac{1}{2}L + z)^2]^{\frac{1}{2}}/c\}}{\{t^2 - [r^2 + (\frac{1}{2}L + z)^2]/c^2\}^{\frac{1}{2}}}\right], \qquad (78a)$$

for $0 \le z \le \frac{1}{2}L$ and

$$\varphi(r,z,t) = - \frac{Q}{4\pi}\left[\frac{u\{t - [r^2 + (\frac{1}{2}L - z)^2]^{\frac{1}{2}}/c\}}{\{t^2 - [r^2 + (\frac{1}{2}L - z)^2]/c^2\}^{\frac{1}{2}}} - \frac{u\{t - [r^2 + (\frac{1}{2}L + z)^2]^{\frac{1}{2}}/c\}}{\{t^2 - [r^2 + (\frac{1}{2}L + z)^2]/c^2\}^{\frac{1}{2}}}\right], \qquad (78b)$$

for $z > \frac{1}{2}L$.

The velocity potential radiated by the line source of finite length is expressed by Eqs. (78) for $0 \leq z < \infty$. It will be noted that the portion of the solution expressed by Eq. (78a) is an even function of z, while that expressed by Eq. (78a) is an odd function of z. As stated previously, the radiated field of the finite line source is symmetric with respect to the plane $z = 0$. It can be readily seen, without repeating the analysis above step-by-step for the case where $z < 0$, that a solution that is valid for the entire interval $-\infty < z < \infty$ can be obtained by introducing the sign function.

$$\text{sgn}(z) = \begin{cases} 1, & z > 0 \\ -1, & z < 0 \end{cases} , \tag{79}$$

as a factor multiplying the entire right-hand side of Eq. (78b).

Referring to Eq. (27), it is seen that the velocity potential, given by Eqs. (78), must be differentiated with respect to time in order to obtain the acoustic pressure field radiated by the finite line. Techniques from the theory of distributions must be applied in order to take the derivative of the singular function $u(t - \alpha)(t^2 - \alpha^2)^{-\frac{1}{2}}$ that appears in Eqs. (78). These techniques are described in Appendix I. Using the results of Appendix I, one obtains the following expression for the acoustic pressure:

$$p(r,z,t) = -\frac{\rho Q}{4\pi}[2\psi(r, 0, t) - \psi(r, \tfrac{1}{2}L-z, t) - \psi(r, \tfrac{1}{2}L+z, t)], \tag{80a}$$

for $-\frac{1}{2}L \leq z \leq \frac{1}{2}L$ and

$$p(r,z,t) = -\frac{\rho Q}{4\pi}\text{sgn}(z)[\psi(r, \tfrac{1}{2}L-z, t) - \psi(r, \tfrac{1}{2}L+z, t)] , \tag{80b}$$

for $|z| > \frac{1}{2}L$, where

$$\psi(r,\mu,t) = \text{Psf}\left[\frac{u[t - (r^2 + \mu^2)^{\frac{1}{2}}/c]t}{[t^2 - (r^2 + \mu^2)/c^2]^{3/2}}\right] . \qquad (81)$$

In Eq. (81), the notation Psf[ ] indicates that the expression within the brackets is a pseudofunction. The particular pseudofunction

$$F(x) = \text{Psf}\left[\frac{u(t - \alpha)t}{(t^2 - \alpha^2)^{3/2}}\right] \qquad (82)$$

that appears in Eq. (81) is a singular generalized function that behaves as the function $t(t^2 - \alpha^2)^{-3/2}$ for $t > \alpha$ and is zero for $t < \alpha$. At $t = \alpha$, the generalized function F has a positive-going singularity.

The pressure field, expressed by Eqs. (80a) and (80b), is continuous across both the plane $z = \frac{1}{2}L$ and the plane $z = -\frac{1}{2}L$. At some observation point $P = (r,z)$ located between these planes, the pressure field, which is expressed by Eq. (80a), is comprised of three components. The first component is a cylindrical wave that is described by the function

$$\psi(r,0,t) = \text{Psf}\left[\frac{u(t - r/c)t}{(t^2 - r^2/c^2)^{3/2}}\right]. \qquad (83)$$

The distances to the point P from the end of the line source located at $z = \frac{1}{2}L$ and from the end located at $z = -\frac{1}{2}L$ are, respectively,

$$d_1 = [r^2 + (\tfrac{1}{2}L - z)^2]^{\frac{1}{2}} \qquad (84a)$$

and

$$d_2 = [r^2 + (\tfrac{1}{2}L + z)^2]^{\frac{1}{2}} . \qquad (84b)$$

Thus, two additional components, which are described, respectively, by the functions $\psi(r, \frac{1}{2}L-z, t)$ and $\psi(r, \frac{1}{2}L+z, t)$, arrive at P--one from each end of the line. These components interfere constructively with

each other, since they have the same sign in Eq. (80a), and destructively with the cylindrical wave.

Suppose the observation point P approaches one of the planes at either $z = \frac{1}{2}L$ or at $z = -\frac{1}{2}L$. For definiteness, suppose it approaches the plane $z = \frac{1}{2}L$. Just beyond this plane, the cylindrical component of the radiated field vanishes. This discontinuous behavior of the component described by the function $\psi(r,0,t)$ is, however, offset by the behavior of the component that is radiated from the end of the line source located at $z = \frac{1}{2}L$. As can be seen from Eqs. (80), the contribution described by the function $\psi(r, \frac{1}{2}L-z, t)$ abruptly changes sign as P crosses the plane $z = \frac{1}{2}L$. The discontinuous behavior in the contributions to the radiated field owing to both $\psi(r,0,t)$ and $\psi(r, \frac{1}{2}L-z, t)$ is, therefore, such that the acoustic pressure remains everywhere continuous.

It is seen from Eq. (80b) that beyond the plane $z = \frac{1}{2}L$, the radiated field consists of two components that arrive from the respective ends of the line source. The component described by the function $\psi(r,\frac{1}{2}L+z, t)$, which is radiated from the end of the source at $z = -\frac{1}{2}L$, is continuous across the plane at $z = \frac{1}{2}L$. It can also be seen from Eq. (80b) that, in the region where $z > \frac{1}{2}L$, this component interferes destructively with the component radiated by the end of the line at $z = \frac{1}{2}L$. Similar behavior of the radiated field occurs at and beyond the plane $z = -\frac{1}{2}L$. In this case, reverse roles are played by the components radiated by the points at $z = \frac{1}{2}L$ and $z = -\frac{1}{2}L$ on the line. That is, the component described by the function $\psi(r, \frac{1}{2}L+z, t)$, which is radiated from the source point at $z = -\frac{1}{2}L$, changes sign as P crosses the plane $z = -\frac{1}{2}L$, while the sign of the component described by $\psi(r, \frac{1}{2}L-z, t)$, which is radiated by the source point at $z = \frac{1}{2}L$, remains the same. Components radiated from the respective ends of the line source again interfere destructively in the region where $z < -\frac{1}{2}L$, just as they do in the region where $z > \frac{1}{2}L$.

CHAPTER V

METHODOLOGY USED FOR EXPERIMENTALLY DETERMINING THE SPATIAL IMPULSE RESPONSE OF A LINE RADIATOR

The theoretical model of the spatial impulse response of a finite line source, which was derived in Chapter IV, can be experimentally investigated by measuring the pressure field radiated by an actual line transducer. The measurement method used is based upon a result from the statistical theory of communication, namely, that the impulse response of a linear system can be obtained by applying a white-noise excitation to the system's input port and then crosscorrelating this input excitation with the response that it generates at the system's output port. In order to apply this method to an input-output experiment in which the linear system is a line transducer and its radiated field, one must also consider the electromechanical network characterizing internal mechanism of the line transducer. This is necessary so that the transducer's spatial impulse response, which is geometrical in origin, can be separated from the overall system response, which is in part determined by the internal structure of the line transducer that is used in the experiment.

The line transducer and its radiated field constitute a linear system with one input port, its electrical terminals, and a infinite continuum of output terminals, the points $\mathbf{r}$ in the fluid surrounding the transducer. A time-varying electrical signal, the voltage $\tilde{E}(t)$ for example, applied to the transducer's input port causes a pressure field $\tilde{p}(\mathbf{r},t)$ at the point $\mathbf{r}$ in the fluid. At a particular point $\mathbf{r}$, then, the impulse response of the linear system comprised of the line transducer and its acoustic field is the pressure $\hat{p}(\mathbf{r},t)$ produced by the electrical signal $\hat{E}\delta(t)$ applied to the input port, where $\hat{E}$ is taken so that

$$\int_{-\infty}^{\infty} \hat{E}\delta(t)\, dt = 1 \text{ V}. \tag{85}$$

The impulse response $\hat{p}(\mathbf{r},t)$ is not, however, the spatial impulse response of the line transducer that is to be measured. Rather, it is the convolution of the spatial impulse response with the impulse response of the linear electromechanical network that represents the electrically excited, mechanically vibrating transducer. That is, the input signal that produces the spatial impulse response of a finite line radiator, as described by Eqs. (80a) and (80b), is the impulsive velocity imparted to the fluid by the source. This impulsive velocity is expressed by the right-hand side of Eq. (59), which is the wave equation for the radiated velocity potential. An electrical impulse applied to the input terminals of a real electroacoustic line transducer will not impart the theoretically specified impulsive velocity to the fluid, owing to the characteristics of the electromechanical network that couples the transducer's electrical terminals to the fluid.

This electromechanical network, if examined in the frequency domain, will be found to have a complicated multi-resonant response. Since an impulsive electrical signal contains spectral components at all frequencies, it will excite all these electromechanical resonances. Such excitation will therefore cause the source transducer to radiate a complex pressure field that is greatly dependent upon the characteristics of the electromechanical network. Those features of the line source's pressure field that are determined by its spatial impulse response function will be obscured by the contribution to the source's field that is caused by the response of the electromechanical network. It is possible however, to obtain an unobscured picture of the spatial impulse response of a line transducer by means of an input-output experiment using cross-correlated noise. The procedure used is an adaptation of a technique discussed by Lee [88].

In order to see how this technique is applied, however, it is necessary to first consider in detail the characteristics of the linear system that is equivalent to the radiating line transducer. This linear system, comprised the line transducer and its radiated field, is

depicted in Fig. 8. The impulse response of the system at the point $\mathbf{r}$ in the transducer's field is $\hat{p}(\mathbf{r},t)$. Suppose the corresponding transfer function is $\hat{H}(\mathbf{r},\nu)$, where ν is the frequency. The functions $\hat{p}$ and $\hat{H}$ are related by the Fourier transform pair

$$\hat{p}(\mathbf{r},t) = \int_{-\infty}^{\infty} \hat{H}(\mathbf{r},\nu) e^{j2\pi\nu t}\, d\nu \tag{86a}$$

$$\hat{H}(\mathbf{r},\nu) = \int_{-\infty}^{\infty} \hat{p}(\mathbf{r},t) e^{-j2\pi\nu t}\, dt\ . \tag{86b}$$

As mentioned previously, the linear system is comprised, first, of an electromechanical network, coupling the electrical port of the line transducer to the fluid. In cascade with this is a second linear system, which can be called the spatial network, coupling the surface of the line transducer to the field point $\mathbf{r}$. Let $h_E(t)$ and $H_E(\nu)$, respectively, be the impulse response and transfer function of the electromechanical network and let $p(\mathbf{r},t)$ and $H(\mathbf{r},\nu)$, respectively, be the impulse response and transfer function of the spatial network pertinent to the point $\mathbf{r}$. Note at this juncture that the total linear system has been decomposed in such a way that the characteristics of the transducer's electromechanical network does not depend upon the nature of the acoustic field that the transducer radiates. For the radiating line transducer, one, therefore, has the relations

$$\hat{p}(\mathbf{r},t) = p(\mathbf{r},t) * h_E(t) \tag{87}$$

$$\hat{H}(\mathbf{r},\nu) = H(\mathbf{r},\nu) H_E(\nu), \tag{88}$$

with the centered asterisk in Eq. (87) denoting convolution.

Assume that the radiating surface of the line transducer is a circular cylinder of length L with a small radius a_0. Also assume that, at the frequency ν, a harmonic electrical signal $E(\nu)$ produces a harmonic velocity distribution $Q(\nu)$ that has an essentially uniform amplitude over

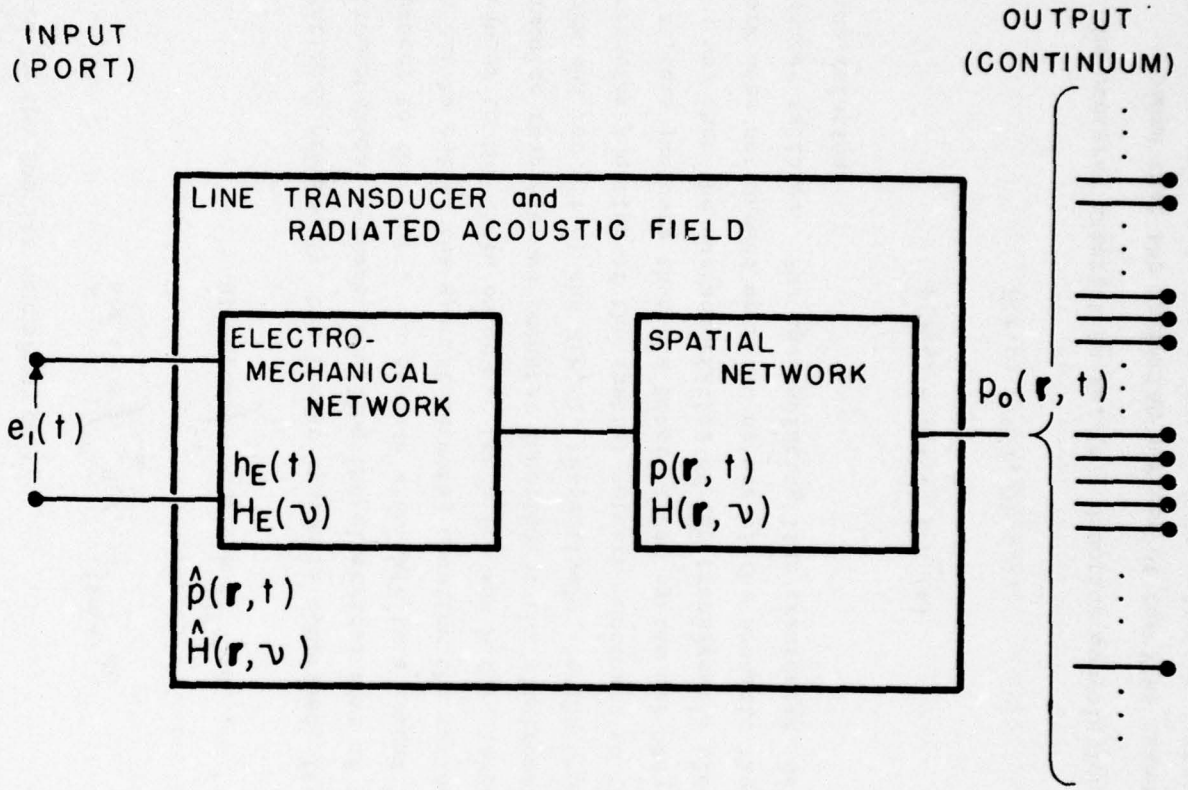

Fig. 8-- Linear-system representation of a radiating acoustic source

the curved portion of this cylinder's surface. Then the function $p(\mathbf{r},t)$ appearing in Eq. (87) will be the spatial impulse response of the line transducer and, if a_0 is sufficiently small, will also be a good approximation to the theoretical impulse response of an ideal line source.

Suppose the continuous random-noise voltage $e_I(t)$ is used to excite the linear system's electrical input. Let the pressure $p_0(\mathbf{r},t)$ result at the point $\mathbf{r}$. If $e_I(t)$ is white noise, its power density spectrum $S_{II}(\nu)$ will have a constant value S at all frequencies. The autocorrelation function $R_{II}(\tau)$ of $e_I(t)$ will then be

$$R_{II}(\tau) = S\delta(\tau) . \tag{89}$$

The input-output crosscorrelation function

$$R_{I0}(\mathbf{r},\tau) = \lim_{T\to\infty} \frac{1}{2T} \int_{-T}^{T} e_I(t)p_0(\mathbf{r},t+\tau)\, dt \tag{90}$$

can be expressed

$$R_{I0}(\mathbf{r},\tau) = \int_{-\infty}^{\infty} \hat{p}(\mathbf{r},t)R_{II}(\tau - t)\, dt, \tag{91}$$

so that, upon substituting the results of Eq. (89) in Eq. (91), one obtains the expression

$$R_{I0}(\mathbf{r},\tau) = S\hat{p}(\mathbf{r},\tau) . \tag{92}$$

Thus, by crosscorrelating the white-noise transducer input signal $e_I(t)$ with the pressure $p_0(\mathbf{r},t)$ it produces at the point $\mathbf{r}$, the impulse response function $\hat{p}(\mathbf{r},t)$ is obtained. This function is, according to Eq. (87), the convolution of the spatial impulse response function, which is sought, with the impulse response of the transducer's electromechanical network.

In order to extract a good representation of the line transducer's spatial impulse response function $p(\mathbf{r},t)$ from the convolution with $h_E(t)$, the input noise signal $e_I(t)$ is bandlimited by means of a filter. The measured input-output crosscorrelation function R_{IO} that results, which can be thought of as a transient signal in the time domain, is then appropriately modified by convolving it with the impulse response of a second filter. The rationale behind this procedure is based upon the assumption that the line transducer's radiated field is generated by the radial motion of a thin cylindrical shell composed of a ferroelectric ceramic. Figure 9 shows the electromechanical equivalent circuit [89]

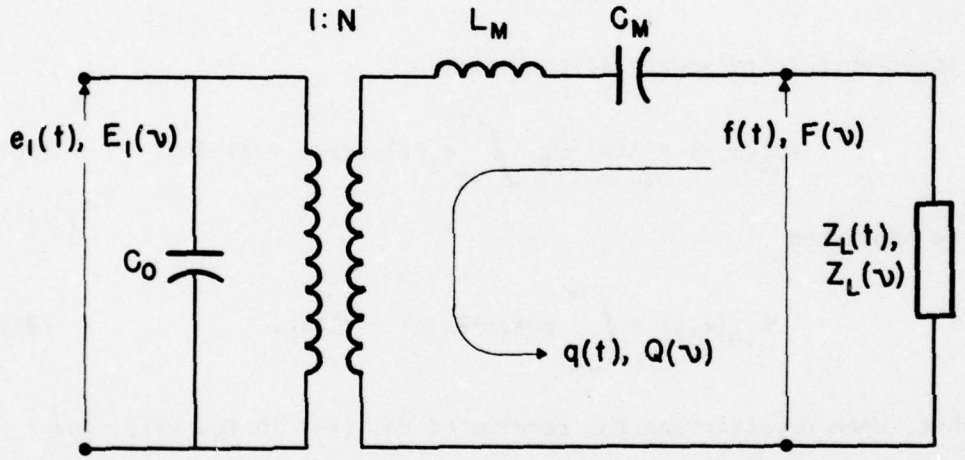

Fig. 9--Equivalent circuit of a ferroelectric cylindrical shell

for a radially poled ferroelectric tube that is plated with metal on its inner and outer curved surfaces. The input voltage $e_I(t)$, applied across these plated surfaces, produces the velocity $q(t)$ at the cylinder's outer curved surface. This surface is in contact with the fluid into which the transducer radiates. The inner curved surface of the cylinder is considered to be free, that is, uncoupled from the fluid surrounding the outside of the cylinder. The values of the circuit elements, C_O, C_M, and L_M shown in Fig. 9 are

$$C_0 = 2\pi L\epsilon_{33}^T[1 - (k_{31}^{\ell})^2]/h \tag{93a}$$

$$C_M = a_0 s_{11}^E/(2\pi Lh) \tag{93b}$$

$$L_M = 2\pi a_0 Lh\rho \tag{93c}$$

in which a_0, h, and L are, respectively, the mean radius, the thickness and the length of the ceramic tube. The quantities ϵ_{33}^T, k_{31}^{ℓ}, and s_{31}^E are, respectively, the dielectric permittivity, coupling constant and elastic compliance constant for the ceramic material of which the radially poled cylinder is composed. The coupling constant k_{31}^{ℓ} is given in terms of the piezoelectric constant d_{31} by the relation

$$k_{31}^{\ell} = d_{31}(s_{11}^E \epsilon_{33}^T)^{-\frac{1}{2}} . \tag{93d}$$

The quantity ρ in Eq. (93c) is the ceramic's density. The turns-ratio N of the equivalent transformer, coupling the electrical and mechanical parts of the circuit, is

$$N = 2\pi L d_{31}/s_{11}^E . \tag{93e}$$

The mechanical force f(t) that is produced acts across the radiation impedance $Z_L(t)$, which is the equivalent mechanical impedance owing to the reaction of the acoustic field on the transducer's radiating surface. The equivalent circuit shown in Fig. 9 gives a good description of the electromechanical behavior of the ferroelectric tube below the tube's lowest circumferential resonance frequency

$$\nu_{RES} = (2\pi)^{-1}(L_M C_M)^{-\frac{1}{2}} . \tag{94}$$

An actual line transducer incorporating such a ferroelectric tube as an active element has a more complicated electromechanical

circuit than the one depicted in Fig. 9. Additional electromechanical elements are always present. For example, there must be an electrical input cable to the transducer. Also there must be a structure supporting the ceramic tube and there must be added material, such as plates capping each of the tube's ends, which isolate the inside surface of the tube from the fluid. Such additional elements cause the electromechanical equivalent circuit representing the complete transducer to be a complicated multiresonant network. However, if the transducer is properly designed, all additional structural and electrical resonances will occur at frequencies well above the frequency ν_{RES} given by Eq. (94). For frequencies sufficiently below ν_{RES} then, an equivalent circuit looking essentially like that in Fig. 9 will adequately represent the actual line transducer, since the electromechanical behavior of the ferroelectric cylinder is the dominant factor in this frequency range.

The radiation impedance $Z_L(t)$ depends upon the behavior of the transducer's radiated pressure field at the vibrating cylinder's outer surface. For this reason, Z_L should be included in the spatial-network portion of the overall linear system, rather than be considered as part of the transducer's electromechanical network. It will be noted that Z_L, which is a time-dependent quantity, can be regarded as the input impedance of the spatial network. Robey [90] developed expressions, which show that both the real and imaginary parts of $Z_L(\nu)$, the radiation resistance and reactance in the frequency domain, have a complicated dependence on ν. However complicated the behavior of Z_L may be in the frequency domain, well below ν_{RES} its magnitude is always small compared to the magnitude of the cylinder's mechanical impedance

$$Z_M = j\omega L_M + (j\omega C_M)^{-1} , \qquad (95)$$

where $\omega = 2\pi\nu$. Therefore, below resonance the velocity component $Q(\nu)$ through Z_M will be little affected by the presence or absence of Z_L in the circuit. Moreover, as sample calculations made according to Eqs. (93b) and (93c) will show, for $\nu \ll \nu_{RES}$

$$(\omega C)^{-1} >> \omega L_M \ . \tag{96}$$

Since it is an impulsive velocity that is the input to the spatial network, one has, for the transfer function $H_E(\nu)$ in Eq. (88), the expression

$$H_E(\nu) = Q(\nu)/E_I(\nu), \tag{97}$$

where the harmonic voltage of amplitude E_I at frequency ν causes the harmonic velocity Q on the transducer's surface. Using the equivalent circuit and Eq. (96), one obtains the result that

$$H_E(\nu) = j2\pi\nu C_M N \tag{98}$$

for $\nu << \nu_{RES}$. Equation (98) can be written in the form

$$H_E(\nu) = \nu/B \ , \tag{99}$$

where the constant B can be expressed

$$B = (j2\pi a_0 d_{31}/h)^{-1} \tag{100}$$

after using Eqs. (93b) and (93e). At frequencies sufficiently below the circumferential resonance of the radiating cylinder, the transfer function $H(\mathbf{r},\nu)$ associated with the spatial network's impulse response can then be expressed as

$$H(\mathbf{r},\nu) = B\hat{H}(\mathbf{r},\nu)/\nu \ , \tag{101}$$

if one substitutes into Eq. (88) the result given in Eq. (99). Equation (101) expresses the important result that, for frequencies sufficiently below resonance, the transfer function associated with the line transducer's spatial impulse response is proportional to the

quotient of the transfer function of the total linear system and the frequency ν.

Suppose the white-noise electrical signal $e_I(t)$ is passed through an ideal bandpass filter before being applied to the input of the line transducer. Then the expression for the line transducer's input autocorrelation function, which corresponds to Eq. (89), is [91]

$$R_{II}(\tau) = S\Lambda \left[\frac{\sin(\pi\Lambda\tau)}{\pi\Lambda\tau} \right] \cos(2\pi\nu_M\tau), \tag{102}$$

in which

$$\Lambda = \nu_{UCO} - \nu_{LCO} \tag{103a}$$

and

$$\nu_M = \tfrac{1}{2}(\nu_{UCO} + \nu_{LCO}) , \tag{103b}$$

where ν_{UCO}, ν_{LCO} and ν_M are, respectively, the upper cutoff, lower cutoff and midband frequencies of the ideal filter's passband. Consider that the passband of the filter is such that ν_{UCO} is sufficiently below ν_{RES}. Then Eq. (96) will hold for all frequencies in Λ. Let the filtered noise voltage at the transducer's input be $e_S(t)$ and let the acoustic pressure that this produces at the point $\mathbf{r}$ be $p_S(\mathbf{r},t)$. Suppose this pressure at $\mathbf{r}$ is measured with a small acoustic receiver that has a uniform sensitivity M_R over a frequency band that is wider than Λ, given by Eq. (103a). If the pressure $p_S(\mathbf{r},t)$ generates the voltage $e_R(\mathbf{r},t)$ at the output of this receiver, then the input-output crosscorrelation function

$$R_{SR}(\mathbf{r},\tau) = \lim_{T\to\infty} \frac{1}{2T} \int_{-T}^{T} e_S(t) e_R(\mathbf{r},t + \tau)\, dt \tag{104}$$

can be expressed by the convolution

$$R_{SR}(\mathbf{r},t) = M_R \hat{p}(\mathbf{r},t) * k_{II}(t) , \tag{105}$$

where R_{II} is now given by Eq. (102). In the frequency domain, the expression equivalent to Eq. (105) is

$$\left.\begin{aligned} S_{SR}(\mathbf{r},\nu) &= M_R \hat{H}(\mathbf{r},\nu) S_{II}(\nu) , \quad \text{for } \nu_{LCO} \le \nu \le \nu_{UCO} \\ &= 0 , \quad \text{elsewhere.} \end{aligned}\right\} \tag{106}$$

In Eq. (106) the power density spectra S_{SR} and S_{II} are, respectively, the Fourier transforms of R_{SR} and R_{II}. If the result given by Eq. (101) is substituted into Eq. (106), one obtains the result

$$\left.\begin{aligned} H_u(\nu) S_{SR}(\mathbf{r},\nu) &= H(\mathbf{r},\nu), \quad \text{for } \nu_{LCO} \le \nu \le \nu_{UCO} \\ &= 0 , \quad \text{elsewhere} , \end{aligned}\right\} \tag{107}$$

in which H_u is the transfer function

$$H_u(\nu) = B(M_R S \nu)^{-1}, \tag{108}$$

with B given by Eq. (100). As one can see from a table of Laplace transforms, the impulse response function $h_u(t)$ corresponding to the transfer function H_u, which is given by Eq. (108), is the step function

$$h_u(t) = Au(t), \tag{109}$$

where A is the constant

$$A = (SM_R a_0 d_{31}/h)^{-1} . \tag{110}$$

Therefore in the time domain, one has from Eqs. (107) and (109) the important result that

$$p(\mathbf{r},t) = Au(t) * R_{SR}(\mathbf{r},t) \ . \qquad (111)$$

That is, the spatial impulse response of the line transducer is proportional to the convolution of a unit step function with the measured crosscorrelation function of the bandlimited white-noise voltage, which is applied to the input port of the transducer, and the voltage produced in a small receiver by the line transducer's radiated pressure field.

The line transducer's spatial impulse response $p(\mathbf{r},t)$ appearing in Eq. (111) is not precisely identical to that quantity appearing in Eq. (87). Since the bandlimited noise voltage $e_s(t)$ contains no frequency components outside the band Λ, the impulse response $p(\mathbf{r},t)$ determined using Eq. (111) will have no such frequency components either. Thus the impulse response $p(\mathbf{r},t)$, when determined using Eq. (111), is that replica of the line transducer's spatial impulse response that would be obtained if the spatial impulse response were passed through an ideal bandpass filter identical to the one which filtered the electrical noise voltage $e_i(t)$ to produce $e_s(t)$. Equation (111) expresses analytically the statement made earlier: a good approximation of an ideal line radiator's spatial impulse response can be determined experimentally by first measuring the input-output crosscorrelation function for a bandlimited white-noise voltage excitation of an actual line transducer and then modifying this correlation function by convolving it with the impulse response of a second linear system. The higher the actual line transducer's resonant frequency, the wider the noise bandwidth Λ can be taken and the more clearly should the measured waveform $p(\mathbf{r},t)$ reveal the features of the line source's spatial impulse response function.

CHAPTER VI

DESCRIPTION OF THE EXPERIMENTAL SYSTEM

The spatial impulse response of a line transducer was measured in a series of experiments that were conducted in a large water tank using bursts of pseudorandom noise. The measurement system used in these experiments will be discussed in a general way in this chapter. Those specific aspects of the experimental apparatus, which must be considered in detail in order to understand particular experimental results, will be discussed in the next chapter, along with the results themselves.

In this chapter, the line transducer for which the spatial impulse response was measured will be described first, along with relevant details of its mounting in the tank. Next, the tank and its experimental electronic suite will be discussed. This will be followed by a description of the realtime pseudorandom noisebursts used in the input-output correlation experiments and a discussion of how such noisebursts are generated using a computer. Relevant aspects of the computer programs for processing and analyzing the experimental data will then be discussed in a general way. Following this, a description of the receiving hydrophones used to detect the pressure field radiated by the line transducer will be given. One should mention here that the experimental system to be discussed utilized a considerable number of commercially available items. It would have been difficult, indeed, to achieve the experimental capability needed to measure a line transducer's spatial impulse response without the availability of such items. From the point of view of the experimental investigator, then, it is important to identify the commercial components in the system and to describe their use. In the interest of clarity, however, such an identification and description will not be included in the discussion to follow, but will be found instead in Appendix II.

The line transducer that was used as a source in the spatial-impulse-response experiments was a Type F36 [92-94] general-purpose line hydrophone. The configuration of the Type F36 hydrophone, which when electrically driven can serve as a line source, is shown in Fig. 10. This figure is taken from Ref. [92]. The actual Type F36 transducer used in the experiments, however, had a U-shaped wire attached to the plate at the end opposite the cable, rather than the plug-and-eye assembly shown in Fig. 10. The active portion of the Type F36 is comprised of an array of seven lead-zirconate-titanate (Clevite PZT-5) piezoceramic cylindrical shells, each endcapped with two glass disks. Electrically, the cylindrical shells are connected in parallel. Each shell has an outer diameter of 19.0 mm (0.75 in), a wall thickness of 160 mm (0.063 in), and is 19.0 mm (0.75 in) long. The cylinders are spaced 28.6 mm (1.125 in) between centers. Each glass-disk endcap is 2.29 mm (0.090) thick. The length of the active portion of the transducer, measured between the outermost endcap surfaces, is 195.1 mm (7.68 in). Each piezoceramic cylinder in the active array is supported within a framework of six steel rods by means of a rubber support ring. The entire assembly is enclosed in a butyl rubber boot that is filled with de-aerated castor oil. The outer diameter of the boot is 44.5 mm (1.75 in). The overall length of the Type F36 transducer used, exclusive of the bushing at the cable end and of the U-shaped wire at the opposite end, is 266.7 mm (10.5 in), which is slightly larger than the corresponding dimension of 254.0 mm (10.0 in) shown in Fig. 10.

As a source, the Type F36 is designed to have a useful frequency range of from 1 to 20 kHz. Figure 11, taken from Ref. [93], shows the transmitting voltage response of the Type F36 transducer that is used in the experiments [95]. The response curve rises steadily at 12 dB-per-octave, except in the vicinity of the first electromechanical resonance of the transducer, which occurs near 24 kHz. The transmitting-voltage-response calibration, shown in Fig. 11, gives the pressure at one meter from the Type F36 per volt applied at the end of the 29m (95 ft) cable

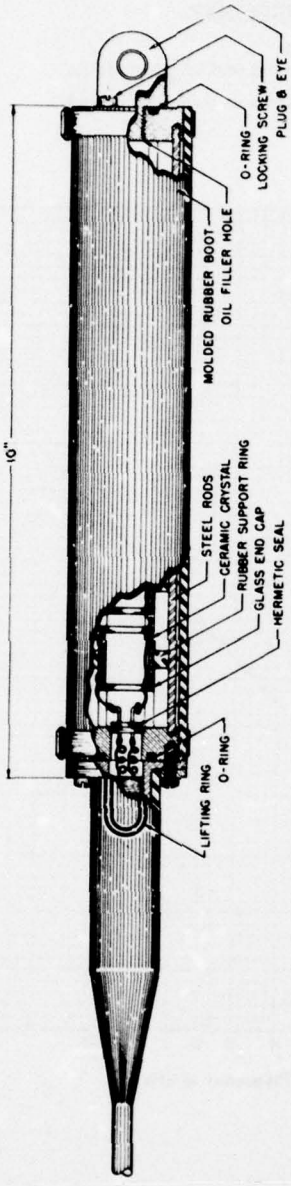

Fig. 10--Type F36 transducer

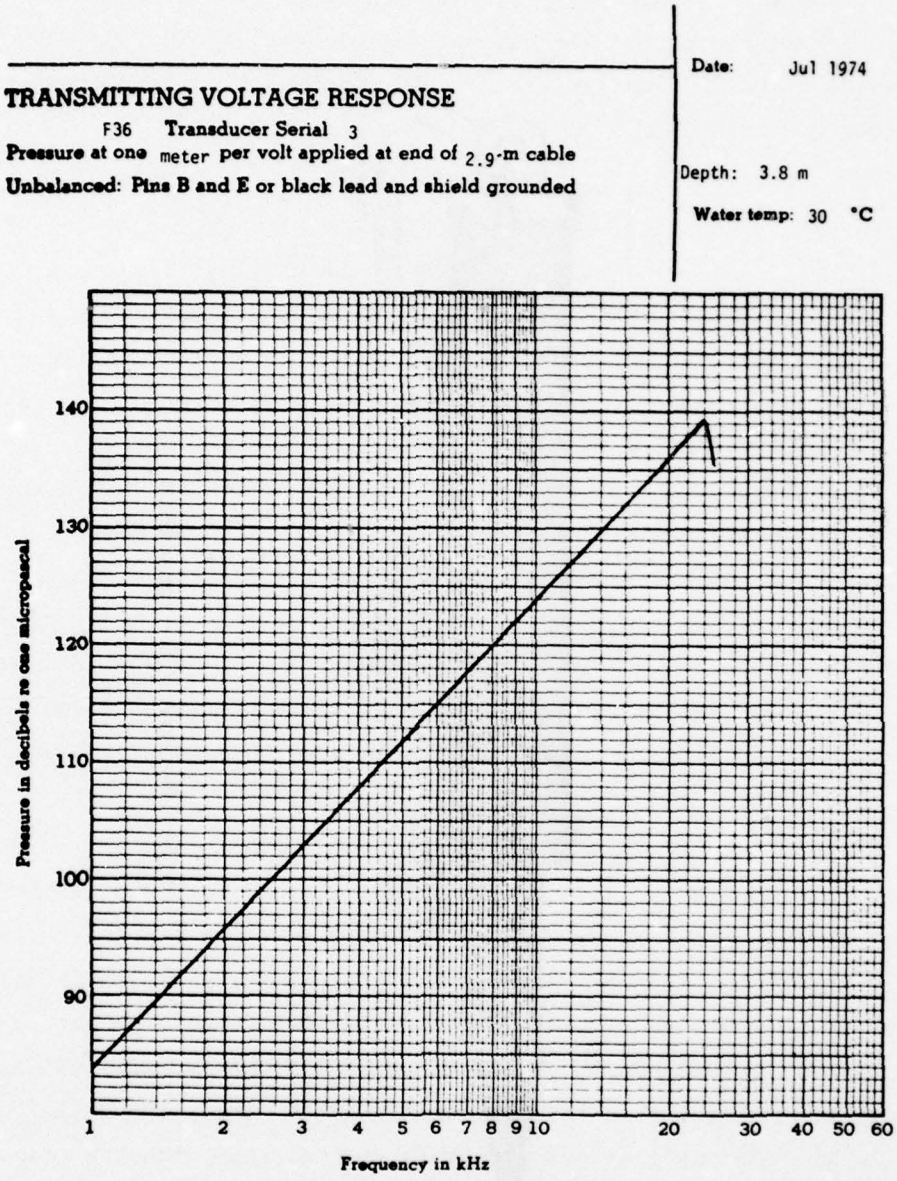

Fig. 11--Transmitting voltage response of the Type F36 transducer

attached to the transducer. The attached cable is a neoprene-sheathed, shielded, twisted pair. The nominal capacitance of the Type F36 transducer with 30.5 m (100 ft) of cable is 600 μF. The DC-resistance is greater than 200 MΩ.

If the Type F36 transducer is to be used as a line source in spatial-impulse-response experiments, it must be mounted so that its line of axial symmetry can be rotated in the horizontal plane about a vertical axis that passes through the center of its seven-element active array. The mounting system that is shown in Fig. 12 was designed and built for this purpose. The mounting system is comprised of a supporting section, shown at the top of the figure, an alignment section, shown at the center, and a transducer-mounting section, shown at the bottom. Use of this design allows the Type F36 transducer to be supported in a horizontal position and enables one to rotate and translate the transducer in the horizontal plane HH'. At the same time, a mounting with the configuration shown will reflect very little of the sound radiated by the transducer to a measuring receiver that is located in the plane HH'. It is important to minimize sound reflection from the supporting assembly, since reflected signals can obscure the structure of the source's spatial impulse response.

The Type 36 transducer is held at the end of the 31.8 mm (1.25 in) diameter lower mounting arm, which is 457.2 mm (18.0 in) long. Part of the center of the arm was cut away and the remaining 152 mm (6 in) portion of this arm, that end closest to the transducer, was bored out to form a tube. A slot wide enough to pass the cable of the Type F36 was machined through one wall of this tubular portion of the arm. The cable bushing of the Type F36 was inserted into this slotted tube with the transducer cable passing out through the cut-away part of the arm. The slotted tube was then tightly compressed over the cable bushing on the Type F36 by means of strap-type hose clamps (Punch-lock). The other end of the lower mounting arm has an axial threaded hole that mates with the screw on an

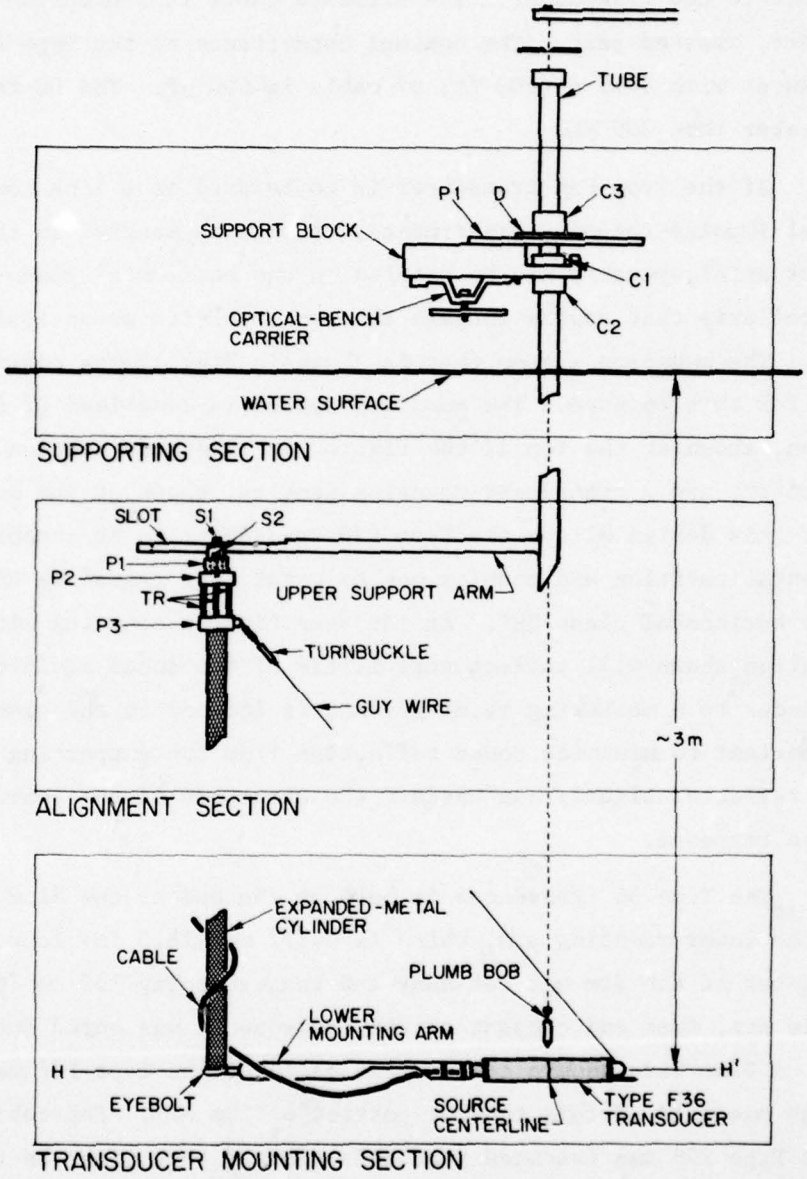

Fig. 12--Mounting system for the Type F36 transducer

eyebolt. The eyebolt is welded to the lower end of a vertical cylinder that is 2.44 m (8 ft) long and 41.4 mm (1.63 in) in diameter. This cylinder is made from 1.6 mm thick expanded-metal sheet. The expanded metal has 67 percent open area and the cylinder fabricated from it thus forms an acoustically transparent support. The lower mounting arm also will not significantly distort the radiated field of the Type F36 in the plane HH', except possibly in the direction of the expanded-metal cylinder, since the diameter of the arm, including the clamps, is less than that of the Type F36 transducer. Moreover, the arm was bored through so that no air can remain trapped in the threaded hole that mates with the eyebolt. Also portions of the arm are machined away so that there are no flat surfaces normal to its axis to cause reflections in the direction of the transducer. The upper end of the transducer mounting assembly is formed from a 3.05 m (10 ft) long tube, 38.1 mm (1.5 in) in diameter. To the lower end of this tube is welded the upper support arm. Screw S1 passes through a longitudinal slot cut vertically in the free end of this upper support arm. This screw clamps the alignment assembly, comprised of the plates P1, P2, and P3 and the four threaded rods TR, to the support arm at any desired position. Plate P3 is welded to the expanded-metal cylinder that holds the lower mounting arm and the Type F36 transducer.

If the axis of the upper 3.05 m tube is vertical, then the mounting system depicted in Fig. 12 can be aligned so that the Type F36 may be rotated in the plane HH' about its center when the tube is rotated about its axis. In order to so align the mounting system, a plumb line is lowered down the axis of the tube. By clamping the alignment assembly to the upper support arm in the proper position, by rotating and tilting the expanded-metal cylinder, using screws S2 and the threaded rods TR, and by tightening the supporting guy wire, using the turnbuckle, one can bring the center of the Type F36 directly under the plumb bob with the axis of the source horizontal. The plane of this axis is established with a spirit level. Alginment of the mounting system

was a two-person operation, with one observer at the Type F36 checking the spirit level and the position of the plumb bob with respect to the center of the Type F36, while the second worker made the necessary adjustments in the alignment section. For this reason, the alignment could not be made in situ. Instead, the system was aligned outside the water tank in which it is used. It was then carefully transported to the water tank and then re-mounted in exactly the same position that it had during the alignment process.

The upper tube of the mounting system is held by the support block shown in the upper part of Fig. 12. The tube is clamped between the two collars C1 and C2, which hold it vertical. The end of the support block is bifurcated. The two arms of this block support collar C1, with the tube passing between them. The plate P1, mounted on the support block, has a V-slot cut into it, which keeps the axis of the tube from shifting its position when the tube is rotated. Collar C3, clamped to the tube, has a divided circular scale D attached to it. When the tube is rotated, this scale is used to determine the transducer's angular orientation. The support block is bolted to an optical-bench carrier. The carrier may be moved along a two-meter optical bench, which is mounted above water surface.

Measurements on the Type F36 source were made in a large cylindrical water tank, with the transducer at a depth of approximately 3 m (10 ft). The water tank used has an inside diameter of 7.09 m (23.25 ft) and a height of 6.71 m (22.0 ft). The usual water depth in the tank is approximately 6.2 m (20.5 ft). The tank is made like a large barrel, having staves of cypress wood, 10 cm (4 in) thick, bound with steel hoops. The tank is free-standing in a large warehouse-like building. A utility building, also free-standing and accessible by a stairway, is built over the tank. The tank is filled with filtered fresh water from the city mains. Once the tank is filled, the water is circulated through a filter and kept chlorinated at a free chlorine level of 0.5 parts per million. Since the warehouse-like building in which the tank is located is neither

heated in the winter nor cooled in the summer, the temperature of the tank water shows seasonal variations. Owing to the mass and heat capacity of the water volume, 246 kl (65100 gal), however, short-term fluctuations in the air temperature do not affect the water temperature in that region of tank in which the Type F36 source and the measuring receiver are located. During the course of any experiment, the water temperature is continually measured by lowering a mercury-in-glass thermometer near the Type F36 and reading the scale by means of a small telescope that is mounted just above the water surface.

The one-room utility building over the tank houses the transducer-positioning equipment and the electronic instrumentation used in the spatial-impulse-response experiments. This instrument room is temperature controlled. One has access to the water tank through a 1.8 m by 4.7 m (5.8 ft by 15.3 ft) rectangular well in the floor. Figure 13 shows a general view of the interior of the instrumentation room. The two-meter optical bench holding the Type F36 mounting system is seen at the center of the picture, with the vertical upper tube of the Type F36 mounting assembly at its center. Other pieces of the experimental apparatus seen in the picture will be discussed at the appropriate time.

Since the radiated field of the Type F36 is to be measured in a confined volume of water, the input-output experiments must be done using pulses or "bursts" of noise having a finite duration so that the effects produced by sound reflection from the tank walls and bottom and from the water surface can be separated from those produced by the sound that is directly radiated to a receiver by the Type F36. Using the dimensions of the cylindrical tank previously described and a value [96] for the sound-speed at 20°C of 1482.343 m/s, one can calculate that the maximum reflection-free pulselength, which can be achieved in a transmission between a point source and a point receiver in the tank, is 4.2 ms. This could only be achieved if the source and receiver were coincident at the center of the tank. Similar calculations show that, for transmission

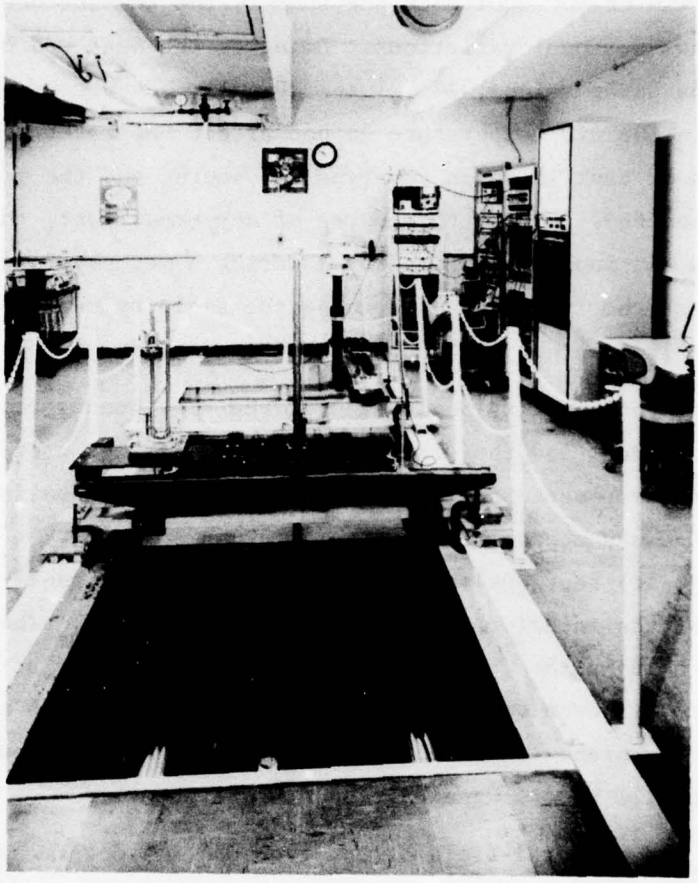

Fig. 13--Water-tank laboratory area

between a point source and receiver at separations of 1 m, 2 m, 3 m, and 4 m, the maximum obtainable reflection-free pulselengths are, respectively, 3.6 ms, 3.1 ms, 2.7 ms, and 2.1 ms. The calculations are based upon the premise that the source and receiver are midway between the water surface and the tank bottom and that the source and receiver are symmetrically disposed with respect to the axis of the cylindrical tank. Under all other circumstances, the maximum pulselengths attainable for these source-to-receiver separations will be less. They will also be less when an extended source, such as the Type F36, is used.

An electronic system was developed and installed in the utility

building above the water tank. This system is capable of generating the noise pulses or "noisebursts" needed in the spatial-impulse-response experiments and of digitally recording the waveforms both of the noise signals supplied to the Type F36, and of the corresponding signals generated in the receiver by the radiation from this source. The electronic instrumentation suite used in the spatial-impulse-response experiments appears at the top right in Fig. 13. A rudimentary block diagram of this instrumentation suite is depicted in Fig. 14. Five main subsystems comprise the electronic system. A pulse-generating subsystem accepts digital data written on magnetic tape. Using the digital data, this subsystem generates an analog signal that is supplied as an input to the Type F36 source. The radiated field produced by the Type F36 is detected by the receiver. The output of the receiver is suitably amplified and processed by the receiver subsystem, and supplied to the waveform-recording subsystem.

The waveform-recording subsystem accepts an analog voltage as an input, digitizes this, and records the digital replica on punched paper tape. The signal from the receiving subsystem, which is the Type F36 output signal, is digitally recorded in this way. In addition, two kinds of input signals to the Type F36 are also digitally recorded by means of this subsystem. These two input signals are voltages proportional, respectively, to the input voltage and to the input current supplied to the Type F36. A Hall-effect current-probe device is used to measure the Type F36 input current. This device produces an output voltage that is proportional to whatever current flows in the conductor passing through the probe head.

A digital timing subsystem supplies the proper clock and trigger signals to the pulse-generating, the receiver, and the waveform-recording subsystems. All subsystems operate in complete synchronism, since they are all controlled by a single clock unit that is part of the timing subsystem. The computer, shown at the top of Fig. 14, is the last of the five subsystems. The computer generates the digital input data for

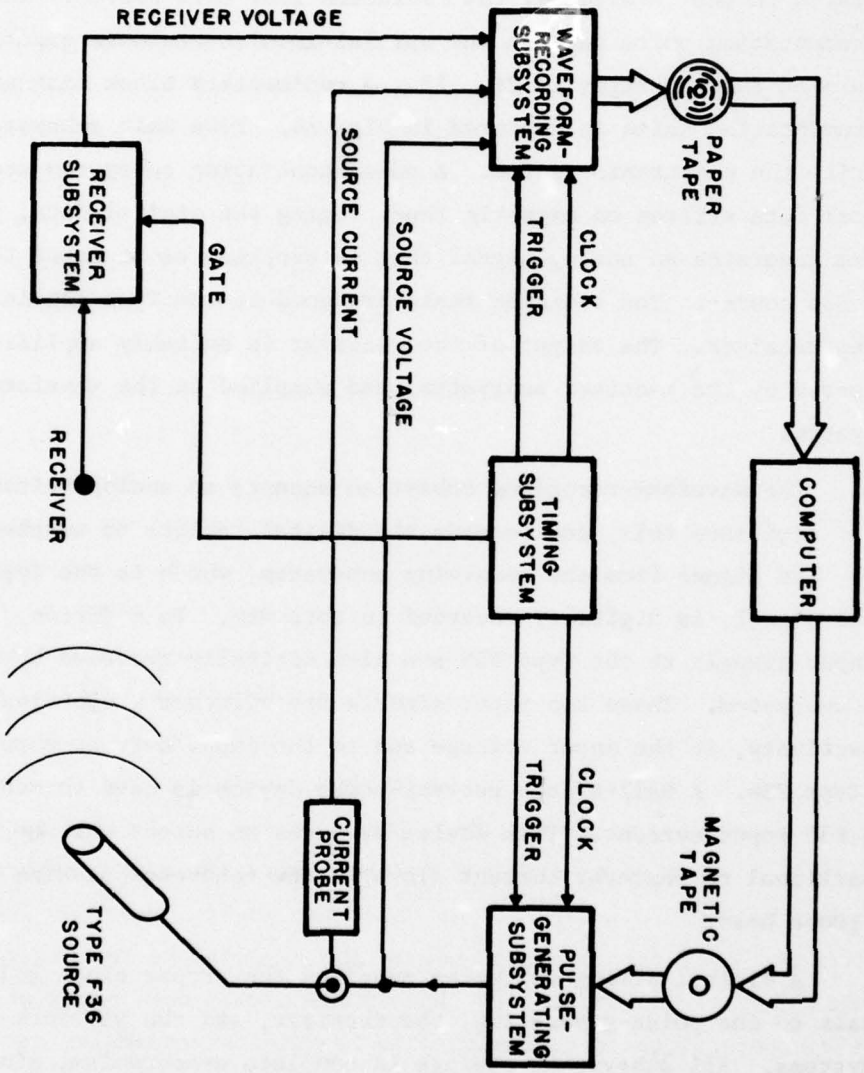

Fig. 14--Electronic instrumentation suite

the pulse-generating subsystem and processes the digital data recorded using the waveform-recording subsystem. All computation is done off-line by a large computer [97] that is not located in the tank utility room as are the other four subsystems comprising the instrumentation suite. In what follows, each of the subsystems will be described in greater detail.

Figure 15 depicts the instrumentation comprising the pulse-generating subsystem that appears in Fig. 14, the electronic-system block diagram. Digital replicas of the noisebursts that serve as inputs to the Type F36 are generated by the computer and stored on the magnetic tape depicted at the top of Fig. 15. Each noiseburst used in the experiment is written on the tape as all or part of a 4096-word record, preceded by an end-of-file mark. The 16-bit words in any record represent, in digital form, samples of the noiseburst that is an input signal to the Type F36. After the magnetic tape is loaded on the tape transport, any desired file can be selected by means of a thumbwheel switch on the buffer/interface unit. The noiseburst record corresponding to this file is then read into a 4096-word semiconductor memory in the buffer/interface, under the control of this latter device. Since any particular noiseburst may be specified by fewer than 4096 samples, the memory word corresponding to the first noiseburst sample, as well as the number of words in the complete noiseburst record, are each set by means of thumbwheel switches on the panel of the buffer/interface. A train of clock pulses and a train triggering pulses is also supplied to the buffer/interface. After one enables the buffer/interface, each triggering pulse causes the digital data stored in the memory to be transmitted to the digital-to-analog converter. The clock pulses control the rate at which the 16-bit memory words are read out from the buffer/interface memory and supplied to the digital-to-analog converter. Thus, each clock pulse causes one sample of the digitized noiseburst to be transmitted to the digital-to-analog converter until the complete digitally represented noiseburst has been transmitted. The transmission begins at the first word selected by the thumbwheel switch on the buffer/interface panel and terminates when the selected

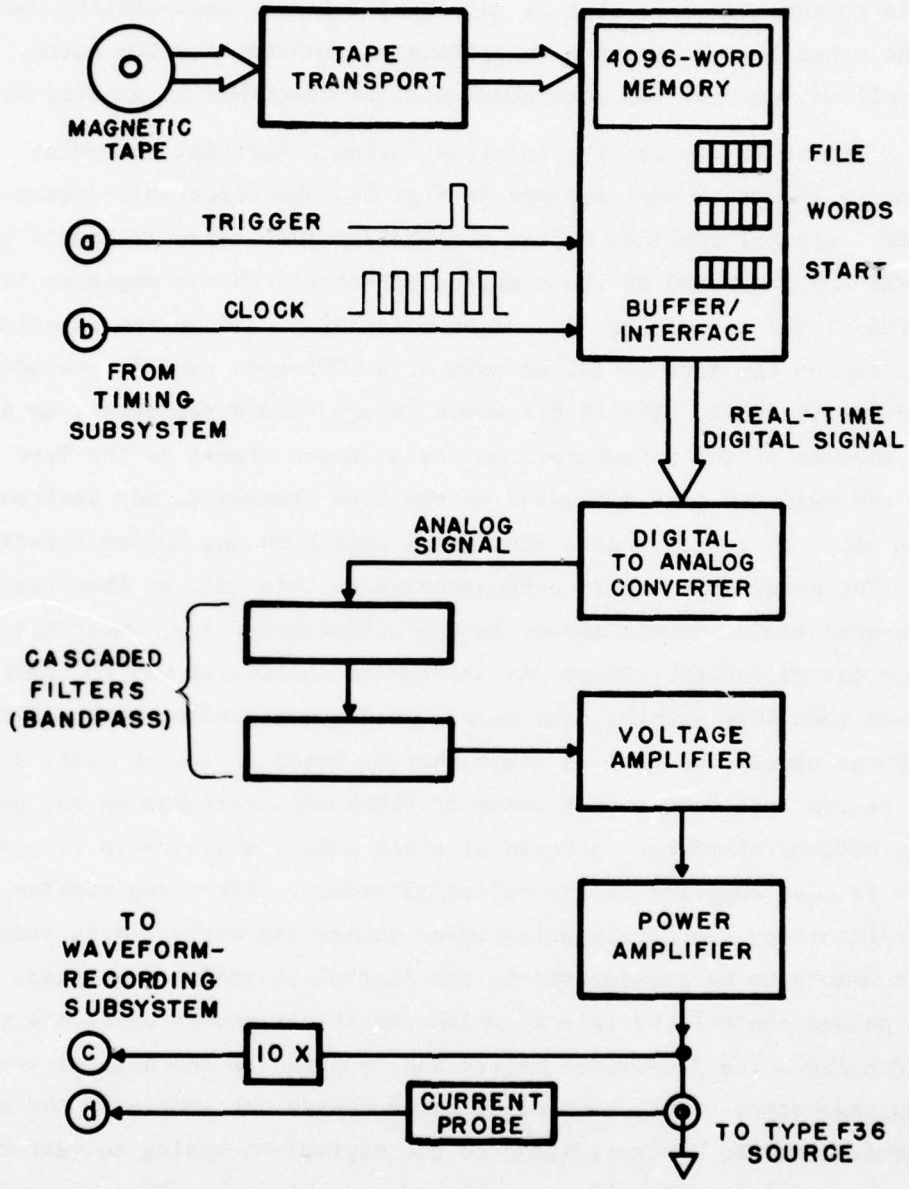

Fig. 15--Pulse-generating subsystem

number of words have been read from memory. After the last specified word is read from memory, the buffer/interface remains quiescent until the next triggering pulse occurs. At this time, the specified number of words is again transmitted seriatium at the clock frequency to the digital-to-analog converter, generating again a replica of the particular noiseburst that is stored in the buffer/interface memory. To produce some different noiseburst, one inhibits the buffer/interface triggering and stops the output from the unit. One then reads the file corresponding to the digital replica of this new noiseburst, from the tape on the transport, into the buffer/interface memory. Once the proper starting word and proper number of samples for this record have been selected via the thumbwheel switches, the buffer/interface is again enabled. The trigger pulses will now repetitively transmit replicas of the new noiseburst to the digital-to-analog converter.

The digital-to-analog converter accepts the sequential digital output of the buffer/interface memory and, using this, generates an analog voltage that replicates the computer-generated noiseburst. Since the digital-to-analog converter in the pulse-generating subsystem is a 12-bit device, only the 12 most significant of the 16 bits in each buffer/interface memory word are used in generating an analog replica. The response characteristics of the digital-to-analog converter limit the maximum frequency at which a 12-bit digital word can be converted to an analog voltage. With the converter used, the data can be read from the buffer/interface memory at a maximum rate of 200 kHz, so that the minimum permissible interval between the clock pulses supplied to the buffer/interface is 5 μs. The spectrum of an analog noiseburst, produced from digital samples supplied at 5 μs intervals, can extend to a maximum upper frequency of 100 kHz, exclusive of the higher-frequency spectral components that are introduced by the digital-to-analog conversion process itself, owing to transient effects.

Cascaded filters are used to bandpass-filter the analog output signals from the digital-to-analog converter. The purpose of these filters is threefold. First, the high-frequency transient artifacts

of the digital-to-analog conversion process must be removed from the noisebursts by lowpass filtering these signals. Second, as a precaution against the introduction of spurious low-frequency coherent signals at the 60 Hz powerline frequency and at harmonics of this frequency, the noisebursts are also highpass filtered. Finally, lowpass filtering is necessary to ensure that all of the spectral components in the noisebursts, with frequencies higher than the first electromechanical resonance frequency of the Type F36 transducer (24 kHz, nominally), have negligibly small amplitudes.

Signals from the digital-to-analog converter are passed through three stages of lowpass filtering and one stage of highpass filtering. The frequency characteristics of each filter stage closely approximates those of an ideal four-pole Butterworth filter. That is, each stage has a passband with unity gain and has an attenuation slope of -24 dB-per-octave, either above or below the cutoff frequency, depending upon whether one is considering a lowpass or a highpass stage. The cutoff frequency of the filter stage is that frequency at which the amplitude of the filter's output voltage, owing to the filter's response characteristics, is 3 dB less than the amplitude of the filter's input voltage. The single highpass stage was set to have a cutoff frequency of 950 Hz, while each of the three lowpass stages has a cutoff frequency of 20 kHz. Thus, the three cascaded lowpass stages have a combined frequency response such that the output voltage is down 9 dB with respect to the input voltage at 20 kHz and have a combined attenuation slope of -72 dB-per-octave above this frequency.

Preliminary measurements with the experimental system had shown that it is necessary to have such a sharply cutoff lowpass response characteristic when filtering the noisebursts that are used as inputs to the Type F36. The filter characteristics used represent a compromise between attainment of a maximum input signal bandwidth and simultaneous rejection of all spectral components near and above the transducer's first electromechanical resonance frequency. Referring to Eq. (102) of

the previous chapter, one sees that the peak of the input autocorrelation function R_{II} becomes wider as the upper cutoff frequency ν_{UCO} diminishes. Thus, the narrower the spectral bandwidth of the input noiseburst to the Type F36, the poorer will be the resolution of the features in the spatial impulse response function. On the other hand, if spectral components in the noiseburst can electromechanically excite the Type F36 at frequencies higher than that of its first resonance, the consequent radiation at these high frequencies will obscure the form of the source's spatial impulse response.

A three-stage cascade filter, with all stages having identical four-pole Butterworth response characteristics, has an overall response characteristic given by the expression [98]

$$V/V_P = [1 + (\nu/\nu_{3dB})^{2p}]^{-N/2} \tag{112}$$

or by the equivalent expression

$$(V/V_P)_{dB} = -(10N)\log[1 + (\nu/\nu_{3dB})^{2p}] \ , \tag{113}$$

with the number of stages N here equal to 3 and the number of poles P here equal to 4. In Eqs. (112) and (113), the quantity V is the filter's output voltage amplitude at the frequency ν and the quantity V_P is the peak output-voltage amplitude that occurs for frequencies within the filter's passband. The frequency ν_{3dB} pertains to a single stage of the filter. It is at this frequency that the output-voltage amplitude is 3 dB lower than the amplitude of the peak voltage occurring in the passband of the stage. In the case in question, ν is 20 kHz for each stage. Using Eq. (113), one calculates that the attenuation produced by the three-stage cascaded filter at 24 kHz, the first electromechanical resonance frequency, is -21.7 dB. Also, one calculates that the -3 dB point on the overall frequency response characteristic of the three-stage filter occurs near 16.9 kHz. Thus, by using the three-stage lowpass

filter, a sufficient, though modest, rejection of the unwanted higher spectral components in the noisebursts is attained, without too severely reducing the bandwidth of the noisebursts.

The output of the filters is passed, via a voltage amplifier, to the input of a 50 W power amplifier. The gain of the voltage amplifier is adjusted so that neither the Type F36 transducer nor the receiving circuits operate in a nonlinear region. The Type F36 is driven directly from the output of the power amplifier. Measurement demonstrated that the power amplifier, when directly driving the Type F36, behaved as a constant-voltage source to within ±0.12 dB over the frequency range from 900 Hz to 24.0 kHz. Such a constant-voltage input to the line transducer was assumed in the analysis previously given in Chapter V.

The input voltage and input current to the Type F36 are measured at the output terminals of the power amplifier, thus excluding the system characteristics of the pulse-generating electronics from the linear system whose impulse response is to be determined. In other words, all modifications to the digitized noiseburst that originally resides on magnetic tape, which are introduced by the electronic system that intervenes between the tape and the transducer's input, are included in the measurement of the transducer's input signal. Since the output voltage of the power amplifier in the experiments is typically in the range of 50 V to 100 V, however, it is necessary to use a voltage-divider network when supplying the transducer input voltage to the waveform-recording subsystem. A high-impedance oscilloscope voltage probe with an attenuation factor of 10 was found suitable for this purpose.

After the acoustic transmission of a noiseburst between the Type F36 and the measuring receiver takes place, the receiver's output voltage is processed by the receiver subsystem that is depicted in Fig. 16. First, the receiver's output voltage is amplified using a sensitive voltage amplifier, operated in a differential mode with a balanced input. Both the differential amplifier circuit within this

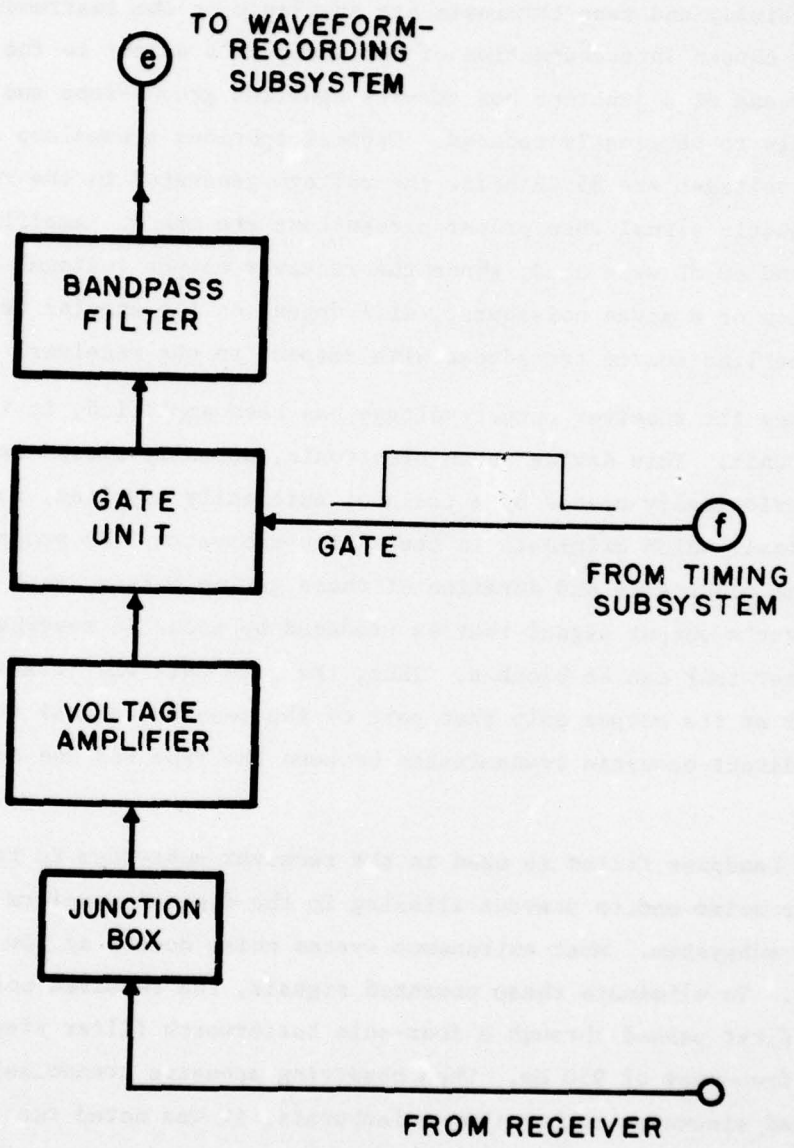

Fig. 16--Receiver subsystem

instrument and its power supply are enclosed by a metal shield, separate from the instrument case and from the circuit chassis. Since separate chassis, shield, and case terminals are available on the instrument panel, a properly chosen interconnection of the receiver's output to the amplifier input by means of a junction box permits spurious ground-loop and crosstalk signals to be greatly reduced. Typical spurious groundloop and crosstalk voltages are 35 dB below the voltage generated in the receiver by the acoustic signal when proper precautions are taken. Amplifier gains of 40 dB and 60 dB were used, since the receiver output voltage, for transmission of a given noiseburst, will depend on the angular orientation of the line-source transducer with respect to the receiver.

Once the receiver output voltage has been amplified, it is passed to a gate unit. This device is an electronic, normally closed switch that is periodically opened by a train of externally supplied, rectangular gating pulses, which originate in the timing subsystem. By properly setting the occurrence and duration of these gating pulses, that part of the receiver's output signal that is produced by acoustic reverberation in the water tank can be blocked. Thus, the gate unit will transmit to the filter at its output only that part of the received signal that is due to a direct acoustic transmission between the Type F36 and the receiver.

A bandpass filter is used in the receiver subsystem to reduce extraneous noise and to prevent aliasing in the digital waveform-recording subsystem. Most extraneous system noise occurs at low frequency. To eliminate these unwanted signals, the received noiseburst is first passed through a four-pole Butterworth filter stage with a cutoff frequency of 950 Hz. When observing acoustic transmissions, using gated sinewaves rather than noisebursts, it was noted that high-frequency effects also were present near the onset and the termination of the signals received from the Type F36. Similar high-frequency effects were also noted near the onset and termination of the input-current signal to this source. It is possible that such high-frequency

effects are produced owing to the fact that the source's radiation impedance is a time-varying parameter. If this is the case, such high-frequency spectral components will also be present in transmitted noisebursts. Since the waveform-recording subsystem samples the signals that it digitizes at 5 μs intervals, such high-frequency spectral components, if not suppressed, could alias the data that this subsystem digitally records. For this reason, all signals used as inputs to the waveform-recording subsystem, including the gated receiver output voltage, are lowpass filtered using a four-pole Butterworth stage with an upper cutoff frequency of 24 kHz. This filter stage attenuates spectral components at 100 kHz, the highest allowable signal frequency when using a 5 μs sampling interval, by 49.6 dB and all components of higher frequency to an even greater degree. Therefore, as a result of this lowpass filtering, the aliasing introduced into the digitized waveforms will be negligibly small.

The waveform-recording subsystem, depicted in Fig. 17, is comprised of a transient recorder, an interface unit and tape formatter, and a paper-tape perforator. An input signal to the transient recorder is sequentially sampled by an internal sample-and-hold circuit, the output of which is digitized by an analog-to-digital converter. Digitized samples of the input signal are stored sequentially in a 2048-word memory at the sampling frequency. The sampling frequency of the transient recorder is controlled by an externally supplied train of pulses occurring at 5 μs intervals. The sampling pulsetrain originates at the timing subsystem, as does the triggering pulse, which initiates the sampling of the input signal supplied to the transient recorder. Digitization by the transient recorder quantizes the input signal amplitude to 8 bits.

Once the digitized signal is stored in the transient recorder's memory, it can be transmitted asynchronously word-by-word at low speed to the paper-tape perforator. An interface unit controls this data transmission. On the paper tape produced by the perforator, resides a sampled 8-bit digital representation of the input noiseburst supplied

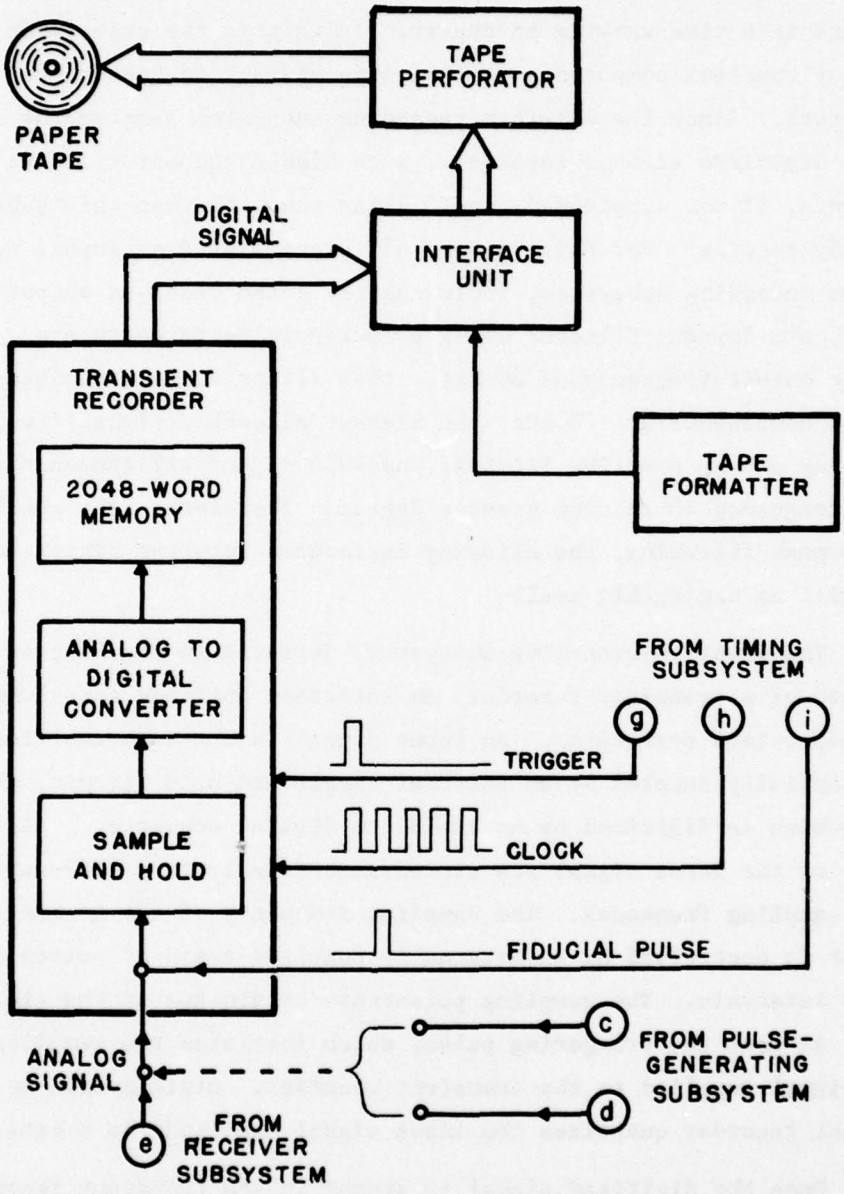

Fig. 17--Waveform-recording subsystem

to the transient recorder. Each experimental noiseburst so digitized can be labeled on the paper tape with extra characters supplied by a paper-tape formatting unit.

One additional timing signal is generated by the timing equipment and transmitted to the waveform-recording subsystem. This timing signal is a fiducial pulse that is added to each input noiseburst on the signal baseline prior to the onset of the burst itself. This fiducial pulse has a width of less than 5 μs and a fixed delay relative to the triggering pulse that is supplied to the buffer/interface to initiate the output of that noiseburst. When a noiseburst is digitized by the waveform-recording subsystem, the fiducial-pulse amplitude is digitized also and stored in a single word in the transient recorder's memory. If the digital record of a noiseburst is examined, this fiducial word is easily distinguished from the digitized record of the noiseburst's baseline that immediately precedes it and follows it. When many noisebursts are digitized in the course of an experiment, this fiducial pulse on each record is used to establish a reference time common to all pulses. It can also be used to determine that a change has occurred in the sequence of timing pulses that go from the timing subsystem to the other devices in the system.

The timing subsystem, depicted in Fig. 18, generates the timing signals needed by all other subsystems. All timing signals are derived digitally from a single 200 kHz sinewave that is generated by a frequency synthesizer. The synthesizer derives this highly stable, spectrally pure sinewave from a crystal-controlled 5 MHz clock. The 200 kHz signal, as well as any other sinusoidal signal from the synthesizer, is phase-locked to the 5 MHz reference frequency. Since all timing signals are derived from one and the same sinusoidal signal, all devices in the system operate in complete synchronism. The 200 kHz clock pulsetrains, which are needed by the buffer/interface for transmitting the digital data and by the transient recorder for sampling the incoming waveforms, are produced by using the 200 kHz sinewave as the input to the externally synchronized pulse generator that is labeled PG1 in Fig. 18. From the output of PG1,

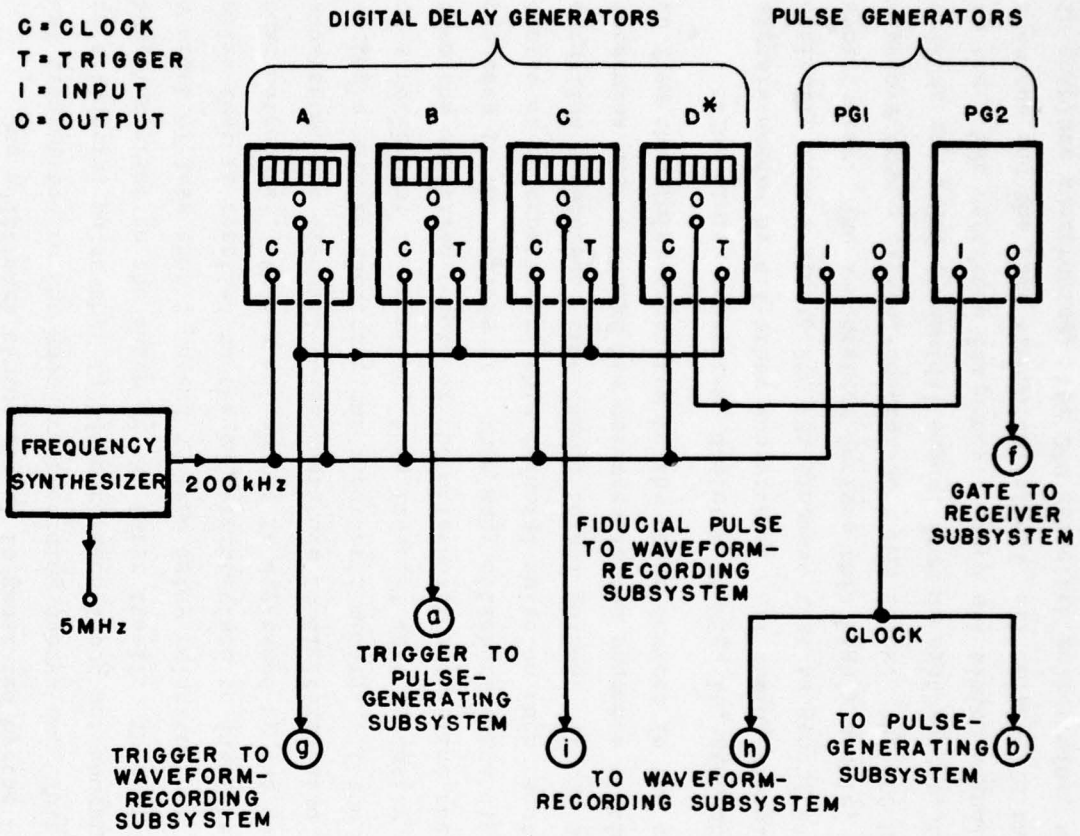

Fig. 18--Timing subsystem

emanates a train of short pulses at 5 μs intervals. The duration of each pulse is determined by the pulse-generator control settings.

All other timing pulses produced by the timing subsystem also occur repetitively. The repetition rate for all these other pulses is the same, but there are various delays inserted by the timing subsystem between corresponding pulses that are transmitted to different parts of the experimental system. For example, the triggering pulse supplied to the transient recorder in the waveform-recording subsystem must be transmitted prior to transmitting the triggering pulse to the buffer/interface unit in the pulse-generating subsystem. The repetition rate of all the triggering pulses is ultimately determined by the acoustic reverberation time in the water tank. After a noiseburst is generated and radiated by the source, a sufficiently long time must elapse for all the signals, which are multiply reflected from the boundaries of the water volume, to decay to an imperceptible amplitude. If the noiseburst is again generated, by again triggering the buffer/interface, before this decay is complete, then the reverberant sound field owing to the previously generated noiseburst will interfere with signal directly transmitted from the source to the receiver.

The pulse repetition rate was derived digitally from the 200 kHz sinewave by using the digital delay generator, labeled A in Fig. 18, as a preset counter. The 200 kHz sinewave is supplied to both the C and T inputs of the digital delay generator and a divisor N is chosen by means of thumbwheel switches on its panel. For every N clock pulses input, the delay generator produces a single pulse at its output terminal O. In the experiments, the divisor chosen was N = 100000, so that the pulse repetition frequency was 2 Hz, or one pulse every 0.5 s.

The output signal from digital delay generator A is transmitted to the waveform-recording subsystem to serve as a trigger and is also supplied as a trigger to the T terminals of three other digital delay generators, which are labeled B, C, and D* in Fig. 18. The 200 kHz

sinewave is the input to the clock terminals C of these same delay generators. Each of the two digital delay generators labeled B and C then produces a pulse that is delayed with respect to the triggering pulse supplied to the terminal T. The delay obtained using a given delay unit will be equal to N_p clock pulses, with the number N_p predetermined by the setting of the thumbwheel switches on the panel of that delay unit. Thus can delayed pulsetrains at a 2 Hz repetition rate be supplied by digital delay generator B, to trigger the pulse-generating subsystem, and by C, to provide the fiducial pulse to the waveform-recording subsystem.

The operation of digital delay generator D* is slightly different, since this unit is internally modified. Rather than generate an output pulse that is N_p clock pulses delayed with respect to its triggering pulse, this unit produces, instead, a rectangular pulse that is N_p clock pulses long. This rectangular pulse, with a digitally determined duration, is then transmitted to pulse generator PG2, which produces a replica pulse of sufficiently high voltage to drive the gate unit in the receiver subsystem.

It was mentioned earlier that a large computer is also a subsystem of the experimental instrumentation suite. Both the pulse-generating subsystem and the waveform-recording subsystem communicate with the computer--the former by means of magnetic tape and the latter by means of punched paper tape. The computer's most important task is to perform the correlation-function computations that are needed in order to obtain the spatial impulse response function of the Type F36 source. Before discussing such correlation computations, however, it is appropriate to consider, first, the computer's other function, namely, generation of the digital pseudorandom noisebursts that are the input signals to the pulse-generating subsystem.

A broadband, white-noise process is to be simulated by an equivalent pseudorandom process. If a true random-noise signal were used to

form the requisite noisebursts, such noise would be required to exhibit a constant power density spectrum over a frequency band encompassing the operational bandwidth of the Type F36 transducer. If this true random noise were obtained from an electronic random-noise generator, the probability density function of its amplitude would be, approximately, Gaussian. Moreover, if the noise generator were properly designed, its output would be stationary in the sense that this probability density function, as well as the power density spectrum of the noise, would not change with time. The experiments to be reported here require a set of pseudorandom, digitally generated noisebursts that are indistinguishable from bursts of true random noise, such as would be created by gating the output of a broadband electronic noise generator. Pseudorandom noisebursts, which simulate a gated, broadband, white-noise, normal process can be digitally generated on the basis of the following theoretical ideas.

Suppose one considers the stochastic process that is described by the ensemble of functions $X(t,\zeta)$, in which t denotes the time and in which the parameter ζ specifies the outcomes, or realizations, of that conceptual random experiment associated with the stochastic process. It can be shown that, if the process is stationary in the strict sense, and if the random variable $X_i = X(t_i,\zeta)$, which is defined by fixing the time at $t = t_i$, has zero mean and, moreover, if, for any two fixed times t_1 and t_2 separated by non-zero interval τ, the random variables $X_1 = X(t_1,\zeta)$ and $X_2 = X(t_2,\zeta)$ are independent, then the random process $X(t,\zeta)$ has a weighted δ-function as its autocorrelation function. Consequently, the process also has a constant power density spectrum at all frequencies and is therefore a white-noise process. If, in addition, the random variable X_1, defined at any fixed time t_1, has a zero-mean Gaussian probability density function, then the white-noise process will also be normal. Since infinite total power is required in any process that possesses a spectral density function that is constant at all frequencies, a white-noise process is physically unrealizable. However a bandlimited white-noise Gaussian process, of the kind discussed in the previous chapter, can be numerically realized using the following method.

Consider first that the random process $X(t,\zeta)$ described above is ergodic so that each realization of the process embodies the statistical properties of the ensemble. Imagine that any realization, the one for which $\zeta = \zeta_0$ say, has been passed through an ideal linear lowpass filter with an upper cutoff frequency ν_U. Then the temporal function $\hat{X}(t,\zeta_0)$ emanating from the output of this filter is such that its spectral density function $S_{\hat{X}\hat{X}}(\nu)$ will have a constant value S at all frequencies ν that do not exceed ν_U, and will be zero at frequencies greater than ν_U. If the autocorrelation function $R_{\hat{X}\hat{X}}$ of $\hat{X}(t,\zeta_0)$ is computed as the temporal average

$$R_{\hat{X}\hat{X}}(\tau) = \lim_{T\to\infty} \frac{1}{2T}\int_{-T}^{T} \hat{X}(t,\zeta_0)\hat{X}(t+\tau,\zeta_0)\,dt, \tag{114}$$

then a result similar to Eq. (102) will be obtained, namely

$$R_{\hat{X}\hat{X}}(\tau) = S(2\pi\tau)^{-1}\sin(2\pi\nu_U\tau). \tag{115}$$

Now, when a realization of a normal process is applied as an input signal to a linear system, the resulting output signal will be a realization of a normal process. Thus, $\hat{X}(t,\zeta_0)$ is a realization of a normal process and, moreover, $\hat{X}$ has a zero mean value, since the mean of $X(t,\zeta_0)$ was zero. Suppose one considers the output process $\hat{X}(t,\zeta)$. This process is the ensemble of temporal functions obtained by filtering each member of the ensemble that comprises the process $X(t,\zeta)$ with a lowpass filter identical to that used to obtain the realization $\hat{X}(t,\zeta_0)$ from $X(t,\zeta_0)$. If the random variables $\hat{X}_1 = \hat{X}(t_1,\zeta)$ and $\hat{X}_2 = \hat{X}(t_1+\tau,\zeta)$ are examined, it is no longer true in general that $\hat{X}_1$ and $\hat{X}_2$ are independent whenever $\tau \neq 0$. However, suppose one samples the realization $\hat{X}(t,\zeta_0)$ at intervals of Δt, where

$$\Delta\tau = (2\nu_U)^{-1}. \tag{116}$$

The sample values thus obtained,

$$\hat{X}_s(\zeta_0) = \{\hat{X}_n(\zeta_0)\} = \{\hat{X}(n\Delta t, \zeta_0)\} \tag{117}$$

with ($n = -\infty, \ldots -2, -1, 0, 1, 2, \ldots \infty$), form a sequence of independent Gaussian random numbers $\hat{X}_n$, having zero mean. Several factors bring about this situation. First, the process $X(t,\zeta)$ is assumed to be ergodic, in which case, its ensemble statistical properties are embodied in the temporal function that is the realization ζ_0. Second, the temporal function $\hat{X}(t,\zeta_0)$, which is the filtered replica of $X(t,\zeta_0)$, contains no spectral component with a frequency greater than ν_U, so that, when it is sampled according to Eq. (116) at the Nyquist frequency $2\nu_U$, the samples obtained are independent. Finally, the lowpass filtering operation does not change the Gaussian character of the process $X(t,\zeta)$.

The above considerations form the basis of digitally simulating a bandlimited, Gaussian, white-noise process. If the sequence i of $(2N + 1)$ independent, normally distributed random numbers

$$\tilde{X}_s(N,i) = \{\tilde{X}_n^i\}\ , \tag{118}$$

where ($n = -N, -N+1, \ldots -1, 0, 1, 2, \ldots N-1, N$), is generated by some means, then the resulting $(2N + 1)$ values $\tilde{X}_n^i$ can be regarded as a sequential sample (with "sample" used here in the statistical sense to denote a set of elements drawn from a population) of size $(2N + 1)$ drawn from one realization, the realization $\zeta = \zeta_0$ say, of the sampled process $\hat{X}_s$ described in Eq. (117). As N increases without bound, the set of values $\tilde{X}_n^i$ will approach the sampled representation $\hat{X}_s$ of the realization $\hat{X}(t,\zeta_0)$ of the bandlimited, Gaussian, white-noise process $\hat{X}(t,\zeta)$. Numerically, of course, only a finite number of sequences $\tilde{X}_s(N,i)$, where ($i = 1, 2, \ldots I$) and where N can depend on i, can be generated.

Each of these I sequences can be regarded in two ways, since an ergodic process is being simulated. On the one hand, the i-th and the j-th such sequence can be regarded as being two samples drawn from different realizations of $\hat{X}_s(\zeta)$, the ζ_i-th realization and the ζ_j-th

realization say. On the other hand, the i-th and j-th sequences may be thought of as being two disjoint samples drawn from a single realization of $\hat{X}_s(\zeta)$, the ζ_0-th realization say. That is, the sequence $\{\tilde{X}_n^i\}$ could represent the sequentially taken sample $\{\tilde{X}(n\Delta t, \zeta_0)\}$ of $\hat{X}_s(\zeta_0)$, with $(n = n_1, n_2, \ldots n_I)$, and the sequence $\{\tilde{X}_n^j\}$ could represent the sequentially taken sample $\{\hat{X}(n\Delta t, \zeta_0)\}$, with $(n = n_J, n_{J+1}, \ldots n_{J+N})$ and with the integer J greater than the integer I. Both of these equivalent alternate interpretations are useful from an experimental standpoint.

A sequence $\{\tilde{X}_n^i\}$ of 2N independent random numbers, which is equivalent to a set drawn from a population with the Gaussian probability density function

$$P(\tilde{X}) = (2\pi\sigma^2)^{-\frac{1}{2}} \exp[-(\tilde{X} - \eta)^2/(2\sigma^2)] , \tag{119}$$

in which η is the mean and σ^2 the variance of the population, can be generated from a sequence $\{\tilde{U}_n^i\}$ of 2N independent random numbers that are drawn from a population with the rectangular density function

$$P(\tilde{U}) = \begin{cases} 1, & 0 < U < 1 \\ 0, & \text{elsewhere.} \end{cases} \tag{120}$$

The method used [99,100] to so generate the sequence $\{\tilde{X}_n^i\}$, transforms each pair of independent random numbers $\tilde{U}_1$ and $\tilde{U}_2$, from the population with the rectangular density function given by Eq. (120), into the pair of independent Gaussian random numbers $\tilde{X}_1$ and $\tilde{X}_2$ by means of the relations

$$\tilde{X}_1 = (-2\sigma^2 \ln \tilde{U}_1)^{\frac{1}{2}} \cos(2\pi\tilde{U}_2) + \eta \tag{121a}$$

and

$$\tilde{X}_2 = (-2\sigma^2 \ln \tilde{U}_1)^{\frac{1}{2}} \sin(2\pi\tilde{U}_2) + \eta . \tag{121b}$$

That $\tilde{X}_1$ and $\tilde{X}_2$ are independent Gaussian random variables, each apparently

drawn from a population with a density function given by Eq. (119), follows [101] from the transformation relation

$$P(\tilde{X}_1,\tilde{X}_2) = |J| P(\tilde{U}_1,\tilde{U}_2) \tag{122}$$

between the joint probability density function $P(\tilde{X}_1,\tilde{X}_2)$ of $\tilde{X}_1$ and $\tilde{X}_2$ and the joint probability density function $P(\tilde{U}_1,\tilde{U}_2)$ of $\tilde{U}_1$ and $\tilde{U}_2$. In Eq. (122), the quantity J is the Jacobian of the transformation inverse to that given by Eqs. (121), viz

$$\tilde{U}_1 = \exp\{-[(\tilde{X}_1 - \eta)^2 + (\tilde{X}_2 - \eta)^2]/(2\sigma^2)\} \tag{123a}$$

and

$$\tilde{U}_2 = (2\pi)^{-1} \arctan[(\tilde{X}_2 - \eta)/(\tilde{X}_1 - \eta)] \, . \tag{123b}$$

One readily calculates the pertinent Jacobian to be

$$\begin{aligned} J &= (\partial\tilde{U}_1/\partial\tilde{X}_1)(\partial\tilde{U}_2/\partial\tilde{X}_2) - (\partial\tilde{U}_1/\partial\tilde{X}_2)(\partial\tilde{U}_2/\partial\tilde{X}_1) \\ &= -(2\pi\sigma^2)^{-1}\exp[(\tilde{X}_1 - \eta)^2/(2\sigma^2)]\exp[(\tilde{X}_2 - \eta)^2/(2\sigma^2)] \end{aligned} \tag{124}$$

so that, from Eq. (122), the relation

$$\begin{aligned} P(\tilde{X}_1,\tilde{X_2}) &= \{(2\pi\sigma^2)^{-\frac{1}{2}}\exp[(\tilde{X}_1 - \eta)^2/(2\sigma^2)\}\{(2\pi\sigma^2)^{-\frac{1}{2}}\exp[(\tilde{X}_2 - \eta)^2/(2\sigma^2)]\} \\ &= P(\tilde{X}_1)P(\tilde{X}_2) \end{aligned} \tag{125}$$

is obtained, which precisely enounces $\tilde{X}_1$ and $\tilde{X}_2$ to be independent Gaussian random variables. Note that the desired mean value η and variance σ^2, which one wishes to obtain in the population from which the sequence $\{\tilde{X}_n^i\}$ is drawn, may be inserted in the transformation that is given by

Eqs. (121). For simulating the normal white-noise process described previously, it is required that $\eta = 0$. The variance σ^2 is then a measure of the total power in the simulated process. As will be described subsequently, this power level is imposed so as to optimize certain characteristics of the experimental noisebursts.

Instead of generating a sequence of Gaussian random numbers $\{\tilde{X}_n^i\}$ from the random sequence $\{\tilde{U}_n^i\}$ with a rectangular distribution, a pseudorandom sequence $\{x_n^i\}$ is generated from a pseudorandom sequence $\{u_n^i\}$, using pairs of values u_1 and u_2 in place of $\tilde{U}_1$ and $\tilde{U}_2$ in Eqs. (121), to generate pairs of values x_1 and x_2, instead of $\tilde{X}_1$ and $\tilde{X}_2$. If the pseudorandom sequence $\{u_n^i\}$ has "statistical" properties that mimic those of the sample $\{\tilde{U}_n^i\}$, then the pseudorandom sequence $\{x_n^i\}$ will be indistinguishable in a statistical sense from the Gaussian random sequence $\{\tilde{X}_n^i\}$. Well-known digital computer techniques [102-104] are available by which sequences of rectangularly distributed pseudorandom numbers can be computed. Although such sequences are repetitive, they have such a long repetition period that computed samples, even those consisting of as many as 10^6 values [105] behave in a random fashion. On the computer [106] used, pseudorandom numbers with the rectangular density function given by Eq. (120) were generated using a program that calls upon a system library function. This system library function uses an algorithm of the multiplicative congruential type. The algorithm meets the criteria set forth for generating pseudorandom sequences of maximal length. It also incorporates a modification introduced in order to avoid the occurrences of abnormally short periods in the least significant bits of the generated values.

From each sequence of Gaussian pseudorandom numbers $\{x_n^i\}$ that is generated, a pseudorandom experimental noiseburst is created. The experimental requirements are imposed upon the sequences. Thus, a typical experiment might require 16 distinct noisebursts, each 2.8 ms in duration. Since the sampling rate in the pulse-generating subsystem is 200 kHz, each of the 16 sequences $\{x_n^i\}$ in this case will consist of 561 Gaussian

pseudorandom numbers. Each such sequence will be generated from one of 16 distinct sets of 562 rectangularly distributed, computer-generated pseudorandom numbers. As has been stated, the specified mean value in Eqs. (121) must be zero. Also, the input signal supplied to the digital-to-analog converter in the experimental electronic system must be in the range between -1.0 and +1.0 V. Therefore, the numbers in any sequence $\{x_n^i\}$ must not exceed unity in magnitude. This would certainly be the case for most sequences of 561 values, if the standard deviation σ in Eqs. (121) was made sufficiently small. However if σ is made small, the full 12-bit word-length of the digital-to-analog converter will not be efficiently used, since most of the digital values of the x_n^i would themselves be small and would therefore only require a few bits to represent them. The only values of x_n^i requiring the full 12-bit word-length of the digital-to-analog converter would then be the infrequently encountered "outliers"--improbable positive or negative values of large magnitude that are accounted for by the tails of the Gaussian probability density function. In order to effectively use the full 12-bit range of the digital-to-analog converter, the standard deviation was taken to be 0.25 V, so that the ±1.0 V full range is $\pm 4\sigma$.

The outliers, those values of x_n^i which exceed in magnitude the ±1.0 V digital-to-analog converter input range, are disposed of by discarding any sequences $\{x_n^i\}$ that contain them. In generating 16 pseudorandom noisebursts, each with 561 values, it was found that only one set had to be rejected owing to the presence of outliers. Thus, 17 sets $\{x_n^i\}$ had to be generated in order to obtain 16 sets of 561 values that include no outliers. A further numerical artifice is also used to tailor the pseudorandom sequences $\{x_n^i\}$ to the experimental requirements. In general, any particular sequence of 561 Gaussian pseudorandom numbers will have neither a zero mean nor a standard deviation of precisely 0.25, since each sequence is but one sample drawn from a population having these statistical characteristics in the aggregate. However, one may numerically impose these characteristics, a zero mean and a standard deviation of

0.25, on each of the 16 sequences by means of a simple linear transformation. Since a linear transformation will not alter the Gaussian character of any sequence $\{x_n^i\}$, all of the 16 experimental sequences can be required to have exactly a zero mean value and contain exactly the same total energy by using this artifice.

Once each of the sets of 561 Gaussian pseudorandom numbers are generated and transformed, each value x_n^i is quantized by rounding to a 16-bit integer with 12 significant bits in order to be compatible with the digital-to-analog converter's word length. These 16-bit digital words are then written on magnetic tape in a format acceptable to the input of the buffer/interface unit in the pulse-generating subsystem. When read from the memory of the buffer/interface unit at a 200 kHz clock rate, a 561-word record gives rise to a unique pseudorandom noiseburst, 2.8 ms in duration, which has an average value of zero and a fixed, predetermined total energy. The energy in the noisebursts, on the average, will be distributed uniformly in the frequency band from 0 to 100 kHz.

Figure 19 depicts the signals resulting from one such pseudorandom noiseburst. The noiseburst at the top of the figure is the voltage that is applied to the input of the Type F36 source. This signal is the noiseburst as it appears after it has been passed through the three cascaded Butterworth lowpass filter stages, each with the upper cutoff frequency of 20 kHz, and through the single highpass Butterworth stage with the 950 Hz lower cutoff frequency. The center and bottom noisebursts shown in Fig. 19 are the voltages generated at a receiver's output owing to acoustic transmissions by the Type F36 that are generated by the noiseburst depicted at the top of the figure. The received noiseburst at the center of Fig. 19 corresponds to an azimuth angle of $\phi = 270°$. This is a source and receiver orientation in which the receiver is normal to the axis of cylindrical symmetry of the Type F36, i.e., "broadside" to the line source. The noiseburst at the bottom of Fig. 19 is generated at an azimuth angle ϕ equal to 180°, a situation in which the receiver is on the axis of symmetry of the Type F36, i.e., the

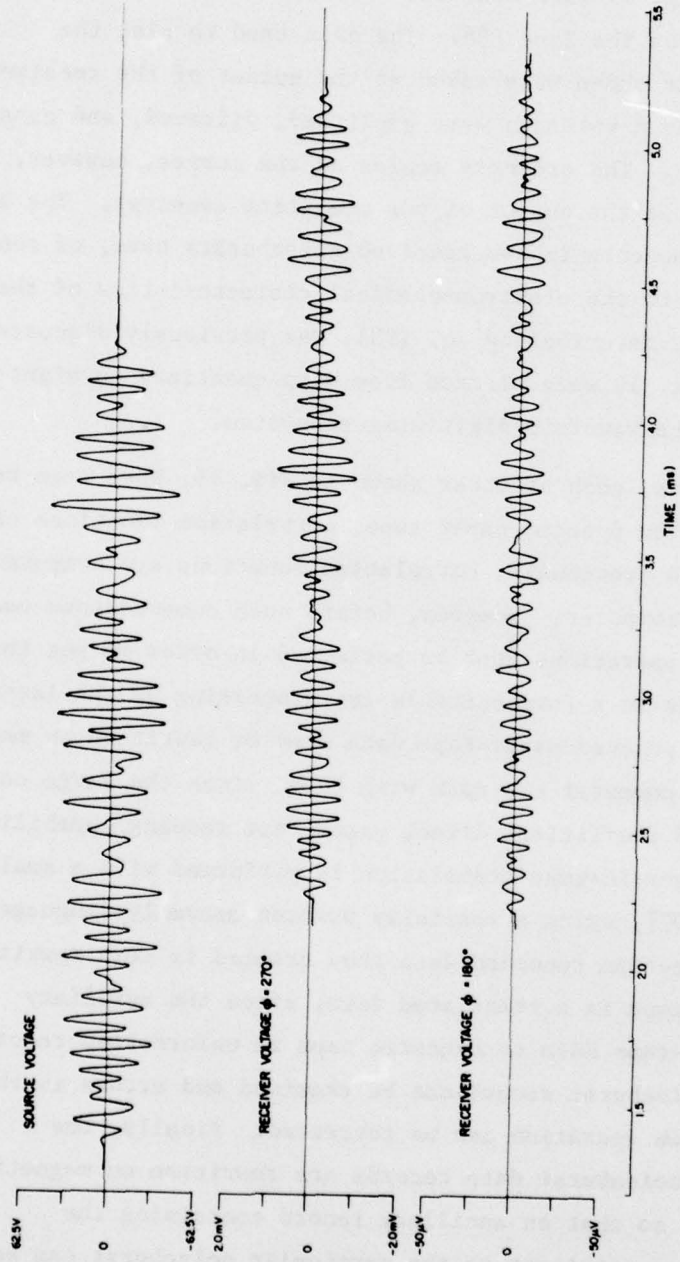

Fig. 19--Experimental pseudorandom noisebursts

receiver is measuring the "endfire" signal from the source. Both received noisebursts shown in Fig. 19 were measured with the center of the receiver 1.32 m from the center of the Type F36. The data used to plot the receiver-voltage signals shown were taken at the output of the receiver subsystem. Thus, received voltages were amplified, filtered, and gated to remove reverberation. The ordinate scales on the curves, however, refer to the actual voltages at the output of the measuring receiver. The high-frequency spectral components in two received noisebursts have, of course, been emphasized, owing to the electromechanical characteristics of the Type F36. This effect, described by Eq. (98), was previously discussed. All three curves in Fig. 19 were plotted from data quantized to eight bits and recorded by the waveform-digitizing subsystem.

Once noisebursts, such as those shown in Fig. 19, have been recorded in digital form on punched paper tape, correlation functions can be computed. As mentioned previously, correlation functions are computed using a large digital computer. However, before such computations can be accomplished, several operations must be performed in order to put the punched-paper-tape data in a form suitable for processing by the large computer. First, the punched-paper-tape data must be rewritten on magnetic tape before the large computer can work with them, since the large computer has a very limited and inefficient direct paper-tape reading capability. This paper-tape to magnetic-tape translation is performed with a small auxiliary computer [107], using a specially written assembly-language program. The magnetic-tape recorded data thus created is next rewritten on a second magnetic tape in a translated form, since the auxiliary computer copies paper-tape data to magnetic tape in unformatted records. At this stage, the noiseburst record can be examined and errors in the paper-tape performation operation can be corrected. Finally, the correctly translated noiseburst data records are rewritten on magnetic tape yet a third time so that an ancillary record containing the experimental parameters pertinent to the particular noiseburst can be

appended to each noiseburst data record. Correlation functions are computed from the noiseburst data records on this magnetic tape.

The noisebursts are considered as transient signals when computing input-output crosscorrelation functions. Consider the two noiseburst records that are represented in Fig. 20. Each of the two records consist of the 2048 words that were the contents of the transient recorder's memory at the time when that noiseburst was digitized. Let the 2048-word sequence $Y^i = \{Y_n^i\}$ be the digital record of a noiseburst voltage that was input to the Type F36 and let the 2048-word sequence $Z^j = \{Z_n^j\}$ be the record of the corresponding noiseburst voltage that was produced at the output of the measuring receiver. At word n_f in both records, the fiducial pulse appears. At word n_1 in record Y^i, the digitization of the Type F36 input signal begins. Suppose this digitized noiseburst consists of N_1 words. Then the actual input noiseburst terminates on word $(n_1 + N_1 - 1)$ as shown. Except for word n_f then, the portion of Y^i prior to n_1 and after word $(n_1 - N_1 - 1)$ represents a digitization of the input signal baseline, which is set to be zero during the initial processing of the data records. Similarly, the output record owing to the digitization of the received acoustic signal begins at word n_2 of record Z^j and terminates at word $(n_2 + N_2 - 1)$, if the received noiseburst consists of N_2 words. Again, except for word n_f, the remainder of the record Z^j is the baseline, which is set to be zero. Owing to the propagation time of the noiseburst from the Type F36 to the receiver, one finds, in general, that $n_2 \geq n_1$. Moreover, owing to the spatial extension of the source, one also finds, in general, that $N_2 \geq N_1$. The input-output crosscorrelation function $R_{YZ}^{ij}(\tau)$ at the discrete values of the delay parameter

$$\tau = m\Delta t, \tag{126}$$

where $(m = -\infty, \ldots -2, -1, 0, 1, 2, \ldots \infty)$ and where Δt is the sampling interval (5 μs in the experiments), is given by the expression

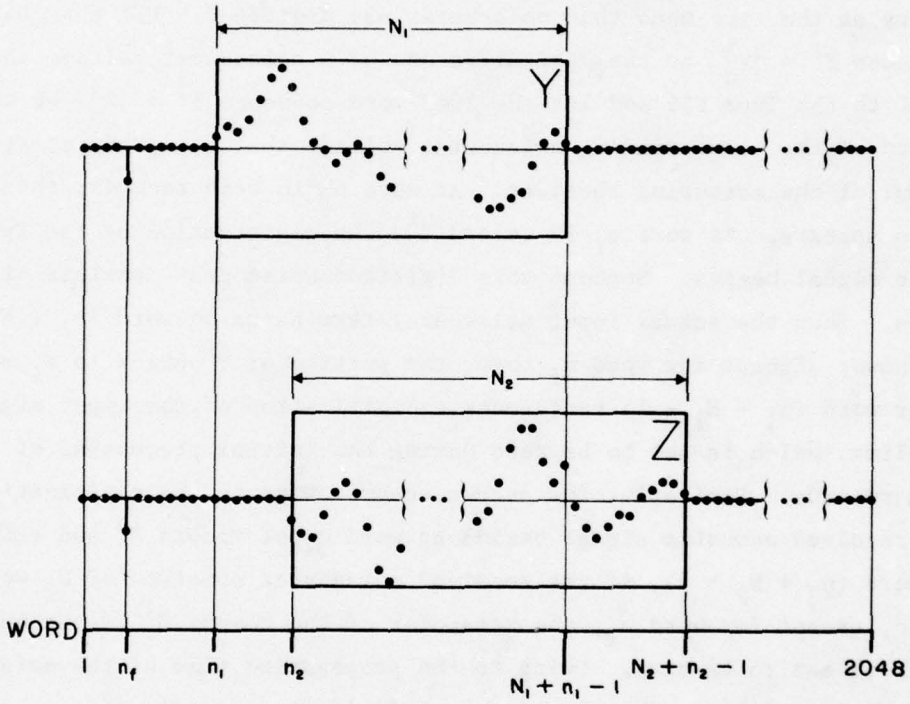

Fig. 20--Representation of recorded noisebursts

$$R_{YZ}^{ij}(m\Delta t)= \begin{cases} 0, & m \le n_2 - n_1 - N_1 \\ \Delta t \sum_{\ell=n_2}^{\Gamma_1+m} Y^i_{(\ell-m)} Z^j_\ell , & n_2 - \Gamma_1 \le m \le n_2 - n_1 \\ \Delta t \sum_{\ell=n_1}^{\Gamma_1} Y^i_\ell Z^j_{(m-\ell)}, & n_2 + n_1 + 1 \le m \le \Gamma_2 - n_1 - N_1 \\ \Delta t \sum_{\ell=n_1}^{\Gamma_2-m} Y^i_\ell Z^j_{(m-\ell)}, & \Gamma_2-\Gamma_1 \le m \le \Gamma_2 - n_1 \\ 0, & m \ge n_2 + N_2 - n_1 , \end{cases} \tag{127}$$

in which

$$\Gamma_\alpha = n_\alpha + N_\alpha - 1, \tag{128}$$

with $\alpha = 1$ or $\alpha = 2$. Note in Eq. (127) that it is the output signal Z^j that is fixed in time, while the input signal Y^i is progressively shifted by discrete values of the delay parameter in the direction of increasing τ.

In addition to computing input-output crosscorrelation functions in the absolute form that is expressed by Eqs. (127), normalized cross-correlation functions $\rho_{YZ}^{ij}(m\Delta t)$ are also computed. Normalized crosscorrelation functions are given by the expression

$$\rho_{YZ}^{ij}(m\Delta t) = R_{YZ}^{ij}(m\Delta t)/M_{YZ}^{ij} , \tag{129}$$

in which

$$M_{YZ}^{ij} = \Delta t \left\{ [\sum_{\ell=n_1}^{\Gamma_1} (Y^i_\ell)^2][\sum_{\ell=n_2}^{\Gamma_2} (Z^j_\ell)^2] \right\}^{\frac{1}{2}} . \tag{130}$$

Since the values of $\rho_{YZ}^{ij}(m\Delta t)$ lie between plus and minus one for all values of m, the normalized crosscorrelation function, given by Eq. (129), is largely independent of such experimental parameters as electrical signal amplitudes, amplifier gain settings and the like. This independence makes the normalized crosscorrelation function useful when studying the structure of the spatial impulse response of the Type F36. On the other hand, in order to determine the effect on the spatial impulse response that is produced by changing a particular experimental parameter, such as the source-to-receiver distance, it is necessary to use the absolute form of the input-output crosscorrelation function that is given by Eqs. (127).

In the preceeding chapter, which discusses the experimental methodology, the spatial impulse response function of the Type F36 is described in terms of the crosscorrelation function of input and output noise signals that are both of infinite duration, rather than in terms of the crosscorrelation function of two noisebursts of finite duration, such as is expressed either by Eq. (127) or by Eq. (129). Any experimental input-output crosscorrelation function must, of course, be determined using noise signal records that are of finite duration. When a pair of records of finite duration are crosscorrelated, each crosscorrelation function obtained is a statistical entity--being one estimate of that crosscorrelation that would be obtained if two infinite records could be crosscorrelated. That is, each pair of noise records of finite duration can be regarded as a paired sample taken from a corresponding pair of records of infinite duration. A characteristic of the population (with the characteristic here being the crosscorrelation function of two infinite noise-signal records) that is determined from one paired sample (with the paired sample here being a finite number of pairs of successive values taken from each of the two infinitely long noise records) will show a statistical variation. Different paired samples, that is, different pairs of finite-duration noise records, will yield different crosscorrelation functions. If a paired sample is large, i.e., if it is comprised of a large number of independent pairs of noise-signal sample

values, then the crosscorrelation function obtained from that one finite-duration paired sample will accurately estimate the crosscorrelation function of the two corresponding infinite records. Conceptually then, one could achieve an estimate of an input-output crosscorrelation function, and hence of the spatial impulse response function of the Type F36 source, with any degree of accuracy desired simply by using one pair of sufficiently long records of input and output noise signals.

It is, however, the size of the water tank used in the experiments that will determine the maximum possible duration of the noise signal records that can be employed when determining crosscorrelation functions. Thus, one is not able to improve the accuracy with which the spatial impulse response of the Type F36 source is estimated to any degree desired simply by increasing the duration of the noisebursts that are used. Highly accurate crosscorrelation-function estimates can be achieved, however, by using the following method, which is completely equivalent to increasing the duration of the noisebursts used. Here it is assumed that one improves the accuracy of an estimate when he reduces its variance.

This method is based upon the fact that any set of I pseudorandom input noisebursts and the corresponding set of I pseudorandom output noisebursts may be regarded either as being I paired samples drawn from I distinct pairs noise signal records, with each signal record being of infinite duration, or else the set may be regarded as I disjoint paired samples taken at different times from a single pair of noise signal records. As stated previously, this dual interpretation follows from the fact that an ergodic stochastic process is being simulated. Suppose, then, that one has I digital records $Y^i = \{Y_n^i\}$ of input noisebursts and the corresponding I digital records $Z^i = \{Z_n^i\}$ of output noisebursts, with ($i = 1,2, \ldots I$). According to the previous discussion, the cross-correlation function $R_{YZ}^{ii}(m\Delta t)$, for one particular value of i, is one estimate of the crosscorrelation function of a pair of infinite noise records Y and Z from which the respective samples Y^i and Z^i are drawn. Since I such sample pairs are available, a more accurate estimate

$R^{I}_{YZ}(m\Delta t)$ of this correlation function is obtained as the average

$$R^{I}_{YZ}(m\Delta t) = \frac{1}{I} \sum_{i=1}^{I} R^{ii}_{YZ}(m\Delta t). \tag{131}$$

The normalized form of this equation is

$$\rho^{I}_{YZ}(m\Delta t) = \frac{1}{I} \sum_{i=1}^{I} \rho^{ii}_{YZ}(m\Delta t). \tag{132}$$

Suppose that each of the input noisebursts Y^i is represented by N_1 values. Then each of the corresponding output noisebursts, Z^i will be represented by N_2 values. The crosscorrelation-function estimate, expressed by Eq. (131), will then be equivalent [108] to crosscorrelating an input noiseburst comprised of IN_1 values and an output noiseburst comprised of IN_2 values. In other words, the input-output crosscorrelation function, which is obtained by averaging the I input-output crosscorrelation functions that result from I input noisebursts of duration T, is equivalent to the input-output crosscorrelation that would be obtained if an input noiseburst of duration IT were used. Thus, by averaging sufficiently many of the input-output crosscorrelation functions that are generated using short noisebursts, a crosscorrelation function can be generated that is equivalent to the correlation function resulting from use of an arbitrarily long input noiseburst. Consequently, the restriction, which is placed on the signal record length, and thereby on correlation-function estimation accuracy, by the confined volume in the experimental water tank, can be circumvented.

Figure 21 illustrates the results of this correlation-function averaging procedure. The normalized autocorrelation functions of eight pseudorandom input noisebursts, each 2.8 ms in duration, were computed according to Eqs. (127) and (129). Figure 21 compares the average normalized autocorrelation function $\rho^{I}_{YY}(\tau)$, which is calculated using Eq. (132) for I equal to 1, 2, 4, 6, 7, and 8. For the autocorrelation functions shown, the timeshift parameter τ is a continuous variable,

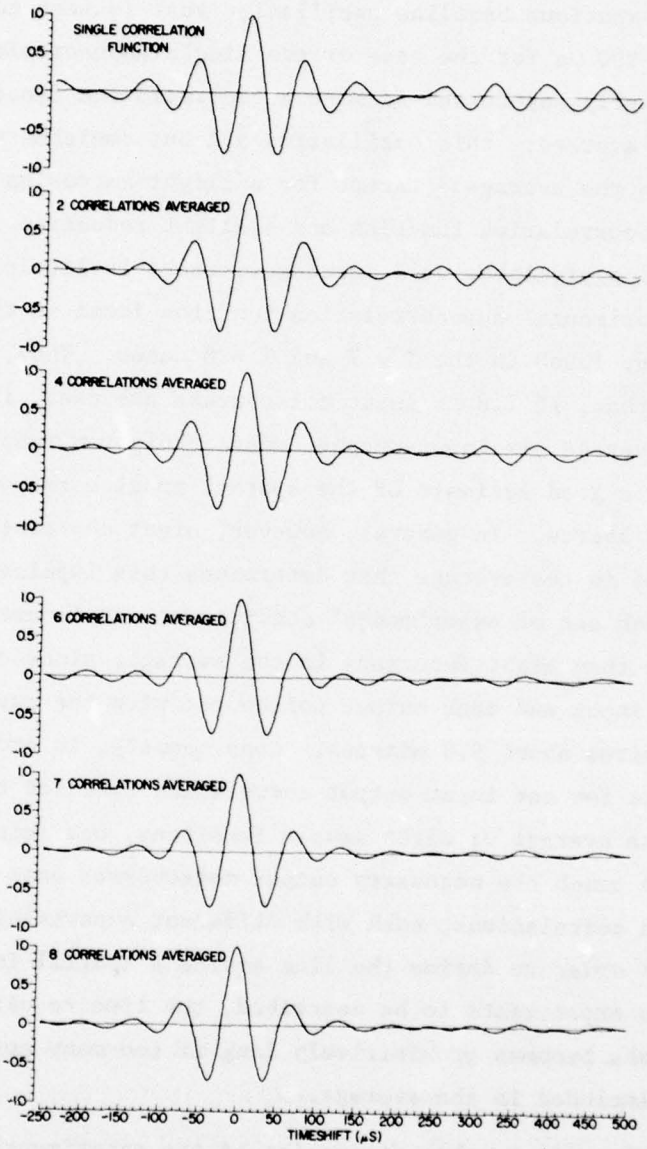

Fig. 21--Averaging the autocorrelation function of the source's input voltage

although the curves are plotted from sampled autocorrelations with $\Delta t = 5$ μs. The spurious baseline oscillation that is seen to occur in the range $|\tau| > 200$ μs for the case of the single autocorrelation function (I = 1) is gradually suppressed as more autocorrelation functions are included in the average: this oscillation all but vanishes when there are six terms in the average. Except for a slight narrowing of the main lobe of the autocorrelation function and a slight reduction in the height of the neighboring sidelobes as I increases, there is little difference between the experimental autocorrelation function found in the I = 6 case and the functions found in the I = 7 and I = 8 cases. Thus, it is found experimentally that, if 2.8 ms input noisebursts are used, it will be sufficient to average six input-output crosscorrelation functions in order to obtain a good estimate of the spatial impulse response function of the Type F36 source. In general, however, eight correlation functions will be included in the average that determines this impulse response function for each set of experimental conditions. It is not practical to include more than eight functions in the average, since digitally recording each input and each output noiseburst with the paper tape perforator requires about 9.6 minutes. Consequently, in order to gather the digital data for one input-output correlation function that is derived from the average of eight sample functions, one requires 77 minutes just to punch the necessary output noisebursts onto paper tape. Since many such correlations, each with different experimental parameters, are required in order to define the line source's spatial impulse response function in the experiments to be described, the time required to gather the acoustic data becomes prohibitively long if too many correlation functions are included in the average.

As final topic in this discussion of the experimental system, the acoustic receivers used to measure the radiated field of the Type F36 source will now be described. Two measuring hydrophones of different sizes were used. Both are commercially manufactured piezoelectric pressure sensors [109]. Both are cylindrically shaped and each has its

sensitive element located near one end and encapsulated in a neoprene sheath that is bonded to a stainless-steel mounting sleeve. The electrical cable emerges from the other end of this sleeve on each receiver.

The larger of the two receivers had a maximum diameter of 9.92 mm (0.391 in) and was 55.6 mm (2.19 in) long with the neoprene sheath comprising 28.6 mm (1.13 in) of this length. The cylindrical mounting sleeve, 7.94 mm (0.313 in) in diameter, accounted for the remaining 26.9 mm (1.06 in) of the total length. This hydrophone has a freefield receiving sensitivity of -209 dB re 1V/μPa. This receiving sensitivity can be considered constant to within ±0.2 dB from 10 Hz to 5 kHz and constant to within ±2 dB from 5 kHz to 40 kHz. This receiver was used to make directional measurements in the farfield of the Type F36 transducer at a fixed distance from this source. A compliant mounting was used to attach the receiver, with its axis of symmetry held vertical, to a vertical stainless-steel rod, which held the receiver fixed in the field of the Type F36.

The smaller of the two receivers was used to probe the field of the Type F36. A small sensitive element in this receiver is encapsulated in a sheath that is only 2.38 mm (0.0938 in) in diameter and 6.35 mm (0.25 in) long. A conical stainless-steel mounting sleeve 95.5 mm (3.75 in) long holds the sensitive element, making the overall length of the receiver 101.6 mm (4.0 in). The sleeve tapers from a diameter of 2.38 mm at the sheath to a diameter of 6.35 mm at the cable. The receiving sensitivity of the hydrophone is -224 dB re 1V/μPa, exclusive of the cable. This receiving sensitivity is constant to within ±0.5 dB from 1.0 Hz to 20 kHz; above 20 kHz, it decreases linearly to approximately -225 dB at 40 kHz. Using a cable 2.44 m (8 ft) long, causes a decrease of about 2 dB in the receiver's sensitivity.

This receiver is mounted, with its axis of symmetry horizontal at the end of a tapered truss. The truss is 3.765 m (148 in) long and is

made of six rods, each 3.18 mm (0.125 in) in diameter, that are welded to a set of rings of progressively increasing diameters, each with a square cross section that is 3.18 mm on a side. This tapered truss, which is light, stiff and acoustically transparent, is fastened to an assembly that is mounted on an optical-bench carrier. The receiver position can be changed by moving the carrier along a one-meter optical bench. The receiver-positioning apparatus is shown in Fig. 22 and also appears in the upper right foreground in Fig. 13.

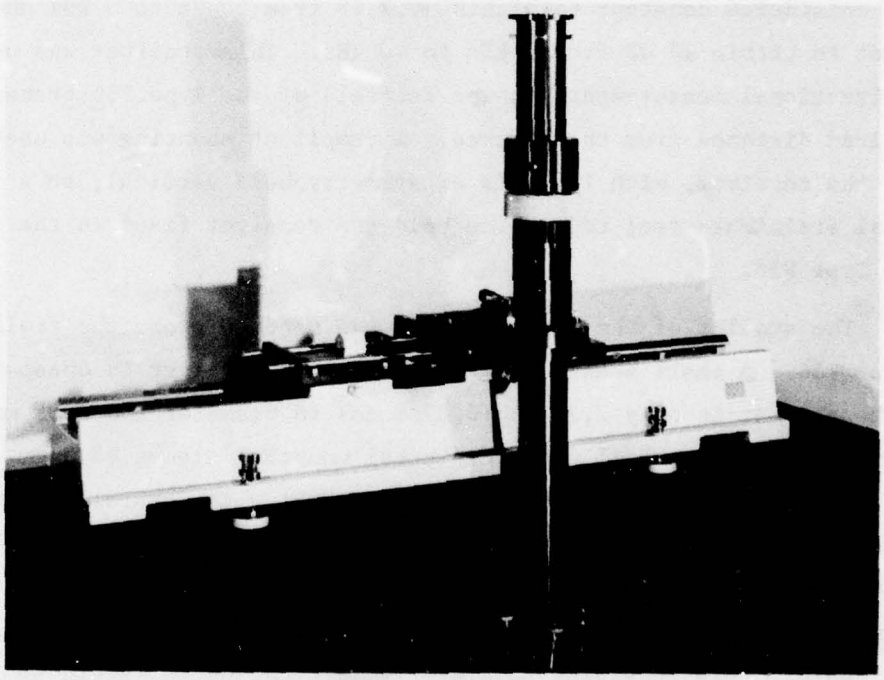

Fig. 22--Receiver-positioning apparatus

The axis of the truss can be kept vertical, when the assembly is moved along the bench, by means of two precision spirit levels, which are accurate to $\pm$10" and which are orthogonally mounted on the assembly that carries the truss. A second carrier is coupled to the assembly that

carries the truss by means of a precision lead screw. By adjusting the lead screw and by using a vernier scale, one can position the carrier that moves the receiver along the optical bench with an accuracy of $\pm$0.05 mm ($\pm$0.002 in). Moreover, by accurately leveling the assembly to maintain the truss axis vertical after the moving the receiver, one can ensure that the motion of the receiver at the end of the truss reproduces the motion of the optical-bench carrier to within $\pm$0.1 mm ($\pm$0.004 in), if one assumes that the precision levels can be read to $\pm$5" and that the distance from the receiver to the point of support for the truss structure is 4.24 m (167 in).

CHAPTER VII

EXPERIMENTAL SPATIAL IMPULSE RESPONSE FUNCTIONS

The spatial impulse response function of the Type F36 transducer was measured, as a function of direction, with the receiver at a fixed distance from the center of the Type F36 source. It is this set of experimental results, defining the source's directional characteristics, that will be discussed in this chapter. In particular, the waveforms of the measured spatial impulse response functions will be compared to those waveforms that are predicted on the basis of the theoretical description of the radiated field of an ideal line source, which was derived in Chapter IV.

In general, the measured spatial-impulse-response-function waveforms agree very closely with the theoretical predictions, except for those cases in which the source's field is measured in the direction of its axis of symmetry, or else, is measured in directions close to axial. However, even in these cases, the theory of the ideal line radiator predicts the essential features of the experimental waveforms. Indeed, the theory may be modified in a simple fashion so that it can also be used to adequately predict the spatial-impulse-response-function waveforms that are measured in axial and near-axial directions. This latter point will be discussed in what follows, along with an explanation of the observed differences between the theoretical and the experimental waveforms in certain regions of the Type F36 source's radiated field.

Measurements were made at 29 different angular positions, with the center of the measuring receiver at a constant distance of 1.324 m (52.12 in) from the axis of the vertical tube in the supporting section of the transducer mounting assembly. (See Fig. 12.) This separation distance was measured with an accurate steel rule to the nearest 1.59 mm (0.0625 in). The angular measurement positions are depicted in Fig. 23,

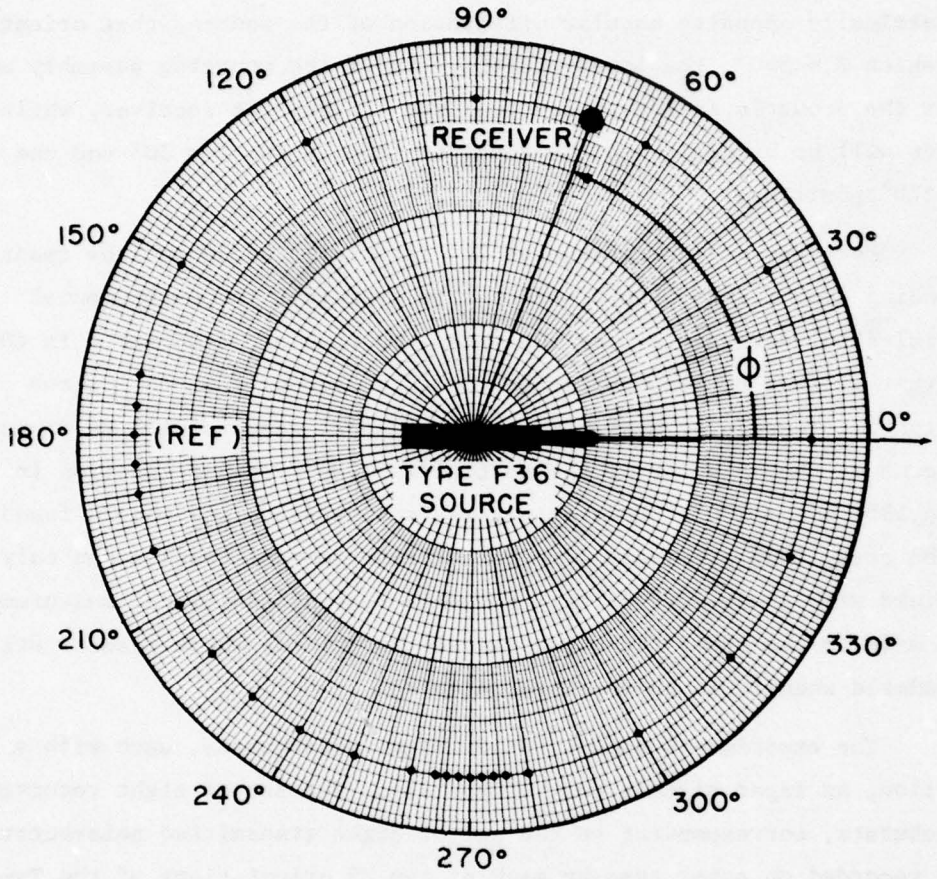

Fig. 23--Measurement positions

in which a plane polar coordinate system is established. The origin of this polar system, which is fixed to the Type F36 source, is located at the center of the source. The plane depicted in Fig. 23 is the plane HH' in Fig. 12. The polar angle ϕ measures the orientation of the Type F36 source with respect to the receiver. The orientation with $\phi = 180°$ is the reference position, which was established visually. In the $\phi = 180°$ position, the axis of symmetry of the Type F36 passes through the measuring receiver, with the source itself between the lower structure

of the transducer mounting assembly and the receiver. Thus, in the diametrically opposite angular orientation of the source, that orientation for which $\phi = 360°$, the lower mounting arm of the mounting assembly will be in the acoustic field between the Type F36 and the receiver, while the source will be broadside to the receiver in both the $\phi = 90°$ and the $\phi = 270°$ positions.

Measurements were taken at 10° intervals throughout the quadrant extending from $\phi = 180°$ to $\phi = 270°$. By symmetry, the experimental spatial-impulse-response-function waveforms that are determined in this quadrant will be representative of those in each of the other three quadrants. Therefore, most of the experimental results will be discussed in terms of the behavior of the spatial impulse response function in the range $180° \leq \phi \leq 270°$. However, it was anticipated, and indeed found to be the case, that precisely symmetrical experimental results can only be attained with great difficulty. For this reason, additional measurements were made in the other three quadrants. Certain of these results will be considered when it is appropriate to do so.

The experiments used a set of eight noisebursts, each with a 2.8 ms duration, as input signals to the Type F36. The set of eight received noisebursts, corresponding to the set of eight transmitted noisebursts, were recorded on paper tape at each of the 29 orientations of the Type F36 that are depicted in Fig. 23. Thus, 232 paper-tape records of received noisebursts were made in addition to the eight paper-tape records that were made of both the Type F36 source's input-voltage and input-current noisebursts. Gathering all the experimental data took nine days of continuous work during a two-week period in May 1976. During the course of the data taking, the temperature in the water tank rose from 18.8°C to 19.6°C, owing to the seasonal transition. Water temperature, which was measured both at the beginning and at the end of each day, was found to be constant during an entire eight-hour measurement period to within approximately ±0.1°C. The experimental results

to be presented are quite insensitive to temperature variations of this magnitude.

The various angular orientations of the Type F36 source with respect to the receiver, which are depicted in Fig. 23, are also tabulated in Table 1, along with the water temperature that existed when received noisebursts were recorded at each particular orientation. The values of the soundspeed [96] that occur at the tabulated water temperatures are also shown in the third column of Table 1. It was intended that each measured spatial impulse response function would be determined from the average of eight input-output crosscorrelation functions. However, eight of the digitized records of received noisebursts were lost, some owing to paper-tape-perforator malfunctions and some owing to problems in magnetic-tape translation and copying operations. Therefore, the fourth column in Table 1 gives the number of received noisebursts that could actually be used in computing input-output crosscorrelation functions, and, hence, also gives the number of such functions that are included in the average that determines the waveform of the source's spatial impulse response for a particular source and receiver configuration. It will be noted that eight input-output crosscorrelation functions are included in most averages and that in no case are fewer than six crosscorrelation functions averaged when determining a spatial impulse response function. Thus, an accurate representation of the Type F36 source's spatial-impulse-response-function waveform can be obtained for each of the 29 orientations at which received noisebursts were recorded.

The waveforms of the Type F36 source's spatial impulse response function, which were measured at a number of the orientations depicted in Fig. 23, are shown in Figs. 24 through 30. These waveforms are determined by the means described in Chapter V, starting with the normalized input-output crosscorrelation functions that are expressed by Eqs. (129) and (130). In Figs. 24 through 30, the ordinate of each waveform is the amplitude of this normalized spatial impulse response function, which

TABLE 1.--Source and receiver orientation angles ϕ at which the spatial impulse response function of the Type F36 source was observed. Temperature T and soundspeed c at each observation angle. Number n of crosscorrelation functions averaged for each orientation when obtaining the waveform of the spatial impulse response function.

ϕ	T (°C)	c (m/s)	n
0°	19.6	1481.108	8
30°	19.6	1481.108	8
60°	19.6	1481.108	7
90°	19.6	1481.108	8
120°	19.6	1481.108	8
150°	19.6	1481.108	8
170°	18.9	1478.916	7
175°	19.9	1478.916	8
180°	18.8	1478.599	8
185°	18.8	1478.599	8
190°	18.8	1478.599	8
200°	18.9	1478.916	8
210°	18.9	1478.916	8
220°	18.9	1478.916	8
230°	18.9	1478.916	8
240°	19.3	1480.174	6
250°	19.3	1480.174	8
260°	19.3	1480.174	7
264°	19.3	1480.174	8
266°	19.4	1480.486	8
268°	19.4	1480.486	8
270°	19.4	1480.486	8
272°	19.6	1481.108	8
274°	19.6	1481.108	7
276°	19.6	1481.108	8
280°	19.6	1481.108	8
300°	19.6	1481.108	8
320°	19.6	1481.108	6
340°	19.6	1481.108	8

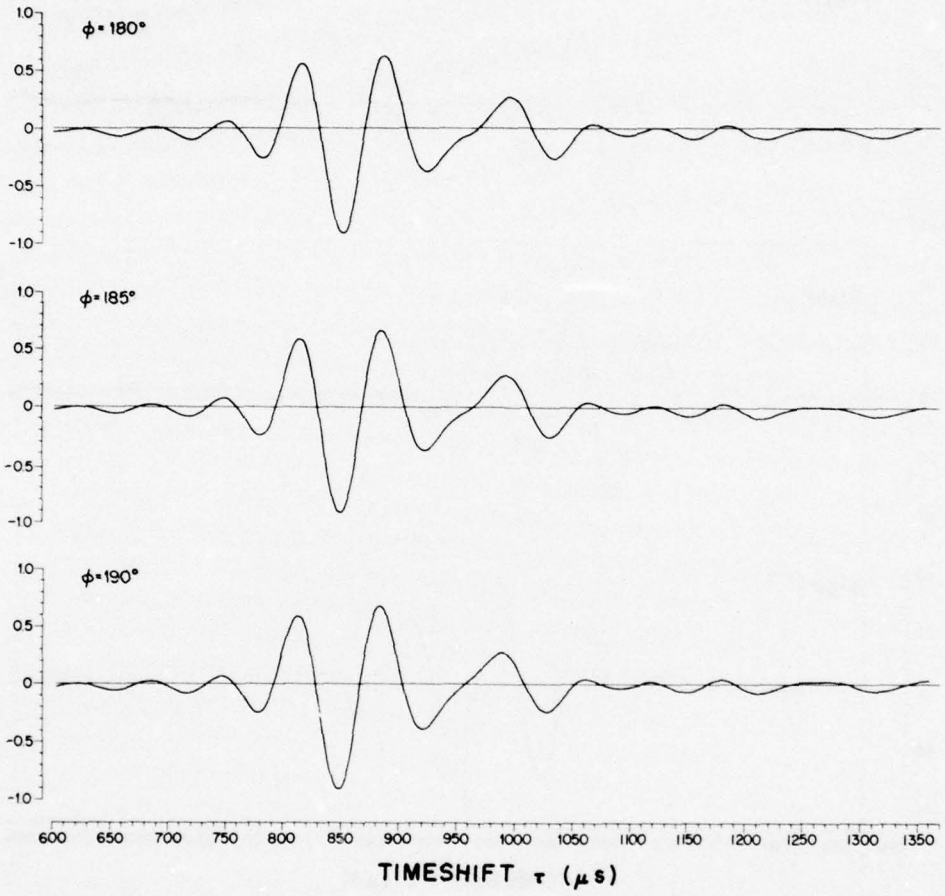

Fig. 24--Experimental spatial-impulse-response-function waveforms: $\phi = 180°$, $\phi = 185°$, and $\phi = 190°$

can be designated as p_0. The abscissa of each waveform is the delay parameter τ, with the scale presented in units of microseconds delay with respect to the time at which the transient-recorder digitization of the received noiseburst began. Thus, the abscissa scales in Figs. 24 through 30 show the time interval from 600 μs to 1350 μs. The occurrence of a given waveform feature corresponds, approximately, to the time it takes

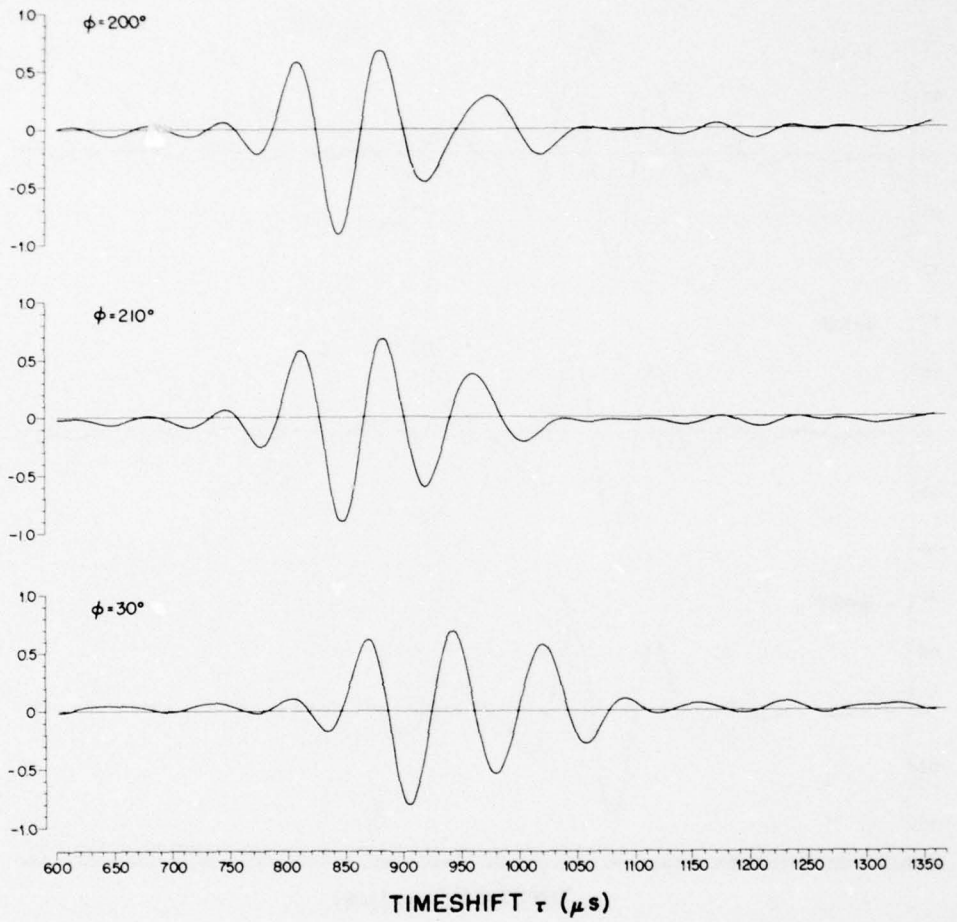

Fig. 25--Experimental spatial-impulse-response-function waveforms: ϕ = 200°, ϕ = 210°, and ϕ = 30°

for an acoustic signal to travel from the source to the receiver. Further remarks concerning this point will be made subsequently.

In Table 2, the amplitudes of the normalized and of the absolute spatial impulse response function are displayed for those waveforms shown in Figs. 24 through 30. Column two of Table 2 gives p_0, the amplitude of the normalized form of the spatial impulse response function, while P_0 in column three is the amplitude of the corresponding absolute function.

TABLE 2.--Comparative amplitudes of the fundamental initial minimum in the observed spatial-impulse-response-function waveform for various observation angles ϕ. The amplitude p_0 pertains to the waveform of the normalized function and P_0 pertains to the waveform of the absolute function. Amplitudes of the waveforms are given at the sampled value of τ that most nearly coincides with the position of the most negative point on the waveform for the minimum in question. Samples of the spatial-impulse-response-function waveform were obtained experimentally at 5 μs intervals so that the waveforms usually attain their extrema between sample values.

ϕ	p_0	P_0 (V^2)	τ (μs)
180°	-0.90233	-1.5235	850
185°	-0.91393	-1.5734	850
190°	-0.90469	-1.5579	850
200°	-0.86743	-1.4386	850
210°	-0.88917	-1.5816	850
30°	-0.80858	-1.3228	905
220°	-0.88713	-1.7025	850
230°	-0.70850	-1.4268	855
240°	-0.63830	-2.7305	875
250°	-0.99540	-8.6207	885
260°	-0.93062	-3.5286	885
270°	-0.85907	-3.5888	885
60°	-0.78962	-1.5127	925
120°	-0.58273	-1.0534	905
300°	-0.82696	-1.6159	880
264°	-0.88895	-3.3069	885
266°	-0.86792	-3.6313	885
268°	-0.86361	-3.6516	885
320°	-0.72678	-1.2503	880
150°	-0.88517	-1.4632	870
340°	-0.48276	-0.6836	845

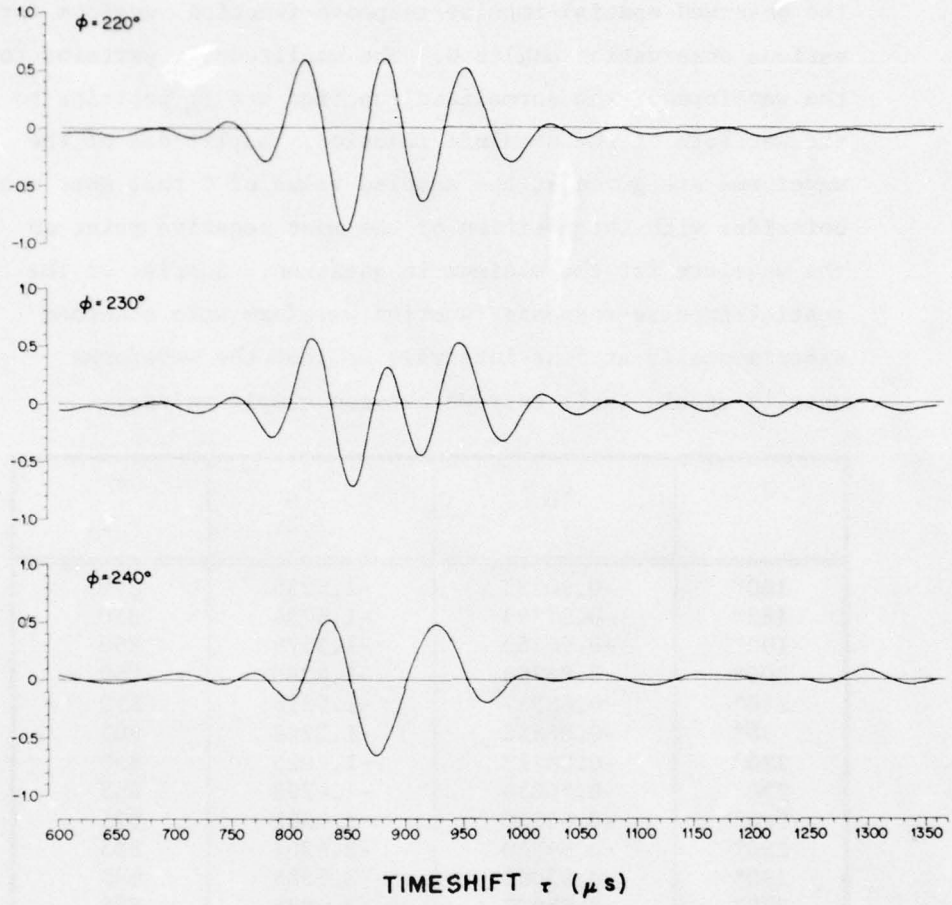

Fig. 26--Experimental spatial-impulse-response-function waveforms: $\phi = 220°$, $\phi = 230°$, and $\phi = 240°$

The amplitude tabulated for each waveform is that amplitude occurring at the sampled value of the delay parameter τ most nearly corresponding to the fundamental initial minimum of the waveform. This value of the delay parameter appears in the fourth column of Table 2.

The waveforms appearing in Figs. 24 through 30 are determined by crosscorrelating the output voltage from the measuring receiver with that

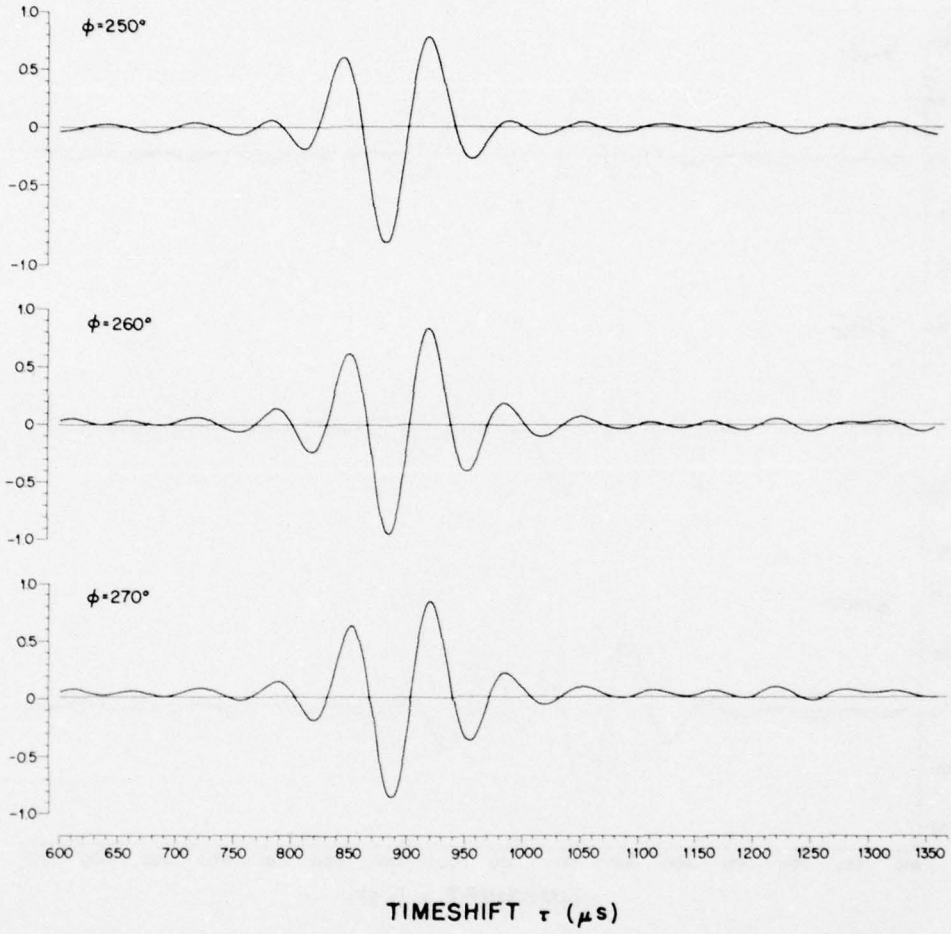

Fig. 27--Experimental spatial-impulse-response-function waveforms: ϕ = 250°, ϕ = 260°, and ϕ = 270°

input voltage to the Type F36 that produced it. For this reason, P_0, the amplitude of the absolute form of the experimental spatial impulse response function, has been given the dimensions of volts-squared in Table 2, although it is proportional to the source's radiated acoustic pressure. It must be emphasized again, however, that the waveforms shown in Figs. 24 through 30 are not the waveforms of the crosscorrelation functions of the input and output voltages of the source and receiver

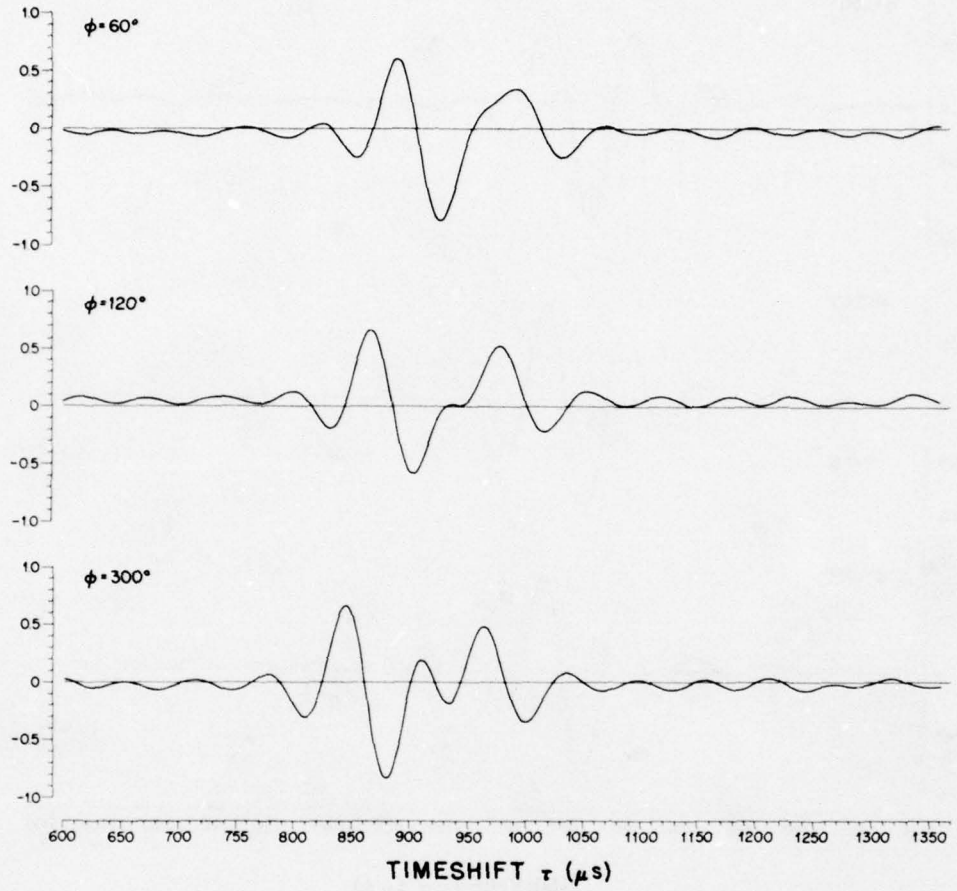

Fig. 28--Experimental spatial-impulse-response-function waveforms: ϕ = 60°, ϕ = 120°, and ϕ = 300°

combination. According to the experimental methodology discussed in Chapter V, these input-voltage/output-voltage crosscorrelation functions must be filtered by convolving each of them with a step function in order to obtain the waveforms of the source's spatial impulse response function that are shown in Figs. 24 through 30. According to the analysis in Chapter V, this filtering operation on measured input-output cross-

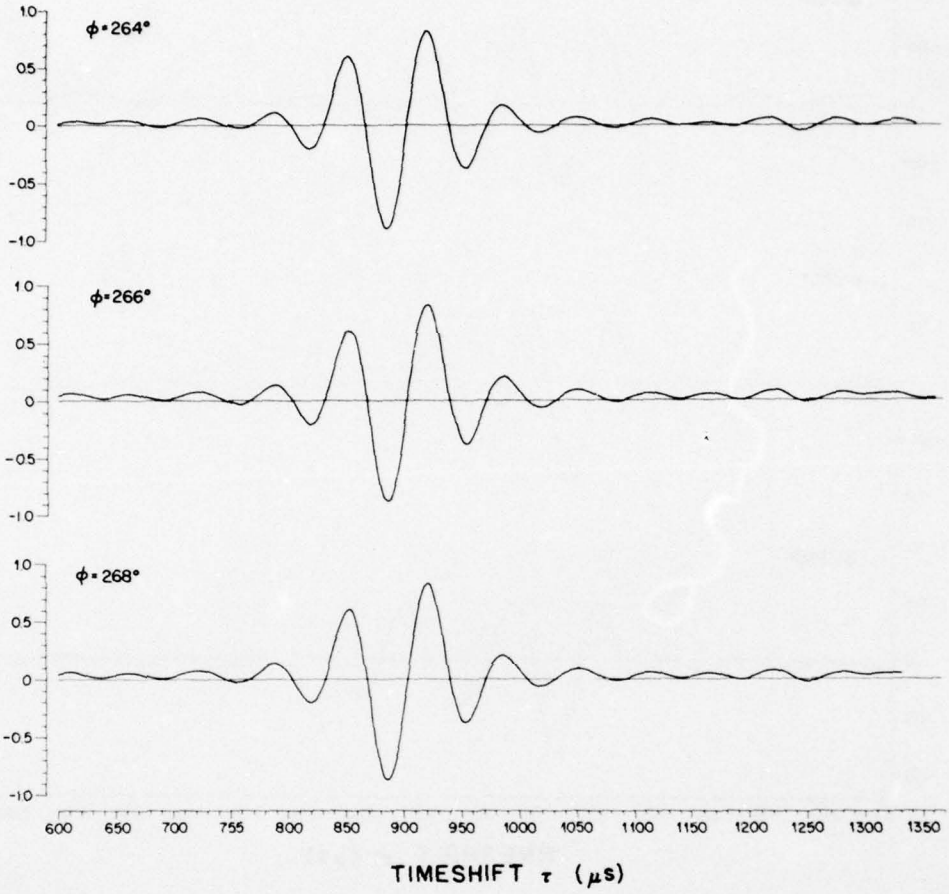

Fig. 29--Experimental spatial-impulse-response-function waveforms: $\phi = 264°$, $\phi = 266°$, and $\phi = 268°$

correlation functions is necessary in order to remove the effect introduced by the mechanical compliance of the vibrating-shell structure within the Type F36 source. (Refer to Fig. 9.) In the equivalent-circuit representation of the radiating source, the mechanical compliance appears as the equivalent capacitor C_M. This capacitor acts as a differentiating element that causes the source's surface velocity to be proportional to the first derivative of the voltage that is applied to the

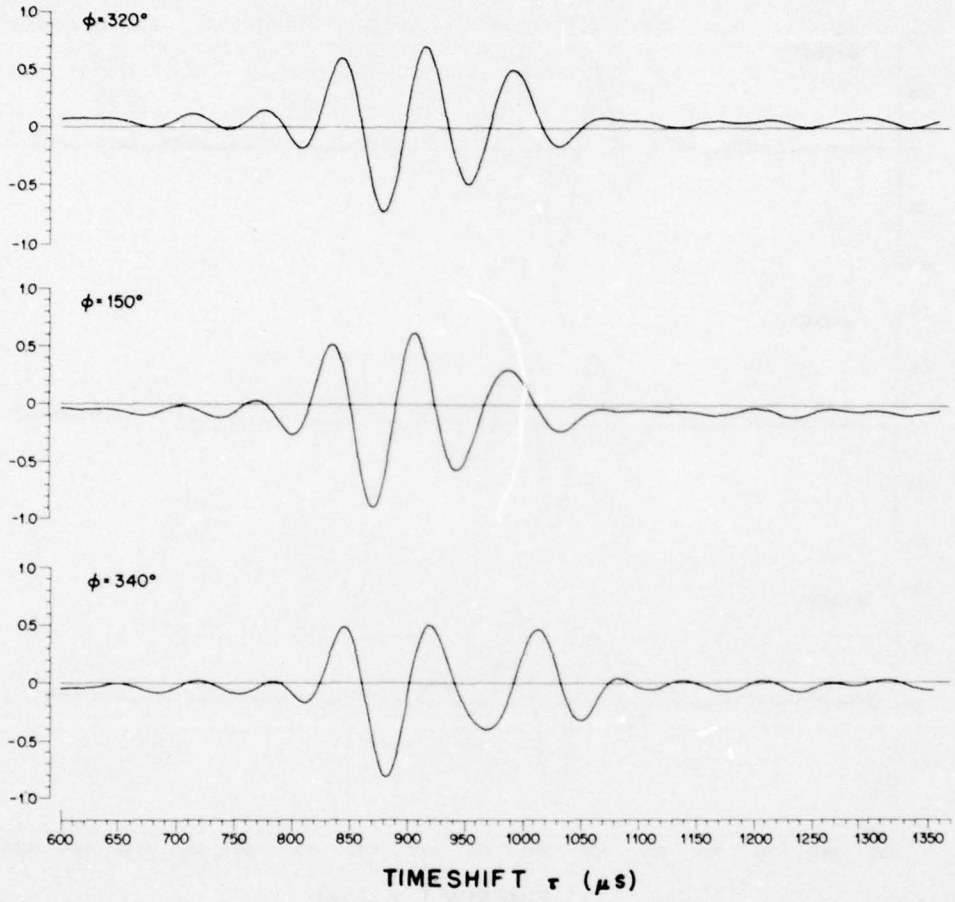

Fig. 30--Experimental spatial-impulse-response-function waveforms: ϕ = 320°, ϕ = 150°, and ϕ = 340°

source's electrical terminals. As a result of the radiating shell's compliance, then, the directly measured input-voltage/output-voltage crosscorrelation function's waveform at any angular orientation is just the first derivative of the waveform of the source's spatial impulse response function at that orientation. Consequently, the convolution of a crosscorrelation function with a step function is clearly just the integration operation that inverts the differentiation performed by the mechanical-compliance element in the Type F36 source's electro-mechanical network.

The relation of the Type F36 source's spatial impulse response function to the directly measured input-output crosscorrelation function is shown in Fig. 31. An unfiltered normalized input-voltage/output-voltage crosscorrelation-function waveform is shown at the top of this figure. This is the waveform of the experimental crosscorrelation

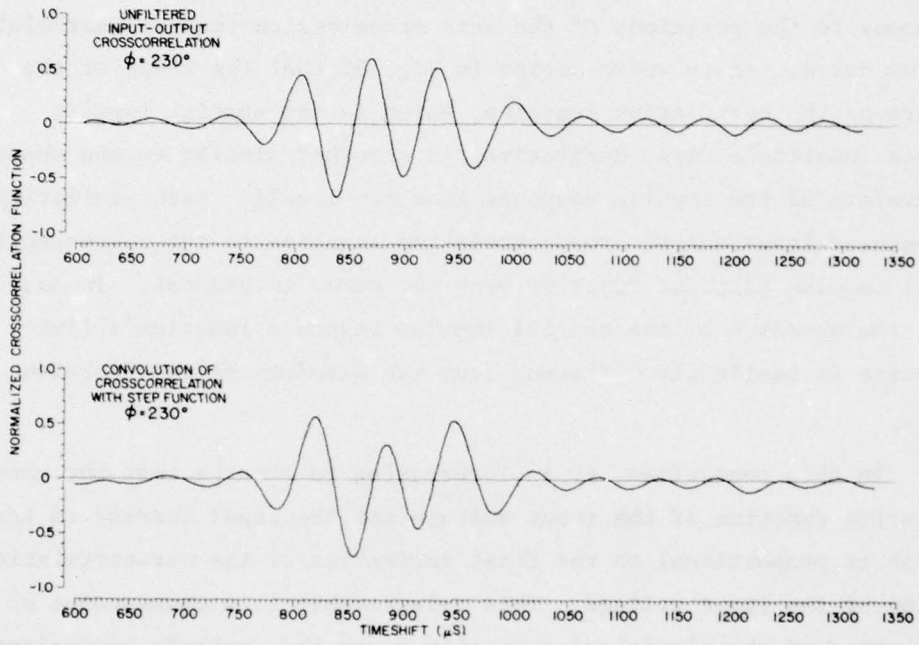

Fig. 31--Measured crosscorrelation function before and after it is filtered

function, measured at the orientation for which ϕ = 230°, before it is convolved with a step function. At the bottom of Fig. 31, the normalized spatial-impulse-response-function waveform that results from the convolution is shown. This same spatial impulse response function appears at the center in Fig. 26. It is clear from Fig. 31 that the waveform of the measured input-output crosscorrelation function, shown at the top of the figure, is the first derivative of the spatial-impulse-response-function waveform shown at the bottom. Thus, the positions along the τ axis of the positive-going and negative-going axis crossings on the lower spatial-impulse-response-function curve coincide very nearly to the

positions of the maxima and minima on the upper crosscorrelation-function curve, since these axis crossings occur at very nearly the positions for which the slope of the spatial-impulse-response-function curve is most pronounced. Thus too, the maxima and minima in the spatial-impulse-response-function curve, where this function's first derivative is zero, correspond to the positions of the axis crossings on the crosscorrelation-function curve. It is worth noting in Fig. 31 that the shape of the waveform of the correlation function, which is the spatial impulse response function's first derivative, is somewhat similar to the shape of the waveform of the impulse response function itself. Such similarity of the measured input-output crosscorrelation function to the corresponding spatial impulse response function does not occur in general. In most cases, the waveform of the spatial impulse response function's first derivative is manifestly different from the waveform of the function itself.

In this connection, it is interesting to observe that the cross-correlation function of the input voltage and the input current to the Type F36 is proportional to the first derivative of the autocorrelation function of the input voltage. This relationship is a consequence of the presence of the electrical capacitor C_0 in the source's equivalent circuit that is shown in Fig. 9. Because the capacitor C_0 shunts the input electrical terminals in the network that characterizes the Type F36, the current flowing into the Type F36, at any frequency ν, is proportional to $j2\pi\nu E_I(\nu)$, where $E_I(\nu)$ is the spectral component of the input voltage at that frequency. Since the input current into the Type F36 is proportional to the first derivative of the input voltage for constant-voltage drive, the waveform of the first derivative of the autocorrelation function of the input voltage (which is shown in Fig. 21) will be the same as the waveform of the crosscorrelation function of the input current and the input voltage. Thus, the shape of the waveform of the measured input-voltage/input-current crosscorrelation function is not similar to the shape of the waveform of the measured input-voltage/input voltage

autocorrelation function. Moreover, if one wished to obtain the spatial impulse response function of the Type F36 from the crosscorrelation function of the received voltage and the input current to the Type F36, he would be required to convolve the measured crosscorrelation function with a ramp function, rather than with a step function. This would be necessary, since the velocity of the radiating surface of the Type F36 would be proportional to the second derivative of the input current supplied to the source under conditions of constant-voltage drive. All of the experimental spatial impulse response functions discussed here, however, will be determined, via convolution with a step function, from input-voltage/received-voltage crosscorrelation functions.

The required convolution of measured input-output crosscorrelation functions with a step function is accomplished by means of the computer. The procedure begins with the computation of the eight input-output normalized crosscorrelation functions that pertain to any particular angular orientation of the Type F36 source. After these normalized cross-correlation functions are averaged according to Eq. (132), the mean-squared value of the resulting average crosscorrelation function is computed. This average normalized crosscorrelation function is then written onto a magnetic tape, which serves as the input to the convolution program. This latter program causes each correlation-function record to be convolved with a step function that has an arbitrarily chosen step height. Each spatial impulse response function resulting from such a convolution has at this stage the correct waveform, but does not yet have the correct amplitude. In order to set the amplitude of the spatial impulse response function, one sets its mean value to be zero and then computes its mean-squared value. The amplitude of the computed spatial impulse response function is then adjusted so that the function will have a mean-squared value identical to that of the original correlation function from which it is obtained by convolution. In other words, one, in effect, passes each average input-output crosscorrelation function through a filter that neither adds nor removes energy from the input signal. The mean-

squared values of the original crosscorrelation function and of the resulting spatial impulse response function are, of course, computed using waveform records of the same duration in both cases.

Now that the preceeding general considerations have been properly dealt with, one may redirect his attention to the experimental results depicted in Figs. 24 through 30, bearing in mind that the results observed in the quadrant for which $180° \leq \phi \leq 270°$ are largely representative of the results obtained in the other three quadrants. Between $\phi = 180°$ and $\phi = 190°$, as will be noted from Fig. 24, there is little change in the waveform of the spatial impulse response function. The waveform changes somewhat but retains this basic shape as ϕ increases further. Indeed, the waveform at $\phi = 210°$, which is shown at the center of Fig. 25, is basically similar to that at $\phi = 180°$, except that the secondary positive maximum, which occurs is near $\tau = 998$ μs for $\phi = 180°$, has moved toward the major minimum in the waveform (that minimum near $\tau = 852$ μs for $\phi = 180°$) so as to be near $\tau = 962$ μs for $\phi = 210°$. (The major minimum is that minimum near $\tau = 847$ μs for $\phi = 210°$.) This secondary positive maximum also increases in amplitude as ϕ increases from 180° to 210°. Further, one sees from the lower curve in Fig. 25 that the waveform at $\phi = 30°$, which is the diametrically opposite position from the $\phi = 210°$ orientation, is basically like the waveform observed at $\phi = 210°$, as is to be expected on the basis of symmetry. The amplitudes and the positions of the corresponding secondary maxima, with respect to the primary minima, are slightly different, however, in the two cases.

As ϕ is changed from 180° to 210°, it is seen that the secondary positive maximum in the waveform grows in amplitude and moves toward the primary minimum. This representative behavior continues with increasing ϕ until the waveform takes on the appearance of that depicted in the center curve of Fig. 26, which occurs in the case when $\phi = 230°$. Somewhere beyond $\phi = 230°$, in the vicinity of $\phi = 240°$, a rapid transition takes place in the waveform as the orientation of the source is changed.

The waveform that results from the transition has attained its basic shape when $\phi = 250°$. As can be seen from Fig. 27, the spatial-impulse-response-function waveform retains this basic appearance in the range $250° \leq \phi \leq 270°$.

Owing to symmetry, the waveforms of the spatial impulse response function observed at $\phi = 60°$, 120°, and 300° should all resemble one another as well as resemble the waveform that is observed at $\phi = 240°$. It can be seen from Fig. 28 that this is not the case. This dissimilarity in waveforms is caused by a small angular misalignment in the transducer-mounting assembly. The effect of this angular misalignment on the waveforms observed near $\phi = 60°$, 120°, 240°, and 300°, however, is greatly magnified, since the shape of the spatial-impulse-response-function waveform varies rapidly in the vicinity of these angles. This point will be discussed in more detail later on.

The experimental waveforms shown in Figs. 27 and 29 illustrate an extremely important result. To appreciate this experimental result, one must first recall some of the consequences of the theoretical analysis developed in Chapter IV. In Chapter IV, it was shown that there are two distinct regions in the acoustic field radiated by a line source of length L. It will be remembered that, in the region outside of the two parallel planes that pass through the ends of the line source and to which the source is perpendicular, the source's field is comprised of two destructively interfering components. These components are radiated by point sources at each end of the line. (See Eq. (80b).) On the other hand, in the region between the two parallel planes, which are separated by the distance L, the source's radiated field is comprised of three components. (See Eq. (80a).) In this latter region, two of the components are radiated by point sources at the ends of the line source and interfere constructively with each other. There also exists an expanding cylindrical wave in this region that interferes destructively with these two constructively interfering components. According to the theoretical picture, when an observation point in the line source's field

crosses either of the planes that delineate the two regions in the field, the acoustic pressure field owing to the cylindrical wave component and the acoustic pressure field owing to the point radiator at the end of the line through which the plane passes, both change discontinuously. The total pressure field, however, remains continuous as one passes from one region in the field to another across one of the two parallel boundary planes.

If one makes a calculation based upon the previous ideas, he finds that, at a distance of 1.324 m from the center of a line source of length L = 210.89 mm (8.303 in), a boundary plane separating the two regions of the source's acoustic field is crossed when $\phi = 265.43°$ and again when $\phi = 274.57°$. (Boundary planes are also crossed when $\phi = 85.43°$ and when $\phi = 94.57°$.) Thus, the uppermost waveform in Fig. 29, that for which $\phi = 264°$, was observed in a region where the source's spatial impulse response function is comprised of only the two components that are radiated by the ends of the Type F36 source. On the other hand, the center and the lowermost waveforms in Fig. 29, and the lowermost waveform in Fig. 27, for which ϕ equals 266°, 268°, and 270°, respectively, were all observed in a region in which the Type F36 source's acoustic field is comprised of three components--a cylindrical wave component and components radiated by each of the source's ends. Since the waveform of the Type F36 source's spatial impulse response function is virtually unchanged when the observation point moves across one of the boundary planes delineating the two field regions, one can conclude, on the basis of the experimental results depicted in Figs. 29 and 27, that the Type F36 source's total acoustic pressure field remains continuous when the components comprising it change discontinuously.

For completeness, Fig. 30 shows the waveforms of the spatial impulse response function that were observed at orientations for which ϕ equals 320°, 150°, and 340°. Using Fig. 23 as a guide, one may compare the waveforms depicted in Fig. 30 with those waveforms related to them by the symmetry that is present the experimental situation.

The spatial-impulse-response-function waveforms observed at other angles are not illustrated because they differ insignificantly from the waveforms that are depicted in Figs. 24 through 30. For example, plots of the waveforms observed at the orientations for which ϕ equals 170° and 175° were compared, respectively, to plots of the waveforms observed at $\phi = 190°$ and at $\phi = 185°$. The comparison, which was made by superimposing the plotted curves on a light table, showed the corresponding waveforms to be virtually indistinguishable from one another. A similar comparison of the waveforms observed at the orientations for which ϕ equals 280°, 276°, 274°, and 272° to the respective waveforms observed at $\phi = 260°$, 264°, 266°, and 268° showed corresponding waveforms to be almost identical. The observation of identical waveforms at equal angular increments on either side of the $\phi = 180°$ orientation and on either side of the $\phi = 270°$ orientation was taken as an indication that the angular misalignment of the transducer-mounting assembly was small.

It will now be shown that the observed spatial-impulse-response-function waveforms for the Type F36 source, which are illustrated by Figs. 24 through 30, are those waveforms to be expected according to the analysis developed in Chapter IV, which describes the radiated field of an ideal line source. Before theoretical and experimental results can be compared, however, two questions must be dealt with, which concern the construction of theoretical spatial-impulse-response-function waveforms. First, one must determine the correct value to use for L, the length of the radiating line source that is equivalent to the actual Type F36 source transducer. Second, one must find an adequate numerical representation of the theoretical equations appearing in Chapter IV, which are expressed in terms of generalized functions, so that theoretical spatial-impulse-response-function waveforms can be constructed using the computer. These two problems are addressed below, commencing with the question of determining the equivalent line length of the Type F36 source.

One first notes that both Refs. [93] and [94] describe the Type F36 transducer as having "...directivity in the vertical (XY) plane...

equivalent to that of an 8-inch (20.3-cm) line." However, if one uses the typical 10 kHz directional response pattern of the Type F36 transducer for the vertical plane, which is enclosed in both Refs. [93] and [94] and if one assumes that this pattern was measured at a temperature of 30°C (the same temperature at which the transducer-calibration curves were obtained), then he will calculate the value of the equivalent line length of the Type F36 to be approximately 210 mm (8.26 in), which is greater than the 203 mm value specified for this quantity. This calculation is based upon the expected angular positions of the nulls in the farfield directional response pattern of a continuous line radiator of length L. (The "vertical...plane" referred to in Refs. [93] and [94] corresponds to the horizontal plane HH' in the experimental arrangement here, since, in practice, the Type F36 is usually deployed with its axis of cylindrical symmetry vertical.) The nulls on either side of the major lobe of such a directional response pattern will occur at the angles ϕ_{1N} that satisfy the relation

$$\sin\phi_{1N} = \pm c/(\nu L), \tag{133}$$

if the line source radiates a harmonic signal with frequency ν, where c is the soundspeed in the acoustic medium. Moreover, the problem of determining the equivalent length L of the Type F36 is not resolved by taking L to be 195.1 mm (7.68 in), which is the overall length of the seven-element array of endcapped cylindrical shells that constitutes the active portion of the Type F36 transducer. A continuous line array this short would not produce directional response patterns like those in Refs. [93] and [94], nor would such a small value of L be consistent with the observed behavior of the spatial-impulse-response-function waveforms.

Nor can one reasonably model the seven-element array within the Type F36 transducer as a seven-element array of discrete point sources, in order to determine L. For an N element discrete array with overall length L', the equation analogous to Eq. (133) is

AD-A053 395 NAVAL RESEARCH LAB WASHINGTON D C F/G 20/1
SPATIAL IMPULSE RESPONSE OF AN ACOUSTIC LINE RADIATOR - A STUDY--ETC(U)
FEB 78 A J RUDGERS

UNCLASSIFIED NRL-8191 SBIE-AD-E000 134 NL

3 OF 3
ADA
053395

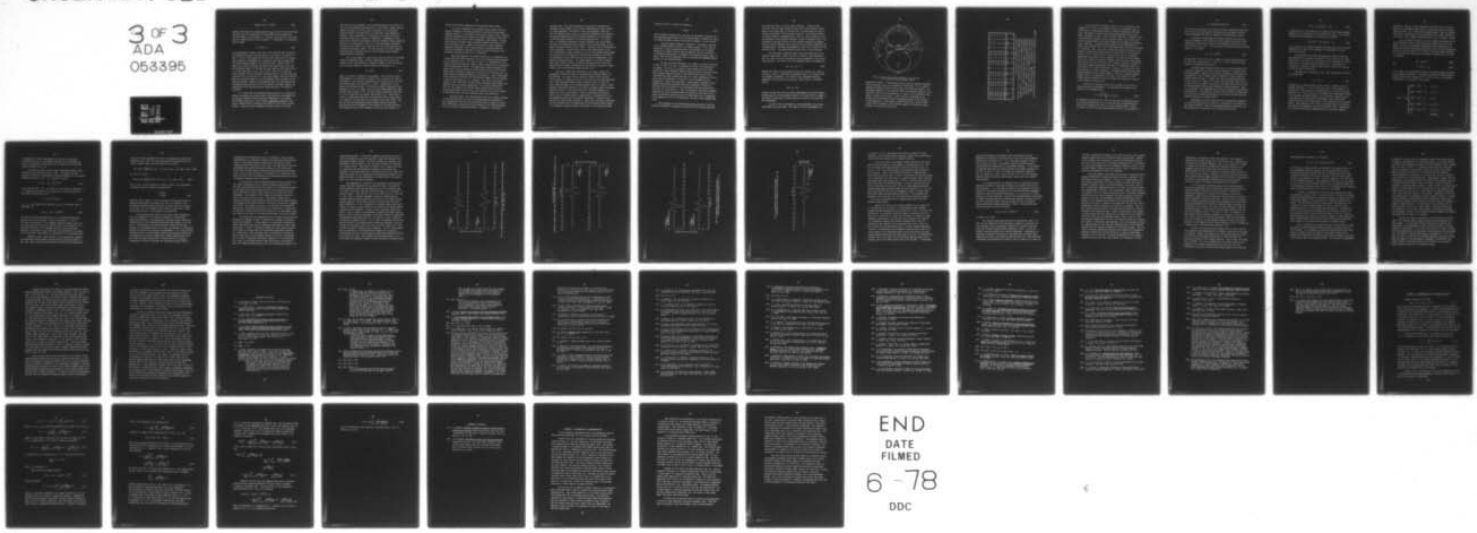

END
DATE
FILMED
6-78
DDC

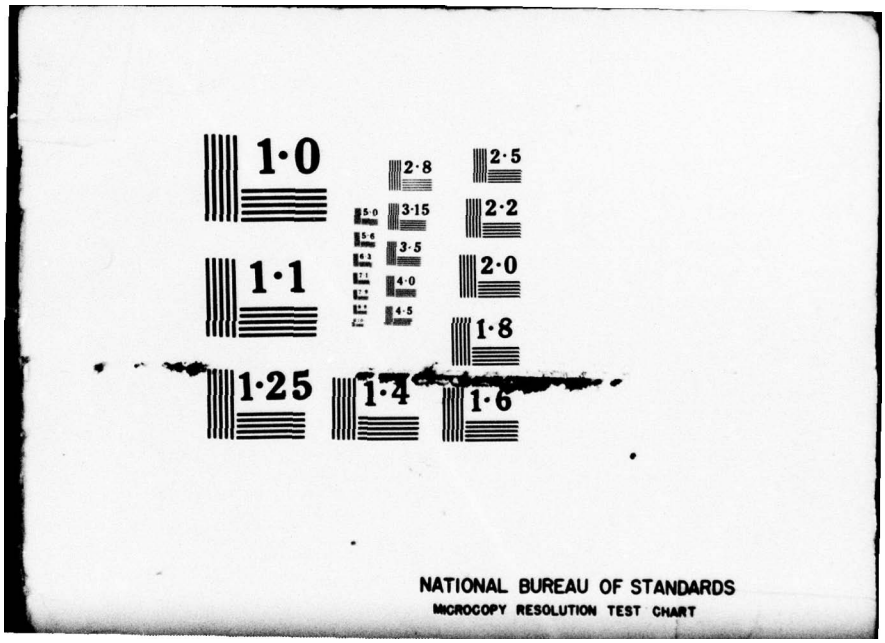
1·0
1·1
1·25
2·8
3·15
3·5
4·0
4·5
5·0
2·5
2·2
2·0
1·8
1·4
1·6
NATIONAL BUREAU OF STANDARDS
MICROCOPY RESOLUTION TEST CHART

$$\sin\phi'_{1N} = \pm c(N - 1)/(N\nu L'). \qquad (134)$$

Equation (134) gives the angular positions ϕ'_{1N} of the first nulls occurring on either side of the major lobe in the discrete array's directional response pattern at the frequency ν. From Eqs. (133) and (134) it is seen that an N element discrete line of length L' is equivalent to a continuous line of length

$$L = L'N/(N - 1) \qquad (135)$$

if the equivalence is made on the basis of the observed null positions in the farfield directional response pattern of the source. The factor of N/(N - 1) in Eq. (135) points out the fact that a line array of discrete point radiators is equivalent to a continuous array that is longer than the overall physical length of the discrete array. However, for N = 7, which is the case in question, one finds on the basis of Eq. (135) that the equivalent length L of the Type F36 array would be 200.0 mm (7.875 in) if L' were taken equal to 171.1 mm (6.75 in), which is the center-to-center spacing of the two outermost cylindrical shells, or else finds that L would be 222.2 mm (8.75 in) if L' were taken equal to 190.5 mm (7.50 in), which is the overall length of the seven-element array, exclusive of the outermost endcaps. Neither the unreasonably short 171.1 mm value nor the unreasonably long 222.2 mm value for the source's equivalent length L is consistent with the observed acoustic characteristics of the Type F36 transducer.

It is clear from the preceding discussion that it is fruitless to attempt to determine the correct value of the equivalent line length L of the Type F36 transducer from the physical dimensions of its internal seven-element array since, from a strictly <u>structural</u> standpoint, this array is unlike either a continuous line array or a line array of point sources. Instead, one must establish the proper value of L for the

Type F36 source by experiment. The preceding discussion also points out how such an experimental determination of L can be made, namely, from the angular positions of the nulls that are present in the directional response pattern of the Type F36 in the plane HH' at any frequency ν. Moreover, such an experimental determination of the Type F36 source's equivalent length can be carried out completely independently of the input-output correlation experiments that were performed using noisebursts. Therefore, the experimental value of L, thus independently determined from directional-response null positions, will not be prejudiced by the correlation-experiment results. Yet once obtained, this value should be consistent with the characteristics of the observed spatial-impulse-response-function waveforms.

If L is the length of a line source, with its center at a distance R from an observation point, then that observation point can be considered to be in the farfield, or Fraunhofer region, of the line source, when the source radiates a harmonic signal with frequency ν, if

$$R > \nu L^2/c \ , \qquad (136)$$

where c, as before, designates the soundspeed. The criterion for the establishment of a line source's farfield that is given by Eq. (136) is conservative. Null-position determination in the acoustic field of the Type F36 was made at the distance R = 1.324 m. Suppose that ν is no greater than 20 kHz and that c = 1487.443 m/s, which corresponds to the temperature of 21.7°C at which the null-position measurements were made. Moreover, when using Eq. (136), one may certainly assume that the value of L for the Type F36 is no greater than 229 mm (9 in). Then with R = 1.324 m, a calculation shows that the observation point is well within the farfield of the Type F36 at all frequencies less than 20 kHz. (One may note that the experimental spatial impulse response functions reported here were all measured in the farfield of the Type F36, since the noisebursts used as input signals to the source were filtered to

suppress the spectral components with frequencies above 20 kHz.)

In order to determine the equivalent source length L from the angular separation of the null positions in the source's directional response pattern, it is necessary to excite the source at each of several harmonic frequencies and to measure the angular positions of the nulls that are created at each of those frequencies. Again owing to the confined volume of the water tank, continuous harmonic excitation of the Type F36 cannot be used. Rather, one excites the source transducer using gated sinusoids, each of which contains an integral number of cycles of the harmonic frequency for which the null positions in the directional response pattern are to be measured.

Such gated sinusoids (so-called "pulsed CW") or "tonebursts" are created using the buffer/interface unit in the pulse-generating subsystem of the electronic suite. (See Figs. 14 and 15.) A modification of the timing subsystem is necessary, however, before tonebursts can be generated with the experimental system. This modification takes advantage of the phase-locked relation between the 5 MHz reference signal and the output signal from the frequency synthesizer (See Fig. 18.), which was set to be 200 kHz when performing experiments with noisebursts. Using a high-speed preset counter, one divides the 5 MHz reference signal by 25 and produces a train or short pulses at 5 μs intervals. The output of the preset counter is then substituted for the 200 kHz sinusoidal timing signal that emanates from the frequency synthesizer in the situation depicted in Fig. 18. Now, however, the 200 kHz timing pulsetrain and all other system timing signals derived from it are produced from, and are thereby in synchronism with, the 5 MHz reference signal from synthesizer.

The clock signal, from pulse generator PG2 in the timing subsystem to the buffer/interface unit in the waveform-generating subsystem, is next disconnected and a new clock pulsetrain, which is needed to control the transmission of digital data from the memory in the buffer/interface unit to the digital-to-analog converter, is supplied to the buffer/

interface unit. This clock pulsetrain is generated by supplying the synthesizer output signal to the external-synchronization input terminal of a pulse generator. The output of this pulse generator, which is a train of repetitive short pulses at intervals determined by the period of the sinusoid emanating from the frequency synthesizer, is then supplied to the clock input terminal of the buffer/interface unit. It is seen that, by varying the synthesizer's output frequency, the rate at which the words are transmitted from the memory of the buffer/interface to the digital-to-analog converter may be varied. Moreover, when the synthesizer's output frequency is varied in this way, no other timing signal in the entire measurement system is altered, since all other system timing signals are derived from the synthesizer's 5 MHz reference signal and not from the synthesizer output, which controls only the word transmission to the digital-to-analog converter. All timing signals in the entire measurement system, however, remain in complete synchronism, since the output signal from the frequency synthesizer at any arbitrary frequency is phase-locked to the 5 MHz reference signal from that unit.

With this timing-system modification, one easily obtains the experimental tonebursts needed for measuring the equivalent length L of the Type F36. One simply writes a series of digital records of sinusoidal signals on a magnetic tape that can be input to the buffer/interface unit. Each sinusoidal signal record is written so that it fills the entire 4096-word memory of the buffer/interface when it is loaded. Every digitally represented sinewave in the series is computed using a different sampling interval, so that each record has a different number N_S of samples per cycle of the sinusoid. Thus, one generates records with values of N_S = 8 samples/cycle, 12 samples/cycle, 16 samples/cycle, etc. Now suppose that one sets the frequency synthesizer to produce a sinusoidal output signal with frequency ν_0. Then, since this signal determines the rate at which words are transmitted from the buffer/interface memory to the digital-to-analog converter, the output of the digital-to-analog

converter will be a sinusoid of frequency

$$\nu = \nu_0/N_S \cdot \qquad (137)$$

Thus by properly choosing both ν_0 and N_S, the synthesizer frequency and the digitized-sinusoid record with the proper number of samples per cycle, an analog sinusoidal voltage at any desired frequency ν can be created.

From this analog sinusoid at frequency ν, a toneburst comprised of any integral number of cycles n_C is easily created. To do this one needs only to start transmitting words from the memory of the buffer/interface at a memory location that corresponds to an axis crossing of the digitized sinusoid and to terminate the transmission after $(n_C N_S + 1)$ words. This can be accomplished simply by setting the thumbwheel-switch controls of the buffer/interface.

For null-position measurements, six tonebursts having frequencies of from 7.5 kHz to 8.0 kHz, in increments of 100 Hz, were generated by this means. The value of n_C chosen at each frequency was that which created the longest possible toneburst having a duration less than 2.8 ms. This frequency range was chosen so that there would be nulls in the resulting directional response patterns for a water temperature of 21.7°C and so that the positions of these nulls at any frequency would be separated by a relatively large angle. Large angular separations can be measured with greater precision than small separations, because the precision [110] with which one can read angles using the divided dial D (See Fig. 12.) is about ±0.1°. Thus, the precision with which an angular separation $\Delta\phi$ can be calculated from the positions of two nulls in the source's directional response pattern is always about ±0.2°, independent of the magnitude of $\Delta\phi$, if the calculation is based on dial-reading error alone.

Null positions in the directional response patterns of the Type F36 were determined by observing the waveform of the received pulse that

was produced by each of the six input tonebursts. Tonebursts were filtered, with the same cascaded filters used in the noiseburst experiments, before being input to the Type F36. An oscilloscope was used to observe the waveform of each received toneburst. The received toneburst was passed through a narrowband filter, with its center frequency set at the frequency of the toneburst sinusoid, in order to minimize noise. The amplitude of the center portion of the received toneburst was observed and the Type F36 transducer was rotated until this observed amplitude had a minimum value. The angle corresponding to such a null position was then read from dial D. The oscilloscope was thus used as a null detector.

The directional response pattern of the Type F36 source in the frequency range from 7.5 kHz to 8.0 kHz is similar to that sketched in Fig. 32. The two nulls at the angles ϕ_1 and ϕ_2 indicated in Fig. 32 are those measured. The value of the null-separation angle is determined as

$$\Delta\phi = \phi_1 - \phi_2 + \pi \, . \tag{138}$$

One-half the value of null-separation angle $\Delta\phi$ is given by Eq. (138) is used in Eq. (133) to calculate the equivalent value of L at each of the six toneburst frequencies. The value of $\Delta\phi$ is determined from the separation of the two nulls at ϕ_1 and ϕ_2, rather than as a difference such as

$$\Delta\phi = \phi_1 - \phi_0 \, ,$$

because, in this way, the null-position measurement can be made without placing any part of the mounting structure of the Type F36 in a region of the source's field where it might perturb the results of the sensitive null measurement.

At each of the six frequencies, ten measurements of ϕ_1 and ten measurements of ϕ_2 were made. The results of these measurements are

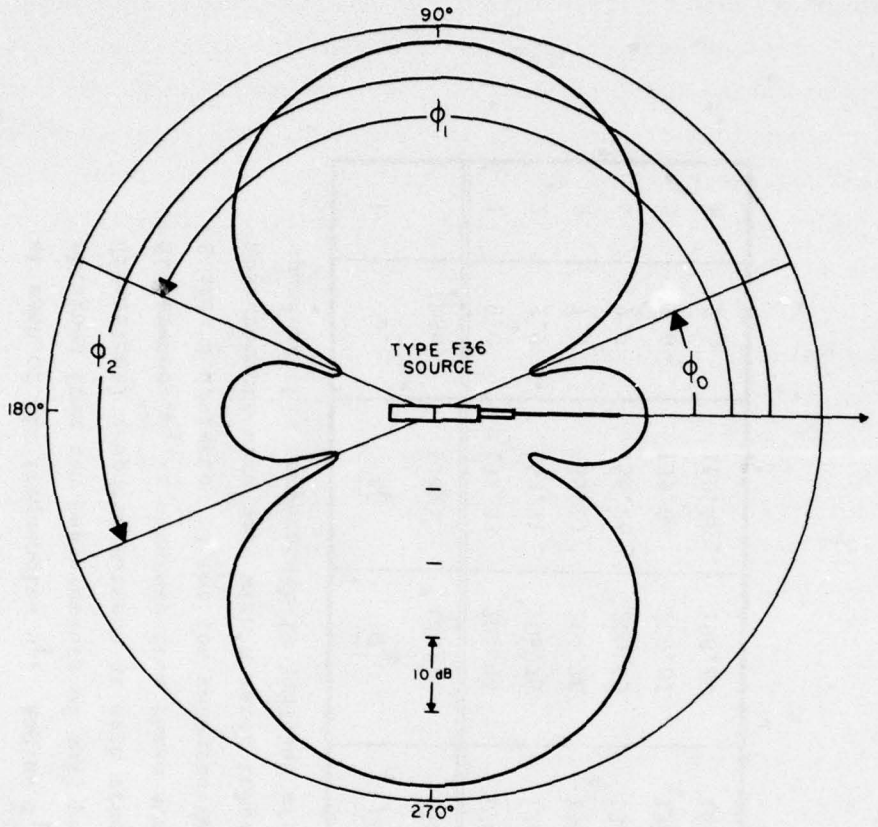

Fig. 32--Typical directional response of the type F36 in 7.5 kHz to 8.0 kHz frequency range

summarized in Table 3. Those tabular entries that are averages determined from ten measured values are designated by placing bars over the symbols heading the columns of Table 3 that contain the entries in question. The equivalent lengths $\overline{L}_i$ of the Type F36, which are determined using Eq. (133) from $\Delta\overline{\phi}_i$ at each of the six frequencies ν_i, where i is a convenient index, appear in column six of Table 3. Since each $\overline{L}_i$ is calculated as an average that is determined from the ten measured values of $\Delta\phi_i$ obtained at each frequency ν_i, the observed standard deviation σ_i of $\Delta\phi_i$ at each ν_i may also be calculated. This quantity appears in the seventh column of Table 3 and will be useful later.

TABLE 3.--Measurement of the equivalent line length $\bar{L}_1$ of the Type F36 source at each of six frequencies ν_i. Angles $\bar{\phi}_1^i$ and $\bar{\phi}_2^i$ are averages obtained from ten measurements of null positions in the source's directional response pattern at each frequency. Average angular difference $\overline{\Delta\phi}_i$ is obtained from these average angles. (See text.) Standard deviation of the ten measured $\Delta\phi_i$ is σ_i. All null-position measurements were made with a water temperature of 21.7°C. The sound-speed at this temperature is 1487.443 m/s.

i	ν_i (kHz)	$\bar{\phi}_1^i$ (deg)	$\bar{\phi}_2^i$ (deg)	$\overline{\Delta\phi}_i$ (deg)	$\bar{L}_i$ (mm)	σ_i (deg)
1	8.0	152.33	207.46	124.87	209.74	0.14916
2	7.9	152.91	206.75	126.16	211.17	0.067495
3	7.8	155.07	204.78	130.29	210.16	0.21402
4	7.7	156.26	203.45	132.81	210.65	0.23623
5	7.6	159.04	200.67	138.37	209.38	0.40073
6	7.5	160.46	198.62	141.84	209.85	0.40682

It will be noted from Table 3 that σ_2, which corresponds to the frequency of 7.9 kHz, is the smallest value of σ_i observed and that σ_i increases for the measurements made at toneburst frequencies lower than this. One expects to obtain a more precise measurement of $\bar{L}_i$ at the higher frequencies in the 7.5 kHz to 8.0 kHz range for two reasons. First, for the particular angles ϕ_1 and ϕ_2 measured (Refer to Eq. (138)), the nulls in question will be more widely separated, the higher the frequency of the toneburst. A constant scale-reading error in determining the angles, then, implies that a more precise measurement of $\bar{L}_i$ can be obtained as ν increases. Also, since one is observing a received toneburst in the presence of system noise when setting the orientation of the Type F36 to produce a null in the direction of the receiver, there is an inherent measurement error owing to one's inability to observe the exact minimum value in the source's directional response pattern with the oscilloscope. This type of error also increases as the frequency decreases, because the system noise remains approximately constant as ν diminishes, while the source level of the Type F36 decreases. Moreover, the resolution of the null positions is further degraded as ν diminishes because the secondary maximum between ϕ_1 and ϕ_2 becomes smaller. When this secondary maximum becomes smaller, the magnitude of its slope in the region of a null likewise becomes smaller and the null becomes more difficult to resolve in the presence of system noise.

Since the six measured values of $\bar{L}_i$ in Table 3 are not all of equal precision, one determines L, the equivalent line length of the Type F36, as the weighted mean

$$L = \bar{L}_2 + \frac{\sigma_2}{6} \sum_{i=1}^{6} (\bar{L}_i - \bar{L}_2)/\sigma_i \ . \qquad (139)$$

The weighting of the $\bar{L}_i$ in Eq. (139) is linear and the weighting factors are inversely proportional to σ_i, so that the most precisely measured values of $\bar{L}_i$ influence the value of L to the greatest extent. Using Eq. (139), the value of L that one determines from the $\bar{L}_i$ in Table 3 is

$$L = 210.89 \text{ mm } (8.303 \text{ in}). \qquad (140)$$

It is this measured value of the Type F36 source's equivalent length that will be used in constructing the theoretical spatial-impulse-response-function waveforms that will be compared to the experimental results.

Theoretical spatial-impulse-response waveforms are constructed, using the computer, on the basis of Eqs. (80), which describe the field radiated by a line source in terms of the generalized function $\psi(r,\mu,t)$ that is given by Eq. (81). It is seen that this function increases without bound as $t \rightarrow t_0$, where

$$t_0 = (r^2 + \mu^2)^{\frac{1}{2}}/c \ . \qquad (141)$$

The function ψ is zero prior to t_0, owing to the step-function factor in Eq. (81), but is not zero for $t > t_0$, i.e., a "tail" follows the singularity in the generalized function ψ.

A suitable approximating function that is finite everywhere must be found to represent ψ in order to use the computer to calculate theoretical waveforms. Moreover, this finite approximating function must be represented by a set of sample values calculated at a finite number of discrete values of time t. Suppose this finite approximating function is called $\hat{\psi}(r,\mu,n\Delta\tau)$, where $\Delta\tau$, the time interval between sample values, is taken to be 5 μs, which is the same as the sample interval in the case of the experimental spatial-impulse-response-function waveforms. Here n is an integer. Upon examining several ways of numerically representing the function $\hat{\psi}$, it was found that the tail, which follows the singularity of ψ, has only an insignificant effect on the result obtained when some arbitrary function is convolved with $\hat{\psi}$.

Subsequently it will be seen that the only important properties of ψ are those that affect the result of a convolution of the function ψ with another function. Thus for calculating theoretical waveforms, one may characterize the function ψ by its singularity and write

$$\psi(r,\mu,t) \approx A(r,\mu)\delta(t - t_0), \tag{142}$$

in which $A(r,\mu)$ is the weight of the δ-function that describes singular behavior of $\hat{\psi}$ at the time t_0 that is given by Eq. (141). The function $\hat{\psi}$ numerically approximating ψ is given by the expression

$$\hat{\psi}(r,\mu,n\Delta\tau) = A(r,\mu)\delta_0(n\Delta\tau - t_0). \tag{143}$$

In Eq. (143), δ_0 is a sampled numerical representation of the δ-function appearing in Eq. (142) and A represents the same quantity in both Eqs. (142) and (143).

Two questions arise when representing the numerical function approximating ψ by the means the quantity $\hat{\psi}$ that is given by Eq. (143). First, what is the value of A, the weight of the δ-function, and second, how shall δ_0, the finite numerical equivalent of a δ-function, be represented? Consider the second question first, namely, the question of representing the function δ_0.

The numerical δ-function δ_0 in Eq. (143) should assume the value zero except when

$$n\Delta\tau - t_0 = 0 , \tag{144}$$

in which case, it should assume a value of unity. However, since the sampling increment $\Delta\tau = 5$ μs is fixed and since n is an integer, it is seen that Eq. (144) cannot be satisfied unless t_0 is itself an integral multiple of $\Delta\tau$. Now the time t_0 is determined by the experimental values of the source's equivalent length L, by the distance R from the center of the Type F36 to the receiver, by the angle ϕ that specifies the orientation of the source with respect to the receiver, and by the sound-speed c. The quantity t_0 is, in fact, the arrival time at the receiver of a particular component in the source's radiated field. Consequently, t_0 is almost never an exact integral multiple of the fixed sampling

interval $\Delta\tau$. That is, in any experimental situation, the one non-zero value of δ_0 will almost always occur at a time other than one at which a sample is taken, i.e., it will occur between samples. Thus, the sampled form of δ_0, if represented in the usual manner, will consist entirely of zero values. Such a sampled representation of δ_0 is, of course, useless.

It is necessary, therefore, to find a sampled representation for δ_0 that assumes a value of unity between two samples and is zero elsewhere. This can be accomplished numerically, by an adaptation of the formula for five-point Lagrange interpolation [111], in the following way. First, one finds n_0, which is the value of n that most nearly satisfies Eq. (144), and also calculates the remainder h derived from it by using the equations

$$n_0 = [[t_0/\Delta\tau]] \tag{145a}$$

and

$$h = (t_0/\Delta\tau) - n_0. \tag{145b}$$

In Eq. (145a), the double brackets denote "the largest integer contained in the bracketed expression." Assuming that times are reckoned from an initial instant that corresponds to n = 0 in Eq. (144), one calculates five samples of δ_0 according to the formula

$$\delta_0(n\Delta\tau - t_0) = \begin{cases} \frac{1}{24}(h^2 - 1)h(h - 2), & n = n_0 - 2 \\ -\frac{1}{6}(h - 1)h(h^2 - 4), & n = n_0 - 1 \\ \frac{1}{4}(h^2 - 1)(h^2 - 4), & n = n_0 \\ -\frac{1}{6}(h + 1)h(h^2 - 4), & n = n_0 + 1 \\ \frac{1}{24}(h^2 - 1)h(h + 2), & n = n_0 + 2 \\ 0, & \text{elsewhere.} \end{cases} \tag{146}$$

The numerical δ-function expressed by Eq. (146) has the required characteristics, for, if any sampled function that is represented as $f(n\Delta\tau)$ is numerically convolved with δ_0, the result will be the time-delayed function $f(n\Delta\tau - t_0)$.

By using Eq. (146), one may obtain an adequate numerical representation for the function δ_0 in Eq. (143). The weight A of this numerical δ-function is determined by noting the behavior of the original generalized function ψ as $t \to t_0$. Consider the factor

$$\xi = t[t^2 - (r^2 + \mu^2)/c^2]^{-3/2} \tag{147}$$

in Eq. (81) at time $t = t_0 + \Delta t$, where Δt is very small in comparison to t_0. Neglecting quantities of the second order, one obtains from Eqs. (141) and (147) the result that

$$\xi \to (\Delta t)^{-3/2} 2^{-3/2} t_0^{-\frac{1}{2}} \tag{148}$$

as $t \to t_0$. The weight of the function δ_0 in Eq. (143) should then be specified to be

$$A(r,\mu) = [(r^2 + \mu^2)^{\frac{1}{2}}/c]^{-\frac{1}{2}} \tag{149}$$

from which the arbitrary numerical factor, the negative three-halves power of two, has been omitted. Since the quantity $(r^2 + \mu^2)^{\frac{1}{2}}$ in Eq. (149) is a distance (it, for example, being the distance from one of the point radiators at an end of the line source to the receiver), one sees that the effect of the singularity in each of the generalized functions ψ that appears in Eqs. (80) will vary inversely as the square-root of the range. Such behavior is characteristic of cylindrical waves.

Using Eqs. (143), (146) and (149), one can numerically represent the theoretical spatial impulse response function that is described by Eqs. (80). This is done by substituting the function $\hat{\psi}$ with appropriate

values of its input parameters for each of the generalized functions ψ appearing in Eqs. (80). The resulting numerical representation of the source's spatial impulse response function will then be

$$\hat{P}(r,z,n\Delta\tau)= -\frac{\rho Q}{4\pi}[2\hat{\psi}(r,0,n\Delta\tau) - \hat{\psi}(r, \tfrac{1}{2}L-z, n\Delta\tau) - \hat{\psi}(r, \tfrac{1}{2}L+z, n\Delta\tau)], \quad (150a)$$

for $-\frac{1}{2}L \leq z \leq \frac{1}{2}L$ and

$$\hat{P}(r,z,n\Delta\tau)= -\frac{\rho Q}{4\pi}\,\mathrm{sgn}(z)[\hat{\psi}(r, \tfrac{1}{2}L-z, n\Delta\tau) - \hat{\psi}(r, \tfrac{1}{2}L+z, n\Delta\tau)], \quad (150b)$$

for $|z| > \frac{1}{2}L$. One can express Eqs. (150) in terms of the experimental coordinates R and ϕ by using the transformation

$$\begin{aligned} r &= R\sin\phi \\ z &= R\cos\phi \ . \end{aligned} \quad (151)$$

Equations (150), however, do not yet describe the theoretical spatial-impulse-response-function waveforms that are to be compared to the experimental waveforms presented earlier, since one must still account for the fact that the experiments were performed using bursts of band-limited white noise as input signals to the Type F36.

The autocorrelation function of the input-voltage noisebursts, which are transmitted to the Type F36 transducer by the waveform-generation subsystem of the experimental electronic system, defines the characteristics of the bandlimited white-noise input signal to the line source. The waveform of this autocorrelation function of the input voltage, in the normalized form, is, in fact, the waveform of the impulse function that excites the source in the experiments. It is seen from the waveforms in Fig. 21 that the input-voltage autocorrelation function has the appearance of the output signal from a linear bandpass filter that would have resulted from excitation of that filter by a δ-function. Consequently, in order to construct the theoretical spatial-impulse-

response-function waveforms that are to be compared to those obtained experimentally, one numerically convolves the normalized autocorrelation function of the input-voltage noisebursts with the spatial impulse response function $\hat{P}$ described by Eqs. (150). The advantage of using the experimental autocorrelation-function waveform in this convolution, rather than the theoretical autocorrelation-function waveform described by Eq. (102), is that by doing so, one includes in the theoretical waveforms all effects that the electronic pulse-generating subsystem has upon the digitally generated input noisebursts.

The theoretical spatial-impulse-response-function waveforms that will appear subsequently are all computed by means described above. The input autocorrelation function in question is the normalized average of the eight autocorrelation functions that can be computed using the eight noisebursts of input voltage, which excite the Type F36 in the experiments. The waveform of this average autocorrelation function is shown as the lower curve in Fig. 21. The computer program used to construct theoretical spatial-impulse-response-function waveforms obtains this average autocorrelation function of the input voltage from a magnetic-tape record. This record is written at the time when the experimental input-output crosscorrelation functions are computed and it resides with the records of these crosscorrelation functions on the same magnetic tape that served as the input to the previously described convolution program.

The theoretical and experimental spatial-impulse-response-function waveforms are compared in Figs. 33 through 36 at a number of different values of the angle ϕ. In these figures, the theoretical waveforms are drawn using dotted lines and the experimental waveforms are drawn using solid lines. In order to facilitate comparisons, each theoretical waveform is made to coincide with the corresponding experimental waveform at a single point. This coincident point is indicated by the bold dot that is found near the first primary minimum in each pair of waveforms. That is, after a theoretical waveform is computed, it is shifted along the τ axis, by introducing either a fixed time delay or time advance, until its primary minimum coincides with the corresponding minimum in the

experimental waveform. A three-point Lagrange interpolation formula is used to determine the time shift necessary to make the theoretical and experimental minima coincide. Once the two minima are coincident, the amplitudes of all the points on the theoretical waveform are multiplied by a constant factor. This factor is chosen so as to require that both the theoretical and the experimental waveforms will have the same amplitude at the single point that is marked by the bold dot. Other than aligning one point on the theoretical and experimental waveforms in the manner described, no other modifications are made either to the experimental or to the theoretical waveforms.

The comparisons of theoretical and experimental spatial-impulse-response-function waveforms that are depicted in Figs. 33 through 36 clearly demonstrate that the theoretical picture of the radiated field of a finite line source, which was derived in Chapter IV, corresponds to physical reality. Thus from Fig. 33, one sees that at both $\phi = 230°$ and $\phi = 120°$, there is excellent agreement between the spatial-impulse-response-function waveform predicted on the basis of the theory and that actually measured. Recall from a previous discussion that the experimental waveform at $\phi = 120°$ is measured in an angular region where small changes in ϕ result in large changes in the shape of the spatial-impulse-response-function waveform. Yet, even in such transition regions, the theory is able to predict the experimental waveforms with great fidelity. Observe in Fig. 34 that the agreement is excellent between the theoretical and experimental waveforms both at $\phi = 260°$ and at $\phi = 270°$. Figure 34 illustrates an important result. For $\phi = 260°$, the radiated field of the Type F36 consists of two destructively interfering components, each one radiated by a pointlike source at an end of the line, while for $\phi = 270°$, the Type F36 source's field has three components. At 270°, the radiated field is comprised of a cylindrical wave component that interferes destructively with the two constructively interfering components radiated by the ends of the line. Thus, whether the observation point is in a region where two components comprise the Type F36 source's radiated field,

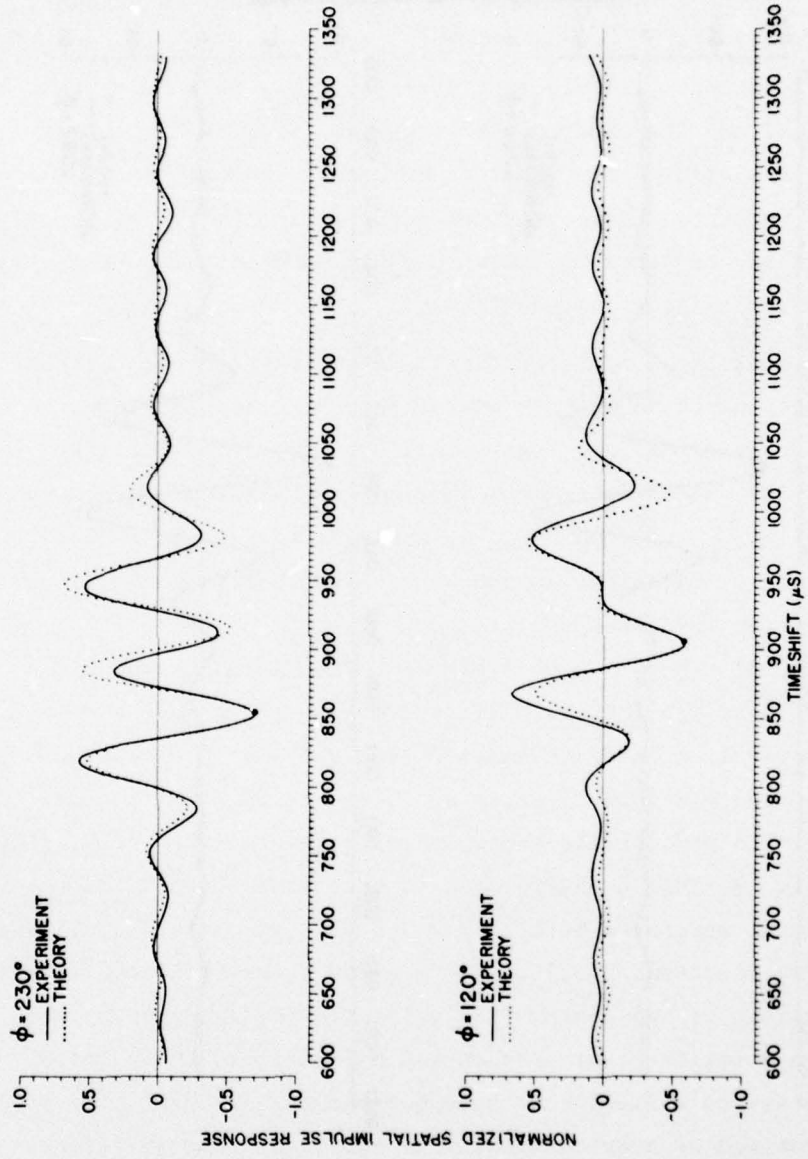

Fig. 33--Comparison of theoretical and experimental spatial-impulse-response waveforms: $\phi = 230°$ and $\phi = 120°$

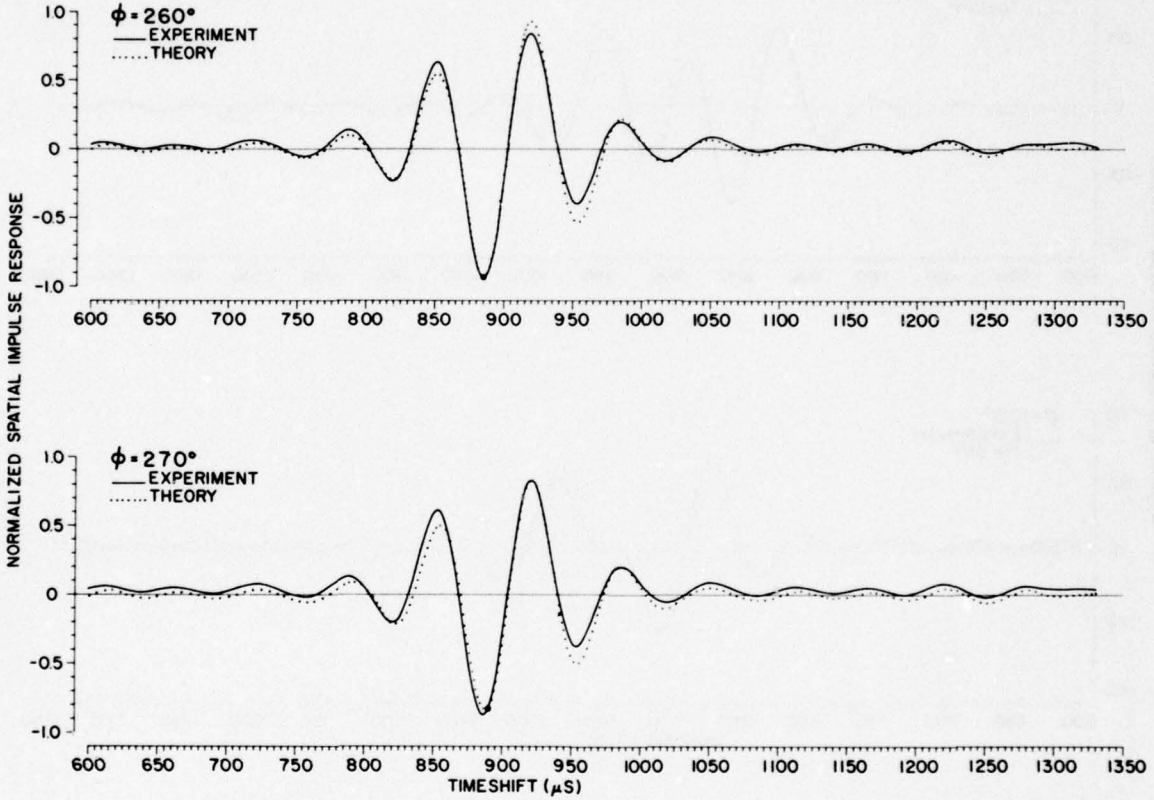

Fig. 34--Comparison of theoretical and experimental spatial-impulse-response waveforms: ϕ = 260° and ϕ = 270°

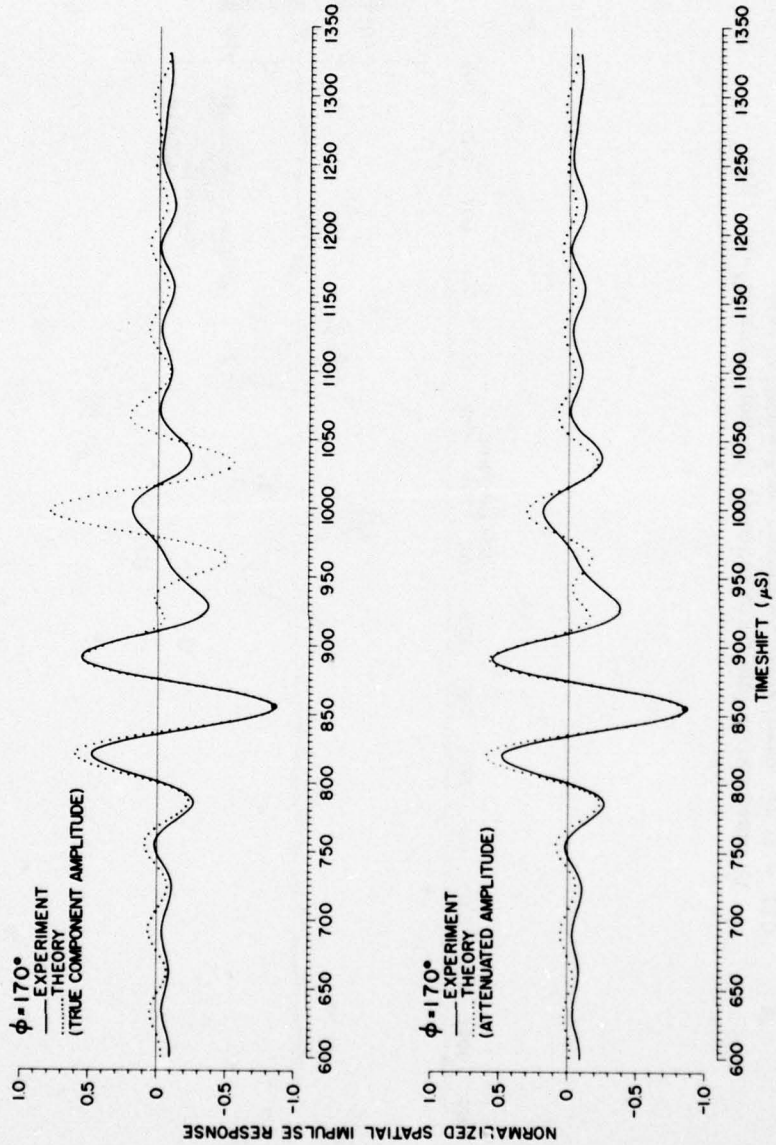

Fig. 35--Comparison of theoretical and experimental spatial-impulse-response waveforms at $\phi = 170°$

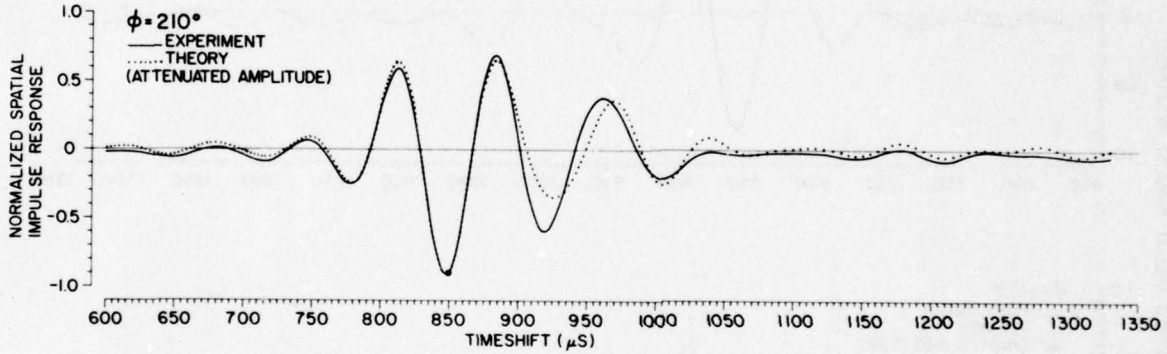

Fig. 36--Comparison of theoretical and experimental spatial-impulse-response waveforms at ϕ = 210°

or whether it is in a region where this field is comprised of three components, the theoretical model accurately predicts the spatial-impulse-response-function waveform that is actually observed.

On the other hand, the agreement between theoretical and experimental waveforms appears at first glance to be rather poor at $\phi = 170°$, if one considers the comparison made in the upper portion of Fig. 35. Now at $\phi = 170°$, the radiated field of the Type F36 source consists of two components. There is an impulse function with a negative-going major peak that arrives, when $\tau = 855$ μs, from the end of the line nearest to the observation point and there is an impulse function with a positive-going major peak that arrives, when $\tau = 997$ μs, from the end of the line most distant from the observation point. As can be seen from the theoretical waveform in the top part of Fig. 35, these negative-going and positive-going impulse-function peaks are well-separated at $\phi = 170°$, but the theory indicates that the two components, though of opposite sign, should have almost the same absolute amplitude. In the experimental waveform at the top of Fig. 35, one observes that the positive peak at $\tau = 997$ μs has an amplitude that is significantly smaller than that predicted theoretically.

However, the theory can be easily modified so as to enable one to correctly predict the shape of the experimental spatial-impulse-response-function waveform, that is observed at $\phi = 170°$. To effect this modification, one introduces a greater degree of attenuation into the factor $A(r,\mu)$, given by Eq. (149), than that which is caused by a range dependence proportional to the inverse one-half power of the distance. In a normalized waveform, this greater attenuation will cause the amplitude of the component that is radiated from the end of the line most distant from the observation point to be more strongly diminished, relative to the amplitude of the component radiated from the end of the source nearest to the observation point, than is the case in the theoretical waveform depicted in the upper part of Fig. 35. For definiteness, consider that $A(r,\mu)$ varies, not as the inverse one-half power of the distance, but as the inverse sixth power of the distance. A theoretical

waveform incorporating this modified inverse-sixth-power distance dependence is compared in the lower part of Fig. 35 to the experimental waveform that is observed at $\phi = 170°$. Here good agreement is seen to exist between the shape of the modified theoretical spatial-impulse-response-function waveform and the experimental waveform. If one applies the modified theory with the inverse-sixth-power distance dependence in the case for which $\phi = 210°$, one obtains the comparison depicted in Fig. 36. Again at $\phi = 210°$, as was the case at $\phi = 170°$, the waveform predicted using the modified theory agrees closely with that observed experimentally.

It is seen from Figs. 33 through 36 that the theoretical picture developed in Chapter IV accurately describes the radiated field of the Type F36 source. It is true that the theory must be modified in order to account for the relative amplitudes of the two radiated-field components observed in axial and near-axial directions (i.e., at and near $\phi = 180°$). However, it is seen from Figs. 35 and 36 that the modification of the theory is readily effected simply by attenuating the component radiated from the end of the line most distant from the observation point by using an inverse-sixth-power distance dependence. That is, for axial and near-axial directions, one uses the relation

$$A(r,\mu) = [(r^2 + \mu^2)^{\frac{1}{2}}/c]^{-6} \qquad (152)$$

in place of Eq. (149).

For axial and near-axial directions of observation, then, it is seen that the unmodified theory developed in Chapter IV, correctly predicts presence of the two components radiated by the ends of the line source and correctly predicts their separation in time. It does not, however, correctly predict their relative amplitudes. Consequently, an additional attenuation factor must be introduced into the theory when computing the shape of the waveforms observed near the $\phi = 180°$ direction. Introducing this attenuation by using Eq. (152) in place of Eq. (149), is,

of course, an arbitrary procedure, but one that is seen to yield relative component amplitudes that are consistent with those observed. However, if one considers the construction of the Type F36 transducer (Refer to Fig. 10.), there appears to be a plausible explanation for the necessity of attenuating the amplitude of the component radiated by the end of the line most distant from the observation point in order to bring the theoretical and experimental results into agreement.

The seven-element array within the Type F36 is constructed using endcapped ferroelectric cylindrical shells as acoustic radiators. The ferroelectric shells are designed to vibrate in a circumferential mode when excited electrically, but owing to elastic coupling, which must be present if Poisson's ratio of the shell material is not zero, there is also a significant longitudinal motion of the ends of each shell during any circumferential vibration. This longitudinal motion causes each of the endcaps to act as a vibrating circular piston. The acoustic radiation from all such piston sources augments the field radiated by the curved surfaces of the seven circumferentially vibrating cylindrical shells. Effects of this radiation from endcaps will be most pronounced in the direction of the axis of symmetry of the Type F36 [112] and will also be significantly large in directions near the axis of symmetry. Thus, in axial and near-axial directions, the radiation from the end of the Type F36 nearest the observation point, owing to endcap motion, will produce an effect greater than that produced by the nearest end of an infinitesimally thin line with the equivalent length. That is, near $\phi = 180°$, the component radiated from the end of the Type F36 nearest the receiver will exhibit an abnormally large amplitude, since this component includes the combined effect of both the infinitesimally-thin-line end-radiation component and the radiation produced by the pistonlike endcap. Thus, in order to construct theoretical waveforms that resemble the experimental waveforms observed with the Type F36 source in axial and near-axial directions, one is required to increase the amplitude of the component radiated from the end of the source nearest to the receiver, or else

equivalently, is required to reduce the amplitude of the component radiated from the most distant end of the source so as to compensate for the effects of the endcap radiation. Also in this connection, it might be expected that there is an additional attenuation produced in the component from the most distant end of the Type F36, owing to the baffling effect of all of the transducer structure between that end of the source and the receiver. Moreover, one suspects that the large end plates, which hold the element-mounting rods on the Type F36, may perturb the shape of the experimental waveforms and axial and near-axial directions owing to the effects of diffraction and reflection.

As is seen from the preceding discussion, the discrepancies between the experimental and the theoretical spatial-impulse-response-function waveforms, which occur in cases of axial or near-axial observation directions, are caused by the failure of the Type F36 transducer to model exactly an ideal line source having only an infinitesimal extension in the radial direction. There is also an additional factor causing discrepancies between the experimental results and those expected theoretically that should be considered before concluding the discussion in this chapter. One aspect of this discrepancy, which was mentioned earlier, is illustrated by the waveforms depicted in Fig. 28 and by that waveform in Fig. 27 for which $\phi = 240°$. By symmetry, one would expect that the waveforms observed at the angles $\phi = 60°$, $120°$, $240°$, and $300°$ should all have the same shape. Noticeable differences exist in the shapes of the experimental waveforms in question, however. Moreover, if one examines all the results depicted in Figs. 24 through 30, a second aspect of the discrepancy manifests itself.

It will be observed from these figures that the time of arrival of a particular field component does not change consistently as the angle ϕ is changed. Suppose, for example, one chooses some particular feature near the onset of the waveform observed at $\phi = 180°$ and notes the successive positions of this feature along the τ-axis in Figs. 24 through 30 as ϕ changes. Here one is assuming that the feature chosen is one produced by the radiation emanating from one end of the Type F36. Consequently, the time τ_a at which this feature appears in the observed

waveform should be governed by the equation

$$\tau_a = C_D + (R^2 + RL\cos\phi + \tfrac{1}{4}L^2)^{\frac{1}{2}}/c, \qquad (153)$$

in which C_D is a delay constant that depends on the characteristics of the experimental electronic system, upon the characteristics of the numerical convolution procedures used in processing input-output cross-correlation functions, and upon the location of the particular feature chosen in the waveform at $\phi = 180°$. The other symbols in Eq. (153) have all been defined previously. Now regardless of the value that one assigns to C_D, he finds that the observed arrival times of particular features in the experimental waveforms, which occur due to end-radiated field components, cannot be predicted by means of Eq. (153) as ϕ is changed.

An error in positioning the Type F36, which occurred when using the apparatus pictured in Fig. 12, accounts both for the lack of similarly shaped experimental waveforms at symmetrical angular positions and for the inconsistent behavior of the arrival times of waveform features as ϕ is varied. The positioning error was caused by small translations of the vertical tube that is clamped between the collars C1 and C2 in the supporting section of the transducer-mounting apparatus. Translational motion of the vertical axis of rotation of the Type F36, as well as of the transducer itself, resulted from this motion of the tube. This unwanted translation occurred as the tube was rotated. It was brought about when, during rotation, the collars C1 and C2 crept along the upper and lower surfaces of the support block instead of turning in place.

Such a translation was possible because it was necessary to clamp the arms of the block tightly between the collars in order to hold the tube vertical. As a consequence, a good deal of manual effort was often needed to change ϕ, since the weight of the movable portion of the assembly was considerable and there was much friction between the surfaces of the collars and of the supporting block. It was found in a preliminary

experimental run that, when the experimenter applied the torque necessary to change ϕ, irregularities in the mating surfaces of the collars and the block arms meshed together and caused the entire assembly to pivot slightly about the point of contact. If sufficient precautions were taken each time ϕ was changed, it was possible to keep the vertical tube pressed against surfaces of the V-slot cut in plate P1 when the transducer-mounting assembly was rotated and to so ensure that the axis of rotation of the source did not move horizontally. Unfortunately, however, when the experimental data appearing in Figs. 24 through 30 were gathered, the axis of rotation did shift slightly during the process. Since the Type F36 underwent a translation when its axis of rotation shifted, the translational motion in question affected both the arrival time at the receiver of the signal from the source, and, to a lesser degree, the angular orientation of the source axis with respect to the receiver. Translation of the axis that occurred when the assembly was rotated clockwise, tended to be offset by motion induced by anticlockwise rotation, because the collars tend to creep along the support block in opposite directions when the assembly is rotated in opposite senses. For this reason, the positioning error in question entered the data in a random fashion, since the acoustic data were gathered in such an order that sometimes a clockwise and sometimes an anticlockwise rotation of the transducer-mounting assembly was required when going from one value of ϕ to another.

The fact that there is experimental error affecting the arrival times of the observed spatial-impulse-response-function waveforms is of little import. If these times had been obtained more accurately, the significance of the experimental results reported here would be neither enhanced nor diminished. On the other hand, while in one sense, it would have been aesthetically more satisfying to have eliminated all positioning error and thereby to have achieved identical waveforms at $\phi = 60°$, 120°, 240°, and 300°, in actuality, the different waveforms, which are observed when the symmetry of the experimental arrangement is perturbed by the error, provide an informative picture of the behavior of the spatial impulse response function in the transition region.

Consider the change in the shape of the spatial-impulse-response-function waveform that occurs in the region between $\phi = 230°$ (See Fig. 26) and $\phi = 250°$ (See Fig. 27). The rapid transition takes place near $\phi = 240°$ as the large sidelobes of the impulse function radiated from the end of the line source most distant from the receiver interfere with similar sidelobes that are part of the impulse function radiated from the opposite end of the line. The central positive peak, which appears in the $\phi = 230°$ waveform owing to constructive interference of impulse-function sidelobes, is diminished near $\phi = 240°$. This condition is depicted by the $\phi = 300°$ waveform at the bottom of Fig. 28. At a slightly greater value of ϕ, this central peak will disappear completely, as is shown by the $\phi = 120°$ waveform at the center of Fig. 28. The $\phi = 120°$ waveform marks the transition between a waveform with three large positive peaks, like that observed at $\phi = 230°$, and a waveform with two such positive peaks, which is fully developed at $\phi = 250°$. Thus, as ϕ is increased still further, a waveform with two positive peaks begins to develop. Such a waveform is shown in the $\phi = 60°$ case that is depicted at the top of Fig. 28. With a further slight increase in ϕ, traces of the rapid transition occurring near $\phi = 240°$, which appear as a distortion in the second positive peak of the $\phi = 60°$ waveform, become faint. In the actual $\phi = 240°$ waveform shown in Fig. 26, they are scarcely visible at all. After such a waveform as that actually observed at $\phi = 240°$ is obtained, a further increase in ϕ only causes the two positive peaks to change in amplitude and move together until the spatial-impulse-response-function waveform attains the shape it has at $\phi = 250°$.

It can be seen from the above description of the behavior of the spatial impulse response function in the transition region near $\phi = 240°$, that the presence of a small positioning error was in a sense fortuitious, since it perturbed the symmetry of the experimental arrangement. Had this perturbation not occurred, the nature of the rapidly changing shape of the spatial-impulse-response-function waveform in the transition region could not have been so readily understood. One should not retain the impression, however, that the transducer-orientation angles ϕ cannot be determined

precisely if sufficient care is exercised, nor should one believe that the basic alignment of the transducer mounting system was in error. Recall that, in the region near $\phi = 180°$, the experimental waveforms obtained at equal angles on either side of the $\phi = 180°$ position were virtually identical and that this was also the case in the region near $\phi = 270°$. Moreover, if one examines the results of the null-measurement experiments that determined L, an estimate of the error inherent in the determination of the angle ϕ can be obtained.

Consider the measured angular null positions $\bar{\phi}_1^i$ and $\bar{\phi}_2^i$ appearing in Table 3. Referring to Fig. 32, one sees that the angles ϕ_1 and ϕ_2 should be symmetrically disposed about the $\phi = 180°$ transducer orientation at all frequencies. Consequently, at any frequency, the difference between ϕ_{AV}, which is the average value of ϕ_1 and ϕ_2, and 180° measures the alignment error inherent in the transducer-mounting system. Using the most precisely measured values of $\bar{\phi}_1^i$ and $\bar{\phi}_2^i$, those for i = 2 obtained using the 7.9 kHz tonebursts, one calculates that $\phi_{AV} = 179.83°$. This value indicates that the alignment was less than 0.2° in error in the anticlockwise direction. (That is, the divided dial used to measure the angles ϕ would have to be rotated 0.17° in the anticlockwise direction in order to make its 180° mark coincide with the actual midpoint between the null positions.) If, on the other hand, the least precisely measured values of $\bar{\phi}_1^i$ and $\bar{\phi}_2^i$ are used, those for i = 6 obtained using the 7.5 kHz tonebursts, one calculates that $\phi_{AV} = 179.54°$. This value indicates the possibility of an alignment error of 0.46°, with the error again occurring in the anticlockwise direction. Most likely, the systematic error in determining ϕ is closer to 0.17° than it is to 0.46°, since, for the reasons examined previously, one would expect that the null measurements obtained with 7.9 kHz tonebursts would be more accurate than those obtained with 7.5 kHz tonebursts. However, even if one used the value of 0.46°, which is obtained from the least accurate experimental measurement, the systematic error he would expect in ϕ would be quite small. Thus, one can see that in the experimental determination of the equivalent line length of the Type F36, the full potential of the measuring system for obtaining an accurate value of ϕ was realized.

REFERENCES AND NOTES

[1] A. Rubinowicz, "Thomas Young and the Theory of Diffraction," Nature 180, 160 (1957).

[2] B. B. Baker and E. T. Copson, The Mathematical Theory of Huygens' Principle (Oxford University Press, London, 1953), 2nd ed., pp. 75-79.

[3] M. Born and E. Wolf, Principles of Optics (Pergamon Press, London, 1959), pp. 448-452.

[4] E. Mach, The Principles of Physical Optics--An Historical and Philosophical Treatment (Dover Publications, Inc., New York, 1953), Chaps. 8 and 14.

[5] F. M. Grimaldi, Physico-Mathesis de lumine coloribis et iride, [Natural philosophy of colored light and rainbows] (Bologna, 1665). This citation was obtained from Refs. [3] and [4].

[6] I. Newton, Opticks (Whittlesey House, McGraw-Hill Book Co., Inc., New York, 1931), Reprinted from the corrected version of the 4th ed. (William Innys, London, 1730), 3rd Bk., Pt. I, Observation 6, p. 326.

[7] Ibid., pp. 326-327.

[8] Ibid., p. 327.

[9] T. Young, "Outlines of Experiments and Inquiries respecting Sound and Light," Philos. Trans. R. Soc. Lond. 90, 106 (1800). This paper was found in a reprinted edition of the Philosophical Transactions, which abridged the complete version. Each paper included in the abridged edition is complete. (C. and R. Baldwin, London, 1809), Vol. XVIII, from 1796 to 1800, pp. 604-626. On p. 615 of this reference, one finds the following statement:

> "When a ray of light passes near an inflecting body, surrounded, as all bodies are supposed to be, with an atmosphere of ether denser than the ether of the ambient air, the part of the ray nearest the body is retarded, and of course the whole ray inflected toward the body ... ".

[10] Ibid., p. 616.
"In inflections, the length of the track of a ray of light through the inflecting atmosphere may determine its vibrations: but, in this case, as it is probable that there is a reflection from every part of the surface of the surrounding atmosphere, contributing to the appearance of the white line in every direction, in the experiments already mentioned [i.e., Newton's observation of the luminous knife-edge], so it is possible that there may be some 2d reflection at the immediate surface of the body itself, and that, by mutual reflections between these 2 surfaces, something like the anguiform motion suspected by Newton may really take place; and then the analogy to the colours of thin plates will be still stronger."

[11] T. Young, "On the Theory of Light and Colors," Philos. Trans. R. Soc. Lond. 92, Pt. I, 12 (1802). The Bakerian Lecture, read November 12, 1801. See in particular, Fig. 4 of Pl. I, facing p. 48.

[12] T. Young, "Experiments and Calculations relative to physical Optics," Philos. Trans. R. Soc. Lond. 94, Pt. I, 1 (1804). The Bakerian Lecture, read November 24, 1803. On p. 12, one finds the following statement:
"I have not, in the course of these investigations, found any reason to suppose the presence of such an inflecting medium in the neighborhood of dense substances as I was formerly inclined to attribute to them; and upon considering the phenomena of the abberation of stars, I am disposed to believe, that the luminiferous ether pervades the substance of all material bodies ... ".

[13] Authors of many of the scientific papers cited in Chapter I state that Young formulated this diffraction model in his celebrated Bakerian Lecture of 1801 (Ref. [11]). This is not correct; the diffraction model is first reported in Ref. [12].

[14] Ref. [4], p. 138.

[15] Ref. [11], p. 26.

[16] Ref. [12], p. 4.
"On the supposition that the dark line is produced by the first interference of the light reflected

from the edges of the knives, with the light passing in a straight line between them, we may assign, by calculating the difference of the two paths, the interval for the disappearance of the brightest light ...".

[17] Ref. [12], p. 6.
"But it may be inferred, from a comparison of all the other observations, that when the obliquity of the reflection is very great, some circumstance takes place, which causes the interval thus calculated to be somewhat greater ...".

[18] T. Young, A Course of Lectures on Natural Philosophy and Mechanical Arts (1807). This citation was obtained from Ref. [4].

[19] T. Young, Miscellaneous Works of the late Thomas Young, ed. by G. Peacock (London, 1855) Vol. I. This citation was obtained from Refs. [1] and [4].

[20] Ref. [4], pp. 279-280.

[21] L. G. Gouy, Ann. Chim. Phys. 6, 8, 145 (1886).

[22] C. V. Raman and K. S. Krishnan, "The Diffraction of Light by Metallic Screens," Proc. R. Soc. Lond. A, 116, 254 (1927).

[23] The fact that the polarization and color of the diffracted light is strongly influenced by the nature of the diffracting edge, lends support to the concept of diffraction put forth by Young, rather than to that envisioned in conventional diffraction theory. Consider the case in which the diffracting screen is a metallic half-plane. If, in accordance with the ideas of conventional diffraction theory, the diffracted field results from the interference of all those Huygens' wavelets that are not blocked by the screen, then all polarization effects, produced by the screen on the diffracted light, can be expected to be quite small. For, if the incident wave consists of an ensemble of Huygens' wavelets, then only a small fraction of those wavelets not blocked by the screen can carry information about the nature of the diffracting edge out into the diffracted field. That is, the edge itself can only be expected to influence the unobstructed Huygens' wavelets in its immediate neighborhood. Since the screen's diffracted field is the superposition of all the unobstructed Huygens' wavelets, and since most of these are wavelets that cannot have been influenced by the properties of the screen, the nature of the screen should have little effect upon the properties of the optical field that will be observed. Yet, as far as polarization and color effects are concerned, the nature of the screen exerts a great influence, according to experiment. If, on the other hand, the diffracted field is caused by a boundary wave

radiated by the edge of the screen, it is clear that the properties of this field could very easily be strongly dependent upon the physical properties of the radiating edge, just as is observed experimentally.

[24] W. Wien, "Untersuchungen über die bei der Beugung des Lichtes auftretenden Absorptionsercheinungen," ["Investigations concerning the absorption phenomena resulting from the diffraction of light"], Ann. Phys. Chem. (Wiedemann) N.F., 28, 117 (1886).

[25] E. Maey, "Ueber die Beugung des Lichtes an einem geraden, scharfen, Schirmrande," ["Concerning the diffraction of light at a straight, sharp, screen-edge"], Ann. Phys. Chem. (Wiedemann) N.F., 44, 69 (1893).

[26] A. Sommerfeld, "Mathematische Theorie der Diffraction," ["Mathematical theory of diffraction"], Math. Ann. 47, 317 (1896).

[27] The discussion that is presented here of the problem of diffraction of an electromagnetic plane wave by a perfectly reflecting half-plane is based largely upon the presentation found in Ref. [3], pp. 567-569.

[28] For example, see Ref. [22], pp. 257-258.

[29] R. W. Wood, Physical Optics (Macmillan Co., New York, 1934), 3rd ed., pp. 220-221.

[30] For example, see Ref. [2], p. 147.

[31] A. Sommerfeld, Optics (Academic Press, Inc., New York, 1954), p. 362.

[32] A. Rubinowicz, "Die Beugungswelle in der Kirchhoffschen Theorie der Beugungserscheinungen," ["The diffraction wave in the Kirchhoff theory of diffraction phenomena"], Ann. Phys. 4, 53, 257 (1917).

[33] G. A. Maggi, "Sulla propagazione libera e perturbata delle onde luminose in un mezzo isotropo," ["On the free and perturbed propagation of light waves in an isotropic medium"], Ann. di Mat. 2a, 16, 21 (1888). Citation obtained from Ref. [34] to follow.

[34] F. Kottler, "Zur Theorie der Beugung an schwartzen Schirmen," ["On the theory of diffraction at black screens"], Ann. Phys. 4, 70, 405 (1923).

[35] A. Rubinowicz, "Zur Kirchhoffschen Beugungstherorie," ["On the diffraction theory of Kirchhoff"], Ann. Phys. 4, 73, 889 (1924)

[36] Ref. [1], p. 161.

[37] A. Rubinowicz, "On the Anomalous Propagation of Phase in the Focus," Phys. Rev. 54, 931 (1938).

[38] C. J. Bouwkamp, "Note on the Anomalous Propagation of Phase in the Focus," Physica (Utr.) 7, 485 (1940).

[39] A. Kalaschinokow, Zh. Russk. Fiz. Chim. Obsc., Fiz. Otdel [Journal of the Russian Physical and Chemical Society, Physics Part] 44, 133 (1912). Citation obtained from Refs. [1], [3], and [48] to follow.

[40] S. Banerji, "On the Radiation of Light from the Boundaries of Diffracting Apertures," Philos. Mag. 6, 37, 112 (1919).

[41] K. Noack, "Eine eigentümliche Beugungsinterferenz," ["A peculiar diffraction interference"], Phys. Z. 23, 228 (1922).

[42] A. Schoch, "Betrachtungen über das Schallfeld einer Kolbenmembran," ["Considerations concerning the sound field of a piston membrane"], Akust. Z. 6, 318 (1941).

[43] H. Stenzel, "Über die Berechnung des Schallfeldes unmittelbar vor einer kreisformigen Kolbenmembran," ["Concerning the calculation of the sound field immediately in front of a circular piston membrane"], Ann. Phys. 5, 41, 245 (1942).

[44] A. H. Carter and A. O. Williams, "A New Expansion for the Velocity Potential of a Piston Source," J. Acoust. Soc. Am. 23, 179 (1951).

[45] O. G. Kozina and G. I. Makarov, "Transient Processes in the Acoustic Fields Generated by a Piston Membrane of Arbitrary Shape," Sov. Phys.- Acoust. 7, 39 (1961).

[46] O. G. Kozina and G. I. Makarov, "Transient Processes in the Acoustic Fields of Special Piston Membranes," Sov. Phys.-Acoust. 8, 49 (1962).

[47] G. N. Ramachandran, "On the Radiation from the Boundary of Diffracting Apertures and Obstacles," Proc. Indian Acad. Sci. 21, (Sect. A), 165 (1945).

[48] D. N. Chetayev, "Ob Izluchenii Zvuka Porshnem," ["About Sound Radiating Pistons"], Dokl. Akad. Nauk SSSR [Sov. Phys.-Doklady] 76, 813 (1951).

[49] K. Osterhammel, "Optische Untersuchung des Schallfeldes kolbenformig schwingender Quartz," ["Optical investigation of the sound field of quartz vibrating in a piston-like manner"], Akust. Z. 6, 6 (1941).

[50] Ref. [12], pp. 7-8.

[51] W. L. Gessert and E. A. Hiedemann, "Ultrasonic Stroboscopes for the Study of Ultrasonic Fields," J. Acoust. Soc. Am. 28, 944 (1956).

[52] J. T. Dehn, "Interference Patterns in the Near Field of a Circular Piston," J. Acoust. Soc. Am. 32, 1692 (1960).

[53] E. M. Kennaugh and R. L. Cosgriff, "The Use of Impulse Response in Electromagnetic Scattering Problems," IRE Nat. Conv. Rec. 6, 72 (1958).

[54] N. G. van Kampen, "An Asymptotic Treatment of Diffraction Problems," Physica (Utr.) 14, 575 (1949).

[55] R. S. Ingarden, "A Generalization of the Young-Rubinowicz Principle in the Theory of Diffraction," Acta Phys. Pol. 14, 77 (1955).

[56] K. Miyamoto, "New Representation of Wave Field," Proc. Phys. Soc. Lond. 79, 617 (1962).

[57] K. Miyamoto and E. Wolf, "Generalization of the Maggi-Rubinowicz Theory of the Boundary Diffraction Wave--Part I," J. Opt. Soc. Am. 52, 615 (1962).

[58] K. Miyamoto and E. Wolf, "Generalization of the Maggi-Rubinowicz Theory of the Boundary Diffraction Wave--Part II," J. Opt. Soc. Am. 52, 626 (1962).

[59] A. Rubinowicz, "The Miyamoto-Wolf Diffraction Wave," Progress in Optics, E. Wolf, ed. (North Holland Publishing Co., Amsterdam, Interscience publisher's division, John Wiley and Sons, Inc., New York, 1965) Vol. IV, Chap. 5., pp. 201-240.

[60] A. Rubinowicz, "Beugungswelle im Falle einer beliebegen einfallenden Lichtwelle," ["Diffraction wave in the case of an arbitrary incident light wave"], Acta Phys. Pol. 21, 61 (1962).

[61] A. Rubinowicz, "Simple Derivation of the Miyamoto-Wolf Formula for the Vector Potential Associated with a Solution of the Helmholtz Equation," J. Opt. Soc. Am. 52, 717(L) (1962).

[62] A. Rubinowicz, "Geometric Derivation of the Miyamoto-Wolf Formula for the Vector Potential Associated with a Solution of the Helmholtz Equation," J. Opt. Soc. Am. 52, 717(L) (1962).

[63] A. Rubinowicz, "Beugungswellen verschiedener Felder im Falle beliebiger einfallender Wellen," ["Diffraction waves in different fields in the case of arbitrary incident waves"], Acta Phys. Pol. 23, 727 (1963).

[64] E. Wolf, "Some Recent Research on Diffraction of Light," Proceedings of the Symposium on Modern Optics, Polytechnic Institute of Brooklyn, March 22-24, 1967 (John Wiley and Sons, Inc., New York, 1967), Vol. XVIII, pp. 433-452, Sect. 1, "The Boundary Diffraction Wave" and Sect. 2, "A Consistent Formulation of Kirchhoff's Diffraction Theory," pp. 433-444.

[65] A. Freedman, "A Mechanism of Acoustic Echo Formulation," Acustica 12, 10 (1962).

[66] A. Freedman, "The High Frequency Echo Structure of Some Simple Body Shapes," Acustica 12, 61 (1962).

[67] A. Freedman, "Transient Fields of Acoustic Radiators," J. Acoust. Soc. Am. 48, 135 (1970).

[68] A. Freedman, "Sound Field of Plane or Gently Curved Pulsed Radiators," J. Acoust. Soc. Am. 48, 221 (1970).

[69] A. Freedman, "Farfield of Pulsed Rectangular Acoustic Radiator," J. Acoust. Soc. Am. 49, 738 (1971).

[70] A. Freedman, "Sound Field of a Pulsed, Planar, Straight-Edged Radiator," J. Acoust. Soc. Am. 51, 1624 (1972).

[71] P. R. Stephanishen, "An Approach to Computing Time-Dependent Interaction Forces and Mutual Radiation Impedances between Pistons in a Rigid Planar Baffle," J. Acoust. Soc. Am. 49, 283 (1971).

[72] P. R. Stephanishen, "Transient Radiation from Pistons in an Infinite Planar Baffle," J. Acoust. Soc. Am. 49, 1629 (1971).

[73] P. R. Stephanishen, "Acoustic Transients in the Far Field of a Baffled Circular Piston Using the Impulse Response Approach," J. Sound Vib. 32, 295 (1974).

[74] P. R. Stephanishen, "Asymptotic behavior of the acoustic near-field of a circular piston," J. Acoust. Soc. Am. 59, 749 (1976).

[75] J. B. Keller, "Geometrical Theory of Diffraction," J. Opt. Soc. Am. 52, 116 (1962).

[76] L. B. Flesen and N. Marcuvitz, Radiation and Scattering of Waves (Prentice-Hall, Inc., Englewood Cliffs, N.J., 1973), pp. 97-98.

[77] E. J. Copson, Asymptotic Expansions (Cambridge University Press, London, 1965). The discussion of the method of stationary phase draws heavily upon the results found in Chapter 4 of this reference.

[78] E. P. Adams, ed., Smithsonian Mathematical Formulae and Tables of Elliptic Functions (Smithsonian Institution Publication No. 2672, Washington, D.C., 1939), Smithsonian Miscellaneous Collections, Vol. 74, No. 1, p. 42.

[79] P. M. Morse and H. Feshbach, Methods of Theoretical Physics (McGraw-Hill Book Co., New York, 1953), Vol. I, p. 462.

[80] G. Doetsch, Theorie und Anwendung der Laplace-Transformation, [Theory and Application of the Laplace Transformation] (Dover Publications, New York, 1943), pp. 200-201.

[81] N. Wiener, "Tauberian Theorems," Ann. Math. 2, 33, 1 (1932), pp. 60-62.

[82] W. Nowacki, Dynamics of Elastic Systems (John Wiley and Sons, Inc., New York, 1963), pp. 368-371.

[83] A. Erdélyi, W. Magnus, F. Oberhettinger and F. G. Tricomi, eds. Tables of Integral Transforms (McGraw-Hill Book Co., New York, 1954), Vol. I, p. 19, Eq. 1.64(4).

[84] Ref., [83], p. 65, Eq. 2.2(20).

[85] Ref. [83], p. 191, Eq. 4.15(11) with $\lambda = 0$.

[86] I. S. Gradshteyn and I. M. Ryzhik, Table of Integrals, Series, and Products (Academic Press, Inc., New York, 1965), p. 316, Eq. 3.364(3).

[87] M. Abramowitz and I. A. Stegun, eds., Handbook of Mathematical Functions, National Bureau of Standards Applied Mathematics Series No. 55 (United States Government Printing Office, Washington, D. C., 1965), Ninth Printing, with corrections, 1970, p. 1028, Eq. 29.3.119.

[88] Y. W. Lee, Statistical Theory of Communication (John Wiley and Sons, Inc., New York, 1960), pp. 323-348.

[89] D. Berlincourt, "Piezoelectric Crystals and Ceramics," Chap. 2 Ultrasonic Transducer Materials, O. E. Mattiat, ed. (Plenum Press, New York, 1971), pp. 72-77.

[90] D. H. Robey, "On the Radiation Impedance of an Array of Finite Cylinders," J. Acoust. Soc. Am. 27, 706 (1955).

[91] J. S. Bendat and A. G. Piersol, Measurement and Analysis of Random Data (John Wiley and Sons, Inc., New York, 1966), p. 85.

[92] R. J. Bobber, Underwater Electroacoustic Measurements (Naval Research Laboratory, United States Government Printing Office, Washington, D.C. 1970), pp. 251-253.

[93] Anon. "USRD Type F36 Transducer," Naval Research Laboratory Instruction Book No. 49 (1966).

[94] Anon. "Operating Instructions for USRL Type F36 Transducer--International Round-Robin Edition," (1965).

[95] The calibration curve in Fig. 11 was obtained at a depth of 3.8 m (12.5 ft) at a temperature of 30°C. Calibration of the Type F36 transducer used in the experiments was performed in July 1974 by the Underwater Sound Reference Division of the Naval Research Laboratory.

[96] V. A. Del Grosso and C. W. Mader, "Speed of Sound in Pure Water," J. Acoust. Soc. Am. 52, 1442 (1972).

[97] The computer used was a medium-speed Control Data Corp. (CDC) 3800 machine, located at the Naval Research Laboratory Research Computation Center. Machine words have a length of 48 bits.

[98] H. P. Westman, ed., Reference Data for Radio Engineers (International Telephone and Telegraph Corp., New York, 1956), 4th ed., pp. 190-193. The pertinent equations in this reference have been modified to express the effect cascading filter stages.

[99] G. E. P. Box and M. E. Muller, "A note on the generation of normal deviates," Ann. Math. Stat. 28, 610 (1958).

[100] M. E. Muller, "A comparison of Methods for Generating Normal Deviates on Digital Computers," J. Assoc. Comp. Mach. 5, 376 (1958).

[101] R. N. Adams and E. D. Denman, Wave Propagation and Turbulent Media (American Elsevier Publishing Company, New York, 1966) pp. 52-53.

[102] J. Moshman, "The Generation of Pseudo-random Numbers on a Decimal Calculator," J. Assoc. Comp. Mach. 1, 88 (1954).

[103] T. E. Hull and A. R. Dobell, "Random Number Generators," SIAM Rev. 4, 230 (1962).

[104] J. Certaine, "On Sequences of Pseudo-Random Numbers of Maximal Length," J. Assoc. Comp. Mach. 5, 353 (1958)

[105] S. Gorenstein, "Testing a Random Number Generator," Comm. Assoc. Comp. Mach. 10, 111 (1967).

[106] The 48-bit per word machine described in Ref. [97] was used for generating pseudorandom numbers.

[107] Paper tape to magnetic tape translation was performed on a CDC 160 computer, which is ancillary to the CDC 3800 machine. The necessary machine-language loader and execution routines were written by Mr. R. D. McCulloch of the Research Computation Center.

[108] Ref. [91], pp. 192-195. The formulas appearing in this reference do not explicitly describe the variance of crosscorrelation functions in the case of sampled transient signal records. However, the experimental situation approximates the conditions of Bendat and Piersoll's example 5.3 sufficiently closely to infer that the variance in the experimental correlation functions is inversely proportional to the duration of the noisebursts correlated. That is, this variance is inversely proportional to the number of samples comprising the noisebursts. It might also be mentioned here that experimental correlation functions were computed with the noisebursts treated both as transient signals in the manner described in the text, and as finite-duration samples of infinite records. In this latter case, lagged-product formulas were used to estimate the correlation functions. Except at very large values of the lag parameter, there were only insignificant differences between the results obtained for experimental correlation functions with the two different estimation techniques.

[109] Both hydrophones used in the experiments were manufactured by the Atlantic Research Corporation. The larger of the two is designated as Model LC-10 while the smaller is Model LC-5. While this manufacturer no longer fabricates these transducers, they are still commercially available from KSP Industries, Inc., as Models VT-102 and VT-106-2, respectively.

[110] There is no vernier scale associated with the divided dial D, so that it is only after some practice that an experimenter attains the ability to read the dial to the nearest 0.1°.

[111] Ref. [87], p. 879, Eq. 25.2.15.

[112] It is likely that radiation from the endcaps between the vibrating cylindrical shells augments the field radiated by the curved surfaces of the shells in such a way that the radiated field near the seven-element array is smoothed out. That is, endcap radiation provides an acoustic field between pairs of radiating shells and causes the seven disjoint cylindrical shells to radiate more like a continuous line array than like a line array of discrete elements.

APPENDIX I--DIFFERENTIATION OF A SINGULAR FUNCTION

Singular functions of the form

$$F(t) = u(t - \alpha)/(t^2 - \alpha^2)^{\frac{1}{2}} \quad , \tag{I.1}$$

with u the unit step function and with α constant, are to be differentiated with respect to the variable t. In the following discussion, let the derivative of any function with respect to t be denoted by a prime superscript. The derivative F'(t) of the function F(t) given by Eq. (I.1) is obtained in two steps. First, the definition of the generalized derivative is applied to F(t). It is next shown that the resultant expression is identical to the expression obtained for the singular generalized function that is defined by the Hadamard finite part [I1, I2] of a certain divergent integral. The generalized function defined by the Hadamard finite part is, therefore, the derivative F'(t) that is sought.

The generalized function f(t) is defined on the real axis $-\infty < t < \infty$ by means of inner products with testing functions $\psi(t)$:

$$< f, \psi > = \int_{-\infty}^{\infty} f(t)\psi(t)\, dt \ . \tag{I.2}$$

The testing functions ψ constitute a space D. Each testing function is defined on the real axis $-\infty < t < \infty$, but vanishes outside a finite interval, $a \leq t \leq b$, which can be different for each different function ψ. Moreover, it is required that the testing functions possess derivatives of all orders. Testing functions are thus continuous. It is to be noted that in order for Eq. (I.2) to define a generalized function f, it is necessary that f(t) be a locally integrable function (i.e., a function integrable in the Lebesgue sense over every finite interval), for only then does the integral in Eq. (I.2) converge.

From Eq. (I.2), the properties of ψ, and an integration by parts, it follows directly that the generalized derivative of the function f can be found using the relationship

$$< f', \psi > = - < f, \psi' > = -\int_{-\infty}^{\infty} f(t)\psi'(t)\, dt \,. \qquad (I.3)$$

Using Eq. (I.3), one can write the derivative of F, given by Eq. (I.1), as

$$< F' \psi > = - \lim_{\epsilon \to 0+} \int_{\alpha+\epsilon}^{B} \frac{\psi'(t)}{(t^2 - \alpha^2)^{\frac{1}{2}}}\, dt, \qquad (I.4)$$

where B is some value so large that both $\psi(t)$ and $\psi'(t)$ equal zero for $t \geq B$. Integrating Eq. (I.4) by parts, yields the expression

$$< F', \psi > = - \lim_{\epsilon \to 0+} \left[\int_{\alpha+\epsilon}^{B} \frac{t\psi(t)}{(t^2 - \alpha^2)^{3/2}}\, dt - \frac{\psi(\alpha)}{(2\alpha\epsilon + \epsilon^2)^{\frac{1}{2}}} \right] . \qquad (I.5)$$

In deriving the result expressed by Eq. (I.5), one uses the fact that

$$\lim_{\epsilon \to 0+} \psi(\alpha + \epsilon) = \psi(\alpha) \,,$$

since ψ is continuous at α.

Now consider the singular function

$$G(t) = - u(t - \alpha)t/(t^2 - \alpha^2)^{3/2}. \qquad (I.6)$$

Since the integral

$$I = < G, \psi > = -\int_{\alpha}^{\infty} \frac{t\, \psi(t)}{(t^2 - \alpha^2)^{3/2}}\, dt \qquad (I.7)$$

does not, in general, converge for all testing functions ψ in D, the expression G(t) is not that of a generalized function. Hadamard [I1] devised a method whereby a finite part of such divergent integrals as that in Eq. (I.7) could be extracted. This finite part can in turn be used to define a singular generalized function. Consider the integral

in Eq. (I.7) expressed in the following form

$$I = - \lim_{\epsilon \to 0+} \int_{\epsilon+\alpha}^{B} \frac{t\psi(t)}{(t^2 - \alpha^2)^{3/2}} \, dt \, , \tag{I.8}$$

in which B is taken to be so large that $\psi(t) = 0$ for $t \geq B$. Let

$$\psi(t) = \psi(\alpha) + (t^2 - \alpha^2)\xi(t) \, . \tag{I.9}$$

Since $\psi(t)$ possesses derivatives of all orders, it can be shown [I2] that the function $\xi(t)$ is continuous for $t \neq \alpha$ and can be extended so as to be continuous at $t = \alpha$. Using Eq. (I.9), one can transform Eq. (I.8) into the expression

$$I = - \lim_{\epsilon \to 0+} \left[\int_{\alpha+\epsilon}^{B} \frac{t\,\xi(t)}{(t^2 - \alpha^2)^{\frac{1}{2}}} \, dt \right.$$

$$\left. - \frac{\psi(\alpha)}{(B^2 - \alpha^2)^{\frac{1}{2}}} + \frac{\psi(\alpha)}{(2\epsilon\alpha + \epsilon^2)^{\frac{1}{2}}} \right] \, . \tag{I.10}$$

The factor $\psi(\alpha)/(B^2 - \alpha^2)^{\frac{1}{2}}$ within the brackets of Eq. (I.10) remains finite as $\epsilon \to 0+$. Also it can be shown in the following way that the integral

$$\int_{\alpha+\epsilon}^{B} \frac{t\xi(t)}{(t^2 - \alpha^2)^{\frac{1}{2}}} \, dt$$

likewise remains finite as $\epsilon \to 0+$. For, since $\xi(t)$ is continuous at $t = \alpha$, one can expand the continuous function $t\xi(t)$ in the integrand of this expression in a Taylor series about that point. The Taylor series is to be written with a finite number of terms in powers of $(t - \alpha)$ plus a remainder term. This series is then integrated, from $t = \alpha + \epsilon$ to $t = B$, term by term. The lowest power of $(t - \alpha)$ that will appear under an integral is $(t - \alpha)^{-\frac{1}{2}}$. The integral involving this term will converge when $\epsilon \to 0+$, as will all the integrals involving higher powers

of $(t - \alpha)$ and that containing the remainder term. The only factor within the brackets on the right-hand side of Eq. (I.10) that diverges, then, as $\varepsilon \to 0+$ is $\psi(\alpha)/(2\varepsilon\alpha + \varepsilon^2)^{\frac{1}{2}}$. The Hadamard finite part of the divergent integral I, given by Eq. (I.8), is obtained by simply discarding this divergent term. Designating the Hadamard finite part of Hfp[ ], one obtains the expression

$$\text{Hfp}[I] = - \lim_{\varepsilon \to 0+} \left[\int_{\alpha+\varepsilon}^{B} \frac{t\xi(t)}{(t^2 - \alpha^2)^{\frac{1}{2}}} \, dt - \frac{\psi(\alpha)}{(B^2 - \alpha^2)^{\frac{1}{2}}} \right]. \tag{I.11}$$

If Eq. (I.9) is solved for ξ and the result substituted into Eq. (I.11), then

$$\text{Hfp}\left[- \int_{\alpha}^{\infty} \frac{t\psi(t)}{(t^2 - \alpha^2)^{3/2}} \, dt \right] =$$

$$- \lim_{\varepsilon \to 0+} \left[\int_{\alpha+\varepsilon}^{B} \frac{t[\psi(t) - \psi(\alpha)]}{(t^2 - \alpha^2)^{3/2}} dt - \frac{\psi(\alpha)}{(B^2 - \alpha^2)^{\frac{1}{2}}} \right]$$

$$= - \lim_{\varepsilon \to 0+} \left[\int_{\alpha+\varepsilon}^{B} \frac{t\psi(t)}{(t^2 - \alpha^2)^{3/2}} \, dt - \frac{\psi(\alpha)}{(2\varepsilon\alpha + \varepsilon^2)^{\frac{1}{2}}} \right]. \tag{I.12}$$

Zemanian [I2] shows that the Hadamard finite part of divergent integrals define singular generalized functions called, following L. Schwartz, pseudofunctions. One thus writes, for the generalized function defined by Eq. (I.12), the expression

$$< \text{Psf}[-u(t - \alpha)t/(t^2 - \alpha^2)^{3/2}], \psi >$$

$$= -\lim_{\varepsilon \to 0+} \left[\int_{\alpha+\varepsilon}^{B} \frac{t\psi(t)}{(t^2 - \alpha^2)^{3/2}} \, dt - \frac{\psi(\alpha)}{(2\varepsilon\alpha + \varepsilon^2)^{\frac{1}{2}}} \right], \tag{I.13}$$

where a pseudofunction is designated Psf[ ]. However, if Eq. (I.13) is compared to Eq. (I.5), one immediately sees that

$$F'(t) = Psf\left[-\frac{u(t-\alpha)t}{(t^2-\alpha^2)^{3/2}}\right]. \qquad (I.14)$$

Thus, the derivative of the function F, specified in Eq. (I.1), is given by Eq. (I.14).

REFERENCES--APPENDIX I

[I.1] J. Hadamard, Lectures on Cauchy's Problem in Linear Partial Differential Equations (Dover Publications, New York, 1952), "Introduction of a New Kind of Improper Integral," Book III, Chapter I, pp. 117-158.

[I.2] A.H. Zemanian, Distribution Theory and Transform Analysis (McGraw-Hill Book Co., New York, 1965), Analysis in this section draws heavily upon this reference, particularly upon the results found in Section 1.4, pp. 15-24, and in Section 2.5, pp. 57-66.

APPENDIX II--INFORMATION ON INSTRUMENTATION

In this appendix, instruments used in the experimental measurement system are identified and, if necessary, briefly described.

Consider first the instruments in the pulse-generating subsystem depicted in Fig. 15. The tape transport is a seven-track synchronous unit, manufactured by Digi-Data Corporation (Model 1700). The digital-to-analog converter is an Analogic Model AN5800 system using, what its manufacturer calls, a transient-free converter unit. The buffer/interface unit is not a generally available commercial item, but was procured on contract from Quad Systems, Inc., (QSI) of Rockville, Maryland in 1975. This company also supplied the system engineering effort necessary to interface the tape transport and the digital-to-analog converter with the buffer/interface unit. The entire integrated system, comprised of the tape transport, the digital-to-analog converter, and the buffer/interface unit, which also includes a Digi-Data NRZI formatter and an Electronic Memories and Magnetics Corporation semiconductor memory system, is designated by QSI as their Model 122. Although the digital-to-analog converter used can only accept 12-bit words at a maximum rate of one word every 5 μs, the buffer/interface unit itself can transmit 16-bit words at 1 μs intervals, so that the integrated system is potentially usable with a faster digital-to-analog converter.

At the output of the digital-to-analog converter, is a Krohn-Hite Model 3202R dual filter, which is followed by a Krohn-Hite Model 3100R bandpass filter. The voltage amplifier is a Scientific Atlanta Series 1116 preamplifier with an adjustable gain setting. This amplifier supplies the input signal to a Krohn-Hite Model DC50A power amplifier. The power amplifier's output current is measured using a Tektronix Type 134 current-probe unit with a P6019 probe; for measurement, the amplifier's output voltage is attenuated by a factor of ten using a Tektronix P6006 probe.

Next consider the instrumentation in the receiver subsystem that is depicted in Fig. 16. The measuring hydrophone signal is supplied to a Scientific Atlanta Model 1116 voltage amplifier, operating with a balanced input. This amplifier's output is supplied to a Scientific Atlanta Model 1112B receiver signal gate. The gated signal is then supplied to a Krohn-Hite model 3100R filter.

In the waveform-recording subsystem depicted in Fig. 17, the transient recorder is a Biomation Model 8100. In the present application, an important feature of this instrument, aside from its large digital memory capacity, is its digitally derived timebase. The paper-tape perforator is a Data Specialties, Inc., PER820 unit. The interface unit, coupling the transient recorder to the tape perforator, is a Model B305 data coupler manufactured by Datacap, Inc., of Chicago, Illinois. The tape formatter is also manufactured by Datacap (Model 2000), but was obtained on contract and is not a standard commercial item. The interface unit not only controls the transmission of digital data between the transient recorder and the tape perforator but also translates this data into ASCII code, so that it can be read on a Teletype module, if necessary.

Consider now the timing subsystem depicted in Fig. 18. Here the frequency synthesizer is a Hewlett-Packard Model 3302B unit incorporating a 5 MHz crystal in a temperature-stabilized oven. Each of the four digital delay generators is a Tektronix DD501 unit. The DD501 unit, designated as D* in Fig. 18, was modified to operate as a pulse generator with a digitally controlled pulselength, in accordance with a suggestion made by the Tektronix, Inc., engineering staff. An internally mounted switch allows one to operate this unit in either the modified mode or in a normal fashion. Both pulse generators PG1 and PG2, shown in Fig. 18, are also manufactured by Tektronix, Inc., the former is their Model PG505, the latter, their Model PG501.

It should also be mentioned that all electronic instrumentation is housed in three specially constructed equipment racks. The 60 Hz power is supplied to each rack through a pair of radio-frequency-

interference filters housed in a steel enclosure in the lower part of the rack. System power to all three racks is supplied from a single source, which was also specially built for this purpose. This source incorporated a Sorgel 7.5 kVA isolation transformer. The primary of this transformer is connected to the lines delivering one phase of the 60 Hz three-phase power that is supplied to the laboratory area. This single-phase input power, however, is supplied to the transformer primary through a pair of 100 A radio-frequency-interference filters, which were salvaged from a radar transmitter. The equipment racks are connected to three of four individually fused AC receptacles, which are wired in parallel to the secondary of the isolation transformer. For safety, the equipment racks and the case of the isolation transformer are grounded to a common bus bar within the power source, which is connected to the ground wire of the power cable that enters the source.

The power supply system described above is an important factor in attaining a measuring system that is largely free of the spurious electrical signals that usually plague the investigator who does acoustic experimentation in a water tank. The precautions taken, not only prevent unwanted transient signals from entering the measuring electronics through the system's power network, but also help to prevent any electrical transients generated by the system's electronic apparatus from being transmitted everywhere else in the measurement system. Use of such an isolated, filtered power system, also seems to make it much less difficult to eliminate troublesome ground-loop and crosstalk problems in the measuring system when they arise.